AZHIKANNICKAL

MATERIAL AND PROCESS MODELS FOR THE FORMING OF ORIENTED POLYMER TUBES

Ph.D.

MATERIAL AND PROCESS MODELS FOR THE FORMING OF ORIENTED POLYMER TUBES

By

ELIZABETH AZHIKANNICKAL, B.Sc., M.Sc. (MECHANICAL ENGINEERING)

A Thesis

Submitted to the School of Graduate Studies

in Partial Fulfillment of the Requirements

for the Degree

Doctor of Philosophy

McMaster University

DOCTOR OF PHILOSOPHY (2008) McMaster University

(Mechanical Engineering) Hamilton, Ontario

TITLE: Material and Process Models for the Forming of Oriented Polymer Tubes

AUTHOR: Elizabeth Azhikannickal, B.Sc., M.Sc. (Mechanical Engineering, Queen's University)

SUPERVISOR: Professor M.K. Jain

NUMBER OF PAGES: xxx, 277

ABSTRACT

The lightweight and good strength of oriented thermoplastic tubes, produced through the ram extrusion process, renders this class of material advantageous from an automotive structural part forming perspective. An analytical model, capable of predicting the forming limits for these materials at elevated temperatures, would avoid the need for difficult and time-consuming tube forming experiments.

The uniaxial tensile stress-strain properties of the oriented polypropylene (OPP) tubes along the axial and hoop direction were determined while methods were developed for obtaining the uniaxial compressive properties of the tube. The uniaxial and biaxial testing of the OPP tubes enabled representation of the experimental plastic work contours for the material at a range of temperatures. The use of the pressure-modified Hill criterion, the concept of plastic work contours in stress space, and the stress strain data from uniaxial testing of the tube allowed accurate prediction of the plastic work contours for the OPP tubes as a function of temperature. The analytical prediction was able to capture the anisotropy, pressure dependency and anisotropic hardening exhibited by the material at elevated temperatures. In addition, the use of a localized necking criterion, which involved the point at which the maximum force along the hoop direction of the tube was reached, allowed the temperature dependent forming limits for the material to be predicted. The forming limits increased with temperature for all of the strain paths considered. In addition, at a given temperature, the forming limits decreased with

increasing strain ratio. The limiting strains achieved with axial end feeding were markedly higher than those in which no axial end feeding was used.

Good agreement was observed between the predicted forming limits and the results from tube forming tests of the material, along a range of strain paths and at various temperatures.

ACKNOWLEDGMENTS

First and foremost I would like to thank my thesis supervisor, Professor Mukesh Jain, for his continued support during my PhD studies. For the diligent and sincere direction that he has given me on all aspects of my experimental and analytical work and for his support of my growth as a researcher. And for the many interesting and thought provoking conversations we've had along the way.

I would also like to thank Mike Bruhis, Research Engineer for the Materials Forming Laboratory of the McMaster Manufacturing Research Institute. I thank him for his enthusiasm and efforts in helping me with all aspects of my experimental work – both on the design side and on carrying out the experiments successfully.

I would like to thank Decoma International Inc., PSAC and the Natural Sciences and Engineering Research Council for financial support for this project. Thanks to Earlby Wakefield of Decoma and Frank Maine and Bill Newson of PSAC for seeing the potential in this project, from both a practical and an academic standpoint. Their help with tube production and material characterization trials is also appreciated.

I extend my appreciation to the members of my Supervisory Committee, Dr. Don Metzger, Dr. Tim Nye and Dr. Shiping Zhu for their helpful suggestions in resolving various research issues and improving the thesis.

I would like to thank the Mechanical Engineering technicians, Joe Verhaeghe, Ron Lodewyks, Dave Schick, Jim McLaren and Mark MacKenzie for their help in resolving various equipment related issues and during the rigorous machining of the OPP tubes for this study. They were always ready and willing to provide support (with a smile).

Thank you to Quan Situ and Mohamed Elnagmi, my colleagues, for making my time in the Materials Forming lab an enjoyable one. A special thanks to Mohamed for modifying and commissioning the hot oil tube forming test rig which I used to conduct the tube tests for this study.

Thank you to Dr. Philip Koshy and Janet Murphy, both of whom always expressed their best wishes for my future, and gave me that extra bit of encouragement and confidence.

Last, but not least, I thank my family for their love and patience.

TABLE OF CONTENTS

LIST OF TABLES

LIST OF FIGURES

NOMENCLATURE

a	material constant in Hosford's yield criterion
A	length of major axis of elliptical die used in tube forming test
A_0	initial cross-sectional area of axial compression sample
A_1	material constant in Inouye (1954) flow stress model
A_r	current cross-sectional are of gauge section of ring hoop tension sample
B	length of minor axis of elliptical die used in tube forming test
B_1	material constant in G'Sell et al. (1983) constitutive model
C_a	yield strength in uniaxial compression along axial direction of a tube (also referred to as the axial compressive stress parameter in pressure-modified Hill criterion to describe biaxial hardening)
C_x	yield strength in uniaxial compression along principal x-direction of a sheet or tube (also referred to as the compressive stress parameter along the x direction of a sheet or tube in pressure-modified Hill criterion to describe biaxial hardening)
C_y	yield strength in uniaxial compression along principal y-direction of a sheet or tube (also referred to as the compressive stress parameter along the y direction of a sheet or tube in pressure-modified Hill criterion to describe biaxial hardening)
C_θ	yield strength in uniaxial compression along hoop direction of a tube (also referred to as the hoop compressive stress parameter in pressure-modified Hill criterion to describe biaxial hardening)

$d\lambda$	constant
D	material constant used in prediction of temperature dependent plastic work contours for OPP tube
D_0	initial outer diameter of thick-walled tube
E	material constant used in prediction of temperature dependent plastic work contours for OPP tube
f	yield function
f_0	constant used in determination of material constants in modified G'Sell constitutive model
F	material constant in pressure-modified Hill yield criterion
F_0	material constant in Hill's (1948) anisotropic yield criterion
F_{12}	material constant in Gol'denblat-Koponov and Tsai-Wu yield criteria
F_a	axial compressive force
F_θ	hoop force per unit length of tube
G_0	material constant in Hill's (1948) anisotropic yield criterion
h	current bulge height of tube formed using an elliptical die
h_0	initial height of axial compression sample
h_1	material constant in G'Sell et al. (1983) constitutive model
h_i	current height of axial compression sample
H	material constant in pressure-modified Hill yield criterion
H_0	material constant in Hill's (1948) anisotropic yield criterion
I	material constant used in prediction of temperature dependent plastic work contours for OPP tube
J	material constant used in prediction of temperature dependent plastic work contours for OPP tube

k	material constant in Inouye (1954) flow stress model
k_1	rate of increase of axial load in a tube forming test
k_2	rate of increase of pressure in a tube forming test
K	material constant in G'Sell et al. (1983) constitutive model
K_1	material constant in Inouye (1954) flow stress model
K_x (or K_a)	material constant in pressure-modified Hill yield criterion
K_y (or K_θ)	material constant in pressure-modified Hill yield criterion
l_a	deformed arc length of tube along axial direction, between minor axis of elliptical die opening, and associated with a bulge height, h
l_{ai}	see B
l_h	deformed arc length of tube along hoop direction, between major axis of elliptical die opening and associate with a bulge height, h
l_{hi}	initial arc length of tube along hoop direction and between major axis of elliptical die opening
L	material constant used in prediction of temperature dependent plastic work contours for OPP tube
m	material constant in G'Sell et al. (1983) constitutive model
m_1	material constant in Inouye (1954) flow stress model
M	stress path
M_1	material constant used in prediction of temperature dependent plastic work contours for OPP tube
n	material constant in Inouye (1954) flow stress model
N	material constant in modified G'Sell model
N_i	total number of plastic work increments
p	internal pressure

P	compressive load applied to axial compression sample
Q	activation energy
R	Universal gas constant
R_a	radius of arc whose length is l_a
R_h	radius of arc whose length is l_h
R_{hi}	initial radius of thin-walled tube
S	constant used in development of modified G'Sell model
t	current thickness of tube
t_0	initial thickness of tube
t_i	time
t_m	half of current wall thickness of tube
T	temperature
T_a	yield strength in uniaxial tension along axial direction of a tube (also referred to as the axial tensile stress parameter in pressure-modified Hill criterion to describe biaxial hardening)
T_x	yield strength in uniaxial tension along principal x-direction of a sheet or tube (also referred to as the tensile stress parameter along the x direction of a sheet or tube in pressure-modified Hill criterion to describe biaxial hardening)
T_y	yield strength in uniaxial tension along principal y-direction of a sheet or tube (also referred to as the tensile stress parameter along the y direction of a sheet or tube in pressure-modified Hill criterion to describe biaxial hardening)
T_θ	yield strength in uniaxial tension along hoop direction of a tube (also referred to as the hoop tensile stress parameter in pressure-modified Hill criterion to describe biaxial hardening)

V	material constant in modified G'Sell model
w	current width of gauge section of ring hoop tension sample
w_0	initial width of gauge section of ring hoop tension sample
W	total plastic work per unit volume
W_a	plastic work per unit volume resulting from deformation along axial direction of tube
W_{inc}	plastic work increment
W_θ	plastic work per unit volume resulting from deformation along hoop direction of tube
Y	yield stress of an isotropic material
Y_c	yield strength in uniaxial compression for an isotropic pressure-dependent material
Y_t	yield strength in uniaxial tension for an isotropic pressure-dependent material
σ_0	yield stress of material
σ_a	stress along axial direction of thin-walled tube
σ_θ	stress along hoop direction of thin-walled tube
σ_{am}	stress along axial direction of thick-walled tube at the mid-wall thickness
$\sigma_{\theta m}$	stress along hoop direction of thick-walled tube at the mid-wall thickness
σ_{hyd}	hydrostatic stress
σ_x, σ_y, σ_z	stresses along principal directions of a sheet or tube
$d\varepsilon_a$	strain increment along axial direction of thin-walled tube
$d\varepsilon_\theta$	strain increment along hoop direction of thin-walled tube

$d\varepsilon_t$	strain increment along thickness direction of thin-walled tube
ε_a	strain along axial direction of thin-walled tube
ε_θ	strain along hoop direction of thin-walled tube
ε_t	strain along thickness direction of thin-walled tube
ε_{am}	strain along axial direction of a thick-walled tube at the mid-wall thickness
$\varepsilon_{\theta m}$	strain along hoop direction of a thick-walled tube at the mid-wall thickness
ε_{as}	strain along axial direction of a thick-walled tube at the outer surface
$\varepsilon_{\theta s}$	strain along hoop direction of a thick-walled at the outer surface
$\dot{\varepsilon}$	strain rate
ρ	strain ratio
ρ_a	radius of curvature of thin-walled tube along axial direction
ρ_θ	radius of curvature of thin-walled tube along hoop direction
ρ_{as}	radius of curvature of thick-walled tube along axial direction and at the outer surface
θ_a	angle subtended between arc whose length is l_a and radius is R_a
θ_h	angle subtended between arc whose length is l_h and radius is R_h
θ_{hi}	angle subtended between arc whose length is l_{hi} and radius is R_{hi}

CHAPTER 1

INTRODUCTION AND OBJECTIVES

1.1 Use of oriented thermoplastics for automotive structural component forming

The draw towards using thermoplastics for potential automotive structural components over metals lies in the fact that thermoplastics have a lower density compared with metals. Some of the other advantages of thermoplastics include their lower cost, corrosion resistance, chemical resistance, ease of processing with the application of heat (compared to room temperature processing) and their low thermal conductivity compared with metals. Thermoplastics are also recyclable, i.e. they can undergo repeatable melt and solidification cycles. However, it was found that sheet forming techniques using thermoplastic sheets, without complex reinforcing agents had inferior properties, such as impact resistance. Therefore, thermoplastics were confined to being used in a wide variety of non-structural automotive parts. Polypropylene, a

commodity thermoplastic, is being used for accelerator pedals, air ducting etc. (McCrum et al., 1997).

Fibre reinforced thermoplastic composites appear to show promise for automotive structural forming since they possess high stiffness and strength and have good impact properties if an appropriate reinforcing agent is chosen. They have become one of the key materials of interest for several industries, most notably the automotive and aerospace industries (Crosby, 1988, Bigg and Preston, 1989, Fallon, 1989). As a result, the study of the material behaviour and forming techniques of such composites has attracted considerable attention in recent years (Smiley and Pipes, 1988, Tsahalis et al., 1990, Michaeli and Jehrke, 1993, Lee and Vogel, 1995a, 1995b). Unfortunately, some of the main problems associated with using polymer composites for forming into automotive structural components include increased weight as well as problems related to recyclability and fibre to matrix adhesion. In addition, due to the presence of the reinforcing agent, the cost of manufacturing a given part would also increase.

The replacement of some high-performance structural materials, such as fibre reinforced composites by more 'commodity' materials such as polypropylene, forces engineers and designers to enhance the properties of the latter for subsequent forming of these materials into automotive structural components. The key to the successful forming of these materials into automotive structural type of components is to ensure a balance of adequate strength and formability at the processing and forming stages. Therefore, from an automotive manufacturing perspective, the development of high modulus and high

strength 'commodity' plastics such as oriented plastics is of interest, in view of their lower weight, cost and ease of recyclability. Also, the lower forces required to deform polymeric materials at room temperature and more so at elevated temperatures, compared with metals, means a lower demand in terms of load capacity from the associated forming equipment. In addition, the option to both uniaxial and biaxial orient thermoplastics (so properties are enhanced in both directions) means more flexibility at the processing stage for obtaining a certain set of properties for good forming and post forming behaviour of the material.

1.2 Description of existing tube forming methods for metals

Hydroforming of metallic tubes is a relatively new technology that is seeing increasingly widespread use in the area of automotive component forming. In the tube hydroforming process, a starting tube is first sealed at its ends via hydraulic actuators. Simultaneous feeding of the tube ends and internal pressurization of the tube (via a pressurizing medium such as water) causes it to expand and fill a die cavity of a given shape (refer to Figure 1.1). Some of the automotive parts produced by the tube hydroforming technology are given below (Koc and Altan, 2001):

- Exhaust system parts usually made of stainless steel for obtaining required structural, thermal and corrosion properties: Exhaust parts, engine tubes, catalytic converters, pressure tubes, tail pipes, connectors and manifolds.

- Chassis parts; common material is low to medium carbon steels and aluminum for structural and cost related reasons: Frame rails, engine sub frames (cradles), roof rails and bows, instrument panels, rear axle frames and radiator frames.
- Engine and power train components: Suspension cross members, hollow camshafts, drive shafts and gear shafts.
- Body and safety parts: Windshield headers, A/B/C pillars, space frame components, seat frames and shock absorber housings.

The primary advantages of the tube hydroforming process over conventional forming processes include reduced part weight, reduced part count, lower component and assembly costs, lower tooling costs, increased strength and stiffness (rigidity) and greater dimensional stability (Singh, 2003). The added axial end feeding also aids in delaying thinning or necking of the material during forming applications that require the material to undergo larger strains. Currently, the tube hydroforming technology has only been applied to metallic materials.

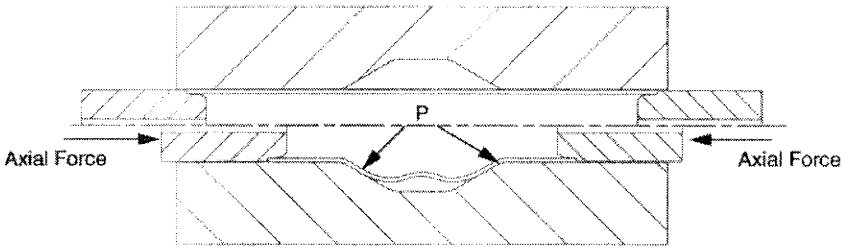

Figure 1.1 Tube forming involving application of internal pressure and axial load (Singh, 2003).

1.3 Description of existing tube and sheet forming methods for thermoplastics

Turning to conventional methods for the tube forming of thermoplastics, stretch blow molding has become an important high-speed production technique since the introduction of the 2-litre carbonated beverage bottle that uses polyethylene terephthalate (PET) resin (Rosato, 1989). During the stretch blow molding process, a temperature conditioned injection preform is inserted into the blow mold cavity and then is rapidly stretched (refer to Figure 1.2). Often a rod is used to stretch the preform in the axial direction with air pressure to stretch the preform in the radial direction (Figure 1.2).

Stretch blow molding is possible for thermoplastic materials such as PET, PVC, polystyrene and polypropylene. The amorphous materials are easier to stretch blow than the partially crystalline types. With the partially crystalline type (such as polypropylene), if the crystallizing is too rapid, the bottle is virtually destroyed during the stretching process (Rosato, 1989). Based on the work on stretch blow-molding 2-litre containers of PVC and PET, average wall thicknesses of 0.3-0.4 mm have been used, however, wall thickness as low as 0.23-0.25 mm have been observed (Rosato, 1989). Due to the fact that axial feeding of the material at its ends is not possible with this process, excessive thinning at locations along the wall may occur. This is not desirable from an automotive in-service performance perspective.

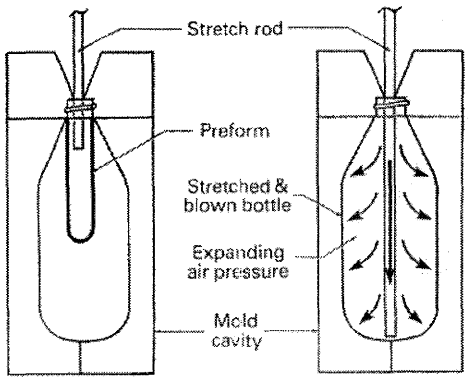

Figure 1.2 Schematic of the stretch blow molding process (Rosato, 1989).

There appear to be a wider range of forming methods applied to thermoplastic sheet materials and these are categorized under the broader term known as thermoforming. Thermoforming uses plastic sheet, which is heated, stretched, cooled, and mechanically cut (Throne, 1999). Traditional pressure forming uses air pressure up to 1 MPa on the free side of the sheet and vacuum on the sheet surface closest to the mold (Throne, 1999). The air pressure is contained in a pressure box that clamps the sheet against the mold surface. Pressure forming is used for thick sheet forming applications when the sheet, at forming temperature, is too rigid to adequately take the shape of the mold surface (Throne, 1999). A schematic of pressure forming is given in Figure 1.3.

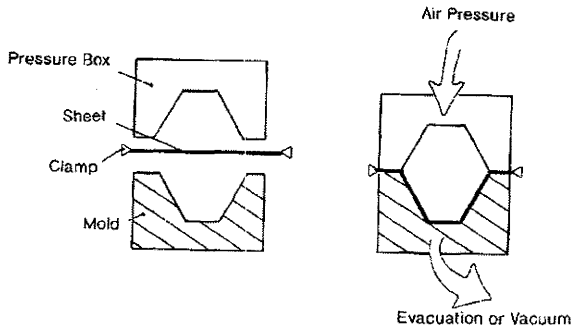

Figure 1.3 Pressure forming (Throne, 1999).

Plug assist thermoforming is a second method used to form polymer sheet materials. The plugs are solid structures of a particular shape that are mechanically driven into the softened sheet during forming. The plugs are mainly used to locally stretch the sheet. The plugs can be made from any heat resistant solid material, including wood, plastics such as nylon, heated aluminum etc. (Throne, 1999). Plugs are used in the forming of thin thermoplastic sheet for products such as drink cups. They are also used in the forming of thicker thermoplastic sheet for products such as tote bins and equipment cabinets (Throne, 1999). A schematic of plug assist thermoforming is given in Figure 1.4.

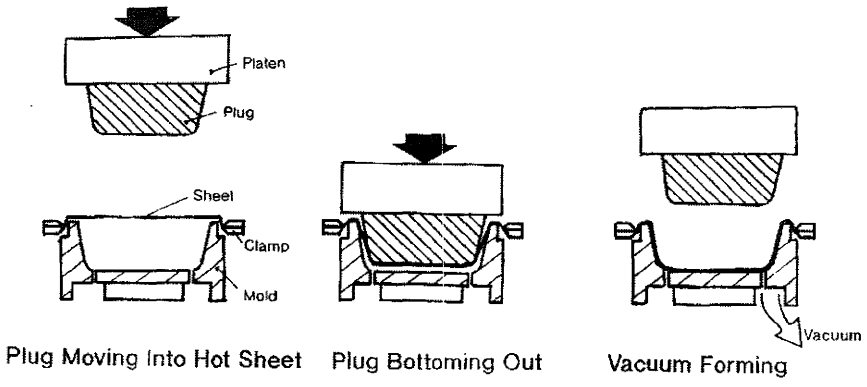

Figure 1.4 Plug assist thermoforming (Throne, 1999).

1.4 Axial feed thermoforming of oriented thermoplastic tubes

The axial feed thermoforming process for thermoplastic tubes is a new process under development in the Materials Forming Laboratory of McMaster University. It merges conventional metal tube hydroforming and blow molding in that a thermoplastic tube is heated to a softened state (as in blow molding) and subsequently formed by the combination of applied internal gas pressure (as in blow molding) and axial feeding of the tube ends (as in tube hydroforming). The primary advantage of this process over blow molding is that a more uniform thickness distribution of the final part results since there is the option to feed the tubes ends during forming. As mentioned previously, axial feeding is not used with conventional blow molding operations. In addition, the cost of the forming equipment for axial feed thermoforming of thermoplastic tubes compared with hydroforming metal tubes is significantly lower. This is because lower forces and pressures are required for the forming of thermoplastics at elevated temperatures compared with metals at room temperature. The broad goal of the present research is to assess the behaviour of oriented polypropylene tube formed by the axial feed thermoforming process at a range of temperatures and strain rates. No work in this area has been conducted, either experimentally or numerically.

1.5 Research issues

In order to assess the feasibility of using oriented thermoplastics, specifically oriented thermoplastic tube, for forming into automotive structural components, an establishment of the forming limit curve for this material at various strain rates,

temperatures and tube draw ratios is required. The forming limit curve identifies the safe and unsafe zones for a material subjected to major and minor strains, typically with ratio of these strains (referred to as the strain path) remaining constant during loading (refer to Figure 1.5). A detailed discussion of forming limit diagrams will be given in Chapter 2. Figure 1.6 shows a typical room temperature forming limit diagram (or FLD) for low carbon steel (Hosford and Caddell, 1993). A FLD is often utilized in establishing the process conditions required to produce good quality parts, i.e. those without areas of localized thinning. An experimental methodology or theoretical framework for establishing the forming limits for oriented thermoplastic tube has not been developed to date.

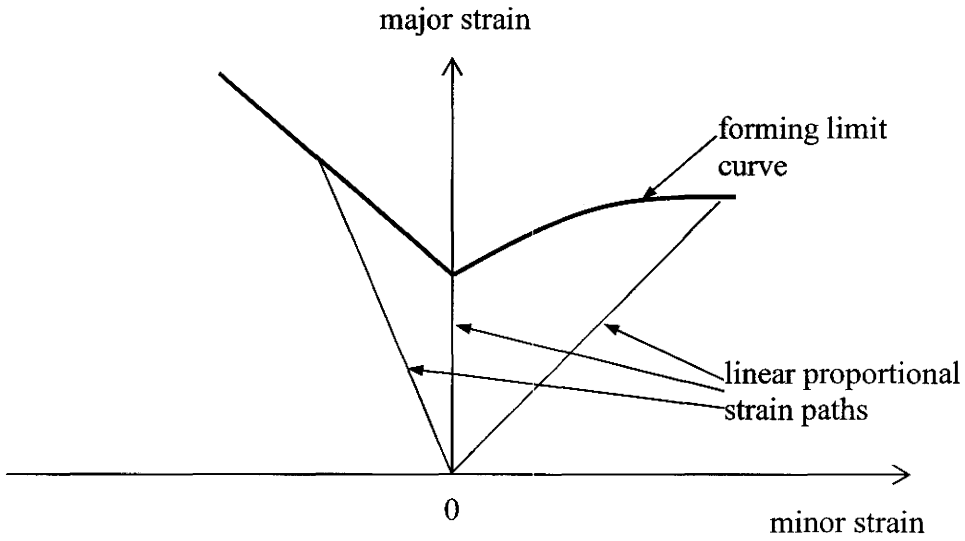

Figure 1.5 Schematic of a typical forming limit diagram showing the forming limit curve and various linear proportional strain paths.

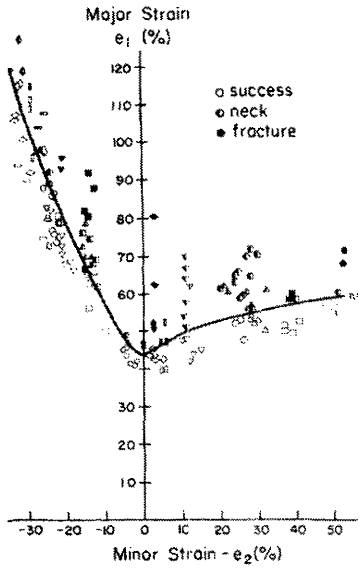

Figure 1.6 Typical forming limit diagram for low-carbon steel (Hosford and Caddell, 1993).

For sheet metal, the forming limits can be determined experimentally and compared with theoretical predictions. The most widely used experimental method involves printing a grid of small circles of diameter, d_0, on a strip of sheet metal before forming (refer to Figure 1.7 (a)). The metal strip is then stretched over a dome (refer to Figure 1.7 (b)) until a neck or fracture is observed (refer to Figure 1.7 (c)). To obtain different strain paths (i.e. ratio of minor strain ε_2 to major strain ε_1), specimen widths are varied. Full-width specimens and good lubrication between the punch and sheet produce conditions close to balanced biaxial tension and very narrow specimens produce conditions close to uniaxial tension (Hosford and Caddell, 1993). For a given strain path, the strains associated with circles wholly or partially in the neck are considered "failed", while the strains in the circles outside of the neck are considered "safe" (Hosford and Caddell, 1993). By plotting the major and minor strains at which strain localization (or

necking) occurs, it is possible to construct a FLD. Due to the tedious and time consuming nature of the experiments to obtain the FLD, many attempts have been made towards prediction of FLDs of sheet metals from the mechanics of the test and theories of plasticity.

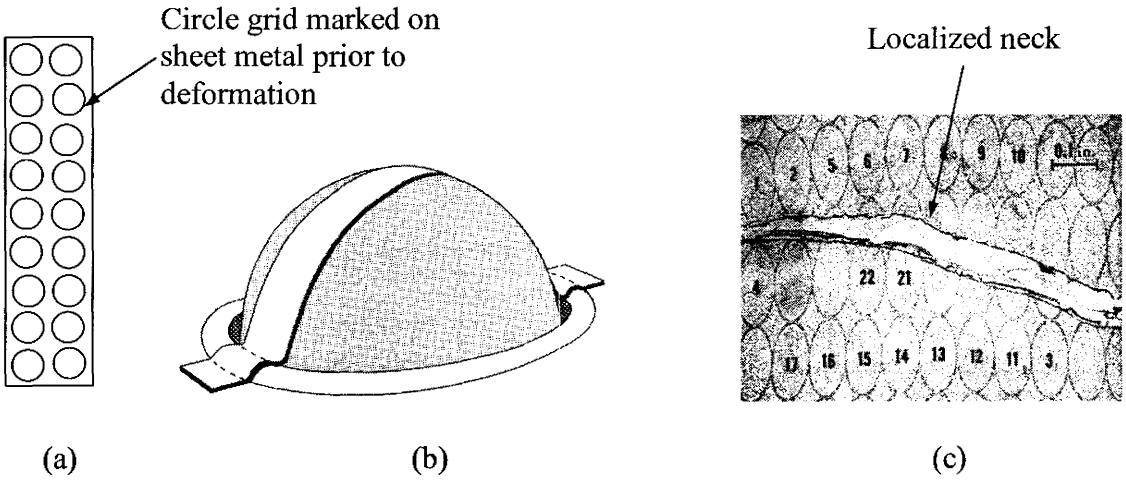

Figure 1.7 (a) Circle grid marked on sheet metal strip prior to deformation (b) Strips of varying widths are stretched over a dome (c) distortion of printed circles near a localized neck in sheet metal (Hosford and Caddell, 1993).

It is important to make a note here that there are several issues associated with obtaining the experimental forming limits for oriented polymer tubes compared with sheet metal. As mentioned earlier, the forming limits for sheet metal can be obtained by the dome test method used on strips of varying widths, in order to obtain strain localization along different strain paths. Assuming that the material is strain rate insensitive, only the width of the specimens and lubrication conditions require variation to obtain different strain paths. Obtaining different strain paths with a tube forming

process, on the other hand, involves the application of internal pressure to the inner diameter of the tube along with simultaneous axial feeding of the tube ends. This combination of loading can be challenging since it must be applied in such a way that the strain path remains constant.

In metal tube hydroforming at room temperature, the material is typically taken to burst, since necking and bursting occur in rapid succession and the test is often difficult to interrupt at neck. Therefore, the point at which the burst occurs can be used as a direct measure of the strains at which localization occurs. A more detailed discussion of the methodology for constructing forming limit diagrams for metal tubes during hydroforming will be made in Chapter 2. It is important to note that with oriented polymer tubes formed at elevated temperatures, the point at which the strain localizes is not necessarily as straightforward to determine. This is because experimental evidence shows that the material does not necessarily burst immediately after strain localization, but, instead, continues to deform within the necked region to much higher strains.

In addition, oriented thermoplastic tubes exhibit much stronger material anisotropy compared with rolled sheet steels. This anisotropy, in addition to the pressure sensitivity exhibited by the oriented thermoplastic tubes, must be accounted for in the theoretical prediction of the forming limits for these materials. Also, since oriented polymers are temperature and strain rate dependent, these parameters are also critical in both the experimental and theoretical establishment of the forming limits.

Caddell et al. (1973) put forth a yield criterion to describe the initial room temperature biaxial yield surface for various oriented thermoplastic tubular materials. A yield criterion is a postulated mathematical expression of the states of stress that will induce yielding or the onset of plastic deformation (Hosford and Caddell, 1993). The particular criterion mentioned above will be referred to as the pressure-modified Hill criterion and its details will be described in Chapter 2. However, the interesting feature of this yield criterion, unlike those typically used for metals, is that it accounts for both the anisotropy and pressure dependency exhibited by oriented thermoplastics. Therefore, this type of a yield criterion is more appropriate for developing models to predict the forming oriented thermoplastic tubes. However, appropriate methodologies for use of this yield criterion for predicting the anisotropic hardening exhibited by the material at elevated temperatures for the purpose of tube forming has not been examined to date.

1.6 Research objectives

The specific objectives of the present research are:

[1]. Assessment of the pressure-modified Hill yield criterion put forth by Caddell et al. (1973) for hot forming applications of oriented polypropylene (OPP) tubes. This objective will involve the development of experimental test methodologies for determination of the uniaxial stress parameters within this yield criterion, along the principal directions of the tube, in tension and compression at various temperatures and strain rates.

[2]. Prediction of the plastic work contours for the OPP tube as a function of temperature and for a given strain rate.

[3]. Development of an analytical model for predicting the forming limits of OPP tubes at various temperatures based on:

1. The yield criterion put forth by Caddell et al. (1973) (refer to objective 1).
2. Prediction of the plastic work contours for the material as a function of temperature (refer to objective 2).
3. A criterion for localized necking of the tube.
4. Mechanics of hot gas (or high temperature) axial-feed tube forming process.

[4]. Validation of the predicted forming limits via tube forming tests using an in-house tube bursting test rig and an on-line optical strain measurement system (ARAMIS) both located in the Materials Forming Laboratory (MFL) in the Mechanical Engineering Department.

CHAPTER 2

LITERATURE REVIEW

2.1 Production of oriented polymers

In recent years, there have been a number of studies focused on the solid-phase processing of polymers as a method for producing high stiffness and strength materials in the form of rods, sheets and tubes (Bekhet et al., 1993). A number of processes exist which allow polymers to be deformed in the solid state. Some of the major techniques are ram extrusion (Farrell and Keller, 1977), hydrostatic extrusion (Nakamura et al., 1972, Hope et al., 1980) and die drawing (Gibson and Ward, 1980, Peguy and Manley, 1984, Richardson et al., 1986, Taraiya et al., 1987).

In the ram extrusion process, an isotropic polymer billet is first heated to a temperature below the melting temperature. It is then forced, by a piston, through a die of reducing cross-section, as shown in Figure 2.1. Depending on the die geometry, ram extrusion can be used to produce rods, tubes, flat or shape profiles. The ram extrusion

process has two main limitations. Firstly, the process must occur quite slowly since high friction exists between the polymer and the metal die. Attempts to extrude at higher rates typically results in the process becoming unstable, and thereby, highly distorted extrudate being produced (Karger-Kocsis, 1999). Secondly, the ram extrusion process is a discontinuous process since preformed billets must be used (Karger-Kocsis, 1999).

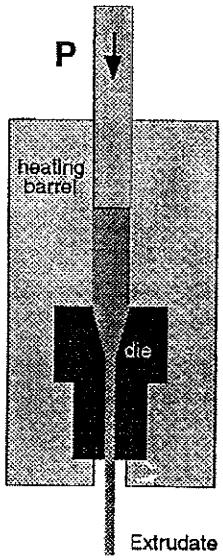

Figure 2.1 Schematic of ram extrusion process (Karger-Kocsis, 1999).

In hydrostatic extrusion, the piston is replaced by fluid under high pressure, and the billet is clear of the walls of the chamber (Ward et al., 2000) (refer to Figure 2.2). Unlike in the ram extrusion process, the fluid acts as a lubricant between the polymer and the die wall, thereby reducing the friction at the polymer/die interface. The haul-off load shown in Figure 2.2 is very small, only enough to ensure that the extrudate emerges from the die straight, and to provide some additional control of the extrusion process (Ward et al., 2000).

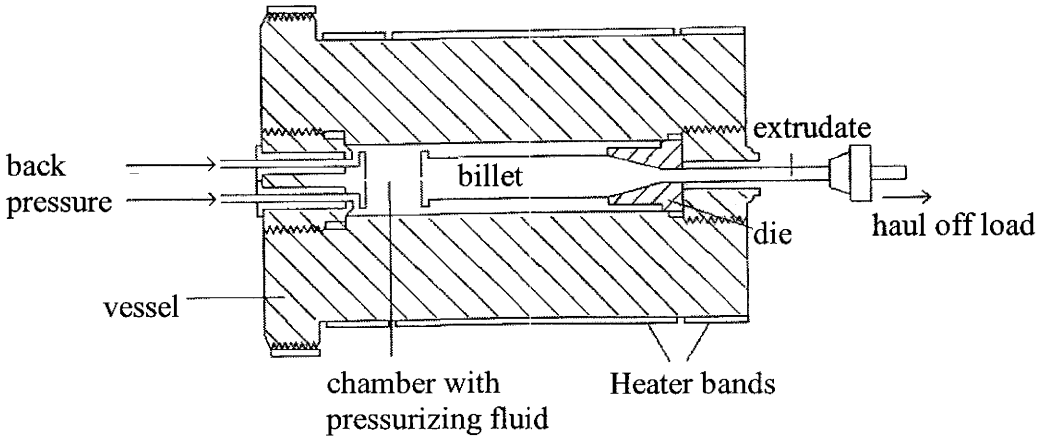

Figure 2.2 Schematic of hydrostatic extrusion process (Ward et al., 2000).

First reports of the hydrostatic extrusion of polymers were given by Buckley and Long (1969) and Alexander and Wormell (1971). In these cases, there was a very moderate enhancement of the mechanical properties of the extrudates through the processing. The first hydrostatic extrusion results exhibiting large enhancement of polymer properties came from the ICI group at the Petrochemical and Polymers Laboratory at Runcorn, Cheshire, U.K. Williams (1973) reported that polypropylene rods could be produced with a Young's modulus of 16 GPa at room temperature. In 1972, Gibson and Ward, who had been employed at ICI, transferred the equipment to Leeds University. Working in collaboration with Cole and Parsons (Gibson et al., 1974), they were able to produce very highly oriented polyethylene rods with a Young's modulus of 60 GPa.

Ward and coworkers (Parsons and Ward, 1982) proposed that the hydrostatic extrusion behaviour of polymers could be understood in terms of two fundamental principles. Firstly, for a given initial isotropic billet, whose chemical composition and

structure are fixed, the mechanical properties of the extrudate are a function of the total plastic strain imposed, i.e. the extrusion ratio. The extrusion (or draw) ratio is defined as the ratio of the cross-sectional area of the billet to the extrudate (Karger-Kocsis, 1999). Secondly, for a given initial isotropic billet, a mechanical equation of state (determined through the mechanics of the extrusion process) and the true stress-strain curve, which is a function of strain rate, temperature and pressure determines the processing behaviour of the material in terms of factors such as extrusion pressure and extrusion rate. However, the primary drawback with the hydrostatic extrusion process is that it is a batch process, so the production rates are much less than those for a continuous process, such as die drawing, which will be treated next.

The die drawing process, which has more recently been developed, is essentially free from the difficulties present with the ram extrusion and hydrostatic extrusion processes. The technical details of the die drawing process have been previously published along with the details of the die drawing behaviour of various polymers (Coates and Ward, 1979, Hope et al., 1981, Selwood et al., 1987, Taraiya et al., 1987). In this process, a polymer billet is heated, and while still in the solid state, it is drawn through a converging die by an axial load. Downstream of the die exit, free tensile drawing occurs, and the material is further axially extended by the drawing load.

The die drawing technique has been used to produce polyethylene, polypropylene and polyvinylchloride (PVC) products of circular and rectangular cross-section. More recently, tubular products have also been made (Craggs, 1990). In this case, the starting

billet has a tubular shape, and it is then drawn through a die and typically over a mandrel. Various mandrel-die configurations are possible as seen in Figure 2.3. Figure 2.3 (a) shows the classic die sinking process in which no mandrel is used. This configuration is of little importance since the hoop stress in the tube wall is compressive (Craggs, 1990). More interesting is the drawing of a tube to a constant bore as the material is highly drawn in the axial direction (refer to Figure 2.3 (b)). The effect of slightly enlarging the bore (Figure 2.3 (c)) is to produce a small amount of drawing in the hoop direction and, therefore, improve the properties in this direction. A significant improvement in hoop properties is achieved using the mandrel-die configuration shown in Figure 2.3 (d), in which the tube has molecular orientation and enhanced properties in both the axial and hoop directions. Polyethylene, polypropylene and PET tubes have been produced by this processing route (Selwood et al., 1987).

It has been shown that the die drawing process is preferred over the other processes discussed because of the relatively high production rates, ease of operation and applicability to nearly all common thermoplastics (Selwood et al., 1987, Ward, 1989). In addition, die drawing has the potential for incorporation into a continuous process, i.e. from granules to the continuous extrusion of the billet to the die drawn polymer (Bekhet et al., 1993).

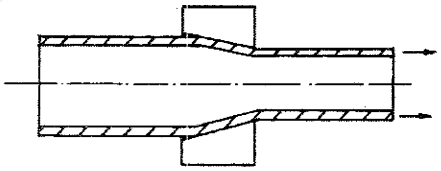

(a) mandrel free drawing

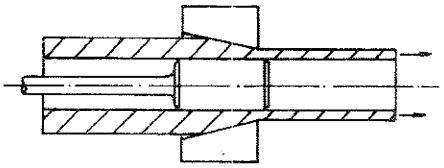

(b) drawing to constant bore

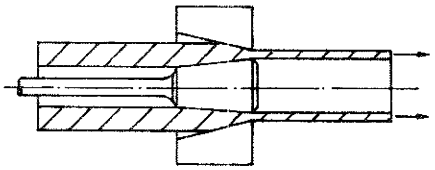

(c) drawing to marginally enlarged bore

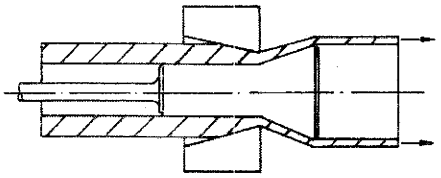

(d) drawing to substantially enlarged bore

Figure 2.3 Mandrel-die configurations for the die drawing of tubes (Craggs, 1990).

2.2 Molecular aspects of oriented crystalline polymers

In order to understand the structure of oriented polymers, it is important to understand the structure of unoriented polymers, from where the oriented structure is derived. Light microscopic examination of thin films of crystalline polymers reveals complex polyhedral objects known as spherulites (McCrum et al., 1997) (Figure 2.4). Each spherulite contains a complex ordered grouping of sub-microscopic crystals that are separated from one another by lamellae of amorphous polymer (Figure 2.4). The crystalline portion of the polymer consists of the packing of the molecules, parallel to one another, within the crystal. The amorphous region of the crystalline polymers consists of long tangled molecules. Since the length of the molecules is greater than the length of the crystals, a given molecule passes through several crystals and several amorphous regions (McCrum et al., 1997). It is these long molecules that allow for the coexistence of the crystal and amorphous regions. The spherulitic structure described above results during the crystallization of a polymer when cooled below its melting temperature.

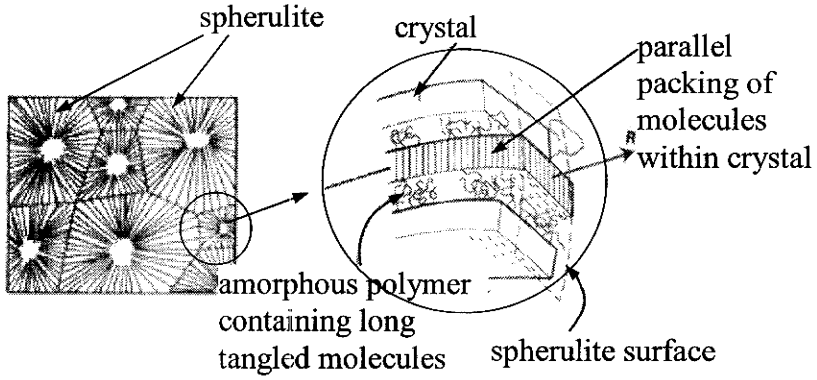

Figure 2.4 Spherulitic structure of polymers (McCrum et al., 1997).

The crystal and amorphous lamellae within the spherulite are of approximately the same thickness. The lateral dimensions of the crystals are much greater than the thickness dimension, and, therefore, the thickness of one crystal can be seen to have the thickness of a sheet of paper (McCrum et al., 1997). The diameter of a spherulite is dependent on the crystallization conditions, but is typically of the order of the wavelength of light (McCrum et al., 1997).

The morphology of an oriented crystalline polymer reveals as the basic structural element the microfibril and not the lamella (Peterlin, 1969). Electron micrographs of a surface replica of a drawn polymer show long, highly aligned microfibrils with lateral dimensions between 100 and 200 angstroms. The length is in tens of micrometers (Peterlin, 1975). During the drawing of a polymer, the folded chain blocks are broken off from the spherulitic lamella and incorporated into the microfibril as shown in Figure 2.5. It has been stated that the microfibril behaves much more as a crystal with locally weak areas originating from the amorphous fraction (Peterlin, 1975). A higher organizational unit is the fibril, i.e. a bundle of parallel microfibrils (Figure 2.5). The fibrils are formed during the drawing from a stack of parallel lamella of the starting material and varying in draw ratio from the adjacent fibril originating from a stack with different lamella orientation. This renders the boundary between adjacent fibrils weak and favours the formation of longitudinal voids (Peterlin, 1975). Highly drawn polymers exhibit an almost complete orientation of the crystal lattice and a high orientation of the amorphous component (Peterlin, 1975). Figure 2.6 shows an electron micrograph of a surface replica of isotactic polypropylene drawn at 100°C to a draw ratio of 5 (Peterlin, 1971). Note the

highly aligned microfibrils as well as the disorientation of the microfibrils bridging the longitudinal voids.

2.3 Mechanical properties of oriented crystalline polymers

The resulting fibrillar structure of an oriented crystalline polymer brings about changes in the mechanical properties of the material. Many examples can be quoted to illustrate how the introduction of orientation during processing affects the properties of solids. Table 2.1 below shows a comparison of hydrostatically extruded polypropylene and forged 0.36% carbon steel (Holliday and Ward, 1975). For the steel, the ratio of ingot diameter to forged rod diameter was 12:1 whereas for the polypropylene, the results shown are for a draw ratio of 5.5. The longitudinal direction in Table 2.1 refers to the direction in which molecular orientation was induced, i.e. the extrusion direction in the case of the polypropylene.

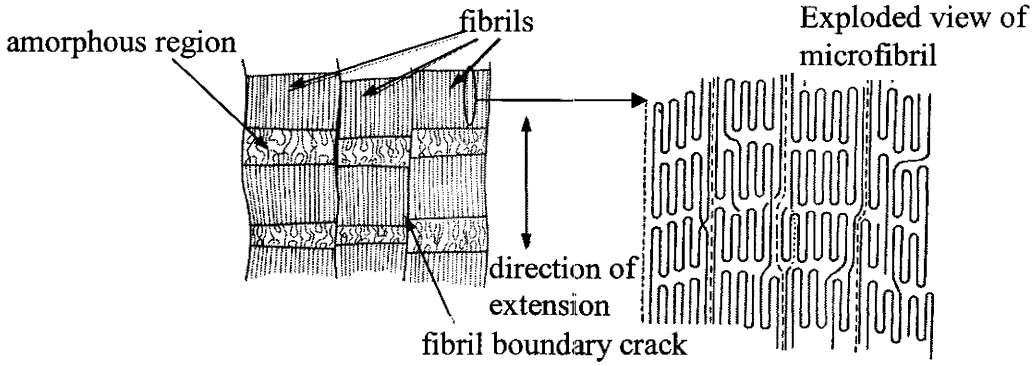

Figure 2.5 Fibrillar structure of an oriented polymer (McCrum et al., 1997).

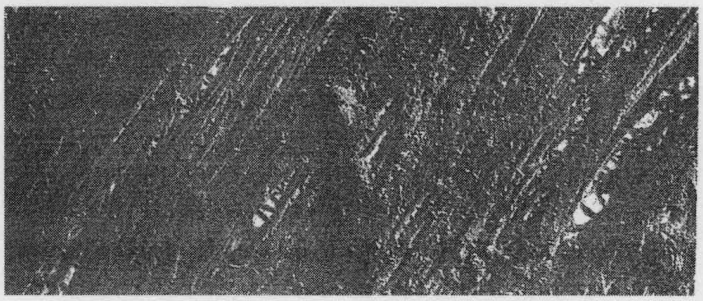

Figure 2.6 Electron micrograph of a surface replica of isotactic polypropylene drawn at 100°C to a draw ratio of 5 (Peterlin, 1971).

Sample	Extrusion ratio	Longitudinal yield strength (MPa)	Longitudinal tensile strength (MPa)	Elongation at break (%)	Impact strength
Carbon steel: ingot	1	290	560	19	56 (J Charpy)
Carbon steel: forged rod	12	340	560	27	102 (J Charpy)
Polypropylene: billet	1	10	22	200	0.3 ft. lb.
Polypropylene: extruded rod	5.5	*	220	24	14 ft. lb.

* No yield drop observed

Table 2.1 Effect of processing on the properties of steel and polypropylene (Holliday and Ward, 1975).

In the case of the carbon steel, forging has improved the ductility and impact strength in the longitudinal direction. Turning to the polymer case, it is important to note that the extent to which it is possible to increase the tensile strength along the longitudinal direction, and the ease with which this can be done, find no parallel with other materials. The results presented in Table 2.1 show that the extruded polypropylene has increased its tensile strength by a factor of 10 and its impact strength by a factor of 47, compared with the starting billet. However, increased strength is accompanied by a significant decrease in the ductility of the extruded polypropylene rod compared with the billet (as indicated by the decrease in the elongation at break).

Inducing molecular chain orientation as a result of processing also brings about some degree of anisotropy in the mechanical properties of the material with direction. In most cases, the degree of anisotropy present depends on the extent to which molecular orientation has been achieved. It is typical for many thermoplastics to be oriented at room temperature by cold drawing (Peterlin, 1975). The solid line in Figure 2.7 shows a typical load-extension curve for an isotropic polymer, having not yet undergone any cold drawing. The rate of strain is low, similar to that used in a normal tensile test. At low strains, the stress rises steadily with increasing strain (refer to Figure 2.7). At A the sample thins to a smaller cross-section at some point within its gauge length with the formation of a neck. Further extension occurs by the movement of this neck through the sample as it thins from its initial state to the final state. If, now, a sample of the drawn material within the neck is taken, and tested (or redrawn) in the longitudinal or fibre direction, the upper dotted line in Figure 2.7 will be obtained. As indicated by the load

extension curve in the longitudinal direction, there is a several fold increase in Young's modulus (as indicated by the greater slope) and a much greater increase in strength. The elongation of the material, however, is greatly reduced. The lower dotted line in Figure 2.7 results from testing the same drawn material in the direction transverse to the orientation direction. In most cases, the stiffness in this direction is lower than the initial stiffness or very nearly equal to it and the strength is always lower (Peterlin, 1975).

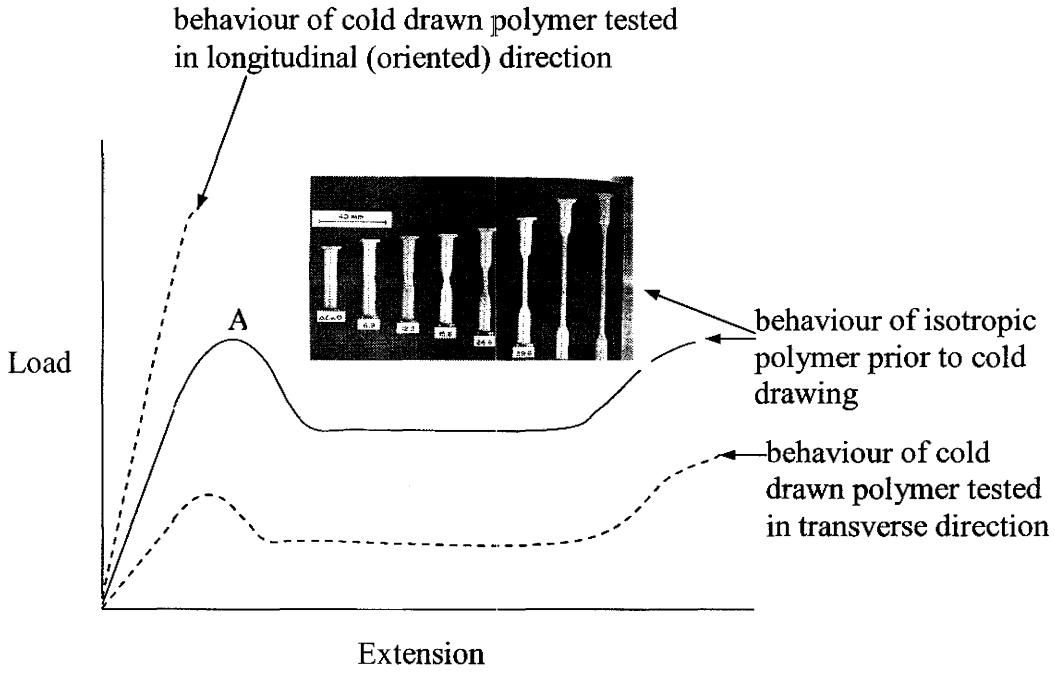

Figure 2.7 Typical stress strain curves for a polymer prior to and post cold drawing (Peterlin, 1975).

It is important to relate the enhancement of the stiffness and strength of oriented crystalline polymers, on a macroscopic scale, to the microscopic features of these materials. In a stress field, the microfibril reacts almost as a rigid structure that is much stronger than any other element of the polymer solid (Peterlin, 1975). This is a consequence of the large fraction of molecules connecting consecutive microfibrils and of the special dense packing of aligned microfibrils, with a large surface to cross-section ratio (Peterlin, 1975). In addition, the longitudinal displacement of a single microfibril is opposed by van der Waals forces along the whole microfibril such that displacement is more difficult than in the case of spherulitic lamella (Peterlin, 1975). The combination of all of the above mentioned effects results in the higher tensile strength and elastic modulus of oriented materials. Also requiring some discussion is the reason for the low modulus and strength in a direction transverse to the orientation direction. As mentioned previously, since adjacent fibrils often vary in draw ratio since they originate from a stack with different lamella orientation, it makes the boundary between adjacent fibrils weaker and favours the formation of longitudinal voids. This causes a significant reduction in the strength of the material in a direction perpendicular to the orientation direction.

As a rule, the increase in elastic modulus, yield strength and tensile strength increase linearly with draw ratio (Peterlin, 1975). It is not entirely correct to assume that this significant modification of mechanical properties is caused by chain orientation. A closer analysis shows that this may be true for the amorphous but not the crystalline component (Peterlin, 1975). It is a consequence of the fact that in a polymer sample with increasing draw ratio, the fraction of fibrous structure is steadily increasing and both the

amorphous orientation and the mechanical properties are proportional to this ratio (Peterlin, 1975). Therefore, the orientation of the crystal lattice may not be a good parameter for the description of the mechanical properties. Also, it fails completely during annealing at higher temperatures in which the crystal orientation is only slightly reduced, in particular if the sample is clamped so that it cannot shrink. However, the mechanical properties are significantly reduced down to the values of the unoriented material (Peterlin, 1975). Infrared dichromism shows a nearly complete loss of orientation of the amorphous component (Glenz and Peterlin, 1971), which seems to indicate that the molecules have almost completely relaxed and assumed a random conformation or have been reduced in number (Peterlin, 1975).

2.4 Experimental methods for determination of loading surfaces

In order to construct an initial experimental biaxial yield surface for a material as well as track its evolution with hardening (i.e represent subsequent loading surfaces), two fundamental considerations must be settled. These are (1) the choice of a suitable test specimen or specimens and the associated testing apparatus which will allow the initial and subsequent loading surfaces to be determined along various stress paths and (2) a definition of initial yield and a method to determine shape of the loading surfaces with subsequent hardening.

2.4.1 Mechanical testing of sheet materials for determination of loading surfaces

2.4.1.1 Uniaxial testing of sheet materials

In order to determine the yield point of a sheet material along a uniaxial stress path, a standard tensile test, typically using a dogbone type of specimen is employed. If the material is isotropic, the true stress-strain curve generated from a uniaxial tensile test along any of the principal directions of the sheet should be approximately equal. However, if the material is suspected to be anisotropic, uniaxial tensile tests are conducted along the principal directions of anisotropy in order to accurately represent the variation in the yield point of the sheet material with direction.

2.4.1.2 Biaxial testing of sheet materials

In sheet forming processes, materials are generally subjected to biaxial loads. Therefore, loading tests which subject the material to a biaxial state of stress are important, for accurately characterizing the biaxial yielding of the sheet material. Determination of the yield point along the plane-strain tension path can be achieved in a sheet specimen with a very wide and short gauge section, where the loading direction is parallel to the shorter gauge section. The difficulty has been in gripping the specimen in such a way that failure does not occur at the gripping location.

The hydraulic bulge test has also become a useful test for its use in characterizing the yield and work hardening characteristics of sheet metals along positive biaxial stress paths. In the bulge test, a thin disc of sheet metal is clamped around its periphery and

then subjected to an increasing fluid pressure applied to one side as shown in Figure 2.8. Several improvements, including a biaxial extensometer (Johnson and Duncan, 1965) and automated hydraulic bulge testers (Young et al., 1981) have simplified the experiment somewhat. For an accurate determination of the stress–strain curves along the principal directions, the geometry of the bulge must be taken into consideration and the strain rate must be constant during bulging (Ranta-Eskola, 1979). The hydraulic bulge test can typically subject the sheet material to strain paths ranging from plane strain to balanced biaxial tension. The resulting stress (or strain) path is typically controlled by the geometry of the die opening, i.e. circular or elliptical. It should also be noted here that the hydraulic bulge test is of limited value in determining the yield point since it relies on the measurement of the curvature of the sheet as it changes from a value of infinity (for a flat sheet) to a finite value as the sheet starts to bulge. Since the measurement of the initial curvature is not accurate, the same can be said about the yield point.

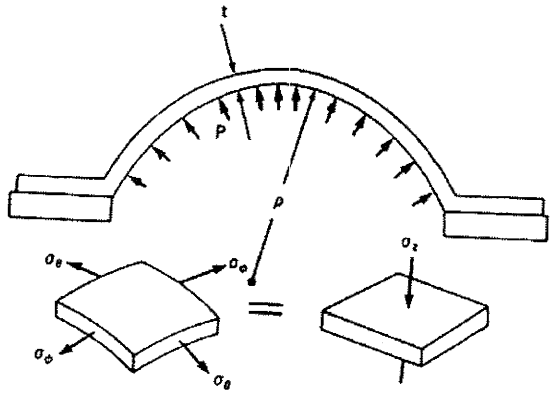

Figure 2.8 Schematic of the bulge testing of a sheet material (Hosford and Caddell, 1993).

Another approach to biaxial tension testing of sheet metals is through the use of cruciform specimens. Figure 2.9 shows two examples of cruciform specimens from previous studies (Ferron and Makinde, 1988, Kuwabara et al., 1998). The cruciform specimens shown in Figure 2.9 (a) have a gauge section that is thinner than that at the periphery. It is not easy to produce this geometry using sheet materials approximately a few mm thick, which are commonly used in sheet stamping operations in industry. Kuwabara and coworkers (1998) designed and constructed a servo-controlled biaxial tensile testing machine and carried out biaxial tension tests on various metallic materials using the cruciform specimen geometry shown in Figure 2.9 (b). Each arm of the specimen has seven slits in order to eliminate any geometric constraint on the deformation of the gauge section. The two principal strains were measured using biaxial strain gauges. The normal stress components in the gauge section were determined by dividing the measured loads by the current cross-sectional area of the gauge section. The current cross-sectional area was determined from the measured values of the plastic strain components and assuming volume constancy.

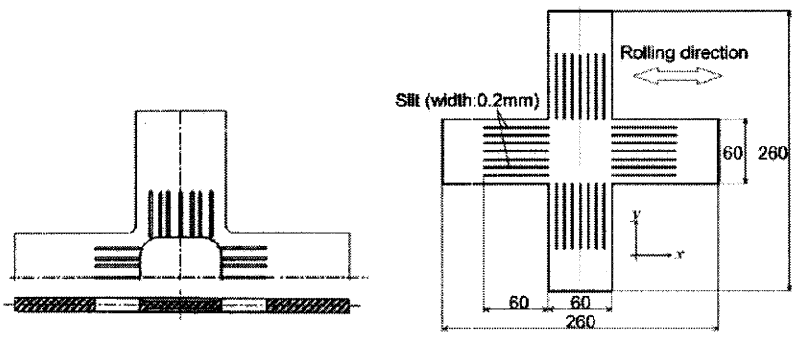

(a) (b)

Figure 2.9 Cruciform specimen geometries discussed in the literature. (a) (Ferron and Makinde, 1988) and (b) (Kuwabara et al., 1998).

The biaxial compression test on adhesively laminated sheet specimens has been found to be quite useful for sheet materials (Tozawa and Nakamura, 1972, Maeda et al., 1998). Figure 2.10 is a schematic diagram showing how various stress states can be obtained using biaxial compression tests on adhesively bonded sheet laminate specimens. A disadvantage of the biaxial compression test is the difficulty in obtaining accurate stress–strain relations because of the friction between the specimen and the tool. In addition, when the plastic deformation behaviour of the material is influenced by the hydrostatic component of stress (Lowden and Hutchinson, 1975, Spitzig et al., 1975), the shape of the loading surfaces obtained from the biaxial compression tests may be different from that obtained from biaxial tension tests. For materials that are influenced by the hydrostatic component of stress, both uniaxial and biaxial tests in tension and compression would, ideally, be required.

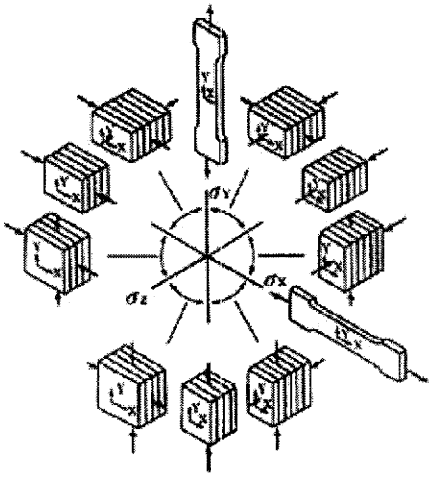

Figure 2.10 Schematic diagram of biaxial compression tests using adhesively bonded laminate sheet specimens (Kuwabara, 2007).

2.4.2 Mechanical testing of tubular materials for determination of loading surfaces

2.4.2.1 Uniaxial testing of tubular materials

For tubular materials, which are isotropic, standard methods for obtaining the uniaxial tensile stress-strain curve along the axial direction of the tube are available and have been explored. One widely used test is the tube axial tensile test, described in ASTM A 370 for steel materials, for example. In this case the tensile sample is cut along the axial direction of the tube. The axial tensile test, in which a full sized tubular specimen is gripped along its length and pulled, has also been used to determine the stress-strain curve (Davies et al., 2000). In the case of plastic materials, the ASTM D 638 standard reports a method for testing full size tubular specimens for obtaining stress-strain properties.

For anisotropic tubes, such as those produced from rolled sheet or by extrusion, the tensile properties along the hoop direction vary from those along the axial direction. Obtaining uniaixial hoop tensile properties of tubular materials is not as straightforward, or well established, particularly beyond the yield point of the material. Caddell and Woodliff (1977) investigated the macroscopic uniaxial and biaxial yield behaviour of oriented polycarbonate, polyethylene and polypropylene at room temperature. The oriented tubes of each material were produced from a solid rod that was loaded in uniaxial tension until a stable neck formed over a specified length. Thin-walled tubes were subsequently machined from the highly oriented (necked) region of the rods (refer to Figure 2.11). In this study, the hoop tensile stress-strain curve close to yield was obtained using the open-ended tube method described by Raghava (1972). For all practical purposes, the authors stated that this approach provided only a hoop stress to be induced in the wall section as internal fluid pressure was increased. However, one would expect that as the pressure is increased, and the material experiences strains beyond yield, an axial stress would develop in the wall in addition to the hoop stress. Therefore, the method may prove difficult for determining purely uniaxial tensile hoop properties of tubular materials to large strains.

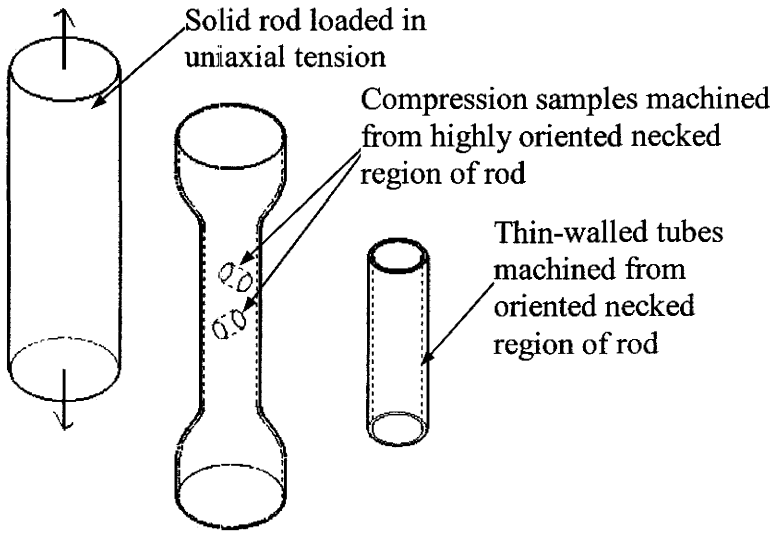

Figure 2.11 Method of production of oriented tube from solid rod loaded in uniaxial tension in the study by Caddell and Woodliff (1977). Cylindrical compression samples were machined along the axial and hoop directions of the highly oriented necked region of the rod.

A test currently used in the metal hydroforming industry for obtaining hoop tensile properties is the flattened ring strip tensile test that is described in ASTM A 370. It is recommended for large diameter tubes (> 203.2 mm in diameter). Most hydroforming tubes, however, are much smaller. For smaller diameter tubes, the additional work hardening resulting from cold flattening of the specimen is a concern.

Wang et al. (2002) devised a ring hoop tension test (RHTT) to determine the uniaxial hoop stress-strain curve of thin-walled tubular materials and outlined a simple data analysis procedure. Figure 2.12 shows a schematic diagram of the gripping device for the ring hoop tension test. An extensometer was installed on the gauge section (refer to Figure 2.13) so that hoop strain could be calculated, which was the key point in the data analysis technique. The reader is referred to the study by Wang et al. (2002) for

complete details of the data analysis procedure used to calculate hoop strains and stresses. In this study, the RHTT was used to determine the uniaxial hoop tensile stress-strain curve for a typical steel hydroforming tube to a strain of 0.45.

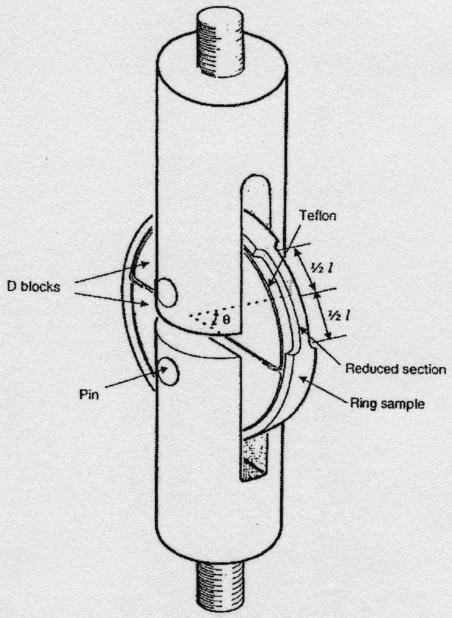

Figure 2.12 Gripping device for ring hoop tension test of tube (Wang et al., 2002).

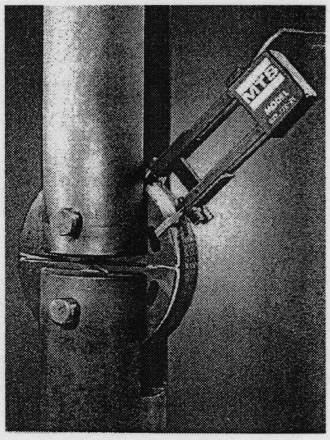

Figure 2.13 Ring hoop tension test assembly with extensometer (Wang et al., 2002).

For a material that is pressure-sensitive, in addition to being anisotropic (i.e. oriented thermoplastic tubes), the uniaxial compressive properties along its principal directions are also required. In the study outlined earlier by Caddell and Woodliff (1977), axial compression tests were performed on solid cylindrical specimens, machined from the highly oriented (necked) area of the rods along the axial direction. The specimens were machined in the vicinity of where the thin-walled tube would subsequently be machined (refer to Figure 2.11). Similarly, to obtain the hoop compressive properties, solid right circular cylinders were machined from material in the necked region transverse to the axial direction (refer to Figure 2.11). It is to be noted that for any thin-walled tube, including thermoplastic tubes, produced through a solid-state extrusion and/or die drawing process, there exists a need to obtain compressive stress-strain properties from specimens machined directly from the tube itself, along its principal directions. This can prove to be a difficult task since there is very little area within the wall thickness from which to machine specimens, especially if one is to eliminate the curvature in the samples originating from the curvature of the starting tube. Currently, no standards for the large strain compression testing of thin-walled tubes have been developed.

2.4.2.2 Biaxial testing of tubular materials

There have been many experimental studies of multiaxial testing of thin-walled metallic tubular specimens loaded in combined tension-torsion or tension–internal pressure modes. Extensive reviews of the early experimental studies have been made by

Michno and Findley (1976) and Hecker (1976). As early as 1968, Woo and Hawkes tested annealed mild steel tubes subjected to a combination of internal pressure (using oil as the pressurizing medium) and axial compressive force. The goal of the work was to deduce a stress-strain curve from the experimental data generated from the tube tests. The equilibrium equations for an element at the middle of the thin-walled bulged tube under internal pressure, p, and axial compressive force, F_a (refer to Figure 2.14), are assumed to be given by:

$$\frac{\sigma_\theta}{\rho_\theta} + \frac{\sigma_a}{\rho_a} = \frac{p}{t} \tag{2.1}$$

and

$$\sigma_a = \frac{p\rho_\theta}{2t} - \frac{F_a}{2\pi\rho_\theta t} \tag{2.2}$$

where σ_a and σ_θ are the axial and hoop stresses respectively, t is the current thickness and ρ_a and ρ_θ are the radius of curvature of the tube along the axial and hoop direction respectively. It should be noted here that if the axial radius of curvature is assumed to be very large (i.e. infinity) in the case of tubes having a very long unclamped section (compared to the diameter), or in cases when the deformation is quite small, it can be assumed that $\rho_a = \infty$ such that the hoop stress via Equation (2.1) reduces to:

$$\sigma_\theta = \frac{p\rho_\theta}{t} \tag{2.3}$$

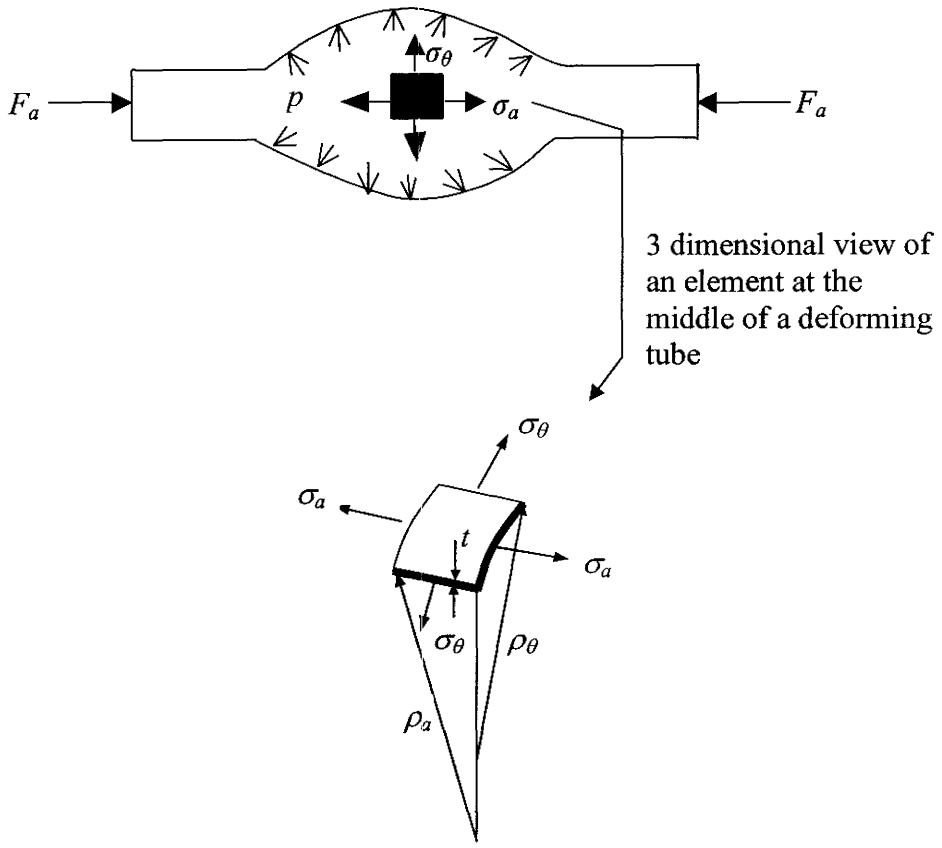

Figure 2.14 Stress state of an element in the middle of a bulging tube.

In the work by Woo and Hawkes (1968), for measuring ρ_a and ρ_θ, the circumference at the mid-length of the specimen was marked before the test. At each stage of bulging, corresponding to a certain p and F_a, the diameter was measured by means of a micrometer, hence ρ_θ could be determined. For obtaining ρ_a, a depth micrometer was used. The difference in the bulge height was measured at intervals of 1.27 mm along the length of the tube, two intervals on each side of the marked

circumference. The value of ρ_a could then be deduced. The axial and hoop stresses were calculated using Equation 2.1 and 2.2. The hoop strain was calculated using the relation:

$$\varepsilon_\theta = \ln \frac{\rho_\theta}{R_{hi}} \tag{2.4}$$

where R_{hi} was the initial radius of the tube. Assuming material isotropy, the Levy-Mises relation was used to calculate the thickness and axial strains. The method used by Woo and Hawkes (1968) for determination of the principal stress and strain components for a tube forming test were simple, but measurements of the geometry of the deforming tube were not recorded continuously throughout the test. Instead, they were measured on an intermittent basis. In addition, the thickness was not measured experimentally, but rather, determined assuming Mises plasticity relations. This would introduce errors in the case of anisotropic tubular materials.

More recently, Sokolowski et al. (2000) evaluated tube formability and material characteristics of 304 stainless steel tube using hydraulic bulge testing. In this case, the tubes were subjected to internal pressure only. Several experiments were run at pressure levels between the bursting pressure and the pressure required to initiate deformation of the material. At each pressure level, the bulge profile, bulge height and thickness distributions were measured over several circumferential locations as indicated in Figure 2.15. Thickness measurements were recorded by sectioning the tube and taking measurements with a digital micrometer. This allowed the strain and stress components to be determined at each pressure level. Although this work was an improvement on that of Woo and Hawkes (1968), in that the instantaneous thickness measurements were

made, continuous (or real time) measurements of the geometry of the bulging tube were not available. Some springback of the tube when it was removed from the testing machine for thickness measurements may also have occurred.

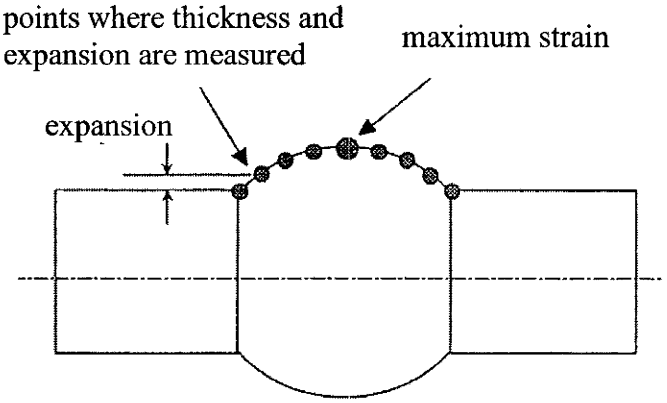

Figure 2.15 Locations of measurement of bulge height, bulge profile and tube thickness in study by Sokolowski et. al. (2000).

Stout et al. (1983) tested 2024 aluminum tubes, heat treated to T6 and T8 tempers, in combinations of tension-internal pressure and tension-torsion loading. The tubes were tested with an MTS servo-controlled axial-torsion-internal pressure testing machine. Several special features of the machine warrant description: 1) The use of a precision axial-torsion load cell permitted combined axial-torsion loading with negligible cross-talk. 2) A rotary motion was applied by a continuous rotary motor, instead of an angle-limited actuator, to permit large torsional strains. 3) The machine was equipped with multiple ported servo-valves and low-noise electronics to obtain smooth low-rate actuator performance. Tubes were tested in tension-torsion or tension-internal pressure at five different ratios of axial tension/torsion or axial tension/hoop tension (0, 0.5, 1, 2 and ∞).

Constant stress ratios were attempted by conducting tests at constant load/torque or load/pressure ratios. Several techniques were used to measure strains continuously throughout the test. At small strains (less than 2%), three-element strain gauge rosettes were employed. Axial and diametral strain gauge extensometers recorded axial and hoop strains from yield to failure. A specially designed rotary extensometer attached to the lower grips provided accurate shear strains. As a final measure, a photoprinted grid of circles was used to measure strains at failure. However, for the tension-internal pressure testing, the method used to calculate the radius of curvature along the axial direction was not outlined in the study. A fully instrumented specimen, mounted in the test fixture, without any rotary extensometer, is shown in Figure 2.16.

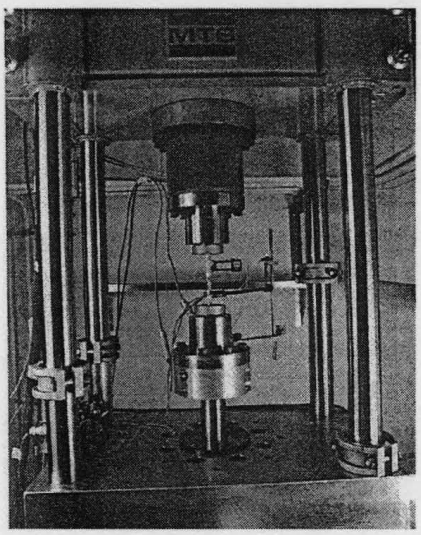

Figure 2.16 Test fixture used to test 2024 aluminum tubes in tension-torsion loading by Stout et al. (1983).

Kuwabara et al. (2003) investigated the anisotropic plastic deformation behavior of extruded 5000 series aluminum alloy tubes, A5154-H112, using a servo-controlled tension-internal pressure testing machine originally designed by Kuwabara et al. (2003) (refer to Figure 2.17). This machine is capable of applying arbitrary stress or strain paths to a tubular specimen using an electrical, closed-loop control system. Axial loads were applied to the specimen by opposing hydraulic cylinders and internal pressure by an intensifier. The deformation behavior of the specimens was measured using a spherometer and two strain gages (used to measure large plastic strains), as shown in Figure 2.18. The spherometer consists of a displacement meter and two wedges. It has the freedom to rotate around an axis vertical to the central axis of the specimen, so that the pointed ends of the displacement meter and the two wedges are always in contact with the bulged surface of the specimen. For real time measurement of ρ_{as} (the axial radius of curvature of the tube), a pantograph-type link mechanism was used (refer to Figure 2.17). This mechanism was originally proposed by Shiratori and Ikegami (1968) and was used so that the center of the specimen was always positioned at the center of the testing apparatus, where the spherometer was located. This testing apparatus appears to be the most well developed to date as real time measurements of strains and curvature during the deformation of the tube are achievable.

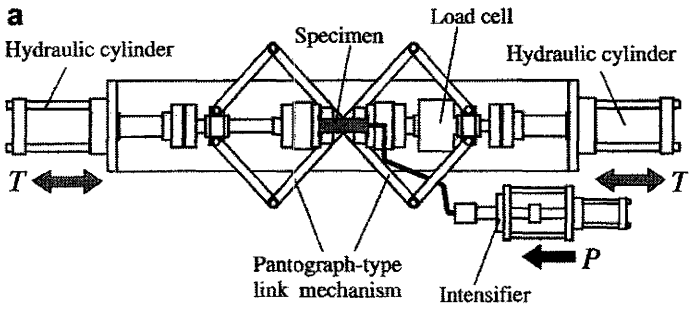

Figure 2.17 Experimental tube forming apparatus designed by Kuwabara et al. (2003).

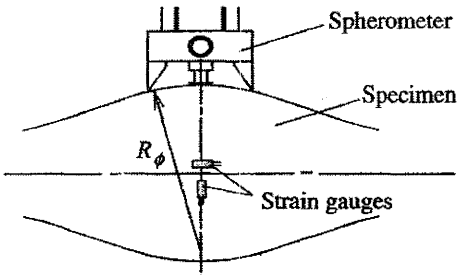

Figure 2.18 Set up of strain gauges and spherometer for apparatus of Figure 2.17 (Kuwabara et al., 2003).

In the above study by Kuwabara et al. (2003), the stress and strain components of the specimens were evaluated at the mid wall. Using thick-walled theory, Jones and Mellor (1967) suggested that the concept of a thin-walled cylinder is an approximation, the accuracy of which varies with stress ratio. They also showed that taking the stress and strain measurements with reference to the mid-thickness of the tube wall gives a better approximation. As such, Kuwabara et. al. (2003) calculated the axial and hoop strains at the mid-wall, ε_{am} and $\varepsilon_{\theta m}$ respectively, using the following relations:

$$\varepsilon_{am} = \varepsilon_{as} - \ln \frac{\rho_{as}}{\rho_{as} - (t_m / 2)} \tag{2.5}$$

$$\varepsilon_{\theta m} = \ln \frac{D_0 \exp(\varepsilon_{\theta s}) - t_m}{D_0 - t_0} \tag{2.6}$$

where ε_{as} and $\varepsilon_{\theta s}$ are the axial and hoop strains, respectively, measured directly from the strain gauges placed at the surface of the tube, D_0 and t_0 are the initial outer diameter, ρ_{as} is the axial radius of curvature measured using the spherometer on the surface of the tube and t_m is half of the current wall thickness of the specimen. The thickness strain was calculated using axial and hoop strains measured at the surface of the tube assuming volume constancy. Subsequently, t_m was determined from the calculated thickness strain. The axial and circumferential stresses, σ_{am} and $\sigma_{\theta m}$ respectively, were calculated as the values at the mid wall, using the following equations based on the equilibrium requirements:

$$\sigma_{am} = \frac{p\pi\left(\left(\left(D_0 \exp(\varepsilon_{\theta s})\right)/2\right) - t_m\right)^2 + F_a}{\pi\left(D_0 \exp(\varepsilon_{\theta s}) - t_m\right) t_m} \tag{2.7}$$

$$\sigma_{\theta m} = \frac{(\rho_{as} - t_m)(D_o \exp(\varepsilon_{\theta s}) - 2t_m)}{(2\rho_{as} - t_m) t_m} p - \frac{(D_0 \exp(\varepsilon_{\theta s}) - t_m)}{2\rho_{as} - t_m} \sigma_{am} \tag{2.8}$$

Compared with the developments in the testing of metallic tubes under a biaxial stress state, much less work in the area of polymer tube forming has been conducted. As mentioned in Section 2.4.2.1, Caddell and Woodliff (1977) investigated the macroscopic uniaxial and biaxial yield behaviour of oriented polycarbonate, polyethylene and polypropylene at room temperature with a proposed anisotropic and pressure-dependent

yield criterion. In order to obtain yield points along biaxial stress paths, thin walled tube tests were also conducted in which a tube was subjected to a combination of internal pressure and axial loading in a manner that produced a reasonably constant stress ratio of σ_a to σ_θ during the test. Standard extensometers were used to measure axial length and diametral changes. However, it was not indicated whether the experimental apparatus and data analysis techniques could be used represent the loading surfaces subsequent to the initial yield surface. Similar was the case with studies by Tuttle et al. (1992) and Bekhet et al. (1994) who examined the initial biaxial yield surface for polyethylene and polypropylene tubes respectively.

From the review of the literature just described, it is important to make note of the fact that most of the tube testing conducted in the past has been at room temperature. Tube forming tests at elevated temperatures are more complicated to perform and analyze. This is because the tests at higher temperatures involve several complicating factors such as temperature uniformity over the entire specimen, stability of the pressurizing medium, strain measurement using contact based methods such as extensometers etc.

2.5 Definition of yield for determination of initial yield surface and subsequent loading surfaces

The methods used to construct an initial yield surface for a sheet or tube material based on the data generated from the tests described above will be reviewed first. It is assumed here that the stress-strain curve for a uniaxial test and the stress-strain curves along the

two principal directions in a biaxial test have been determined. The definition of yield along a uniaxial strain path will be considered first. This is not always straightforward, though, since most materials do not exhibit a clearly defined yield point. An exception to this statement is the case of mild steel, which exhibits a well defined yield point. For a work hardening material, however, yield point is not as clear. Figure 2.19 shows some of the possible definitions that have been used and/or are currently being used in such circumstances. These are: (A) the proportional limit; (B) a small measurable permanent set, for example 10 microstrain; (C) the conventional engineering offset of 0.2% strain; (D) point of tangency of stress-strain curve with a multiple of elastic slope; (E) an extrapolation method in which the elastic strain is neglected (F) an extrapolation method in which the elastic deformation is included. The effect of the definition of yield on the yield surface has been considered by Hsu (1966), Hill (1967) and Haythornwaite (1968).

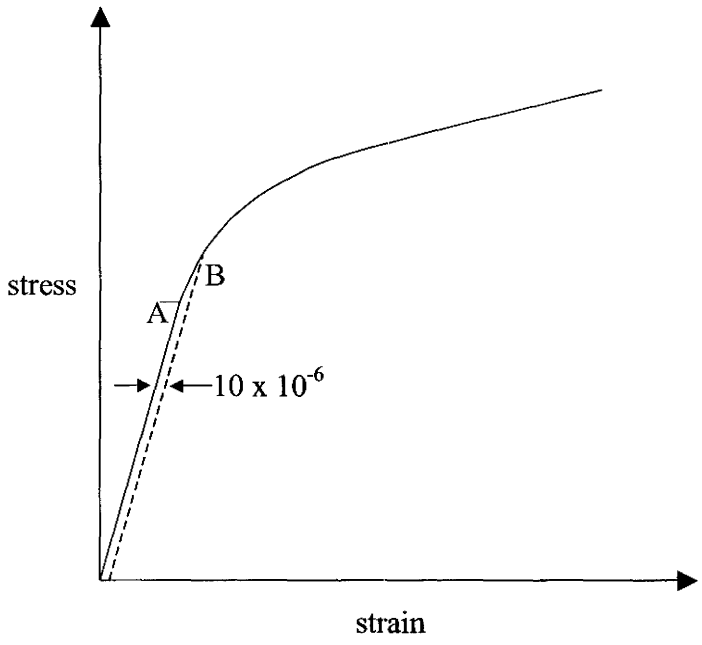

A – deviation from linearity
B – small measurable offset

Figure 2.19 Various definitions of yield along a uniaxial strain path A - deviation from linearity, B - use of a small measurable offset (Michno and Findley, 1976).

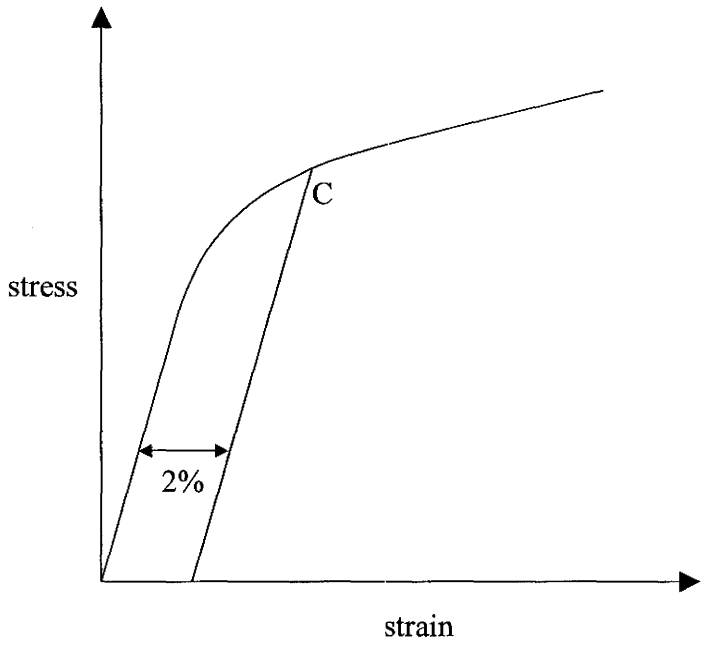

C – 2% offset

Figure 2.19 *cont.* Various definitions of yield along a uniaxial strain path C - 2% offset (Michno and Findley, 1976).

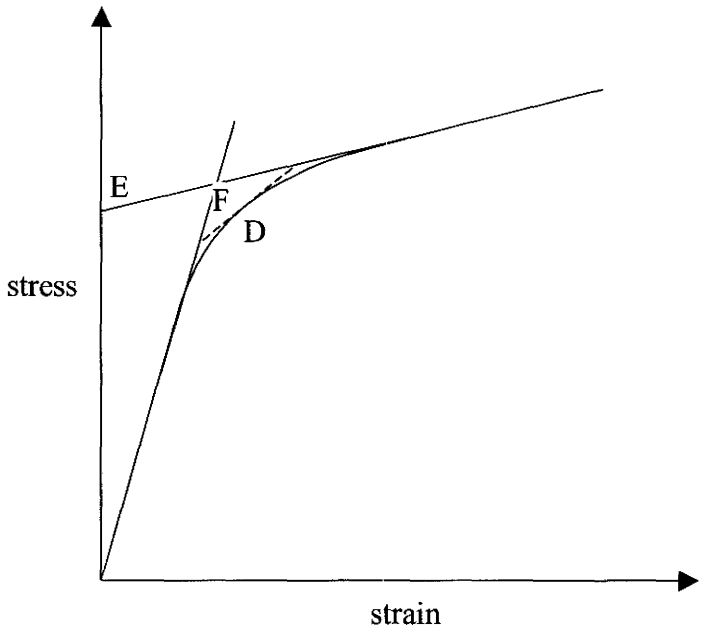

D – slope equal to constant x elastic slope
E – extrapolation of post yield slope to ordinate
F – intersection of elastic slope and definition E

Figure 2.19 *cont.* Various definitions of yield along a uniaxial strain path D - slope equal to constant x elastic slope, E – extrapolation of post yield slope to ordinate, F – intersection of elastic slope and definition E (Michno and Findley, 1976).

The yield point becomes somewhat more difficult to define from the stress and strain components generated along the two principal directions in a biaxial stress test. One method for determination of the yield point from a biaxial stress test is via the concept of an "effective" or "equivalent" stress/strain curve. A single effective stress-strain curve allows use of one of the definitions of yield outlined above. Bekhet et al. (1994) in their study of the biaxial yielding behaviour of oriented polypropylene determined an effective stress-strain curve based on the Mises yield criterion and then subsequently used a 0.5% offset rule for the determination of the yield point. This method introduces some ambiguity in the determination of the yield point as it requires the use of an existing theoretical yield criterion. In addition, the validity of this approach for the determination of the subsequent loading surfaces is somewhat questionable, since each subsequent surface depends on the use of the assumed effective stress-strain relationship. This approach does, however, appear more reasonable for isotropic, Mises type materials, compared with anisotropic materials.

A second method, for defining the yield point from a biaxial stress test, was used in the study by Caddell and Woodliff (1977) on the macroscopic yielding of polymer tubes. The individual values of σ_a and σ_θ from a given biaxial stress test were plotted against an effective strain function associated with the Mises yield criterion. A typical plot is shown in Figure 2.20, where the values of σ_a and σ_θ connected with yielding were found using a 0.3% offset rule. The authors stated that this approach was supported by the fact the ratio of σ_a and σ_θ which defined yielding via a plot such as Figure 2.20

agreed closely with the applied stress ratio for a given test. Although an effective stress definition was not used, an effective strain definition was still employed.

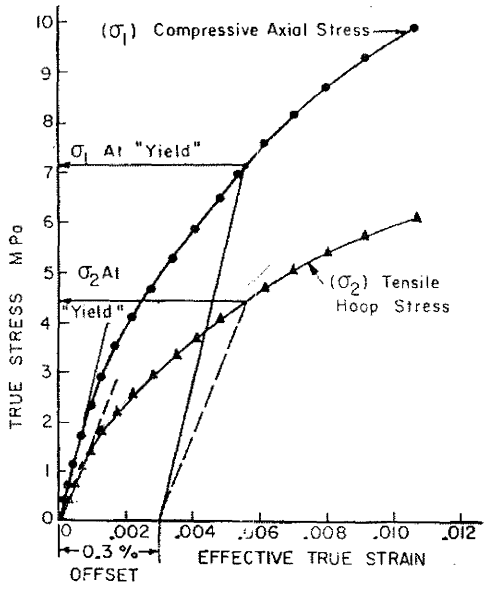

Figure 2.20 Definition of yield point from biaxial tube test used in study by Caddell and Woodliff (1977).

A third method used to construct the initial and subsequent yield surfaces for a sheet or tubular material involves the notion of the contour of plastic work in stress space (Hill and Hutchinson, 1992, Hill et al., 1994, Barlat et al., 1997). The following is the method for constructing contours of plastic work considering a tubular material. A uniaxial tension test in the axial direction of the tube is first carried out, and the uniaxial true stress, σ_a, and plastic work, W, dissipated per unit volume are determined for particular values of the axial logarithmic plastic strain, ε_a^p. The uniaxial tension test in the hoop direction of the material and biaxial tension tests with the stress ratio, σ_a:σ_θ, held at specific proportions are then carried out. Finally, groups of stress points for

which the same amount of plastic work as W is needed, are plotted in principal stress space so as to construct contours of plastic work corresponding to particular values of ε_0^p. It is effectively an initial yield surface for the material only when ε_a^p is taken to be sufficiently small (Kuwabara, 2007). This method also appears to have more of physical basis than previously discussed methods. For illustration purposes, Figure 2.21 shows the plastic work contours for extruded aluminum alloy tube for values of the axial logarithmic strain ranging from 0.2% (effectively an initial yield surface for the material) to 25% (Kuwabara et al., 2005).

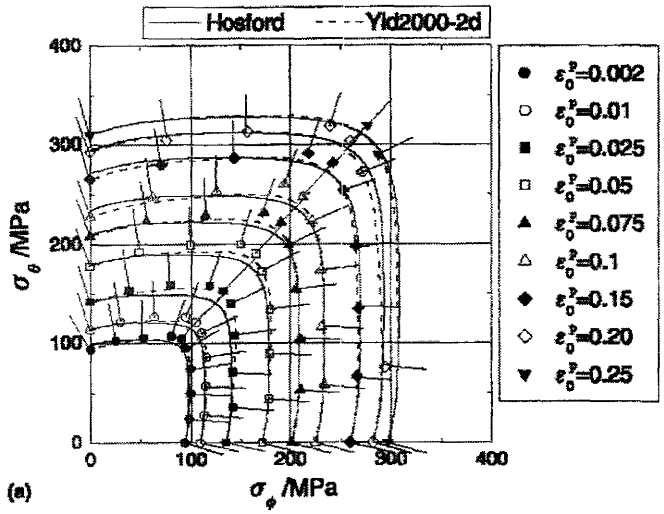

Figure 2.21 Contours of plastic work for extruded aluminum alloy tube (Kuwabara et al., 2005).

2.6 Review of theoretical yield criteria

2.6.1 Theoretical yield criteria applied to metals

One of the simplest theoretical yield criterion for representing the biaxial yield surface for isotropic, pressure insensitive materials is the von Mises criterion, which is given in principal plane stress space by:

$$\sigma_x^2 + \sigma_y^2 + (\sigma_x - \sigma_y)^2 = 2Y^2 \tag{2.9}$$

where σ_x and σ_y are the principal stresses and Y is the yield stress of the material. The yield criterion given by Equation (2.9) is simple to use since only one constant requires definition. However, most of the materials used in forming applications possess some degree of anisotropy. This is true for rolled sheets used in stamping operations and extruded tubes used in hydroforming applications. In this case, one must look to other criteria to accurately predict their behaviour.

Hill (1948) formulated a quantitative treatment of plastic anisotropy without regard to its crystallographic origin. He assumed a homogeneous material characterized by three orthogonal axes of anisotropy, *x*, *y* and *z*. In a rolled sheet, it is conventional to take *x*, *y* and *z* to be the rolling, transverse, and through-thickness directions, respectively. It is important to note here that along any given direction, the tensile and compressive yield strengths are equal, i.e. the material is not pressure sensitive. His proposed anisotropic yield criterion, in principal plane stress space, and assuming material symmetry along the *y*-*z* plane, has the form:

$$H_0\sigma_x^2 + F_0\sigma_y^2 + H_0(\sigma_x - \sigma_y)^2 = 1 \tag{2.10}$$

where F_0 and H_0 are constants which characterize the anisotropy. The constants F_0 and H_0 can be evaluated from simple tension tests, and if $F_0 = H_0$, the criterion given by Equation (2.10) reduces to the Mises criterion given by Equation (2.9). The constants in Equation (2.10), in terms of the tensile yield stress along the x direction, T_x, and the tensile yield stress along the y direction, T_y, are given as:

$$F_0 = \frac{1}{2}\left(\frac{2}{T_y^2} - \frac{1}{T_x^2}\right) \tag{2.11}$$

$$H_0 = \frac{1}{2}\left(\frac{1}{T_x^2}\right) \tag{2.12}$$

Hill's criterion applied to crytallographically textured fcc and bcc metals showed that it overestimates the effect of the anisotropy on the shape of the plastic work contours (Kuwabara, 2007). The trends of the calculations are much better represented by a yield criterion given by Hosford (1979) and Logan and Hosford (1980). This criterion, in principal plane stress space, and assuming material symmetry along the y-z plane, has the form:

$$H_0|\sigma_x|^a + F_0|\sigma_y|^a + H_0|\sigma_x - \sigma_y|^a = 1 \tag{2.13}$$

Note that the Hill yield criterion given by Equation (2.10) is obtained from the Hosford criterion for the case of $a=2$. Also, $a = 6$ is recommended for bcc metals and $a = 8$ is recommended for fcc metals (Hosford and Caddell, 1993). It was found that the plastic work contours calculated using Hosford's yield criterion with $a = 6$ agreed more closely with the experimental contours than those calculated using Hill's quadratic yield criterion

for IF steel and hot rolled Al-killed steel sheet (Ikeda and Kuwabara, 2004). Hill's quadratic yield criterion tended to overestimate the flow stresses in the vicinity of equibiaxial tension for the IF steel (Ikeda and Kuwabara, 2004).

Other anisotropic yield criteria have been developed to date, but their relative merits and downfalls will not be discussed here. What should be highlighted, however, is the fact that the metals commonly used for forming applications are not affected by the hydrostatic component of stress. In other words, these materials are pressure insensitive, and as such, their yield strengths in tension and compression can be assumed to be equal.

2.6.2 Theoretical yield criteria for isotropic polymers

Polymeric materials, unlike most metallic materials, are pressure sensitive with respect to their yielding behaviour. Several yield criteria have been proposed to account for the pressure sensitivity of isotropic polymers. A complete review of these criteria will not be given here, however, the interested reader is referred to the reviews by Paul (1968) and Ward (1971). One suggested criterion of interest is called the pressure-modified Mises criterion. In principal plane stress space, this criterion is expressed as:

$$\sigma_x^2 + \sigma_y^2 + (\sigma_x - \sigma_y)^2 + 2Y_c(Y_c - Y_t)(\sigma_x + \sigma_y) = 2Y_cY_t \qquad (2.14)$$

where Y_t and Y_c are the yield strengths in uniaxial tension and compression, respectively, and assumed to be independent of material direction. The first three terms of the above equation are the same as those for the Mises criterion (refer to Equation (2.9)), while the term, $(\sigma_x + \sigma_y)$, includes the effect of hydrostatic stress. When $Y_t = Y_c$, Equation (2.14)

reduces to the Mises criterion. According to Raghava et al. (1973), this criterion was originally proposed by Schleicher in 1926, and was suggested independently by Stassi-D'Alia (1967). Raghava et. al. (1973) were the first to apply the criterion to polymers. It has since been successfully used to predict the room temperature pressure-sensitive yield response of several polymers including polyvinylchloride (Raghava et al., 1973), polycarbonate (Raghava et al., 1973, Freire and Riley, 1980) and polyethylene (Raghava and Caddell, 1974).

For illustration purposes, Figure 2.22 compares the isotropic Mises criterion with the pressure-modified Mises criterion, for a thermoplastic tube with assumed values for the tensile and compressive yield strengths. As indicated by Figure 2.22, neglecting the pressure sensitivity of this material could markedly affect the biaxial yield surface in all four quadrants in stress space. The effect, of course, depends on the extent of the asymmetry in the tensile and compressive yield strengths of the material.

2.6.3 Theoretical yield criteria for anisotropic pressure dependent polymers

Several yield criteria have been proposed for use with pressure sensitive anisotropic polymers. The few key criteria, which have been compared to experimental biaxial yielding data from the testing of oriented polymer tubes, will be reviewed here.

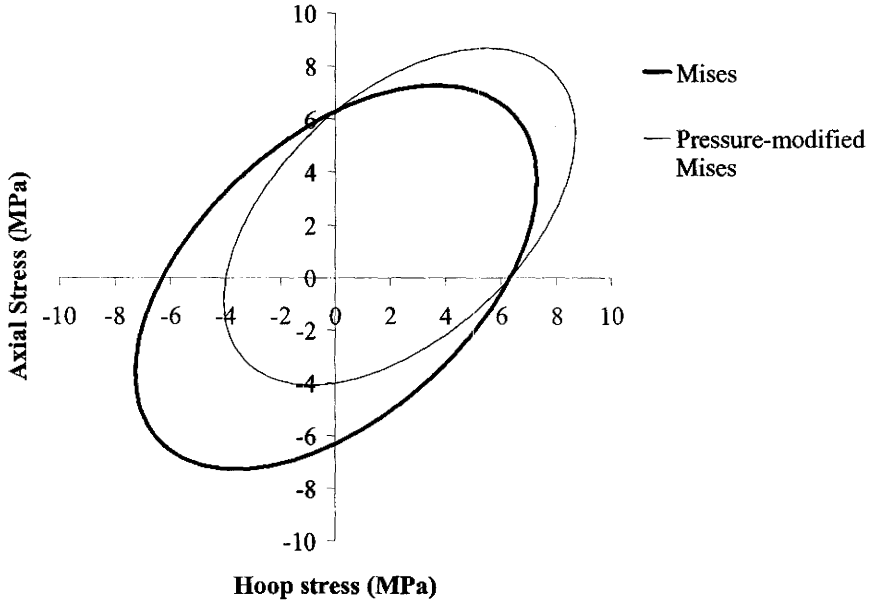

Figure 2.22 Comparison of Mises and pressure-modified Mises criteria for a thermoplastic material assuming values for material constants.

The first criterion of interest is that due to Gol'denblat and Koponov (1965), which in principal plane stress space is given mathematically by:

$$\frac{C_x - T_x}{2C_xT_x}\sigma_x + \frac{C_y - T_y}{2T_yC_y}\sigma_y + \left[\left(\frac{C_x + T_x}{2T_xC_x}\right)^2 \sigma_x^2 + \left(\frac{C_y + T_y}{2C_yT_y}\right)^2 \sigma_y^2 + 2F_{12}\sigma_x\sigma_y\right]^{0.5} = 1 \quad (2.15)$$

where T_x and T_y are the tensile yield strengths and C_x and C_y are the compressive yield strengths along the principal directions respectively. In addition

$$F_{12} = \frac{0.5}{(T_xC_xT_yC_y)^{0.5}} \quad (2.16)$$

The second criterion is one by Tsai and Wu (1970). It is given mathematically, in principal plane stress space as:

$$\frac{C_x - T_x}{C_x T_x}\sigma_x + \frac{C_y - T_y}{T_y C_y}\sigma_y + \frac{\sigma_x^2}{T_x C_x} + \frac{\sigma_y^2}{T_y C_y} + 2F_{12}\sigma_x\sigma_y = 1 \tag{2.17}$$

where F_{12} is as for the Gol'denblat-Koponov theory above. The similarity of the first two terms of the Tsai-Wu criterion with that of the Gol'denblat and Koponov criterion should be noted.

The third criterion of interest is called the pressure-modified Hill criterion, and was suggested independently by Stassi-D'Alia (1967) and Caddell et al. (1973). The pressure-modified Hill criterion for a transversely isotropic material (with material symmetry in the y-z plane) subjected to plane stress is given by:

$$2H\sigma_x^2 + (H+F)\sigma_y^2 - 2H\sigma_x\sigma_y + K_x\sigma_x + K_y\sigma_y = 1 \tag{2.18}$$

where

$$H = \frac{1}{2|T_x||C_x|} \tag{2.19}$$

$$H + F = \frac{1}{T_y|C_y|} \tag{2.20}$$

$$K_x = \frac{|C_x| - T_x}{|C_x|T_x} \tag{2.21}$$

$$K_y = \frac{|C_y| - T_y}{|C_y|T_y} \tag{2.22}$$

The first three terms of the pressure-modified Hill criterion are equivalent to the Hill yield criterion given by Equation (2.10). It is the K_x and K_y terms within the pressure-modified Hill criterion that account for the difference in tensile and compressive yielding. Also worth noting is the equivalence of all of the terms within the pressure-modified Hill criterion and the Tsai-Wu criterion, except for the coefficient of the $\sigma_x\sigma_y$ term which is the point of difference between the two criteria.

The pressure-modified Hill criterion has been successfully used to predict the room temperature yield response of a few oriented polymers, including polyvinylchloride (Caddell and Woodliff, 1977), polycarbonate (Raghava and Caddell, 1974, Caddell and Woodliff, 1977) and polypropylene (Shinozaki and Groves, 1973, Caddell and Woodliff, 1977). It should be mentioned here that the studies listed above were centered on the room temperature yielding of oriented polymeric tubes. No work examining the effect of elevated temperature on the uniaxial and biaxial yielding of oriented thermoplastic tubes, for use in subsequent formability studies, has been conducted to date. In addition, no studies related to the biaxial hardening behaviour of oriented thermoplastic tubes (at room or elevated temperature) has been conducted.

Bekhet et al. (1994), in their study of the biaxial yielding behaviour of oriented polypropylene tube, compared various yield theories in biaxial stress space for anisotropic pressure-dependent materials. Values were assumed for the material constants within the yield criteria being compared, i.e. it was assumed that $T_x = 2\,T_y = 0.4\,C_x = 0.8\,C_y$. This resulted in the F_{12} being equal to $1.0/C_xT_x$ in the Tsai-Wu criterion.

The choice of material constants caused the Tsai-Wu and Gol'denblat-Koponov theories to reduce to the same expression. Figure 2.23 compares the Tsai-Wu and pressure-modified Hill criterion. The marked difference in the two criteria appears in the third quadrant, and arises from the fact that the coefficient of the $\sigma_x\sigma_y$ term of the Tsai-Wu criterion is twice that of the pressure-modifed Hill criterion.

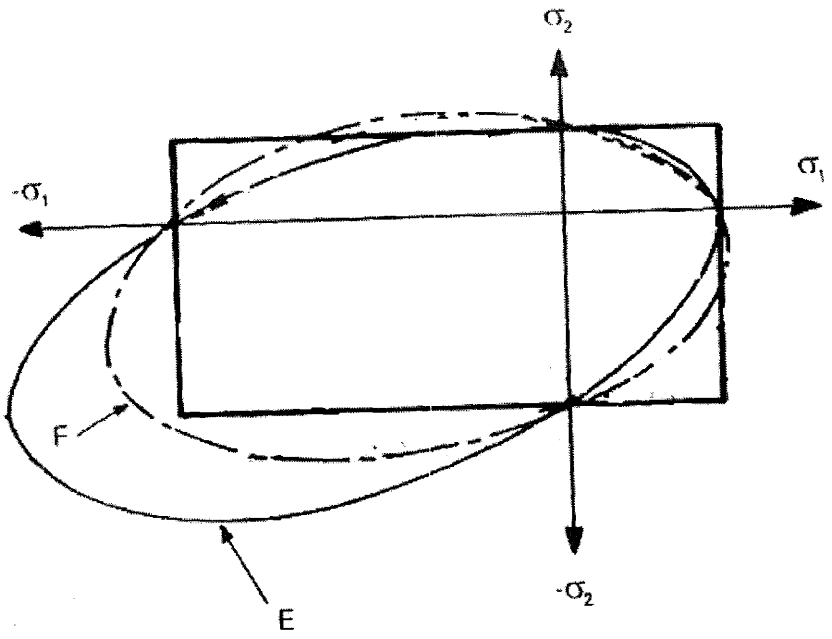

Figure 2.23 Comparison of Tsai-Wu criterion (E) and pressure-modified Hill criterion (F) for an anisotropic, pressure-dependent material (Bekhet et al., 1994).

2.6.3.1 Flow rule for pressure-modified Hill yield criterion

Flow rules, relating stress and strain have been developed for plastic deformation. In general, the flow rules can be stated as:

$$d\varepsilon_{ij} = d\lambda \frac{df}{d\sigma_{ij}} \tag{2.23}$$

where f is a function of σ_{ij} that describes yielding (i.e. the yield criterion). Using Equation (2.32), and the pressure-modified Hill yield criterion, the strain increments are given by the following expressions (see Appendix A for complete derivation):

$$d\varepsilon_x = 2d\lambda\left[H(2\sigma_x - \sigma_y) + \frac{1}{2}K_x\right] \tag{2.24}$$

$$d\varepsilon_y = 2d\lambda\left[F\sigma_y + H(\sigma_y - \sigma_x) + \frac{1}{2}K_y\right] \tag{2.25}$$

$$d\varepsilon_z = 2d\lambda\left[-H\sigma_x - F\sigma_y + \frac{1}{2}K_y\right] \tag{2.26}$$

Both the pressure-modified Hill yield criterion and the strain components given by Equations (2.24) to (2.26) will subsequently be used in the development of the analytical model used to predict the forming limits for the OPP tube in Chapter 4.

2.7 Temperature and strain rate dependent constitutive models for polymers

In general, in order to model the tube forming of materials, in addition to a yield criterion, an appropriate constitutive model for predicting the hardening is required. For oriented thermoplastics, an appropriate flow stress model should be capable of predicting the behaviour of the material from initial yield up to relatively large strains at a range of

temperatures and strain rates. It is of particular importance that the constitutive model captures the temperature dependency of the oriented material. This is because the orientation, originally induced during extrusion, may relax to some extent upon heating and prior to forming. The nature of this relaxation will affect the subsequent formability of the material.

Many constitutive models have been developed for thermoplastics over the years. Some of these models account for the room temperature behaviour of the material while others also account for temperature and/or strain rate effects. However, little work has been done in the assessment of the applicability of existing constitutive models, or the modification of such models, for characterizing the axial tensile behaviour of oriented thermoplastic materials. Tate et al. (1988) showed that the constitutive laws typically used for metals could predict the experimental flow stress data for polypropylene sheet, along the oriented direction. More specifically, it was indicated that the flow stress model originally put forth by Inouye (1954) was able to predict the strain, strain rate and temperature dependence of the flow stress. The Inouye model is given mathematically by:

$$\sigma = K_1 \varepsilon^n \dot{\varepsilon}^{m_1} \exp\left(\frac{A_1}{Tk}\right) \tag{2.27}$$

where ε is the strain, $\dot{\varepsilon}$ is the strain rate, T is the temperature and K_1, n, m_1, A_1 and k are material constants. However, in the study by Tate et al. (1988), a comparison of the experimental flow stress curves with the prediction via the Inouye model at selected temperatures and strain rates was not presented for the oriented polypropylene sheet.

Therefore, whether or not the constitutive model given by Equation (2.27) could capture the large strain behaviour of the material at various temperatures and strain rates was not clear.

A three-parameter, non-linear constitutive model was put forth by Zhou and Mallick (2002) for predicting the temperature and strain rate dependent behaviour of unfilled and talc-filled polypropylene. The model, although able to capture material hardening or softening, was derived in terms of engineering stress and strain as opposed to true stress-strain, which is the form required for large strain forming analyses. Hyperelastic models, which are typically used to capture the non-linear elastic behaviour of rubber materials have also been used to model semi-crystalline polymers at elevated temperature and strain rates. However, hyperelastic models, which are essentially curve fitting equations, often require the use of a large number of material constants for its definition at a single temperature and rate condition. Therefore the modification of such models for predicting effect of temperature and strain rate, in addition to strain, on oriented thermoplastics appears less attractive. A model by Ball et al. (1981), which is also hyperelastic in nature and accounts for the effects of temperature, was applied to the high temperature stretching of polypropylene to large strains by Sweeney et. al. (1997). Five constants were required to fully define the model, and two of the constants involved specification of the number of per unit volume of cross-links and sliplinks in the system. These parameters become harder to determine since they are microscopic in nature and may not be directly applicable to oriented crystalline polymers whose fundamental unit is the microfibril. In addition, the model does not account for the effect of strain rate.

G'Sell et al. (1983) demonstrated that the true stress-strain behaviour of high density polyethylene as a function of strain rate could be modeled with the following expression:

$$\sigma(\varepsilon,\dot{\varepsilon}) = K[1-\exp(-B_1\varepsilon)]\exp(h_1\varepsilon^2)\dot{\varepsilon}^m \tag{2.28}$$

where σ is the stress, ε and $\dot{\varepsilon}$ are the strain and strain rate and K, B_1, h_1 and m are material constants. It should also be noted here that Equation (2.28) is formulated in such a way that at a given temperature, the effects of strain and strain rate are expressed in a multiplicative manner, i.e. $\sigma(\varepsilon,\dot{\varepsilon}) = f(\varepsilon)\times g(\dot{\varepsilon})$. The term $[1-\exp(-B_1\varepsilon)]$ accounts for the short period of flow at the beginning of straining. It is derived based on the response of a standard Maxwell element, made up of a spring with elastic constant, E, and a dashpot, which is assumed to have non-Newtonian behaviour with a response compliant to a power law. The term $\exp(h_1\varepsilon^2)$ in Equation (2.28) accounts for the dramatic hardening that takes place at large strains in the material. The interesting feature of the model is that at small strains, the term given by $\exp(h_1\varepsilon^2)$ approaches 1 and the strain behaviour is governed by the term $K[1-\exp(-B_1\varepsilon)]$. The form of this term is also similar to that of the Voce constitutive equation (Voce, 1948) in that the stress saturates at high strains. On the other hand, at large strains, the term $[1-\exp(-B_1\varepsilon)]$ approaches 1 and strain behaviour is controlled by the $K\exp(h_1\varepsilon^2)$ term.

The primary advantages of the model put forth by G'Sell et al. (1983) is that it is formulated in terms of true stress and strain, which makes it amenable to large strain forming analyses. In addition, the constants within the model can easily be determined

via tensile tests of the material at various strain rate conditions. The model is also able to capture the dramatic hardening, which takes place in thermoplastics at large strains. Based on experiments in this study, oriented polypropylene (OPP) also exhibits this dramatic hardening at large strain and at elevated temperatures (refer to Figure 2.24). The main limitation of the model is that it does not account for the effect of temperature, which is essential for modeling the high temperature forming of these materials.

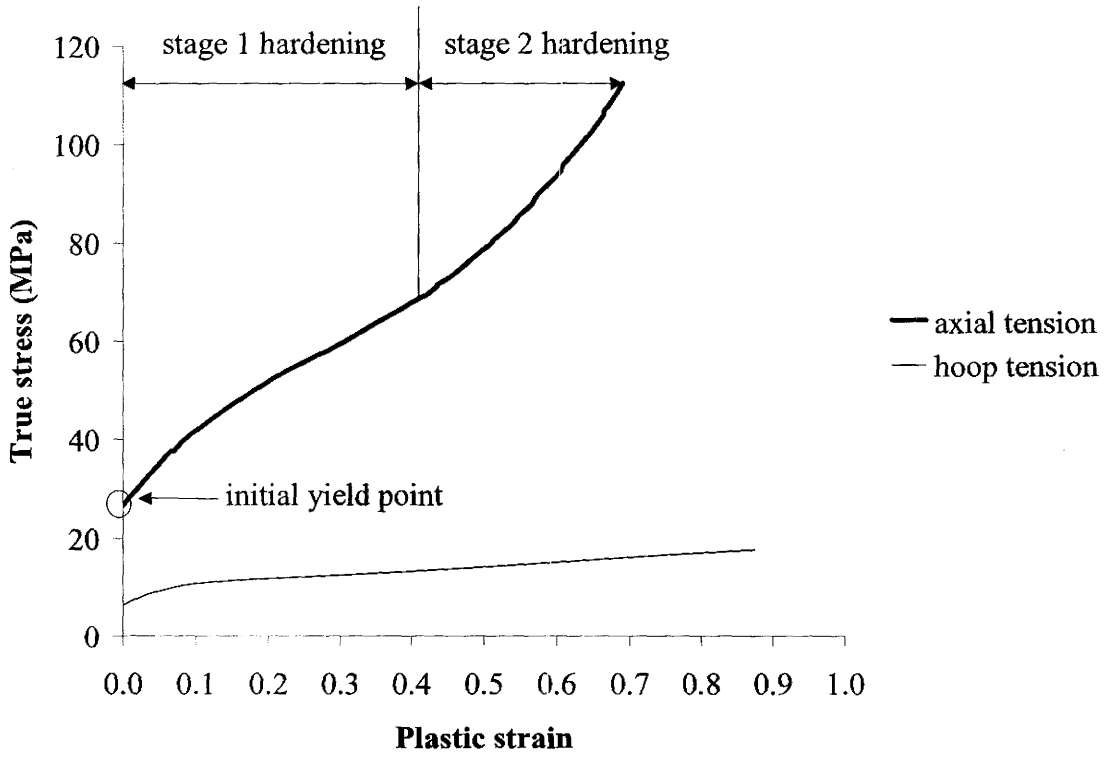

Figure 2.24 Plastic stress strain curves obtained from testing of OPP tube, of draw ratio 5.0, along the axial and hoop direction at a temperature of 130°C and at a strain rate of 0.044/second.

2.8 Criteria for localized necking of tube during forming

In general terms, the condition of instability relates to the attainment of a maximum force, pressure etc. at which the material would continue to deform in a relatively uncontrolled manner. However, this does not imply that additional and useful uniform deformation always ceases at instability, as is true in a uniaxial tensile test (Hosford and Caddell, 1993). For the case of a thin-walled tube subjected to internal pressure and axial feeding, two characteristic points during the deformation are the point at which the maximum pressure is reached and the point at which the maximum wall force is reached. It is important to note that the maximum wall force does not occur at maximum pressure. It occurs at a strain larger than that at which the maximum pressure is reached. For this reason, the maximum wall force condition is more commonly taken as a localized necking criterion for tubular materials.

Consider a tube that is subjected to an internal pressure, p, and an axial compressive force, F_a, as in a typical forming test. For an element at the middle of the bulged tube, the equilibrium equations were given earlier in Section 2.4.2.2. Assuming that the hoop stress is larger than the axial stress, necking can be correlated with the maximum tensile force per unit length of the tube along the hoop direction. If F_θ is the hoop force per unit length of the tube, then

$$F_\theta = t\sigma_\theta \tag{2.29}$$

Localized necking results when the hoop force per unit length reaches a maximum, i.e. when

$$d(F_\theta) = 0 \tag{2.30}$$

or from Equation (2.29), when

$$d(t\sigma_\theta) = 0 \tag{2.31}$$

Substituting Equation (2.31) into (2.3) results in localized necking occurring when

$$d(p\rho_\theta) = 0 \tag{2.32}$$

Combining Equations (2.32) and (2.3) gives the localized necking condition as

$$d(p\rho_\theta) = \sigma_\theta dt + t d\sigma_\theta = 0 \tag{2.33}$$

or

$$\frac{d\sigma_\theta}{\sigma_\theta} = \frac{-dt}{t} \tag{2.34}$$

Also

$$\frac{dt}{t} = d\varepsilon_t \tag{2.35}$$

Therefore, after substitution of Equation (2.35) into (2.34), the theoretical condition for localized necking thus becomes,

$$\frac{d\sigma_\theta}{\sigma_\theta} = -d\varepsilon_t \tag{2.36}$$

Researchers studying the metal tube hydroforming process have identified localized necking of a thin-walled tube to occur when the maximum force in the hoop direction is reached (Koc and Altan, 2001, Kim and Kim, 2002, Brunet et al., 2004). Validation of this criterion or selection of an alternate criterion to predict the localized necking of thermoplastic tubes subjected to biaxial stresses has not been examined to

date. However, a simple argument to support this criterion for its application to oriented thermoplastic tubes can be made here. Figure 2.7 shows that local necking occurs when sample of an oriented thermoplastic is pulled in a direction transverse to the orientation direction. This necking occurs quite early and at the point when the load reaches a maximum. The material does not exhibit this necking when it is pulled along the orientation direction (refer to Figure 2.7). Hence, the use of a necking criterion involving the maximum force in the hoop direction of the tube during biaxial forming has a definite physical basis for oriented polymers.

2.9 Forming limit diagrams

The limits of the formability of metals subjected to plane stress are commonly represented by forming limit curves (FLCs). These curves specify the magnitudes of strain at the onset of localized necking for proportional strain paths. The FLC is commonly used for assessing the forming severity of sheet metals in real press forming operations. However, the FLC is not as useful a concept in multistage forming operations which typically involve multi-linear (non-proportional) strain paths. Experimental (Graf and Hosford, 1993, Graf and Hoford, 1994) and numerical (Chu, 1982, Barata da Rocha et al., 1985, Gotoh, 1985, Kuroda and Tvergaard, 2000) studies on the formability of sheet metals subjected to nonproportional loading have revealed that the FLC is path-dependent. This means that forming limit strains of a sheet metal subjected to nonproportional loading may not be predicted using a single limit curve in strain space.

2.9.1 Experimental forming limit determination for tubular materials

The method for the experimental determination of the forming limit curve for sheet metal was summarized briefly in Chapter 1. The experimental determination of the forming limit curve for tubular materials will be reviewed in this section. Tube forming tests in which the material is subjected to simultaneous internal pressure and axial load is a common method for the determination of the experimental forming limits for tubular materials. In most cases (i.e. forming of metal tubes at room temperature), the forming process is stopped when the internal pressure is reduced suddenly due to tube explosion or burst so that the time from fracture initiation to final failure is very small, and thus, the material characteristics are hardly affected by the damage (Kim et al., 2005).

In the study of the forming limit stresses of steel tubes subjected to non-proportional loading by Yoshida and Kuwabara (2007), forming limit strains were determined by first measuring data of the outer diameter, D, and the thickness, t, of a burst specimen. The outer diameter was measured at three positions, 60°, 90° and 120° in the circumferential direction from the position where fracture occurred. The thickness was measured every 30° in the circumferential direction, except for the portion where fracture occurred. These measured data were averaged and used to determine the forming limit strains.

In the case of materials that locally neck, but fracture considerably after necking occurs, alternate experimental methods for forming limit determination would be required. In this case, a clear physical indication that necking has occurred (as in the case

of bursting) is likely not available or may be subjective. This has been observed with the oriented polypropylene tubes used in this study.

CHAPTER 3

MECHANICAL CHARACTERIZATION OF OPP TUBE FOR DETERMINATION OF PLASTIC WORK CONTOURS

3.1 Basic physical properties of OPP tube

The polypropylene resin used to produce the OPP tubes was a homopolymer from British Petroleum (BP), whose grade was 10-6014 and melt flow index was 0.7. Appendix B provides details of the preparation of the polypropylene tubular billets that were subsequently ram extruded. Also, details of the ram extrusion process used to produce the oriented polypropylene tubes used in this study are also described in Appendix B.

In order to determine the physical properties of the oriented polypropylene tube, such as its crystallization and melting temperatures, a differential scanning calorimetry

(DSC) test was performed. Figure 3.1 shows the results of a DSC test for an oriented polypropylene tube with a draw ratio of 4.5. The first peak in Figure 3.1 gives the crystallization temperature of the material (approximately 119°C) and the second peak gives the melting temperature (approximately 163°C). Another important parameter, which can be determined from the results of a DSC test, is the percentage crystallinity of the material. Thermoplastics can vary in their degree of crystallinity depending on the type of polymer as well as the methods by which they were processed.

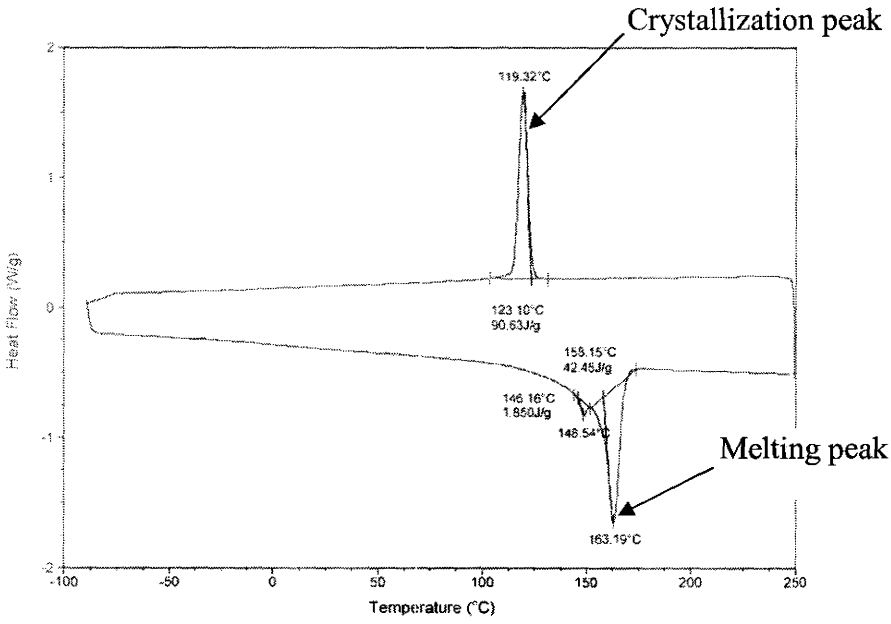

Figure 3.1 DSC test result for oriented polypropylene tube of draw ratio 4.5.

3.2 Uniaxial mechanical testing of OPP tube at elevated temperatures

In order to experimentally represent the plastic work contours for oriented (anisotropic), pressure-dependent polypropylene tube, uniaxial mechanical tests were conducted. Specimens were tested in (tension and compression) along principal directions of the tube at various elevated temperatures and strain rates. The naming convention for the three principal directions of the tube are given in Figure 3.2. The details of the testing are described in the sections to follow.

All uniaxial tensile and compression tests were performed on a MTS servo hydraulic test machine equipped with an environmental chamber. The tension and compression tests along a given direction were conducted at 4 different temperatures (110°C, 130°C, 140°C and 150°C) and two crosshead velocities (1 mm/minute and 20 mm/minute). The initial strain rates corresponding to 1 mm/minute and 20 mm/minute are 0.0022/second and 0.044/second respectively. To ensure repeatability of the results, the tension and compression tests along the axial and hoop directions were repeated 2-3 times at 110°C and 130°C and corresponding to the two strain rates (at a draw ratio of 4.0). The repeatability of the test results were, in general, quite good (refer to Appendix C). Also, in the case of the compression tests, silicone oil was applied to the top and bottom surfaces of each sample (prior to heating) for improved lubrication.

The true stress strain curves from the uniaxial mechanical tests were determined using the constancy of volume assumption. It is known that the elastic Poisson's ratio for polymers is of the order of 0.35, a value less than that required for incompressibility (ν =

0.5). However, Duffo et al. (1995), in their studies of the tensile behaviour of a commercial grade of isotactic polypropylene tested up to 150°C, found the relative volume expansion to be less than 2.5%. In this case, the constancy of volume assumption can be used without the introduction of a large error.

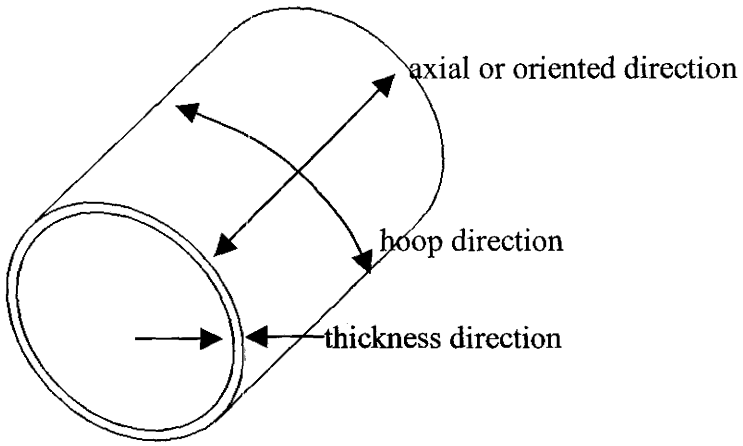

Figure 3.2 Naming conventions for three principal directions of OPP tube.

3.2.1 Axial compression test

For the determination of the axial compressive properties of the OPP tube, a ring compression test was employed. It is important to note here that there are no standards specifying the specimen geometry for the large strain compression testing of thin-walled tubes. However, the thick-walled ring compression test applied to metallic specimens has been used to generate the large strain flow curves at elevated temperatures and strain rates (Osakada et al., 1991, Robinson et al., 2004). The thick-walled ring specimen

dimensions were chosen such that the ratio of outer diameter to inner diameter to height was 6:3:2 (Osakada et al., 1991). With this sample geometry, the ratio of wall thickness to height is 0.75, which is 50% greater than the minimum diameter to height ratio of 0.5 commonly used to avoid buckling during the large strain compression of a solid cylindrical metallic specimen (Dieter, 1961). This indicates that as one moves from the compression testing of a solid cylinder to a thick-walled ring, the height of the ring progressively approaches the wall thickness of the ring.

The ISO 604 standard outlines methods for the determination of the compressive properties of plastics at room temperature. The standard indicates that for the compression testing of smaller size cylindrical specimens, the ratio of diameter to height should be 0.5. Therefore, for the case of the compression testing of thick-walled plastic rings, one may choose to use a wall thickness to height ratio of 0.75, just as in the case of the compression testing of the thick-walled metallic rings outlined above. However, for the compression testing of thin-walled plastic rings, which is of interest in this study, it is proposed that the height of the sample be close to or slightly smaller than the its wall thickness (i.e. wall thickness to height ratio of 1 or slightly greater). With the intent of avoiding buckling and minimizing barreling of the sample, a ratio of wall thickness to height of 1.2 was selected. The ring samples had a height of 2.64 mm and a wall thickness of 3.175 mm (based on a tube with an O.D. of 50.8 mm and an I.D. of 44.45 mm). Figure 3.3 shows an OPP ring sample prior to compression testing.

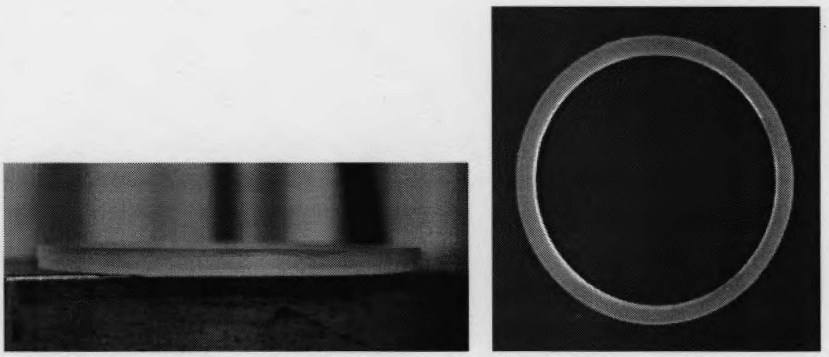

front view top view

Figure 3.3 Axial ring compression specimen prior to testing.

To convert the load-displacement curves obtained from the axial compression tests to true stress-strain curves, the following formulas were used:

$$\sigma = \frac{P \cdot h_i}{A_0 \cdot h_0} \tag{3.1}$$

$$\varepsilon = \ln \frac{h_i}{h_0} \tag{3.2}$$

where P and h_i are the measured instantaneous load and height respectively, and A_0 and h_0 refer to the initial cross-sectional area and height of the compression specimen respectively.

To determine whether buckling occurred during the axial compression test, plots of the load versus displacement at room temperature and at 150°C were examined and are shown in Figure 3.4, for a tube of draw ratio of 5. No significant drop in the load occurred as the deformation progressed at both temperatures, indicating that buckling of the sample did not occur. On the other hand, preliminary tests of ring samples of draw ratio 5.0 with larger heights (i.e. close to 12.7 mm) showed a dramatic drop in the load

curve close to the yield point. This was consistent with visual observation of buckling in these samples.

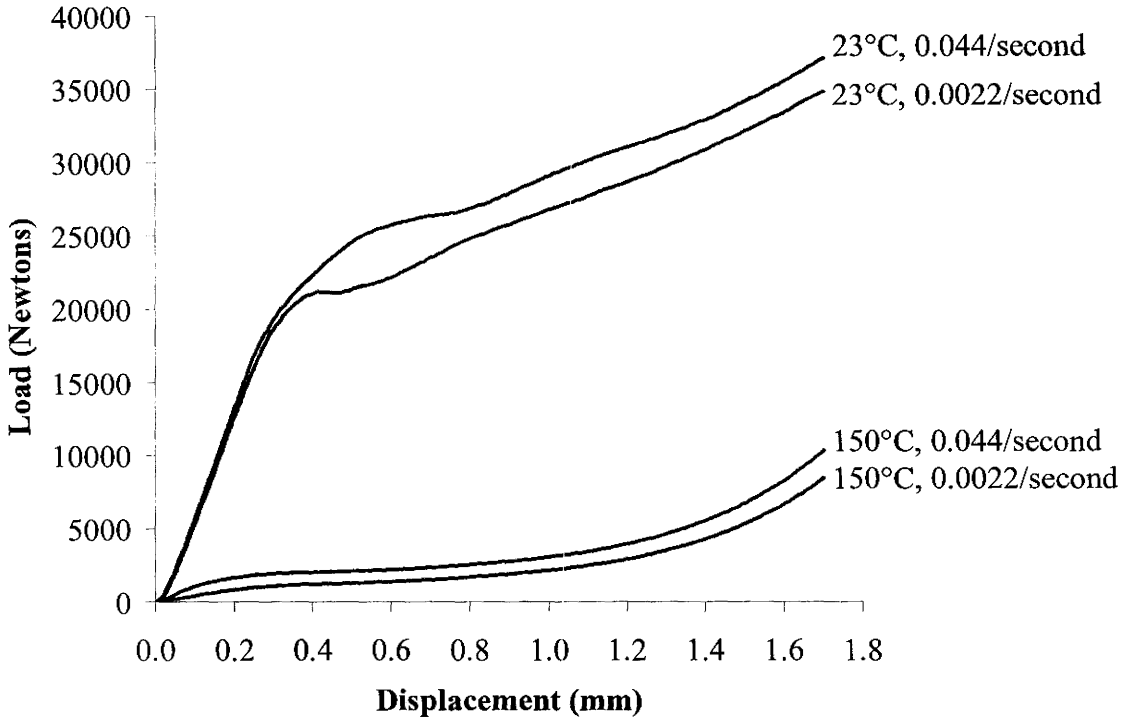

Figure 3.4 Load-displacement curves generated from axial compression test at two temperatures (room temperature and 150°C) and two rates (0.0022/sec. and 0.044/sec.) for a tube draw ratio = 5.0.

Figure 3.5 and 3.6 show the true stress-strain curves for samples of draw ratios 5 and 4 respectively tested at three temperatures and strain rates. For a given strain level, as the temperature increases, the corresponding stress decreases. Also, for a given strain, the stress increases as the testing rate increases for all of the temperatures studied. As the temperature reaches 150°C, the stress-strain curve appears to flatten out and show a steady but gradual rise to a strain of 1.

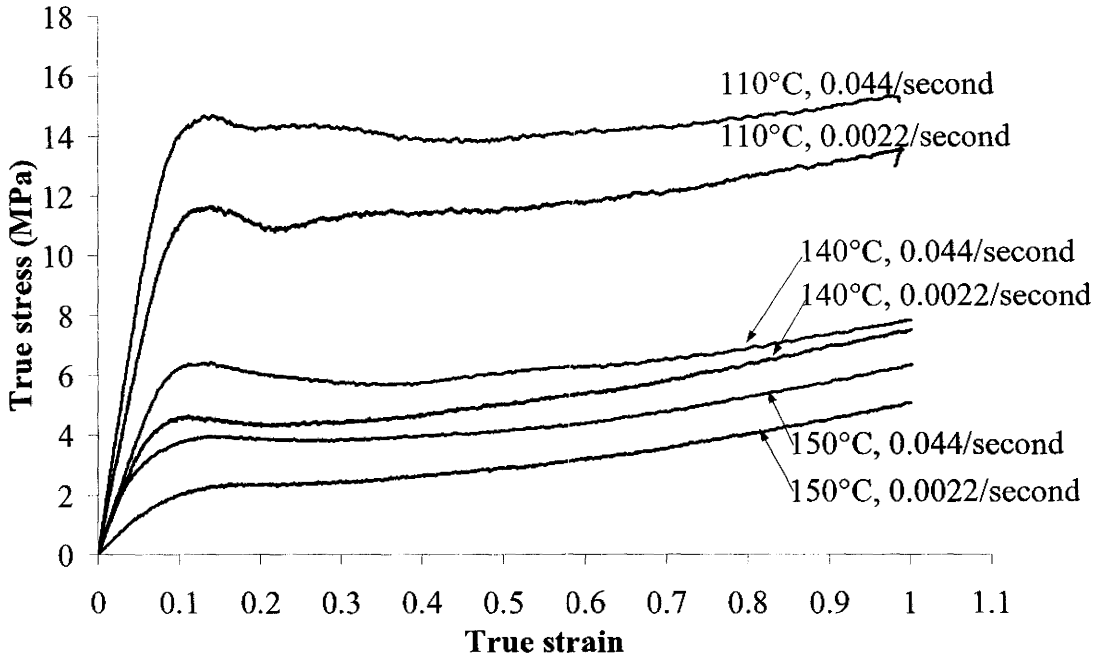

Figure 3.5 True stress strain curves determined from axial compression test of OPP tube of draw ratio 5.0 at three temperatures (110°C, 140°C and 150°C) and two strain rates (0.0022/second and 0.044/second).

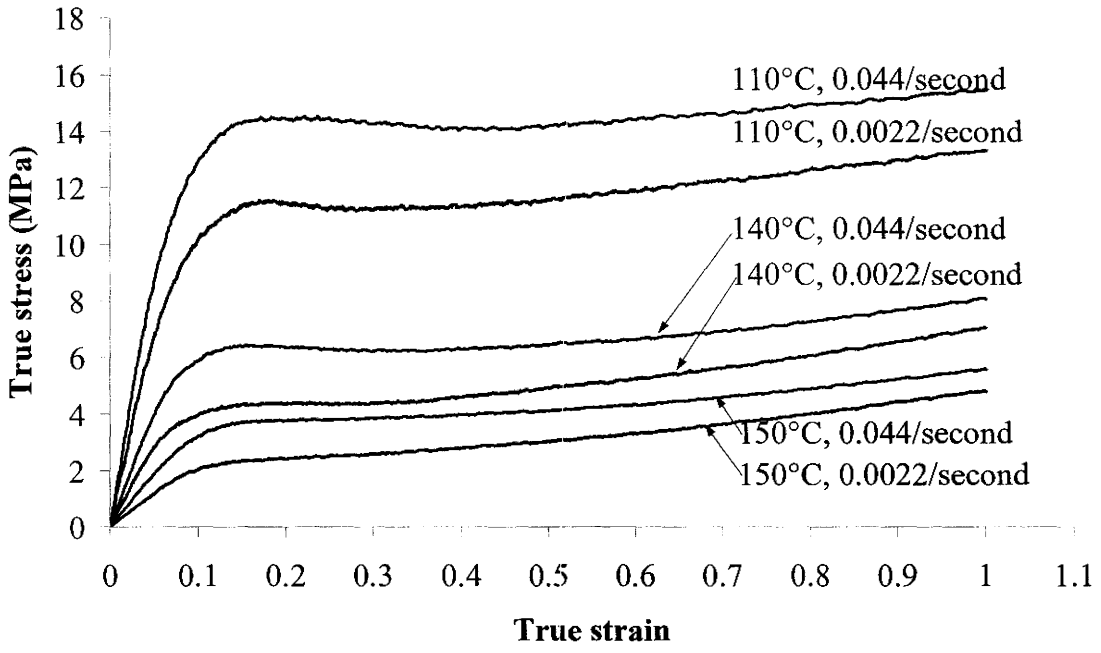

Figure 3.6 True stress strain curves determined from axial compression test of OPP tube of draw ratio 4.0 at three temperatures (110°C, 140°C and 150°C) and two strain rates (0.0022/second and 0.044/second).

3.2.2 Thickness compression test

The second test involved the compression of specimens to obtain properties along the thickness direction of the tube. Since the specimens used for the thickness compression test were machined from the wall of the tube, the height of the samples could be no larger than the wall of thickness of (3.175 mm). To keep the specimen dimensions in conformity with ISO 604 standard, square cross-sectional specimens were machined from the wall of the tube. The height of the specimens was chosen to be less than the wall thickness of the tube to eliminate any curvature resulting from the geometry of the tube. Specimen dimensions were chosen such that they had a length, width, and height of 5.28 mm, 5.28 mm and 2.64 mm respectively (refer to Figure 3.7).

It should be mentioned here that an attempt was made to construct a laminated sample made up of multiple rectangular cross-section specimens machined from the wall of the tube. The intention was to produce a sample, which had the dimensions required by the ISO 604 standard for the compression testing of plastic materials. However, the adhesive between the individual polypropylene specimens did not remain intact and this procedure had to be abandoned. In addition, the use of an adhesive in compression tests can be somewhat questionable as its properties often get incorporated into the behaviour of the overall sample.

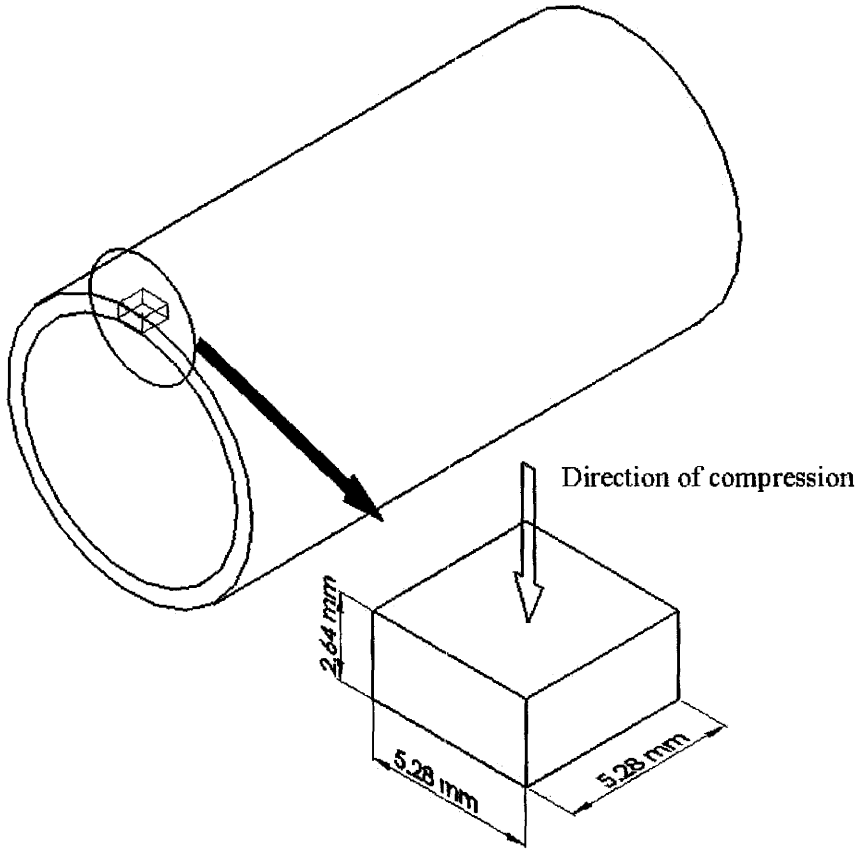

Figure 3.7 Geometry of specimen used for thickness compression test.

Figures 3.8 and 3.9 show the true stress-strain curves obtained from the thickness compression test at three temperatures and two strain rates for draw ratios of 5.0 and 4.0 respectively. At large compressive strains (i.e. greater than 60%), there is a significant increase in stress with strain, with this characteristic being more pronounced at the lower temperatures studied. The magnitude of this hardening decreases progressively as the temperature increases. This feature of the stress-strain curves is consistent with those obtained from a study of the large strain compression of oriented polyethylene terephthalate (PET) above the glass transition temperature (Boyce et al., 2000), as well a

study of the effects of strain rate and temperature on the compressive deformation of polymethylmethacrylate (PMMA) (Arruda et al., 1995). Both studies involved the uniaxial compression of samples that were solid (cylindrical in the case of PET and cubic in the case of PMMA).

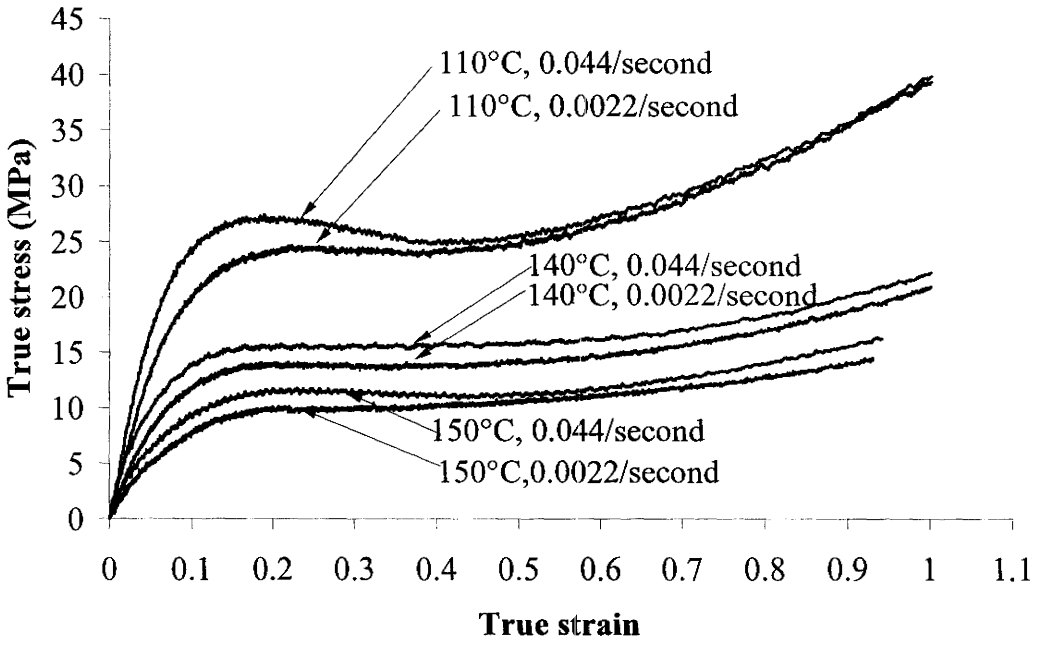

Figure 3.8 True stress strain curves determined from thickness compression test of OPP tube of draw ratio 5.0 at three temperatures (110°C, 140°C and 150°C) and two strain rates (0.0022/second and 0.044/second).

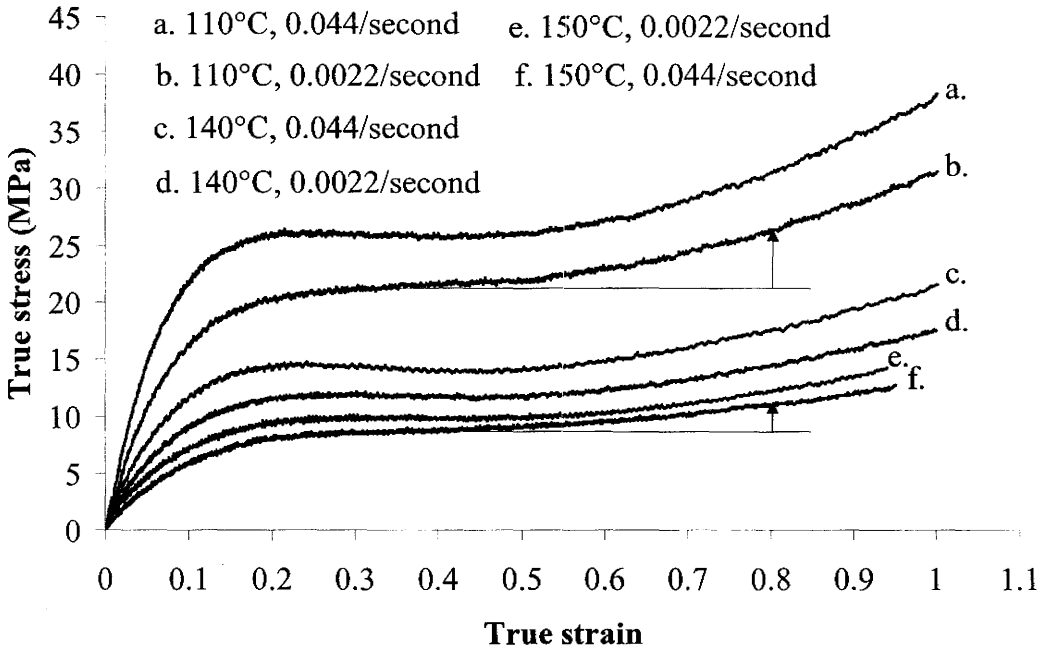

Figure 3.9 True stress strain curves determined from thickness compression test of OPP tube of draw ratio 4.0 at three temperatures (110°C, 140°C and 150°C) and two strain rates (0.0022/second and 0.044/second).

Figure 3.10 shows the thickness compression sample before and after deformation at a temperature of 110°C, a strain rate of 0.0022/second and corresponding to a tube of draw ratio of 5.0. The interesting feature is that little to no flow of material occurs along the axial (or orientation) direction compared to the hoop direction (or transverse to the orientation direction). This indicates that the material is in an anisotropic state at this elevated temperature, causing the sample's cross-section to change from square to one that is nearly rectangular. This characteristic emphasizes the need for quantifying the compressive flow behaviour of this material, through appropriate test methods such as the ones outlined in this study, along its principal directions. This will ultimately allow for a better understanding of the change in the state of anisotropy of the material with temperature and strain rate.

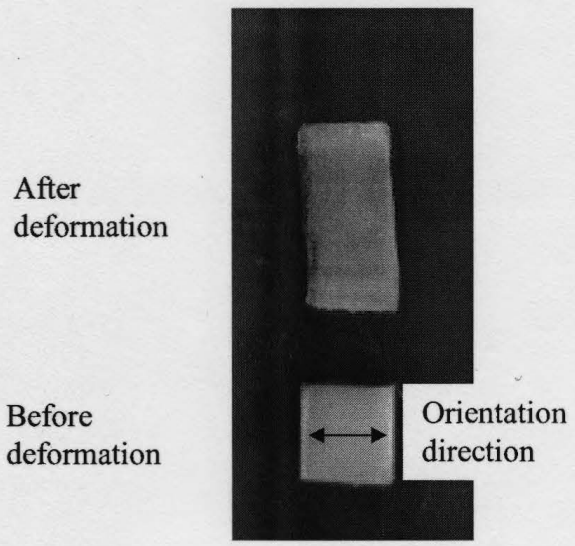

Figure 3.10 Thickness compression sample before and after deformation at 110°C and a strain rate of 0.0022/second (tube draw ratio 5.0).

3.2.3 Axial tensile test

For determination of the axial tensile properties of the OPP tube, tension specimens were machined along the axial direction of the tube. The geometry of the specimens was in accordance with the ASTM D 638 Type V specimen. The gage length of the specimen was 7.62 mm and the width of the narrow section was 3.175 mm. A miniature specimen was chosen from the standard in order to keep the curvature, resulting from the tube geometry, to a minimum along the width of the sample. The localized necking and cold drawing phenomenon common with isotropic polymeric materials tested in tension did not occur in any of the samples tested along the axial (or oriented) direction. The deformation along this direction was quite uniform. Figure 3.11 shows a sample tested in tension along the axial direction at 140°C and a strain rate of 0.0022/second at various stages of the deformation (tube draw ratio = 5.0).

In situ full-field strain measurements during the tensile deformation of the sample were made using a commercially available digital image correlation (DIC) system (ARAMIS version 4.7). In order to use the ARAMIS system, a random black and white speckle pattern was applied to the front surface of each sample, along its gage length using an air gun (refer to Figure 3.11). The principle of DIC is based on the distribution of grey scale values of a rectangular area (facet) in the initial image (captured by a single CCD camera) and subsequent images of the same area under deformation. Details of the method are described in the ARAMIS version 4.7 manual (2000). Figures 3.12 and 3.13 show the true stress-strain curves from the axial tensile test of tube of draw ratio 5.0 at

the two strain rates considered. Both figures show that at a given rate, the overall shape of the stress-strain curves does not change significantly. A dramatic hardening is observed at strains larger than 0.7 at all of the temperatures and rates considered. Note here that the test corresponding to 130°C and a rate of 0.044/second, shows a marked reduction in the true strain value at the end of the test. This is due to the fact that the test was stopped earlier than the others, since the deformation was out of the field of view of the camera.

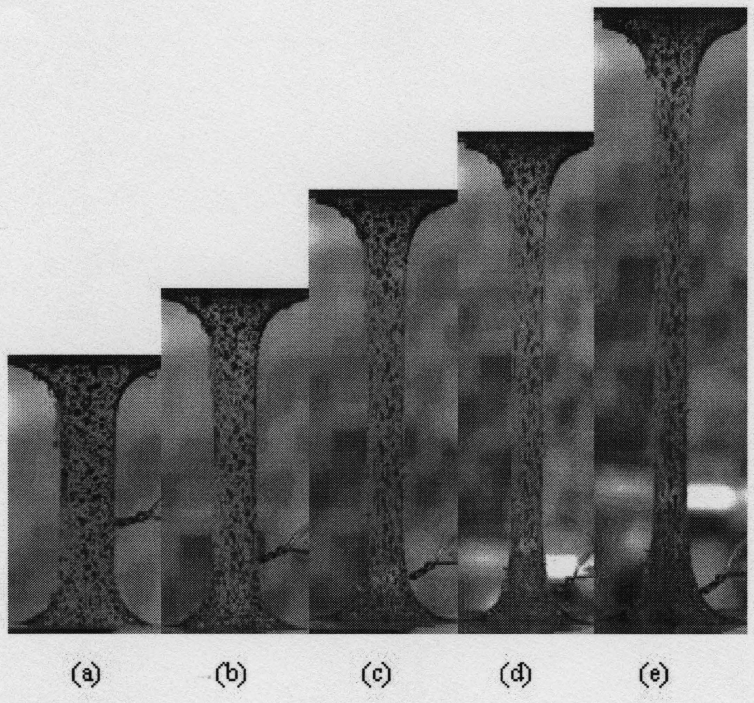

Figure 3.11 Axial tensile sample machined from OPP tube (draw ratio 5.0) and tested at 140°C and a strain rate of 0.0022/second at various stages of the deformation (a) initial state, (b) 39% true strain, (c) 67% true strain, (d) 86% true strain, and (e) 94% true strain.

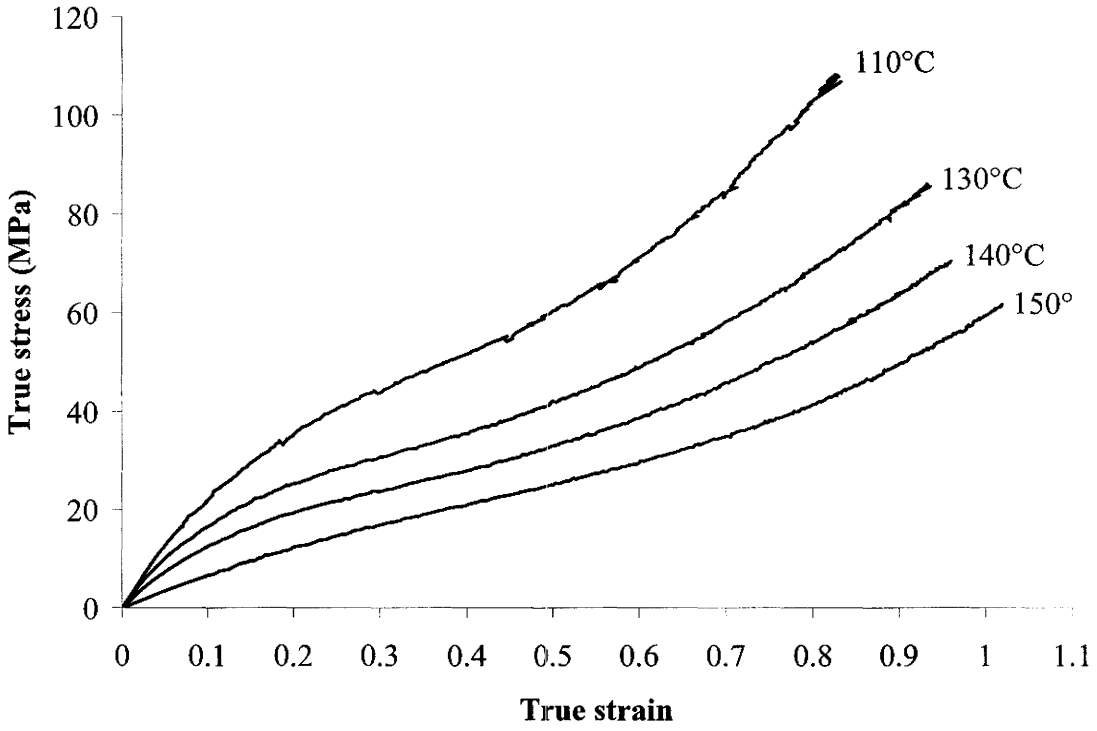

Figure 3.12 True stress strain curves determined from axial tensile test of OPP tube of draw ratio 5.0 at four temperatures (110°C, 130°C, 140°C and 150°C) and a strain rate of 0.0022/second.

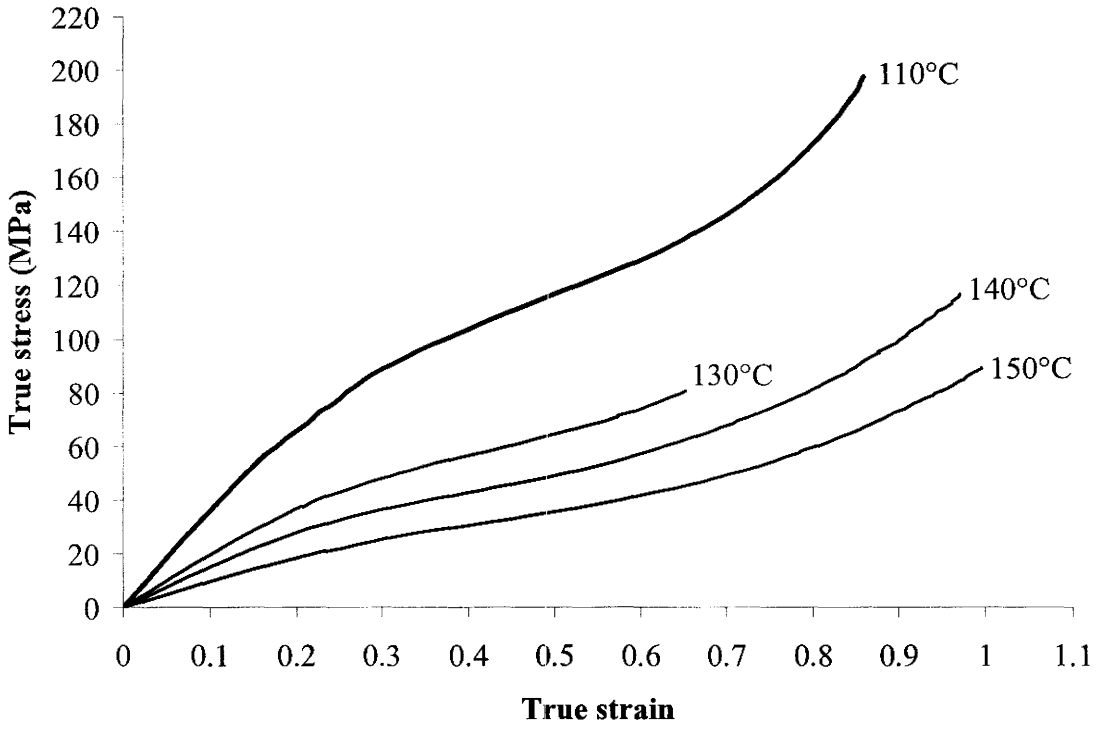

Figure 3.13 True stress strain curves determined from axial tensile test of OPP tube of draw ratio 5.0 at four temperatures (110°C, 130°C, 140°C and 150°C) and a strain rate of 0.044/second.

3.2.4 Ring hoop tension test (RHTT)

In order to obtain the stress-strain behaviour of the OPP tube along the hoop direction, the ring hoop tension test (RHTT), first proposed by Wang et al. (2002) and described in Chapter 2, was utilized. Figure 3.14 shows a photograph of the gripping device for the ring hoop tension test. The two semi-circular discs (or D-blocks) were

held in the grips, which were installed on an MTS servohydraulic testing machine, fitted with an environmental chamber for conducting the elevated temperature tests. Separation of the grips (and hence the D-blocks), resulting from movement of the lower actuator, caused hoop expansion of the ring specimen. Figure 3.15 shows the initial geometry of the ring hoop specimens prior to testing. Specimens 9.53 mm wide and with a gage section in accordance with the ASTM D 638 Type V specimen were used.

Due to the inhomogeneous nature of tensile flow along the hoop direction of the OPP tube (i.e flow localization associated with necking and the propagation of the neck along the hoop direction), it was necessary to measure strain "locally" within the neck, for accurate determination of the true stress-strain behaviour. The ARAMIS optical strain measurement system was used once again. For this test, the random speckle pattern was applied to the thickness surface of the gage section of the sample (refer to Figure 3.15) since this was the surface that would subsequently be used to measure hoop strain.

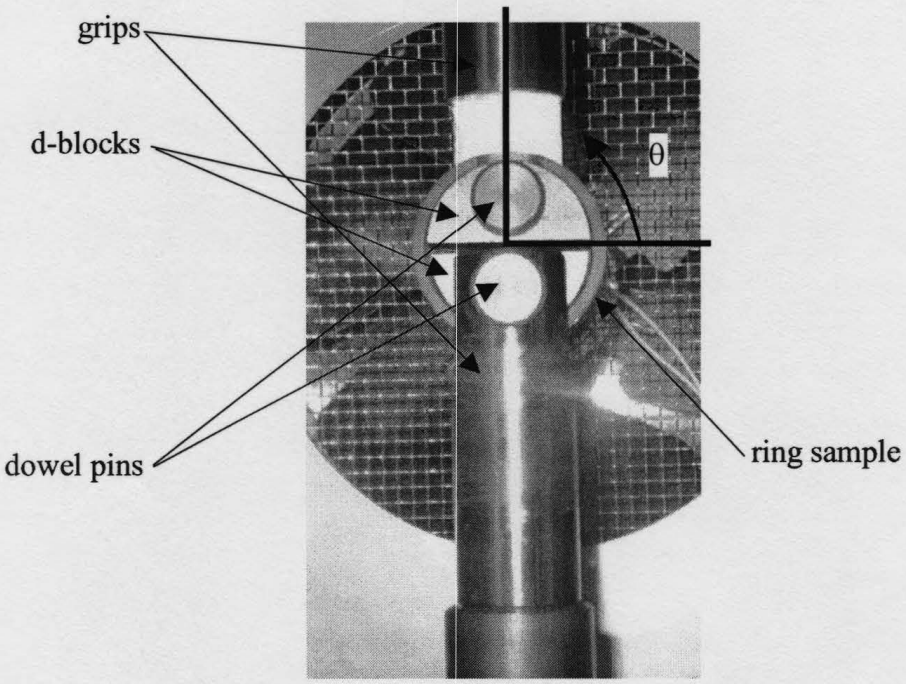

Figure 3.14 Gripping device for ring hoop tension test used in current study.

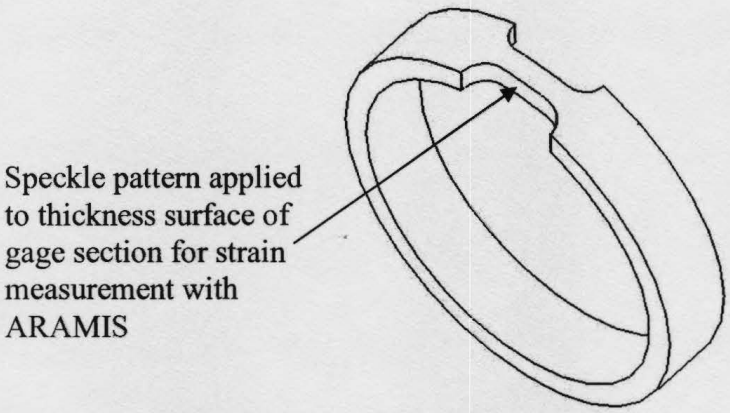

Figure 3.15 Geometry of ring hoop tension specimen prior to testing.

An examination of the set-up for the ring hoop tension test indicates that it is possible for the middle of the gage section of the specimen to be positioned anywhere between 0 and 90° along one quarter of the edge of the upper D-block (refer to θ in Figure 3.14). It is expected that the deformation mode and the friction condition between the D-block and the specimen, when it is positioned at various locations along the edge of the block will vary. In order to choose the most appropriate position of the specimen, three potential orientations of the specimen were tested (θ = 0°, 70 ° and 90°) (refer to Figure 3.16), and the resulting deformation and strain distribution across the thickness of the sample were examined. Note here that tests in which the center of the gauge section was positioned at greater than 0° but smaller than 70° were found to be problematic since a portion of the gauge section was found to have lost contact with the upper D-block as the D-blocks separated and the material experienced larger strains. For the purposes of this simple case study, the tests at the three different orientations were conducted at 110°C, a strain rate of 0.0022/second and with a tube of draw ratio 4.5.

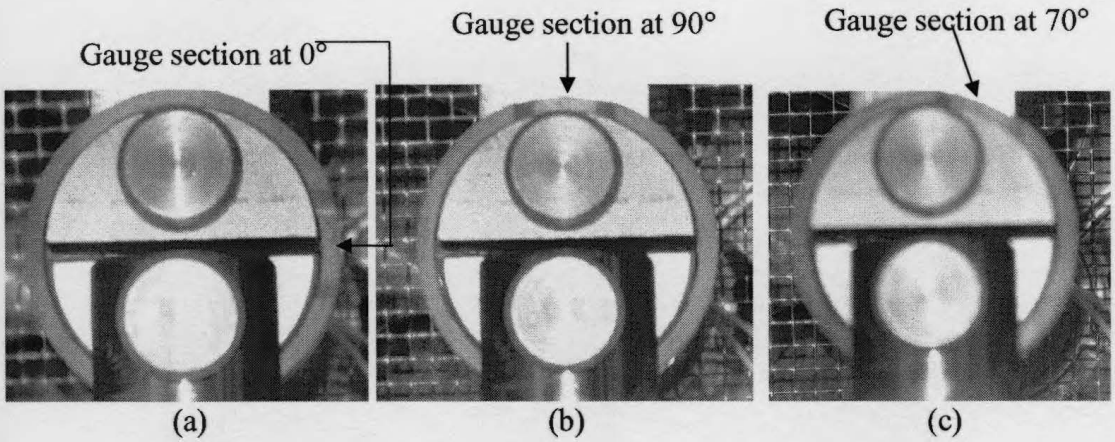

Figure 3.16 Three orientations of gauge section of ring hoop tension sample around D-block.

3.2.4.1 RHTT sample oriented at $\theta = 0°$

It was found that when the gage section was oriented at 0° (Figure 3.16 (a)), progressive separation of the D-blocks caused the gage section of the ring to change its shape and inside radius. In other words, flattening of most of the gage section was observed (refer to Figure 3.17). The strain distribution (both major and minor strains) varied across the thickness of the ring, moving from the inside diameter toward the outer diameter. Figure 3.18 shows the variation in the major strain along section 0 at various stages of the deformation. Note that each stage refers to the deformation at an interval of time, with all intervals of time being equal throughout the test. The variation in the major strain along the thickness appears to increase as the overall deformation increases. At stage 240 of the deformation, a variation of close to 15% is present in the major strain between the beginning and end of section 0. The variation can be attributed to the fact that the strains developing during the straightening of the gage section varied between the inner diameter and the outer diameter, with this effect likely being more pronounced with tubes having a larger wall thickness. This variation in the strain along the thickness did not allow this sample orientation to be used for determining the stress-strain response of the material along the hoop direction.

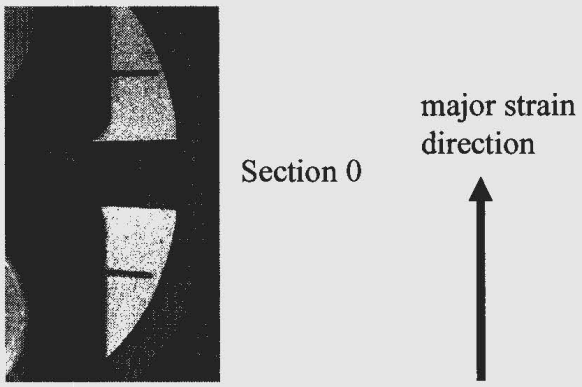

Figure 3.17 Straightening of gage section when ring hoop tension sample oriented at θ = 0° around D-block (corresponding to a tube of draw ratio 4.5 tested at 110°C and a strain rate of 0.0022/second).

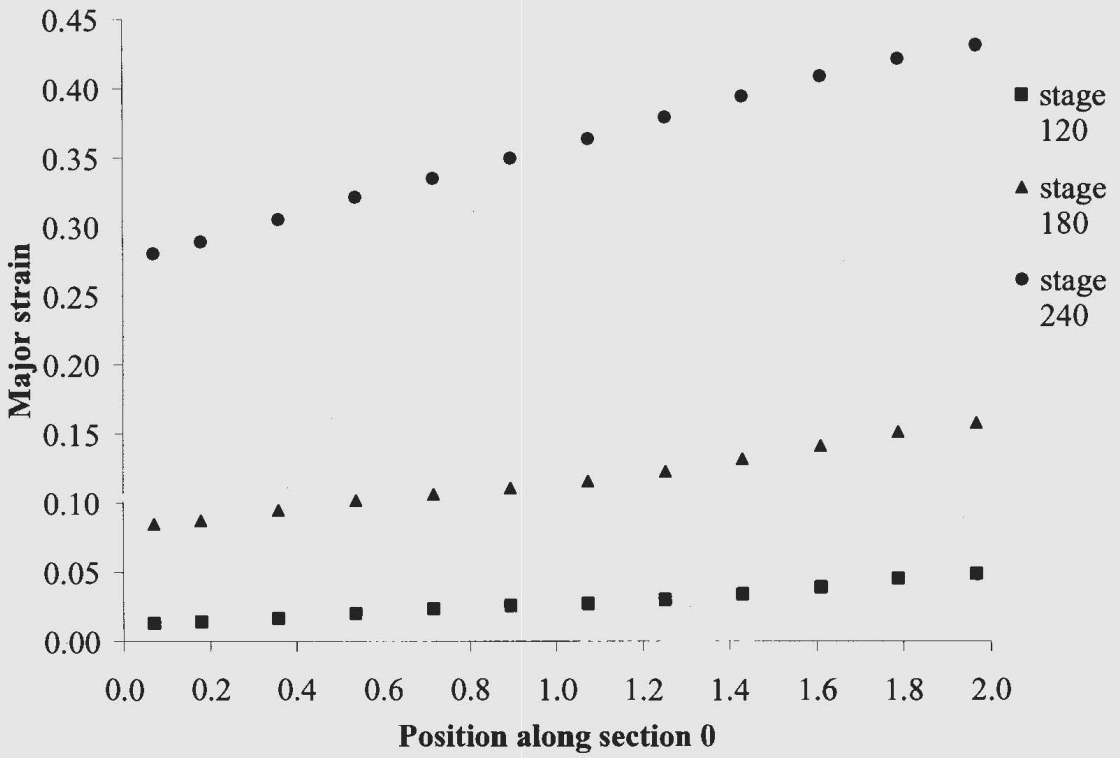

Figure 3.18 Variation of major strain along section 0 of ring hoop tension sample oriented at 0° (corresponding to a tube of draw ratio 4.5 tested at 110°C and a strain rate of 0.0022/second).

3.2.4.2 RHTT sample oriented at θ = 90°

The second orientation was one in which the sample was oriented at 90° (refer to Figure 3.16 (b)). In this configuration, it was found that up to a major strain level of approximately 20%, the material deformed relatively uniformly around the edge of the D-block. However, as the major strain increased above 20% and load transmitted to the ring also increased, the friction between the ring and the D-block became more significant. This is indicated by the central area of the ring material along the gage section undergoing little to no flow compared with the area on both sides of it, which eventually begin to neck. Figure 3.19 shows the section (section 0) along which the major strains are measured. Figure 3.20 shows the variation in the major strain along section 0 at various stages of the deformation. As indicated in Figure 3.20, the large peaks in the curve at stages 150 and 180 correspond to the two necks that develop in the sample.

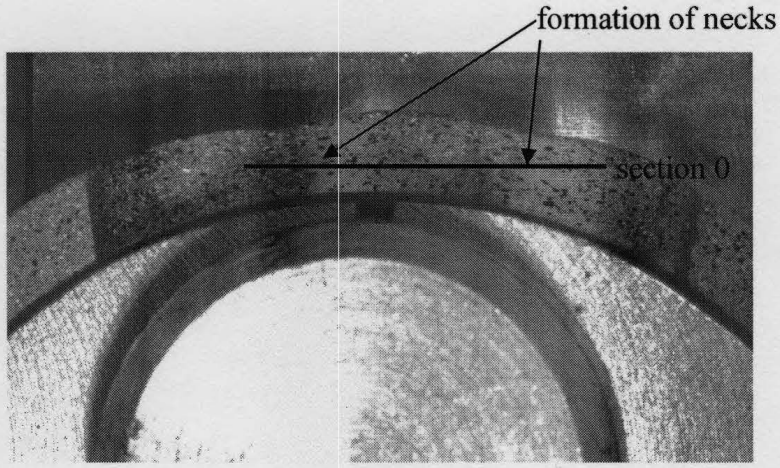

Figure 3.19 Location of section 0 and development of two necked regions along gage section of ring hoop tension sample oriented at θ = 90° (corresponding to a tube of draw ratio 4.5 tested at 110°C and a strain rate of 0.0022/second).

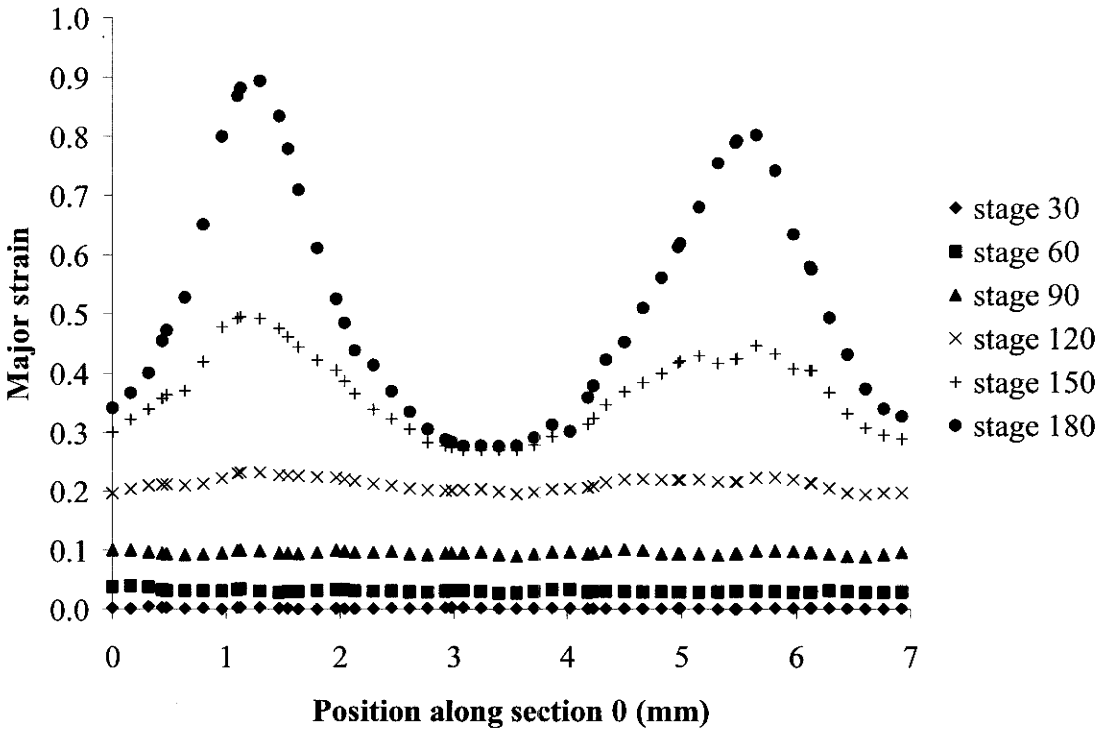

Figure 3.20 Variation of major strain along section 0 of ring hoop tension sample oriented at $\theta = 90°$ (corresponding to a tube of draw ratio 4.5 tested at 110°C and a strain rate of 0.0022/second).

3.2.4.3 RHTT sample oriented at $\theta = 70°$

The final orientation tested was one in which the sample was oriented at 70° along the edge of the insert (refer to Figure 3.16 (c)). An examination of the major strain distribution across the thickness of the sample, along section 0 in the necked region, (Figure 3.21) as the deformation progressed, showed the strains to be quite uniform across the thickness (refer to Figure 3.22). For all subsequent RHTT tests at elevated temperatures, a sample orientation of 70° was used.

In order to plot the true stress stain curves for the OPP tube along the hoop direction at various temperatures, the strain data obtained from the ARAMIS system and a method for determination of the true stress in the specimen as the deformation progressed was required. The details of the method for the plotting of the true stress strain curves are described in the flowchart given in Figure 3.23. A point was selected within the necked region of the sample, in the last stage of the deformation. The major and minor strain data at this point for all previous stages was used in the generation of the true stress strain curve.

Figures 3.24 and 3.25 show the stress strain curves obtained from the hoop tensile test at four temperatures and a strain rte of 0.0022/second and 0.044/second respectively.

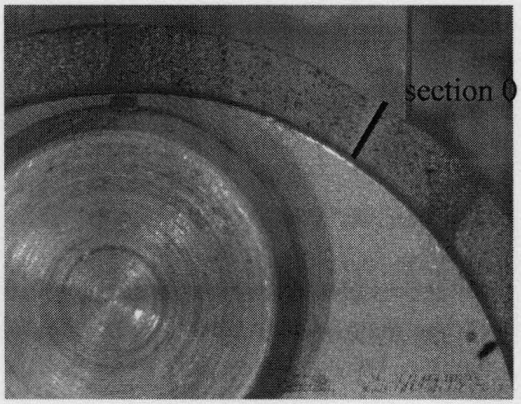

Figure 3.21 Location of section 0 of ring hoop tension sample oriented at θ = 70° (corresponding to a tube of draw ratio 4.5 tested at 110°C and a strain rate of 0.0022/second).

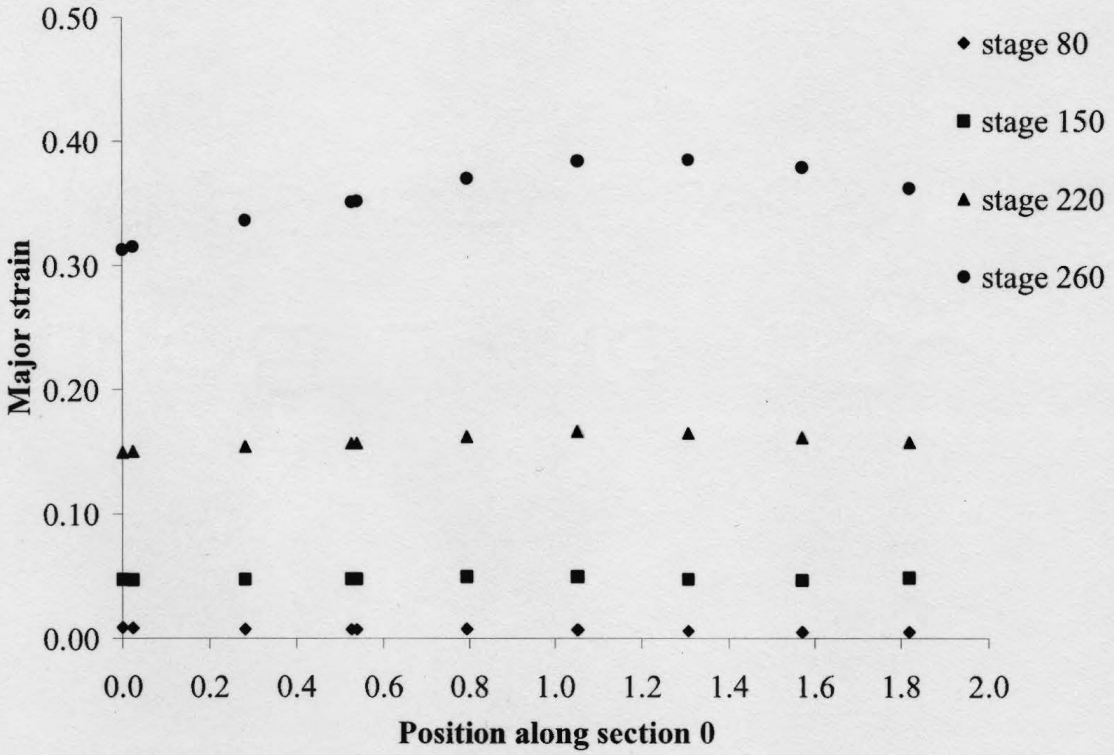

Figure 3.22 Variation of major strain along section 0 of ring hoop tension sample oriented at θ = 70° (corresponding to a tube of draw ratio 4.5 tested at 110°C and a strain rate of 0.0022/second).

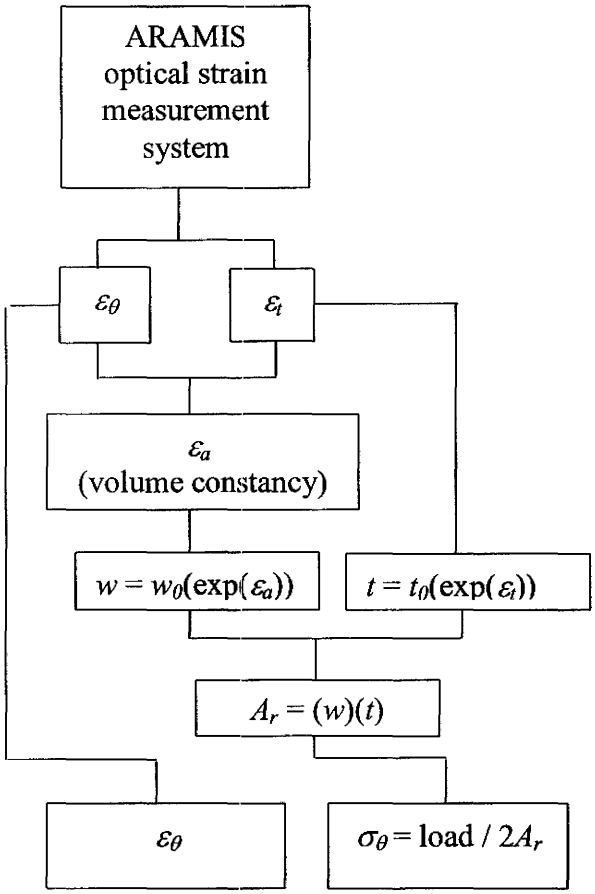

Figure 3.23 Flow chart for plotting true stress strain curve from ring hoop tension test. Symbols - ε_θ = hoop strain, ε_t = thickness strain, ε_a = width strain, w = current width, w_0 = original width, t = current thickness, t_0 = original thickness, A_r = current area.

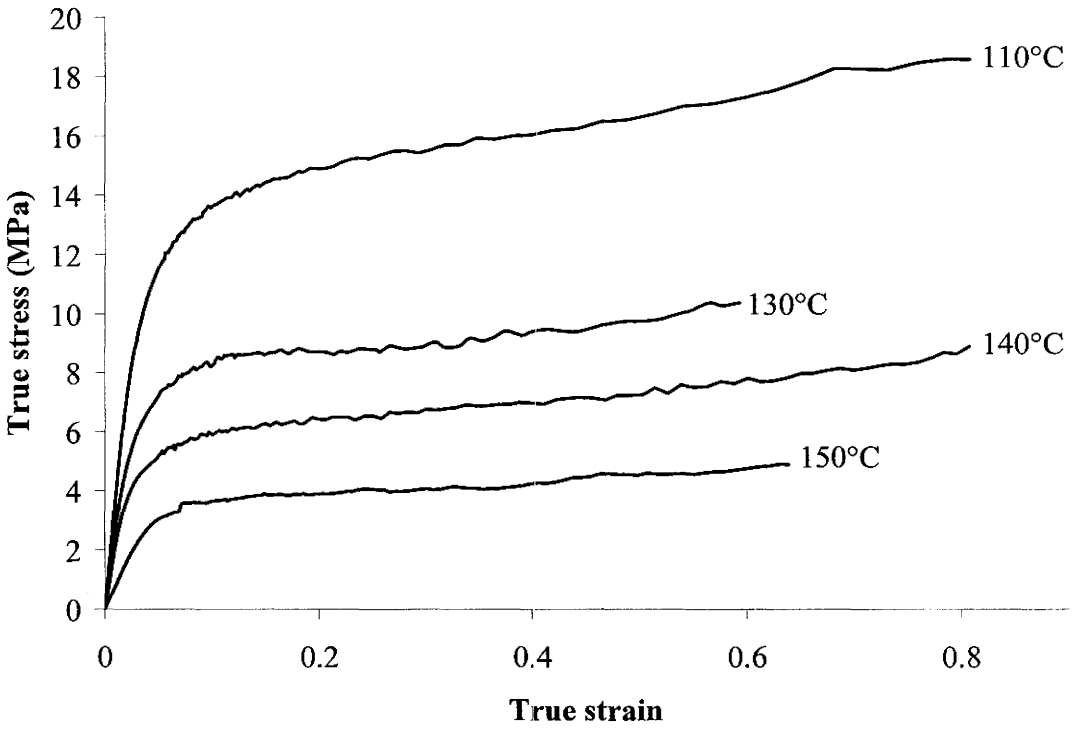

Figure 3.24 True stress strain curves determined from ring hoop tension test of OPP tube of draw ratio 5.0 at four temperatures (110°C, 130°C, 140°C and 150°C) and a strain rate of 0.0022/second.

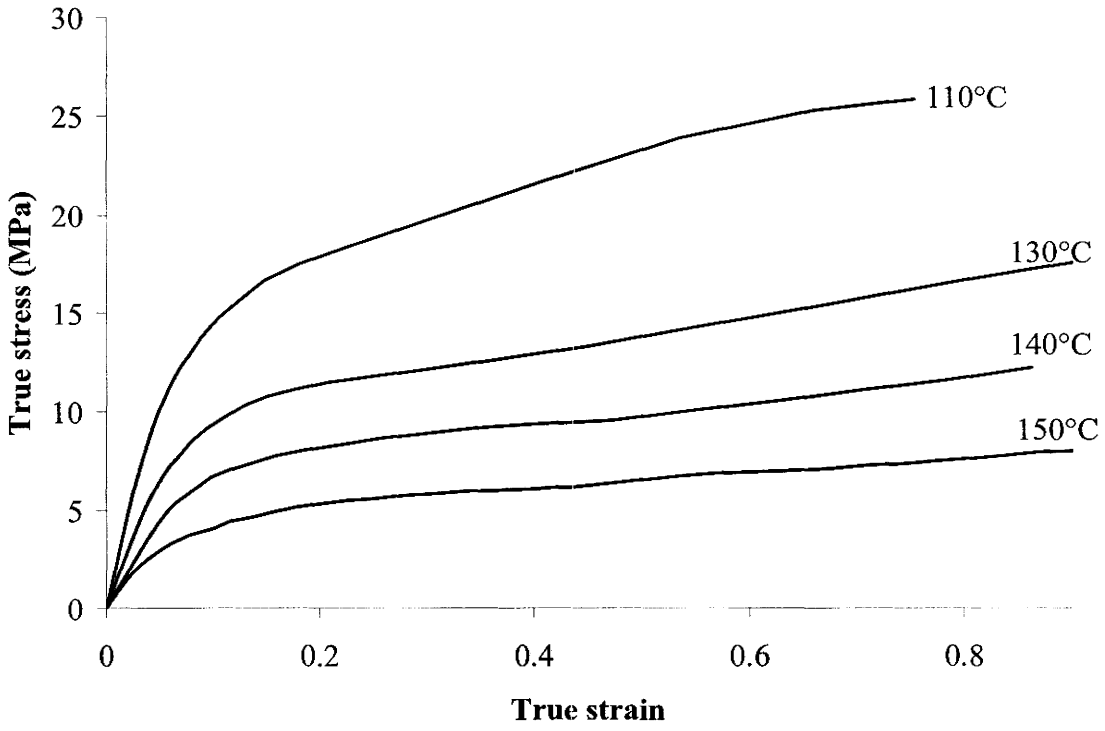

Figure 3.25 True stress strain curves determined from ring hoop tension test of OPP tube of draw ratio 5.0 at four temperatures (110°C, 130°C, 140°C and 150°C) and a strain rate of 0.044/second.

A point to note here with regard to the stress-strain curves obtained in tension and compression along the axial and hoop directions of the tube is the significant anisotropy in the hardening of the material. To illustrate this fact, Figure 3.26 shows the true stress-strain curves at 150°C and a cross-head velocity of 1 mm/min. obtained from the axial tensile, RHTT, axial compression and thickness compression tests for a tube of draw ratio 5.0. As indicated in this figure, the yield and hardening behaviour is markedly anisotropic, where the axial tension hardening is most dramatic. The stress-strain curves along the hoop tensile, axial and compression and thickness compression directions appear to flatten out at strains in excess of 0.15.

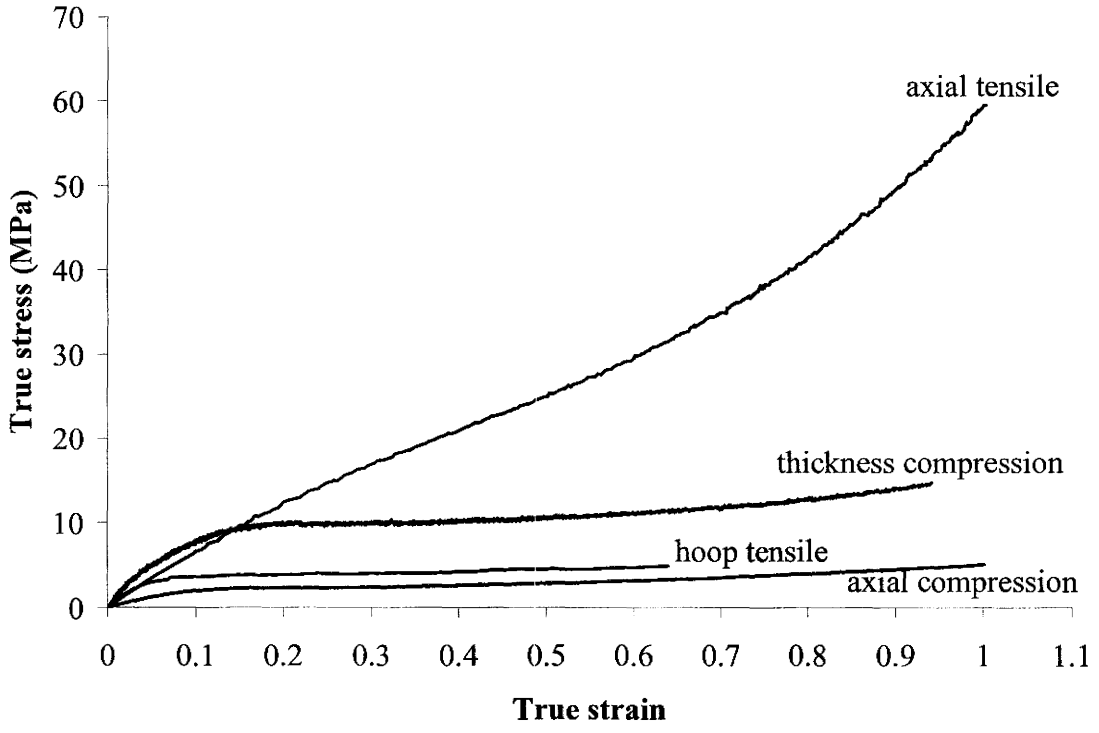

Figure 3.26 Comparison of axial tensile, axial compression, hoop tensile and thickness compression stress strain curves for OPP tube of draw ratio 5.0, tested at 150°C and a strain rate of 0.0022/second.

3.3 Tube forming tests at elevated temperatures

3.3.1 Description of test rig

A test rig for the high temperature tube forming of thermoplastic tubes with axial end feeding was designed and fabricated. Each end of the tube was sealed with a cylindrical plug, which had a taper at its end (as shown in Figure 3.27). The taper at the end of each plug ensured good sealing of the tube by accommodating variations in the inner diameter of the extruded tubes. Once the tube was sealed between the plugs, the tube ends (44.5 mm from each end) were clamped between two die halves, which had the same taper geometry as the plugs (refer to Figure 3.27).

Three copper tubes, connected to a hot air gun having various heat settings, were used to circulate hot air around the outside of the OPP tube sample (refer to Figure 3.28). Heated silicone oil was circulated through the inner diameter of the tube and used as the pressurization medium. Both sources, the hot air gun and the heated silicone oil, working simultaneously, were used to heat the entire tube to the desired temperature. The setting of the hot air gun and the temperature of the silicone oil to achieve a desired tube temperature were determined through the following simple experiment. Two holes were drilled into the wall thickness of a tube (starting from the outside surface), and which had a diameter close to that of the thermocouples used. One hole was drilled slightly before reaching the inside wall thickness and the other was drilled up to the mid-wall thickness. A thermocouple was placed in each hole, such that a temperature reading for both the inside diameter and mid-wall thickness were obtained. A third thermocouple was also

attached to the outside surface of the tube. The heat settings for the hot air gun and the temperature setting for the silicone oil were slowly increased/adjusted simultaneously. This continued until, eventually, the three thermocouple temperatures stabilized to the desired temperature. During an actual tube test, one thermocouple was positioned on the surface of the tube near the region where the biaxial strains would be measured. The heat setting for the hot air gun and the temperature of the silicone oil were set to the values required to achieve a given temperature, based on the experiment described above. The thermocouple contacting the surface of the tube verified the tube temperature. A temperature variation of approximately 2-3°C, across the surface of the sample, would be expected in any given test. Figure 3.28 shows the complete tube forming test rig with the tube sample installed. Thin-walled OPP tubes of various lengths were pressurized (or pressurized and axially fed) such that both axial and hoop stresses (and strains) were induced in the tube walls.

3.3.2 Selection of loading rates in tube forming tests

For a given temperature, tube geometry and stress path in a biaxial tube test, a method for selecting the rate at which the internal pressure (or internal pressure and axial load) was increased was required, such that, by some measure, it was "equivalent" to the loading rate used in the uniaxial tests at the same temperature. This is particularly important since polymers are rate dependent materials. Since oriented polymers are also known to be pressure sensitive at room temperature, it was assumed that the hydrostatic stress would have an effect on their yielding behaviour at elevated temperatures.

Therefore, the hydrostatic stress rates used in the uniaxial tests were also imposed on the biaxial tests. The method used to calculate the axial load rate and/or the internal pressure rate required to induce a constant hydrostatic stress rate (equal to that used in the uniaxial test) along a given biaxial load path is described below. A similar procedure was used by Tuttle et al. (1992), in which a constant octahedral shear stress rate was imposed along all loading paths.

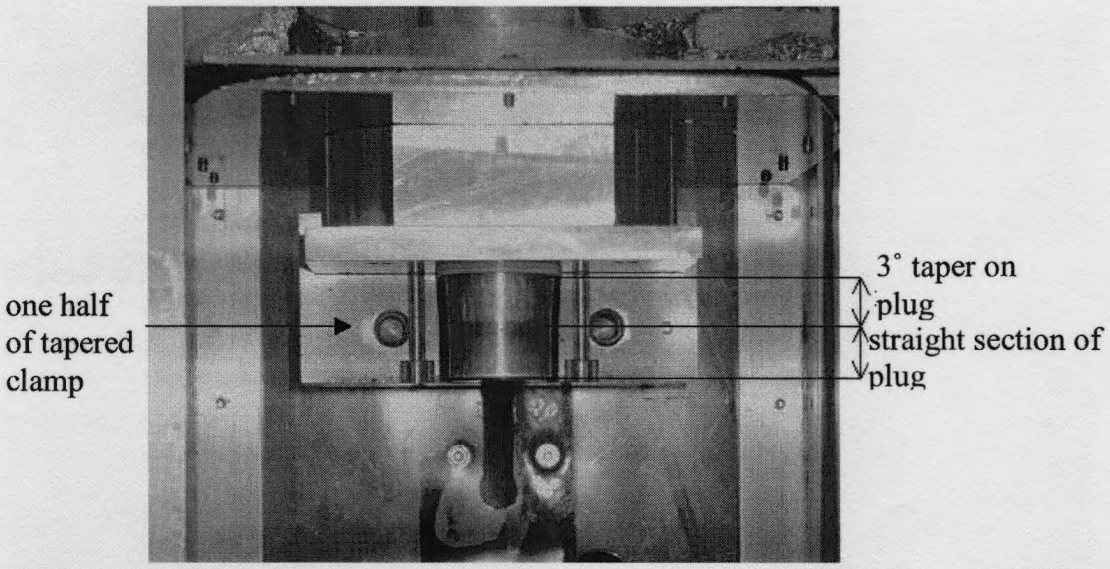

Figure 3.27 Exposed tapered geometry of cylindrical plug between which tube was sealed (prior to tube assembly).

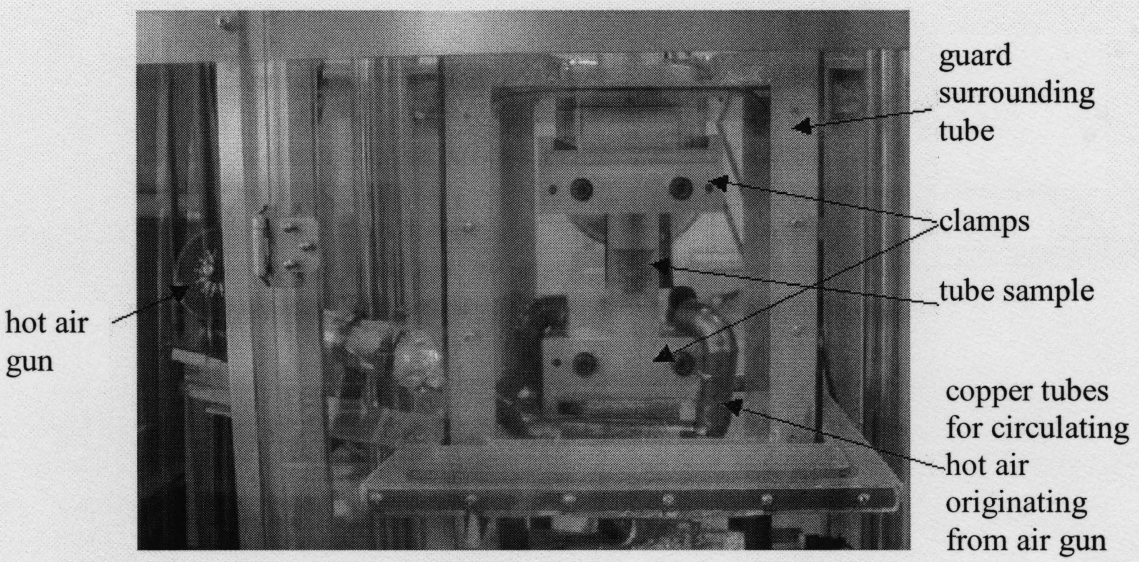

Figure 3.28 Complete tube forming test rig with tube sample installed.

Both the axial load, F_a, and the internal pressure, p, were initially zero at the start of each test, and were subsequently increased at a constant rate, k_1 and k_2 respectively. Thus, at time t_i after the start of a test:

$$F_a = k_1 t_i \tag{3.3}$$

$$p = k_2 t_i \tag{3.4}$$

The stresses induced in the wall of a thin walled tube at time t_i are given by:

$$\sigma_a = \frac{t_i}{2t}\left(k_2 \rho_\theta - \frac{k_1}{\pi \rho_\theta}\right) \tag{3.5}$$

$$\sigma_\theta = \frac{k_2 t_i \rho_\theta}{t} \tag{3.6}$$

$$\sigma_t \approx 0 \tag{3.7}$$

where

ρ_θ = hoop radius of the tube

t = tube wall thickness

The hydrostatic stress, σ_{hyd}, is given by:

$$\sigma_{hyd} = \frac{\sigma_a + \sigma_\theta + \sigma_t}{3} \tag{3.8}$$

Substituting Equations (3.5)-(3.7) into Equation (3.8), the hydrostatic stress rate, (σ_{hyd}/t_i) induced by a given combination of k_1 and k_2 is given by:

$$\left(\frac{\sigma_{hyd}}{t_i}\right) = \frac{1}{3t}\left(\frac{k_2\rho_\theta}{2} - \frac{k_1}{2\pi\rho_\theta} + k_2\rho_\theta\right) \tag{3.9}$$

The slope of any loading (or stress) path can be given as:

$$M = \frac{\sigma_a}{\sigma_\theta} = \frac{k_2\pi\rho_\theta^2 - k_1}{2k_2\pi\rho_\theta^2} \tag{3.10}$$

The axial load rate, k_1, and the internal pressure rate, k_2, required to induce a constant hydrostatic stress rate (equal to that used in the uniaxial test) along a biaxial load path of slope M can be determined by combining Equations (3.9) and (3.10):

$$k_1 = \left(\frac{\sigma_{hyd}}{t_i}\right)(3t)\left[\frac{\pi\rho_\theta(2M-1)}{(-M-1)}\right] \tag{3.11}$$

$$k_2 = -\left(\frac{\sigma_{hyd}}{t_i}\right)(3t)\left[\frac{1}{(-M-1)\rho_\theta}\right] \tag{3.12}$$

3.3.3 Continuous biaxial strain measurement during tube forming test

The axial and hoop strains over the entire surface of the deforming tube were determined with the ARAMIS optical strain measurement system. A random black and

white speckle pattern was applied to the surface of the free (i.e. unclamped) section of the tube prior to forming (Figure 3.29). Individual images of the pattern were recorded at different stages of the deformation using two CCD cameras positioned at specified incident angles from the viewing direction (refer to Figure 3.29). The approximate dimensions for the observation window used by the ARAMIS system are given in Figure 3.30. Position coordinates (*x, y, z*), displacement and strains in 3D of points on the surface of the tube and within the observation window were calculated automatically using photogrammetric evaluation procedures (ARAMIS version 4.7 manual, 2000). Therefore, at any stage of the deformation, the axial and hoop strains at any location within the observation window were known.

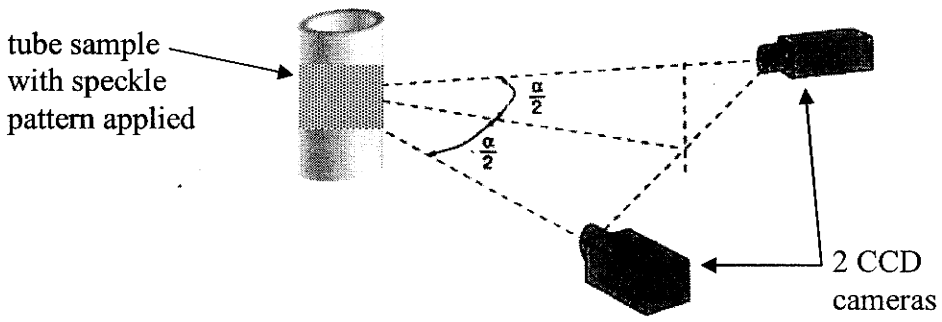

Figure 3.29 Positioning of two CCD cameras for use with ARAMIS strain measurement system.

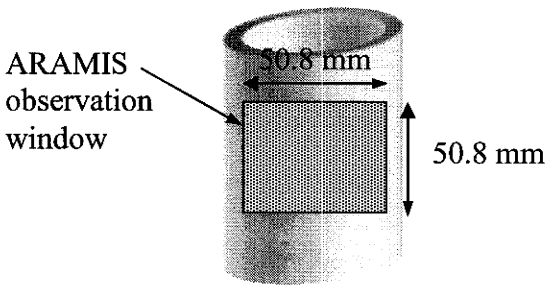

Figure 3.30 Dimensions of observation window used for strain measurement with ARAMIS optical system.

This chapter outlined the test methods used to determine the true stress-strain behaviour of the OPP along its principal directions in both tension and compression. A ring compression test was used to determine the axial compressive properties while a square cross-sectional specimen machined from the wall thickness of the tube was used to obtain hoop compressive properties. In addition, a standard tensile specimen machined along the axial direction of the tube and the ring hoop tension tests were used to determine the axial tensile and hoop tensile properties respectively. Both the uniaxial and biaxial mechanical tests of the OPP tube were used to construct the plastic work contours for the material at various temperatures. The method of construction of the experimental plastic work contours and their use in predicting the forming limits for the tube are presented in Chapter 4.

CHAPTER 4

DEVELOPMENT OF ANALYTICAL MODEL FOR PREDICTION OF FORMING LIMITS OF OPP TUBE

This chapter presents the development of an analytical model for prediction of the forming limits for the OPP tube at different temperatures. The model makes use of the pressure-modified Hill yield criterion as proposed by Caddell et al. (1973). In the present work, the uniaxial stress parameters in the above yield criterion (i.e. T_a, T_θ, C_a and C_θ) have been proposed as a function of temperature of forming and various experimentally based relationships for the uniaxial stress parameters as a function of temperature will be presented. Specifically, T_a will be referred to as the axial tensile stress parameter, T_θ the hoop tensile stress parameter, C_a the axial compressive stress parameter and C_θ the hoop compressive stress parameter. The above-mentioned development, along with the mechanics of axial-feed and internal pressure based tube forming, and a well-established strain localization criterion, is then utilized to obtain forming limits for a range of strain paths of relevance to tube forming. The characteristics of the model are exploited to

reveal trends consistent with the existing data. Unless otherwise stated, all data corresponds to a tube of draw ratio 5.0 tested at a strain rate of 0.0022/second.

4.1 Experimental representation of plastic work contours for OPP tube at elevated temperatures

As a first step towards the development of the analytical model, an assessment of 3 of the most relevant and easy to use yield criteria, presented earlier in Chapter 2 (Section 2.6), was made. Since these criteria needed to be assessed for a range of temperatures, a methodology for plotting the experimental orientation (and temperature) dependent stress data, from the uniaxial and biaxial testing of the tube, was devised using the notion of contours of plastic work (i.e., area under the appropriate stress-strain curve) in stress space. For example, the axial tensile stress parameter, T_a, corresponds to the area under the axial stress versus axial strain curve for a plastic work of 1.25×10^5 N/m^2 (Figure 4.1). The other three uniaxial stress parameters, namely axial compression, hoop tension and hoop compression corresponding to the above plastic work value are similarly plotted in Figure 4.1. This data is obtained from OPP tubes that were tested uniaxially in the axial and hoop directions at 140°C.

It is important to make note that the above methodology makes use of the area under the true stress-strain curves generated from the uniaxial mechanical tests, rather than from the plastic stress-strain curves. Therefore, total work, rather than plastic work, is being calculated. However, since it is assumed that the elastic strains are small and can be taken to occur at constant volume (refer to Section 3.2), total work and plastic work

are taken to be equal. Therefore, from this point forward, the area under the uniaxial true stress-strain curves will correspond to a given plastic work value.

In order to plot the biaxial stress points corresponding to a given plastic work contour, the results from experimental tube forming tests were employed. The description of the tube forming test rig as well as the test procedure with the use of the ARAMIS optical strain measurement system were outlined in detail towards the end of Chapter 3 and will not be discussed here. However, the process details of the five tube forming tests performed at 140°C are summarized in Table 4.1. Note here that the five tube tests are labeled as stress paths 1-5. Stress paths 1 and 2 were obtained from tube tests involving internal pressurization and axial end feeding, whereas stress paths 3-5 were obtained by pressurizing the tube without any axial feeding.

The procedure for obtaining biaxial stress points along a given stress path, with each point corresponding to a value of plastic work can be illustrated with the help of Figure 4.2 and 4.3. Figure 4.2 is a flowchart outlining the methodology for the determination of the continuous biaxial stress path corresponding to a given tube forming test. Figure 4.3 describes the method of determination of biaxial stress points along a biaxial stress path corresponding to increasing levels of plastic work.

Figure 4.4 shows all experimental points from uniaxial and biaxial test data. A closed loop joining all experimental points can be referred to as the plastic work contour corresponding to a plastic work value of 1.25×10^5 N/m^2. A similar procedure is utilized

for the construction of the plastic work contours for various discrete levels of plastic work from continuous uniaxial and biaxial stress-strain data.

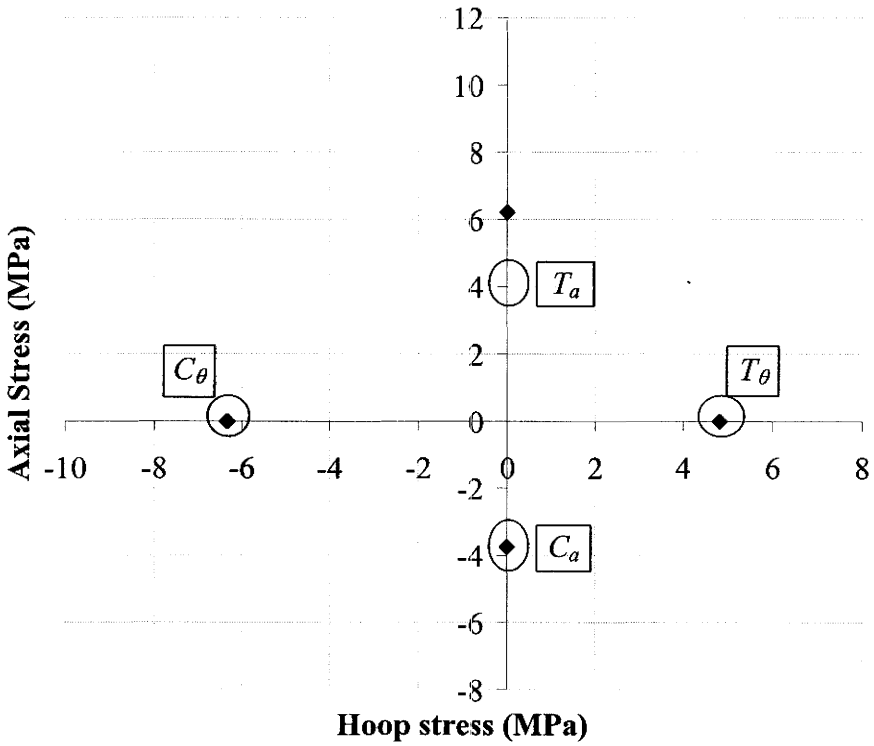

Figure 4.1 Experimental plastic work contour for OPP tube tested at 140°C and corresponding to a plastic work of 1.25×10^5 N/m^2. Note only uniaxial stresses making up this plastic work contour are shown.

Stress path number	Initial free section length of tube (mm)	Pressure increase rate (Pa/second)	Axial end feed (mm)	Feed rate (mm/second)
1	66	2.76×10^4	19	0.2
2	66	2.76×10^4	12	0.2
3	66	2.76×10^4	-	-
4	38	2.76×10^4	-	-
5	15	2.76×10^4	-	-

Table 4.1 Tube forming test specifications for OPP tube tested at 140°C.

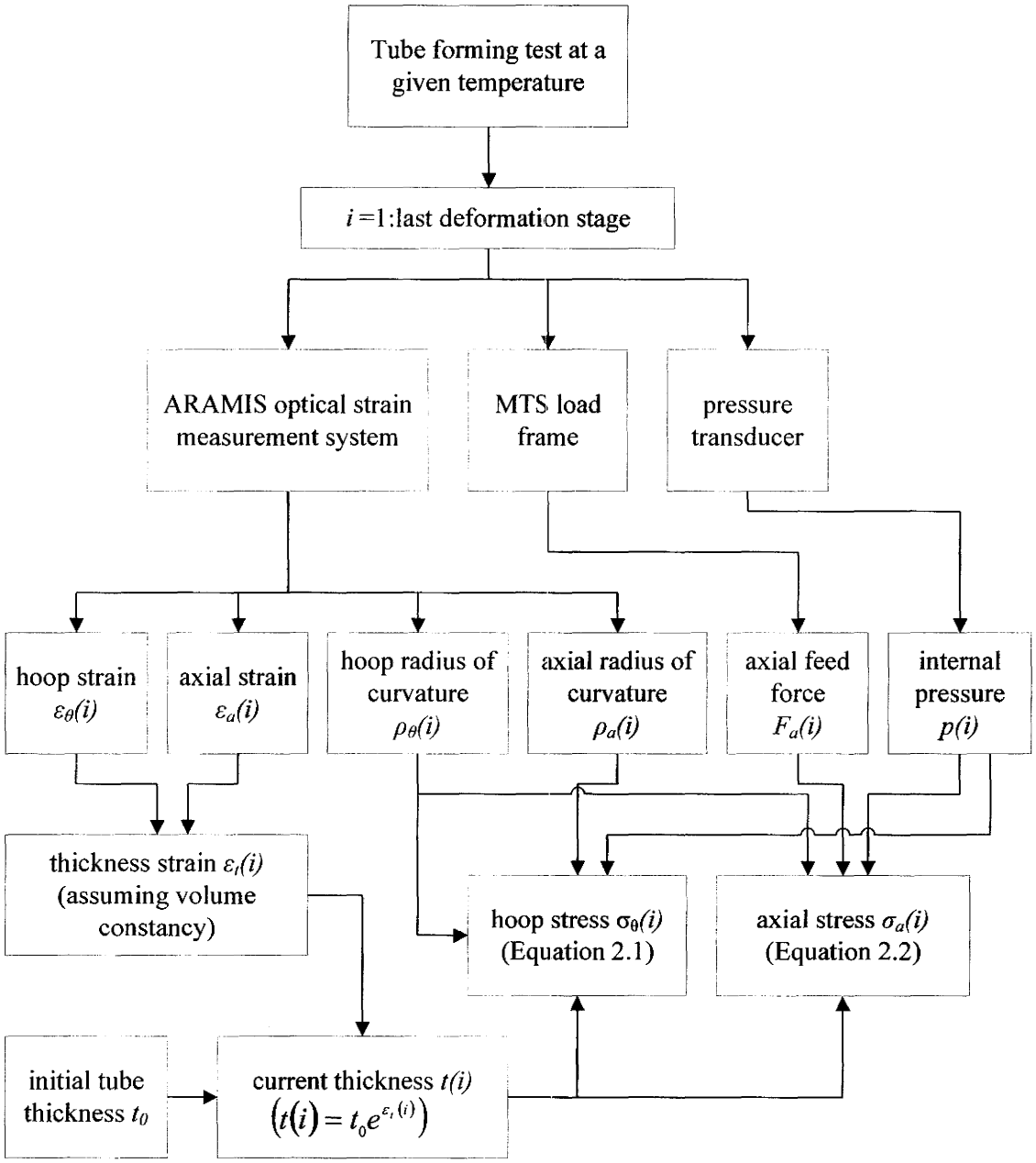

Figure 4.2 Method of determination of continuous biaxial stress path for a tube forming test.

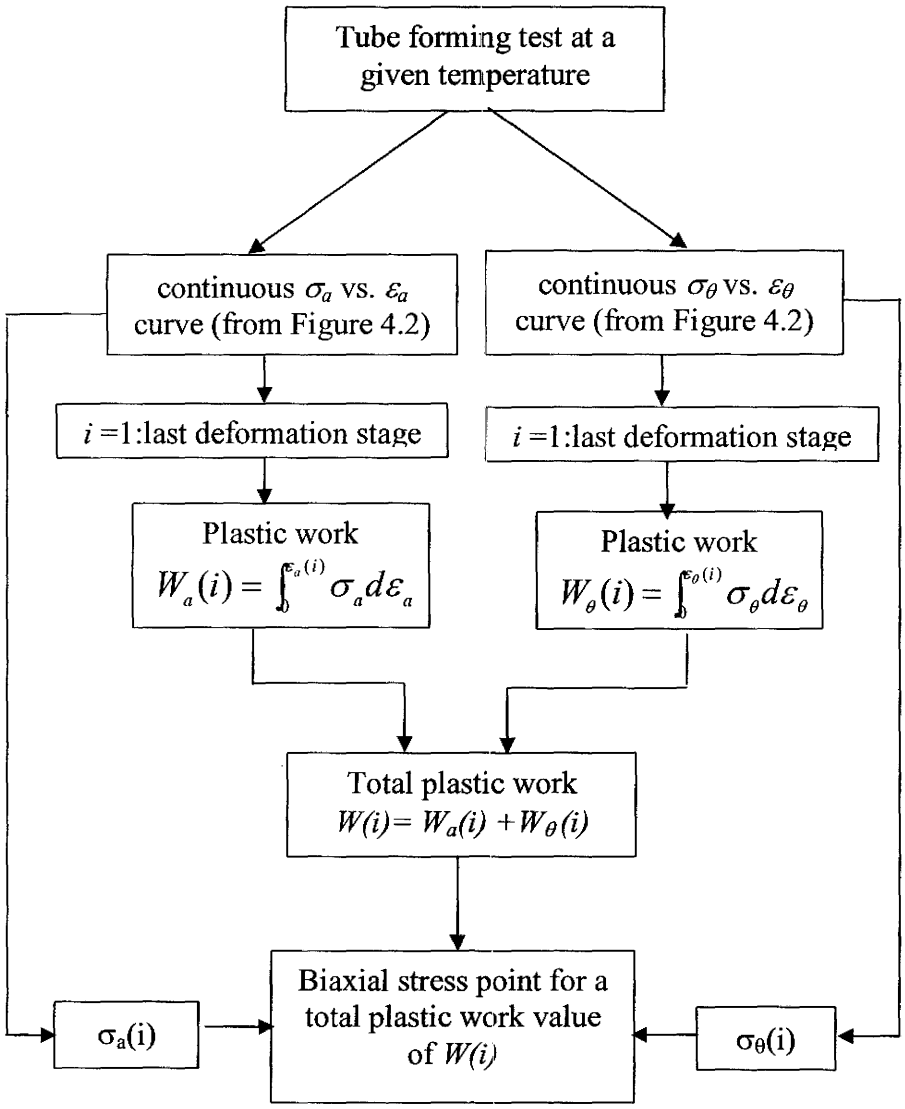

Figure 4.3 Method of determination of biaxial stress point along a biaxial stress path corresponding to a given plastic work value.

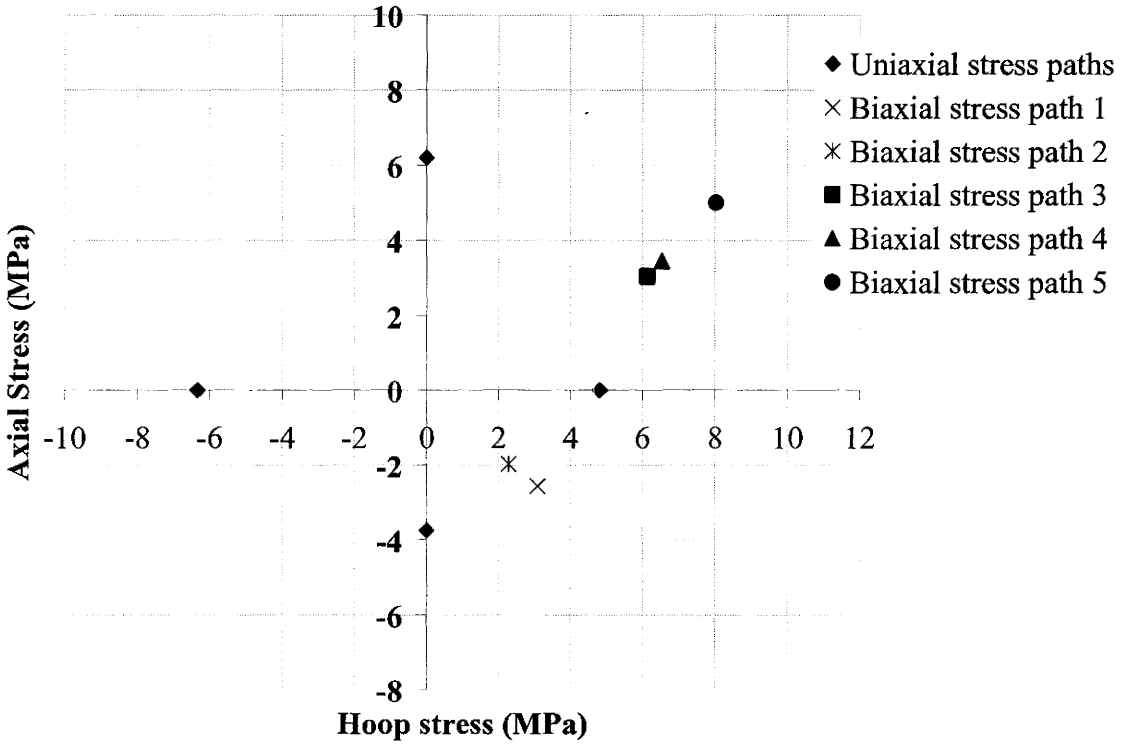

Figure 4.4 Experimental uniaxial and biaxial stress points for OPP tube tested at 140°C and corresponding to a plastic work of 1.25×10^5 N/m^2.

4.2 Comparison of theoretical yield criteria for use in prediction of plastic work contours for OPP tube

In order to select an appropriate yield criterion for the prediction of the plastic work contours for the OPP tube, the fit of three theoretical yield criteria to the experimental plastic work contour given in Figure 4.4 will be compared. The three yield criteria that will be compared here are the pressure-modified Mises criterion, the Hill anisotropic criterion and the pressure-modified Hill criterion by Caddell, Raghava, and Atkins. All three of these criteria were reviewed earlier in Chapter 2.

There is some subjectivity in fitting the Hill anisotropic and pressure-modified Mises yield criteria to the data points shown in Figure 4.4. There are at least two different ways that it could be done as described in Table 4.2. Method 1, for example, involves constraining the plastic work contour in such a way that it passes through the axial tension and hoop (or thickness) compression data points while it is unconstrained elsewhere. Similarly, method 2 involves constraining the plastic work contour with respect to axial compression and hoop tension and keeping it free elsewhere. The resulting fitted curves from the two methods are shown in Figures 4.5 and 4.6. Clearly, from Figure 4.5, the pressure-modified Hill captures both the uniaxial and biaxial yield behaviour of the OPP tube quite accurately. However, the pressure-modified Mises and Hill anisotropic criteria provide poor representations of the experimental data. Figure 4.6, based on method 2, seems to provide slightly better agreement of the pressure-modified Mises and Hill anisotropic criteria to the experimental data but none are as satisfactory as the pressure-modified Hill yield criterion. Therefore, the pressure-modified Hill criterion was subsequently utilized in the prediction of the plastic work contours for the OPP tube as the material work hardened from zero strain (considered the yielding point).

Mechanical test	Uniaxial stress parameter (MPa)	Uniaxial stress parameter used in method 1 fitting			Uniaxial stress parameter used in method 2 fitting		
		Pressure-modified Hill	Hill anisotropic	Pressure-modified Mises	Pressure-modified Hill	Hill anisotropic	Pressure-modified Mises
Axial tension	6.2	x	x	x	x		
Hoop tension	4.81	x			x	x	x
Axial compression	3.75	x			x	x	x
Hoop (thickness) compression	6.34	x	x	x	x		

Table 4.2 Uniaxial stress parameters used to define three theoretical yield criteria in method 1 and method 2 fitting.

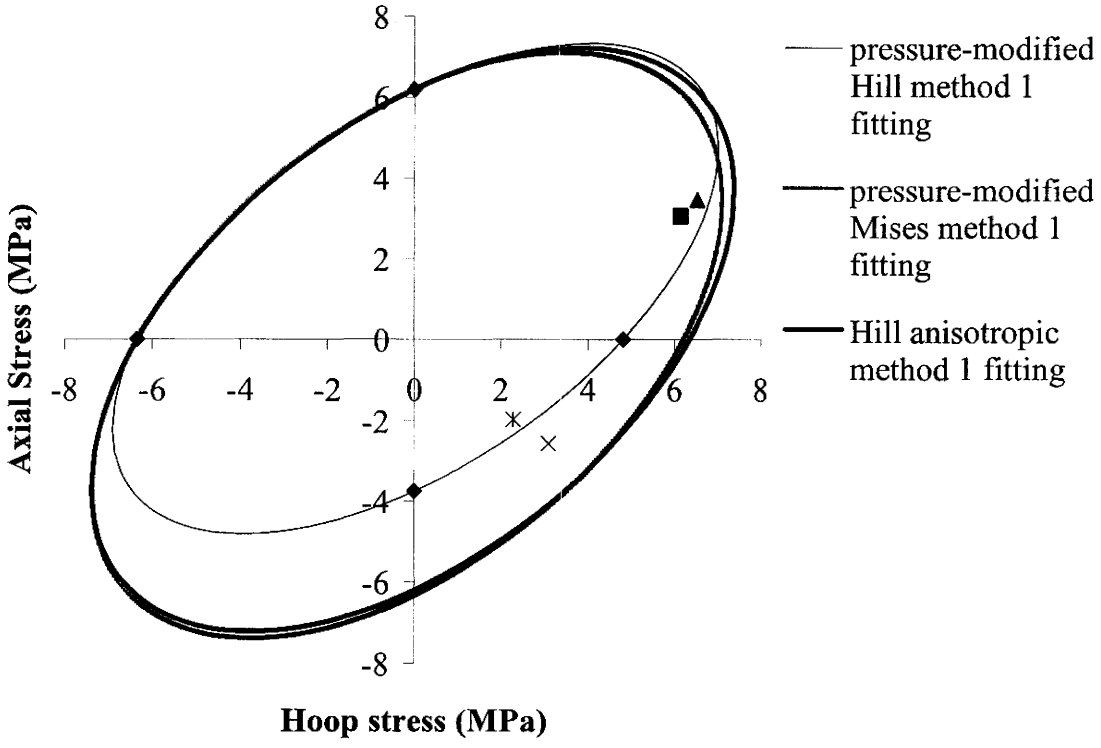

Figure 4.5 Experimental plastic work contour for OPP tube tested at 140°C (as given in Figure 4.2) and the fit of the three theoretical yield criteria listed in Table 4.2 under method 1 fitting.

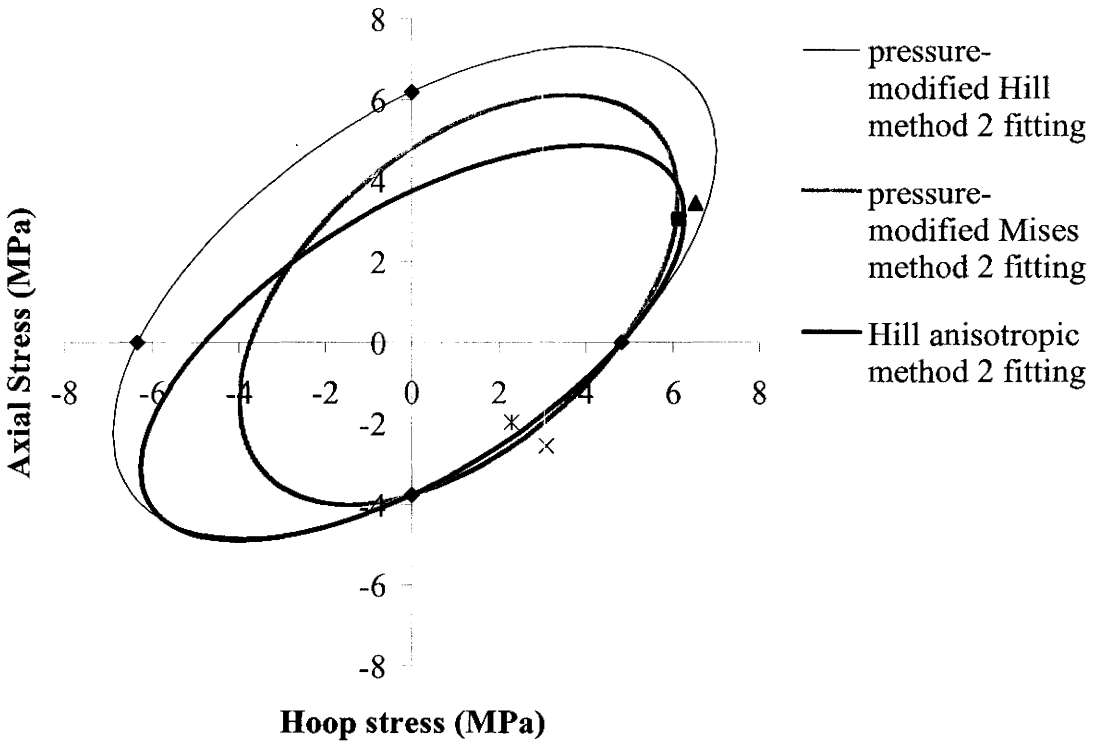

Figure 4.6 Experimental plastic work contour for OPP tube tested at 140°C (as given in Figure 4.2) and the fit of the three theoretical yield criteria listed in Table 4.2 under method 2 fitting.

4.3 Prediction of plastic work contours for OPP tube using pressure-modified Hill yield criterion

Based on a review of the literature presented in Chapter 2, related to the application of the pressure-modified Hill yield criterion for characterizing the biaxial yielding of various oriented polymers, the fit of the theoretical yield criterion to only the initial yield surface was examined. However, in order to simulate the large strain forming of these materials, at various temperatures, there is a need to predict the plastic work contours as the material work hardens. As described in Chapter 3, the oriented polypropylene tubes harden anisotropically, where hardening along the axial direction dominates.

In order to predict the plastic work contours, at a given temperature and strain rate, the plastic work contour concept described in Section 4.1 was used. Once the values of T_a, T_θ, C_a, and C_θ, for a given plastic work are known, Equations (2.19) – (2.22) can be used to calculate the corresponding values of H, F, K_a and K_θ. Finally, Equation (2.18) can be used to construct the theoretically predicted plastic work contour corresponding to a given plastic work value. More accurately stated, then, the values of H, F, K_a and K_θ become a function of plastic work such that:

$$H, F, K_a, K_\theta = f\left(T_a, T_\theta, C_a, C_\theta\right) = f(W) \tag{4.1}$$

Figure 4.7 shows the contours for various levels of plastic work for the OPP tube using the method described above. For simplicity, only values of the uniaxial tensile and compressive stresses along the axial and hoop direction corresponding to a given amount

of plastic work were used to construct each contour and are given by the diamond shaped markers. The solid line passing through the uniaxial data for each plastic work contour corresponds to the fit obtained with the pressure-modified Hill criterion given in Equation (2.18).

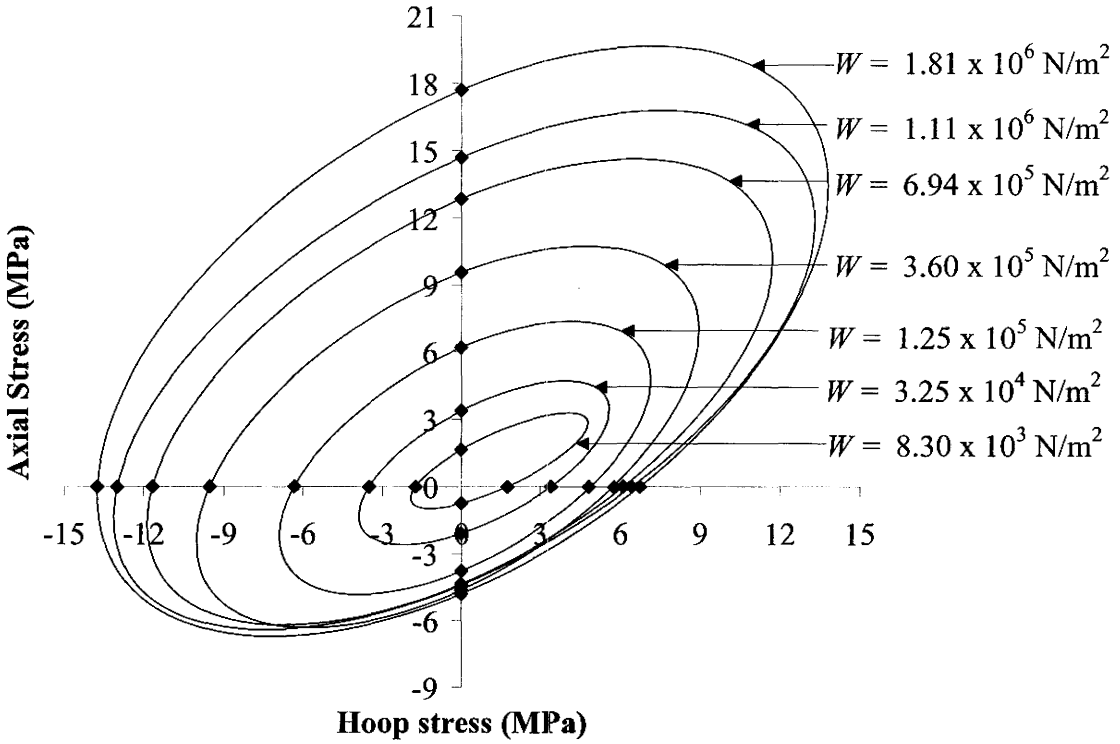

Figure 4.7 Experimental plastic work contours for OPP tube tested at 140°C and constructed using uniaxial data points only. Also shown are the predicted contours using the pressure-modified Hill criterion.

In order to check the validity of the predicted plastic work contours, given in Figure 4.7, for biaxial stress states, the results from the experimental tube forming tests (refer to Table 4.1) were employed once again. Figure 4.8 shows the predicted contours for various levels of plastic work (as in Figure 4.7) as well as the experimental stress paths obtained from the five tube forming tests given in Table 4.1.

Figures 4.9 to 4.13 compare the predicted contours (as in Figure 4.7) with each of the individual experimental biaxial stress paths given in Figure 4.8. Each biaxial stress path is shown separately for clarity. The markers along each stress path indicate the axial and hoop stress combination corresponding to the same plastic work values for which the predicted contours were generated. In general, good agreement exists between the predicted plastic work contours and the biaxial stress points taken at an equivalent value of plastic work. One should also make note of the significantly non-linear shape of all of the stress paths except for stress path 3, which is nearly linear. The non-linearity of stress paths 1 and 2, occurring early on in the deformation, can be attributed to the axial feeding of the tube ends.

Figure 4.14 compares the predicted plastic work contours and experimentally obtained contours for OPP tube tested at 110°C and corresponding to various levels of plastic work. Good agreement also exists between the predicted contours and the results of the biaxial tube test at 110°C.

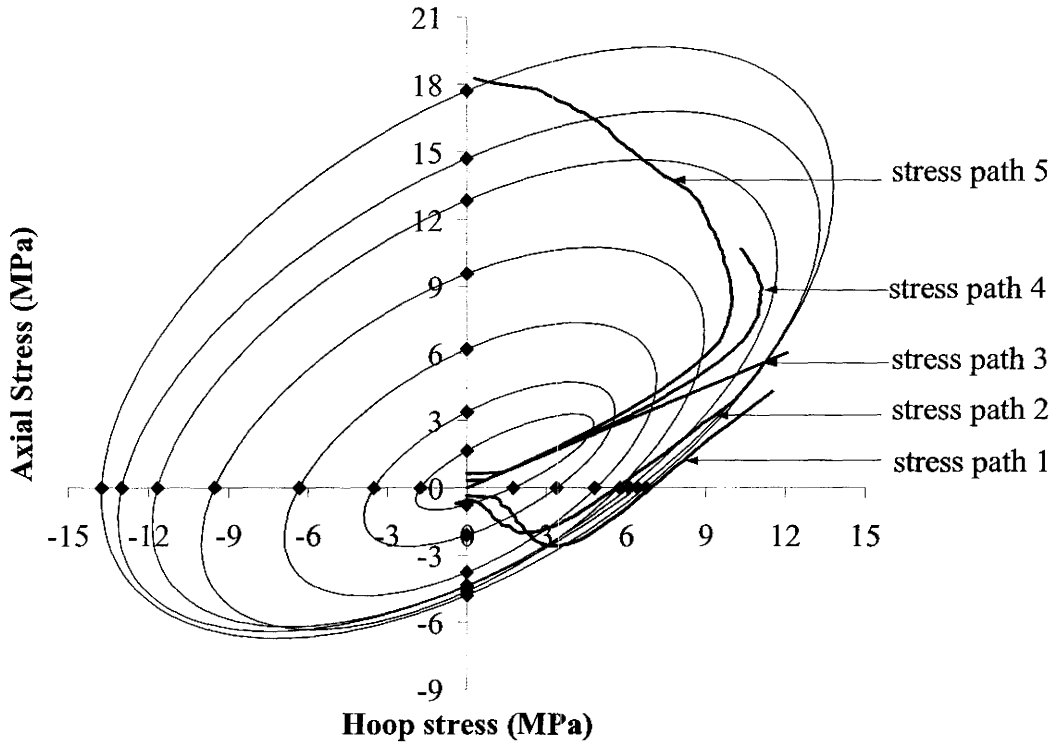

Figure 4.8 Five stress paths obtained from tube forming tests detailed in Table 4.1 overlaid on Figure 4.7.

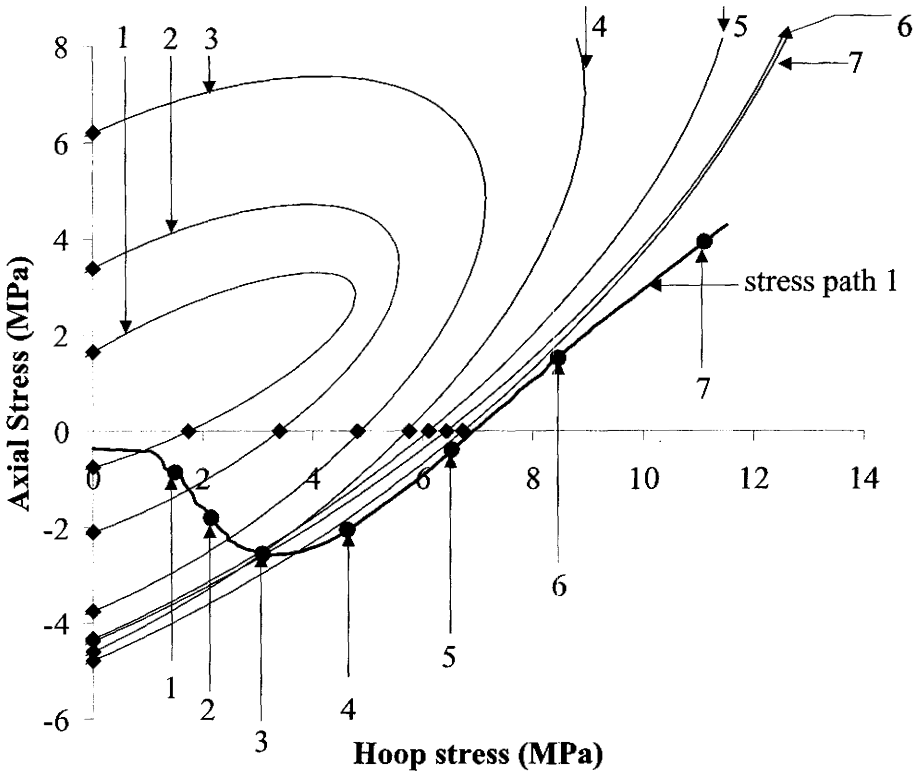

Number	Plastic work value (N/m^2)
1	8.30×10^3
2	3.25×10^4
3	1.25×10^5
4	3.60×10^5
5	6.94×10^5
6	1.11×10^6
7	1.81×10^6

Figure 4.9 Comparison of predicted plastic work contours and experimentally obtained contours (using uniaxial data and stress path 1 from tube forming test) for OPP tube tested at 140°C.

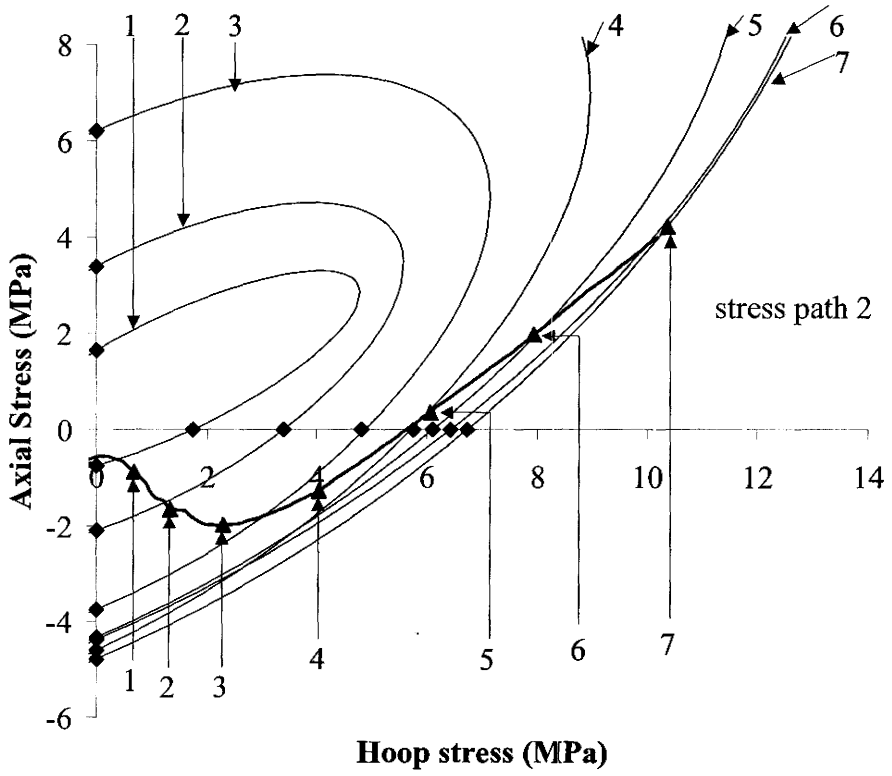

Number	Plastic work value (N/m^2)
1	8.30×10^3
2	3.25×10^4
3	1.25×10^5
4	3.60×10^5
5	6.94×10^5
6	1.11×10^6
7	1.81×10^6

Figure 4.10 Comparison of predicted plastic work contours and experimentally obtained contours (using uniaxial data and stress path 2 from tube forming test) for OPP tube tested at 140°C.

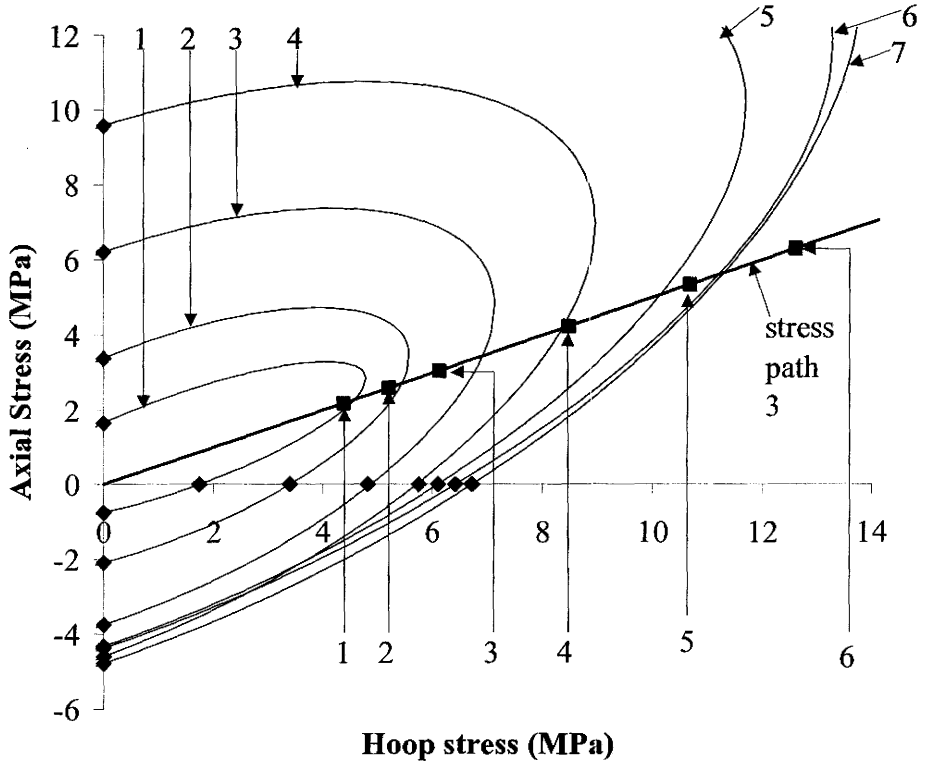

Number	Plastic work value (N/m^2)
1	8.30×10^3
2	3.25×10^4
3	1.25×10^5
4	3.60×10^5
5	6.94×10^5
6	1.11×10^6
7	1.81×10^6

Figure 4.11 Comparison of predicted plastic work contours and experimentally obtained contours (using uniaxial data and stress path 3 from tube forming test) for OPP tube tested at 140°C.

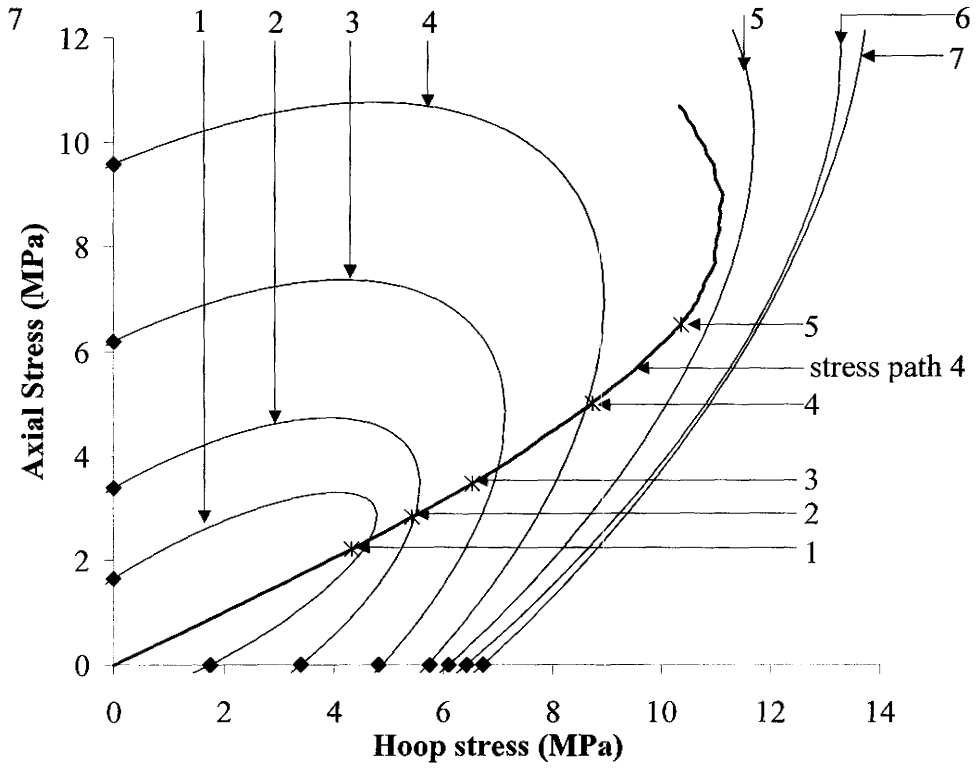

Number	Plastic work value (N/m^2)
1	8.30×10^3
2	3.25×10^4
3	1.25×10^5
4	3.60×10^5
5	6.94×10^5
6	1.11×10^6
7	1.81×10^6

Figure 4.12 Comparison of predicted plastic work contours and experimentally obtained contours (using uniaxial data and stress path 4 from tube forming test) for OPP tube tested at 140°C.

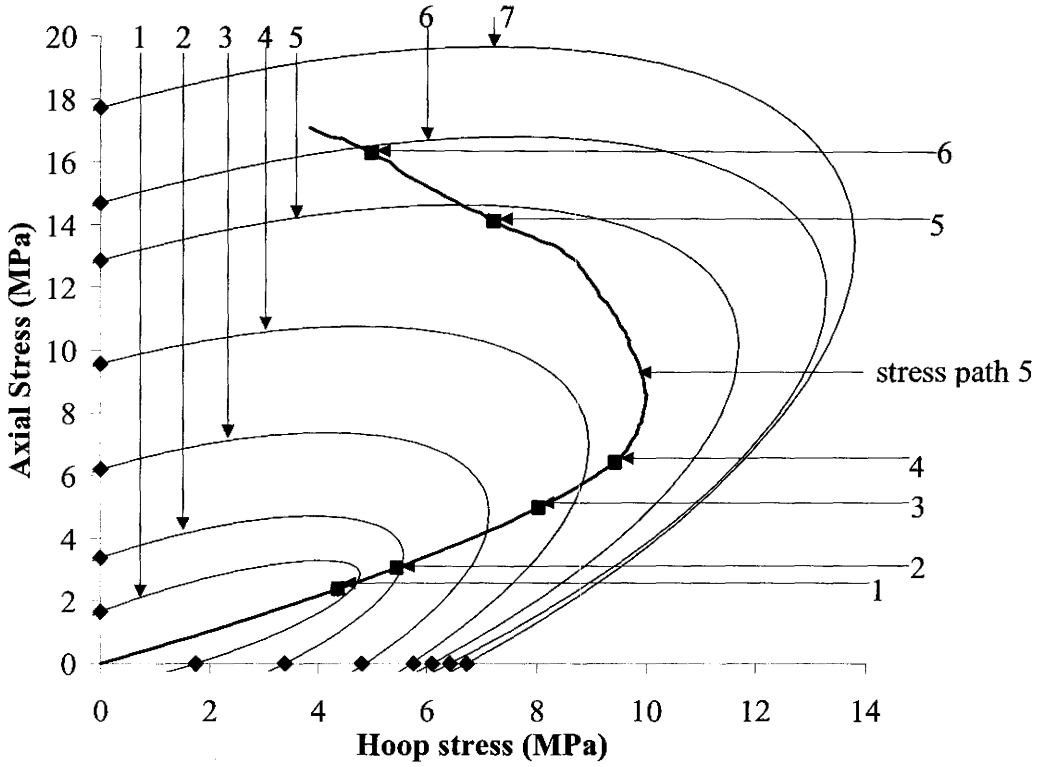

Number	Plastic work value (N/m^2)
1	8.30×10^3
2	3.25×10^4
3	1.25×10^5
4	3.60×10^5
5	6.94×10^5
6	1.11×10^6
7	1.81×10^6

Figure 4.13 Comparison of predicted plastic work contours and experimentally obtained contours (using uniaxial data and stress path 5 from tube forming test) for OPP tube tested at 140°C.

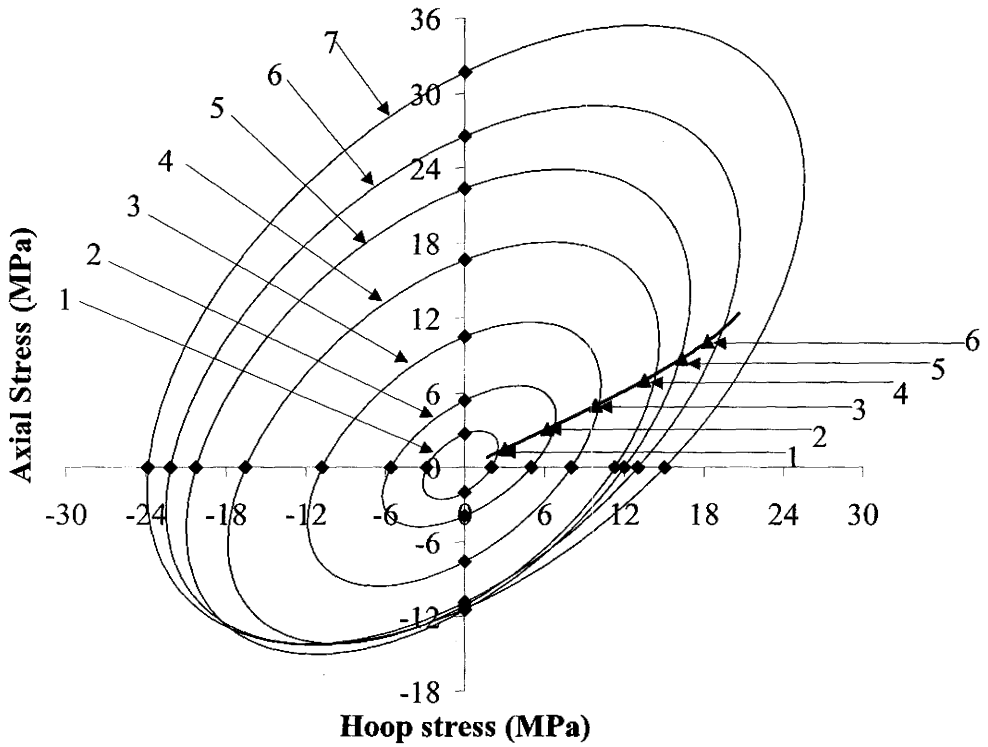

Number	Plastic work value (N/m^2)
1	1.40×10^4
2	5.61×10^4
3	2.18×10^5
4	6.33×10^5
5	1.27×10^6
6	1.95×10^6
7	3.14×10^6

Figure 4.14 Comparison of predicted plastic work contours and experimentally obtained contours for OPP tube tested at 110°C.

4.4 Prediction of temperature dependent plastic work contours for OPP tube

4.4.1 Approach 1 - prediction of temperature dependent uniaxial stress parameters in pressure-modified Hill criterion

In this section, temperature dependent plastic work contours of increasing magnitude are obtained. This is accomplished by analyzing the temperature dependency of each of the uniaxial stress parameters in the pressure-modified Hill criterion, i.e. T_a, T_θ, C_a and C_θ corresponding to a given value of plastic work. The results are shown in Figures 4.15 to 4.21 for seven different plastic work contours of increasing magnitude. Interestingly, a linear relationship between each of the uniaxial stress parameters and temperature in the range 110°C and 150°C is observed in almost all cases. The data was fitted with a linear least square curve fitting procedure to extract the fit parameters for all of the experimental data. The fitted lines, the fit parameter values, and the quality of fit in terms of the correlation coefficient (or R square value) are presented in each of the figures mentioned above. It is to be noted that the R square coefficients are close to 1 for all of the cases considered.

It is to be noted that the values of T_a and C_θ are approximately equal at the temperatures considered and for plastic work values ranging from 4.20×10^6 N/m^2 to 1.25×10^6 N/m^2. In an attempt to reduce the number of experiments for defining the temperature dependent plastic work contours for the OPP tube, as well as the number of experimentally determined parameters, a simple case study was performed. Firstly, it was assumed that value of T_a was equal to C_θ at the temperatures considered and

corresponding to the range of plastic work values up to $1.67x10^6$ N/m^2. In addition, the value of the each of the uniaxial stress parameters (in the pressure-modified Hill criterion) at 110°C and 150°C (determined experimentally) was used to predict the value of the same parameter at 130°C and 140°C assuming a linear relationship between temperature and the parameter for a given plastic work value. Table 4.3 illustrates the method for the case of the plastic work equal to $4.20x10^5$ N/m^2.

The method described above was used to predict the values of the uniaxial stress parameters at 130°C and then, subsequently, to predict the plastic work contours at this temperature for the previous set of plastic work values. These plastic work contours based on predictions using linear fit to experimental data (at 110°C and 150°C) are compared with the predictions using experimental data (at 130°C) in Figures 4.22-4.28. In general, good agreement can be observed between the predicted and measured contours for most of the plastic work values. However, as the plastic work value increases (refer to Figures 4.27 and 4.28), the agreement between the two contours is slightly poorer. However in the first and fourth quadrants of the stress diagram (forming regime), the agreement can still be considered acceptable.

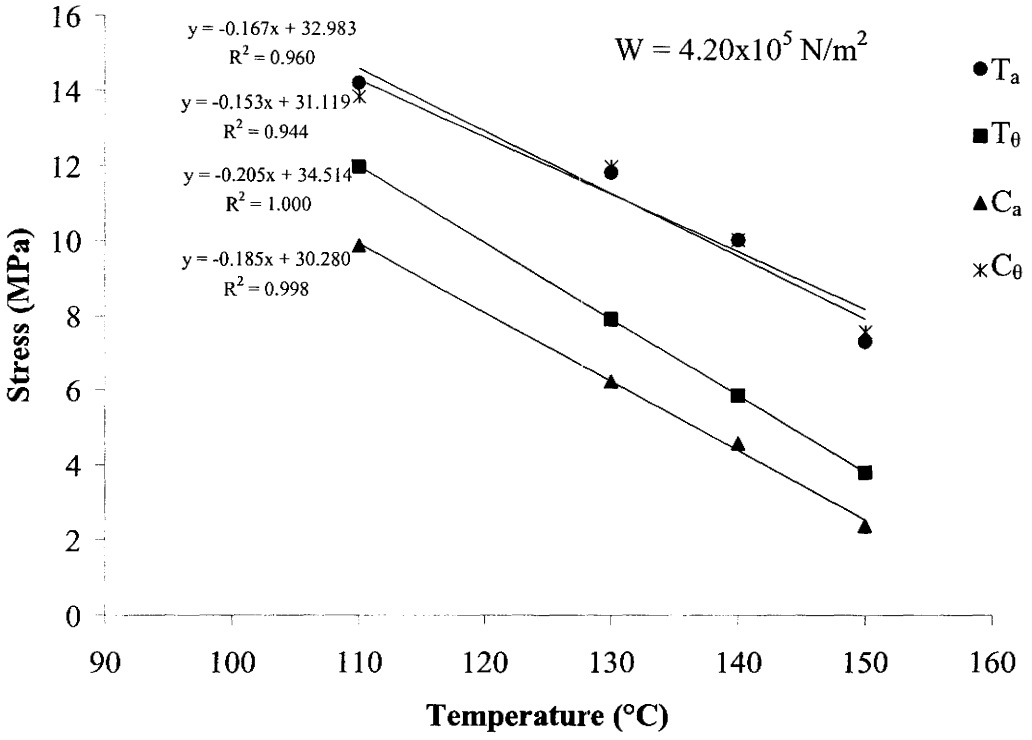

Figure 4.15 Effect of temperature on pressure-modified Hill uniaxial stress parameters corresponding to a plastic work of 4.20×10^5 N/m^2.

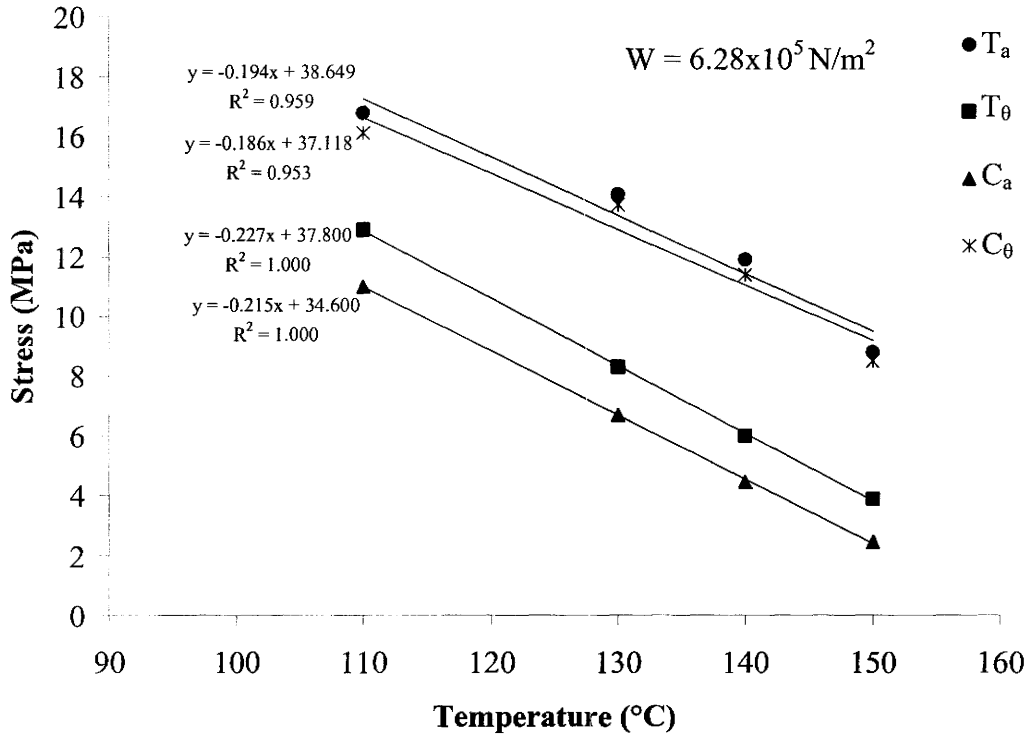

Figure 4.16 Effect of temperature on pressure-modified Hill uniaxial stress parameters corresponding to a plastic work of 6.28×10^5 N/m^2.

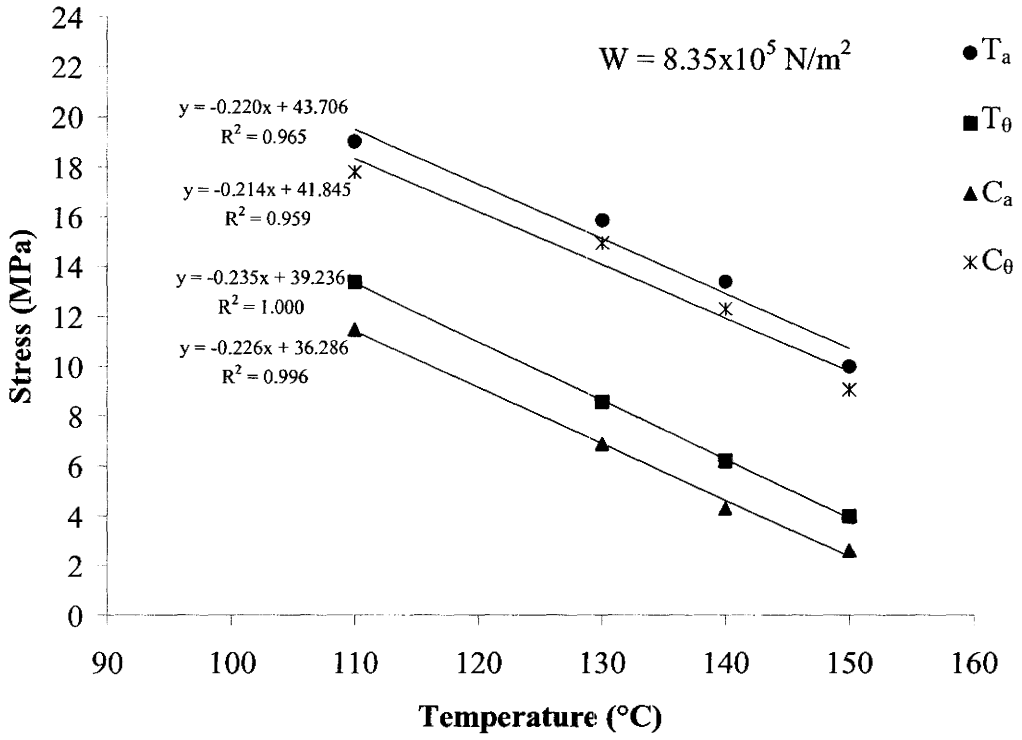

Figure 4.17 Effect of temperature on pressure-modified Hill uniaxial stress parameters corresponding to a plastic work of 8.35×10^5 N/m^2.

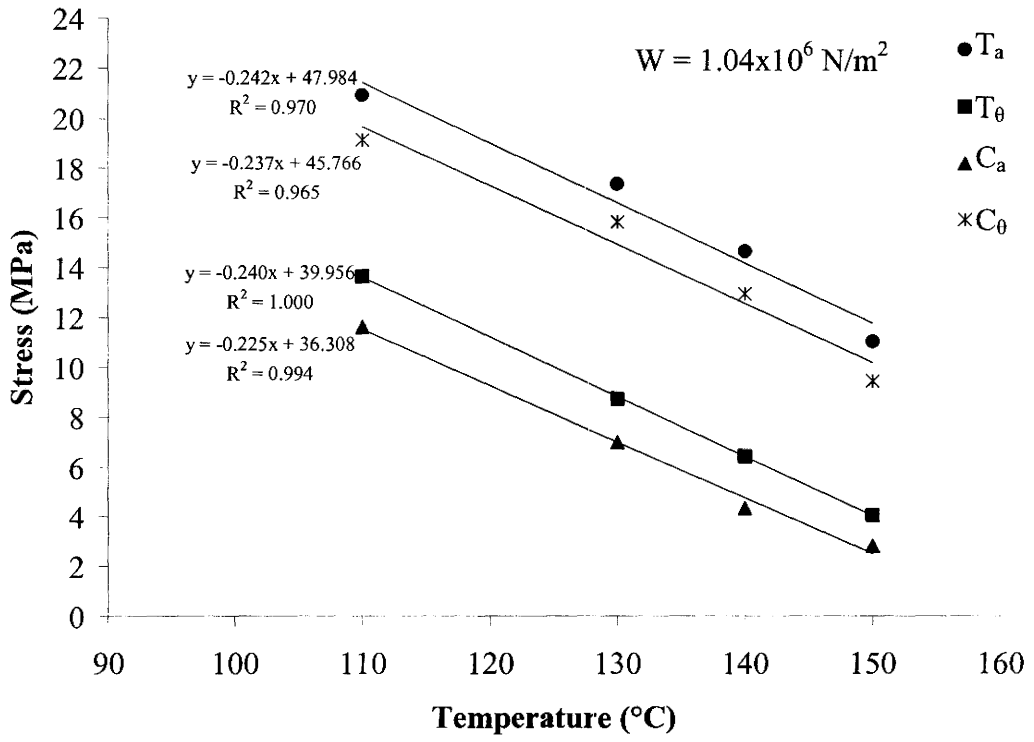

Figure 4.18 Effect of temperature on pressure-modified Hill uniaxial stress parameters corresponding to a plastic work of 1.04×10^6 N/m^2.

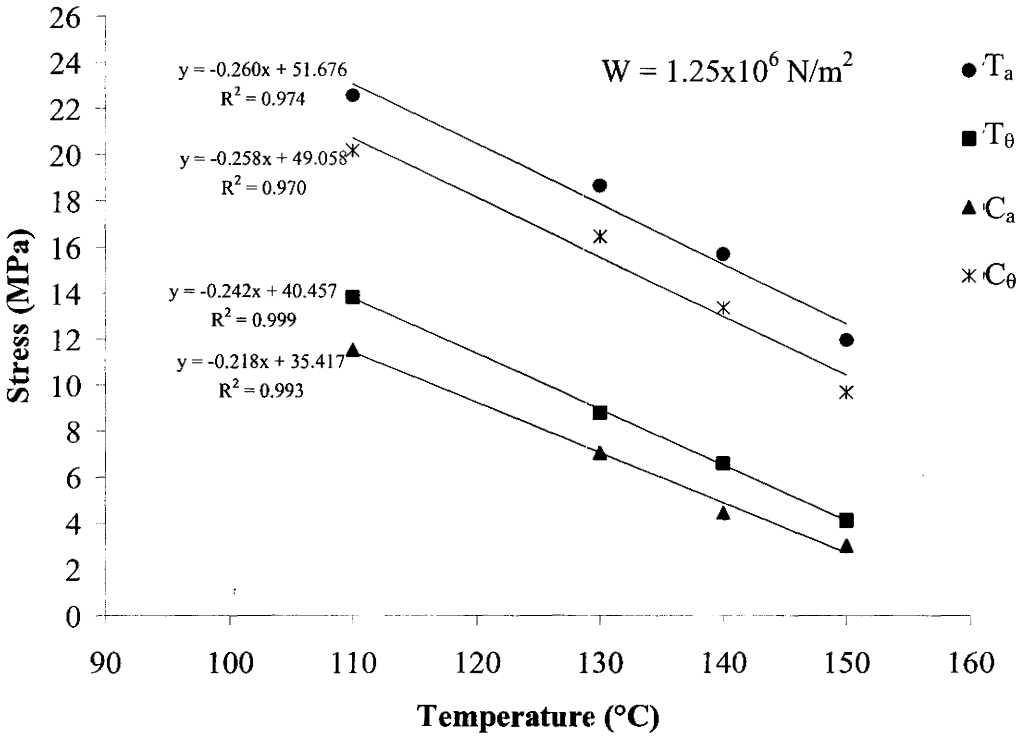

Figure 4.19 Effect of temperature on pressure-modified Hill uniaxial stress parameters corresponding to a plastic work of 1.25×10^6 N/m^2.

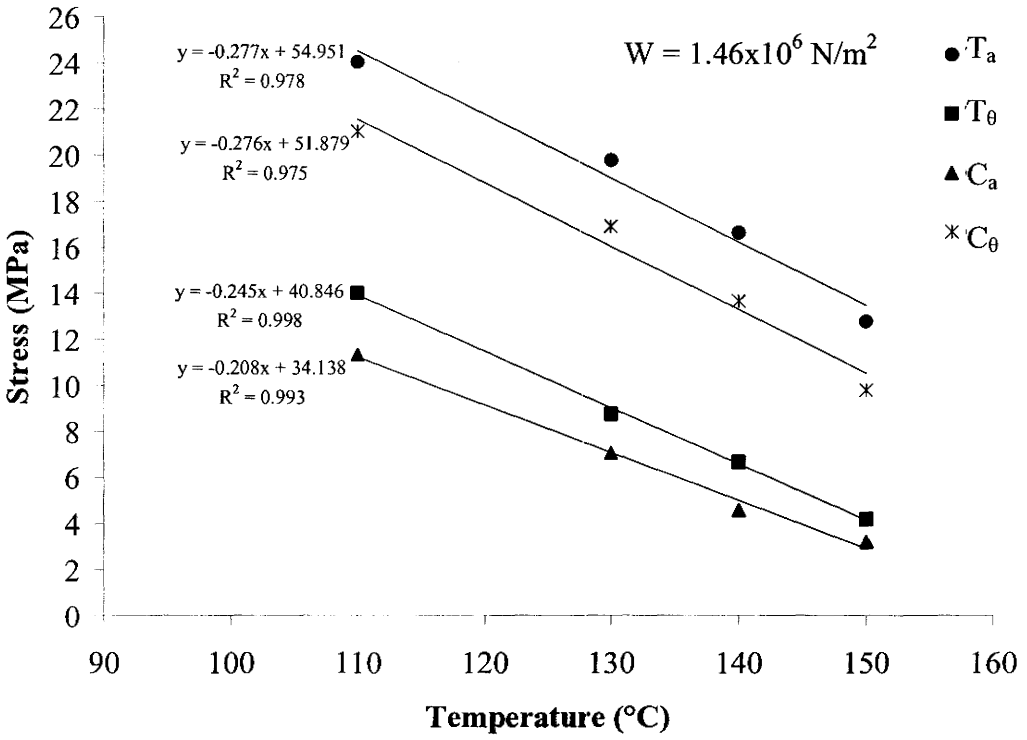

Figure 4.20 Effect of temperature on pressure-modified Hill uniaxial stress parameters corresponding to a plastic work of 1.46×10^6 N/m^2.

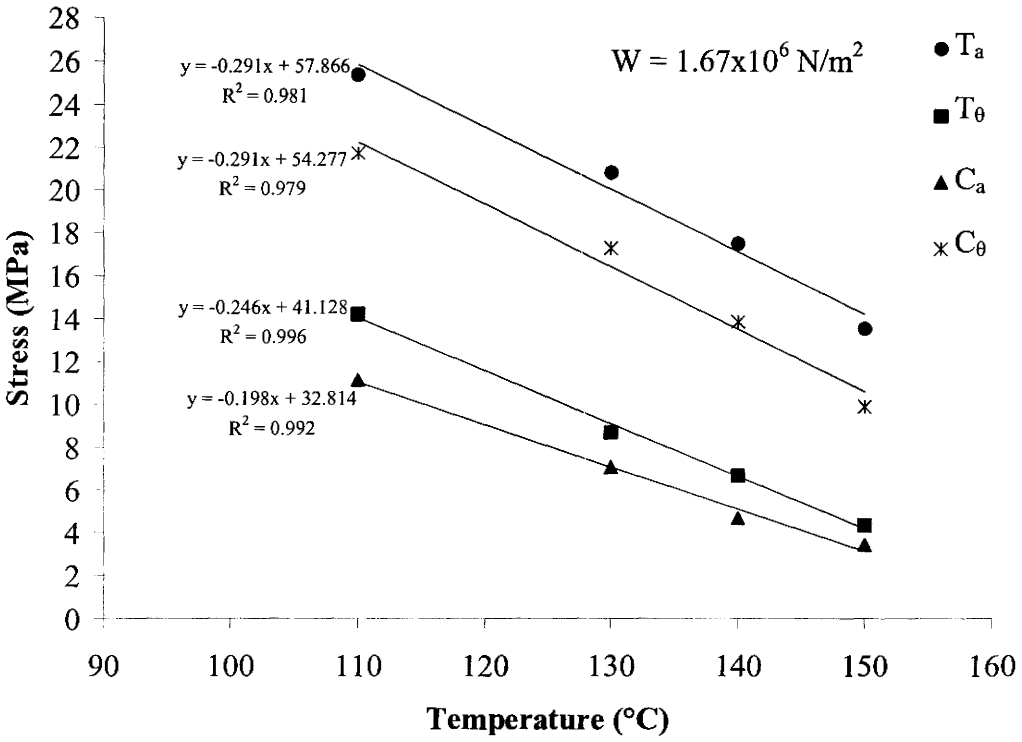

Figure 4.21 Effect of temperature on pressure-modified Hill uniaxial stress parameters corresponding to a plastic work of 1.67×10^6 N/m^2.

Temperature (°C)	Experimentally determined uniaxial stress parameters in pressure-modified Hill criterion				Uniaxial stress parameters (in pressure-modified Hill criterion) based on linear fit to experimentally determined parameters at 110°C and 150°C			
	T_a (MPa)	T_θ (MPa)	C_a (MPa)	C_θ (MPa)	T_{ap} (MPa)	$T_{\theta p}$ (MPa)	C_{ap} (MPa)	$C_{\theta p}$ (MPa)
110	14.20	11.99	9.88	13.84	14.20	11.99	9.88	14.20
130	11.81	7.91	6.23	11.97	10.75	7.89	6.13	10.75
140	10.01	5.85	4.58	10.01	9.02	5.84	4.26	9.02
150	7.30	3.80	2.38	7.56	7.30	3.80	2.38	7.30

Table 4.3 A comparison of experimentally measured pressure-modified Hill uniaxial stress parameters and prediction of the same parameters based on a linear fit to experimentally determined parameters at 110°C and 150°C (corresponding to a plastic work of 4.20×10^5 N/m^2).

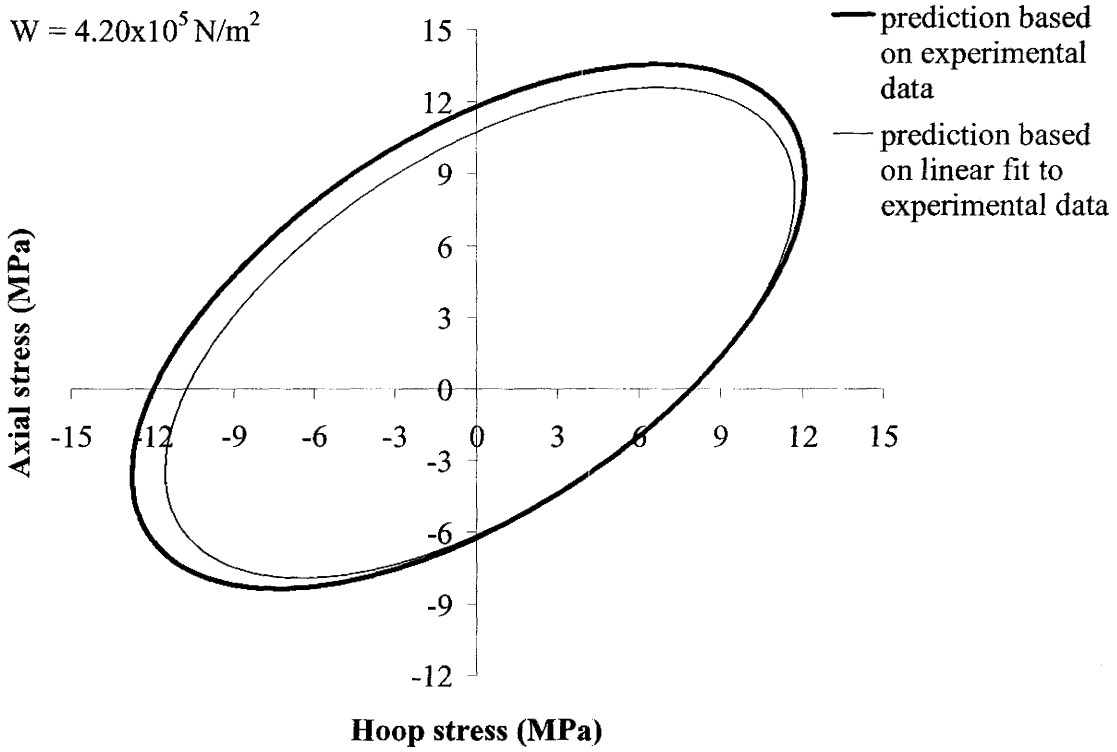

Figure 4.22 Comparison of plastic work contours obtained from fitting of the pressure-modified Hill criterion to the four uniaxial stress parameters, determined experimentally at 130°C (referred to as the "prediction based on experimental data") to that based on a linear interpolation to the uniaxial stress parameters obtained experimentally at 110°C and 150°C (referred to as the "prediction based on linear fit to experimental data"). The comparison is for a plastic work of 4.20×10^5 N/m^2.

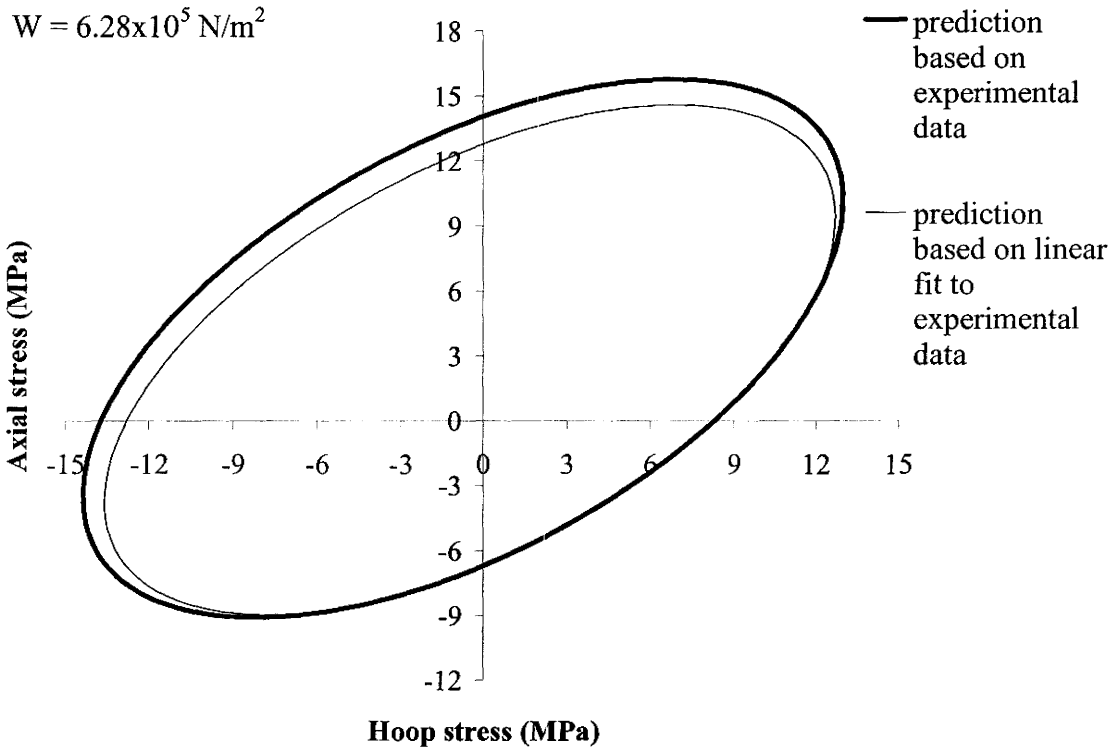

Figure 4.23 Comparison of plastic work contours obtained from fitting of the pressure-modified Hill criterion to the four uniaxial stress parameters, determined experimentally at 130°C (referred to as the "prediction based on experimental data") to that based on a linear interpolation to the uniaxial stress parameters obtained experimentally at 110°C and 150°C (referred to as the "prediction based on linear fit to experimental data"). The comparison is for a plastic work of 6.28×10^5 N/m^2.

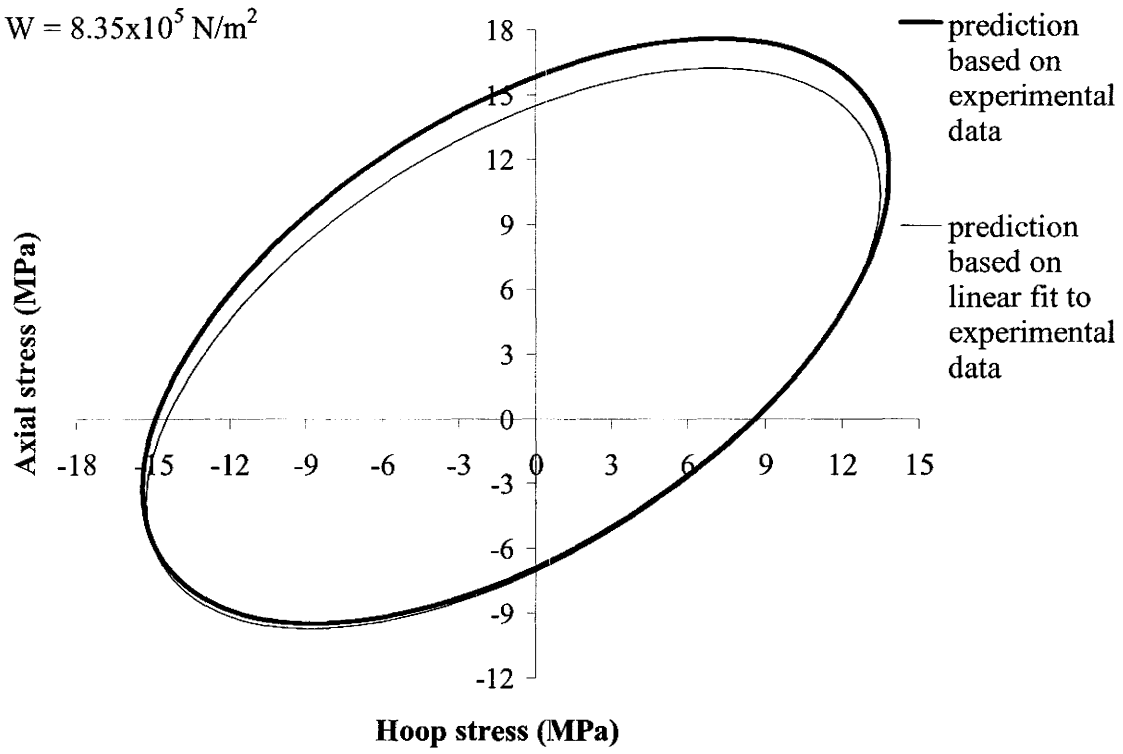

Figure 4.24 Comparison of plastic work contours obtained from fitting of the pressure-modified Hill criterion to the four uniaxial stress parameters, determined experimentally at 130°C (referred to as the "prediction based on experimental data") to that based on a linear interpolation to the uniaxial stress parameters obtained experimentally at 110°C and 150°C (referred to as the "prediction based on linear fit to experimental data"). The comparison is for a plastic work of 8.35×10^5 N/m^2.

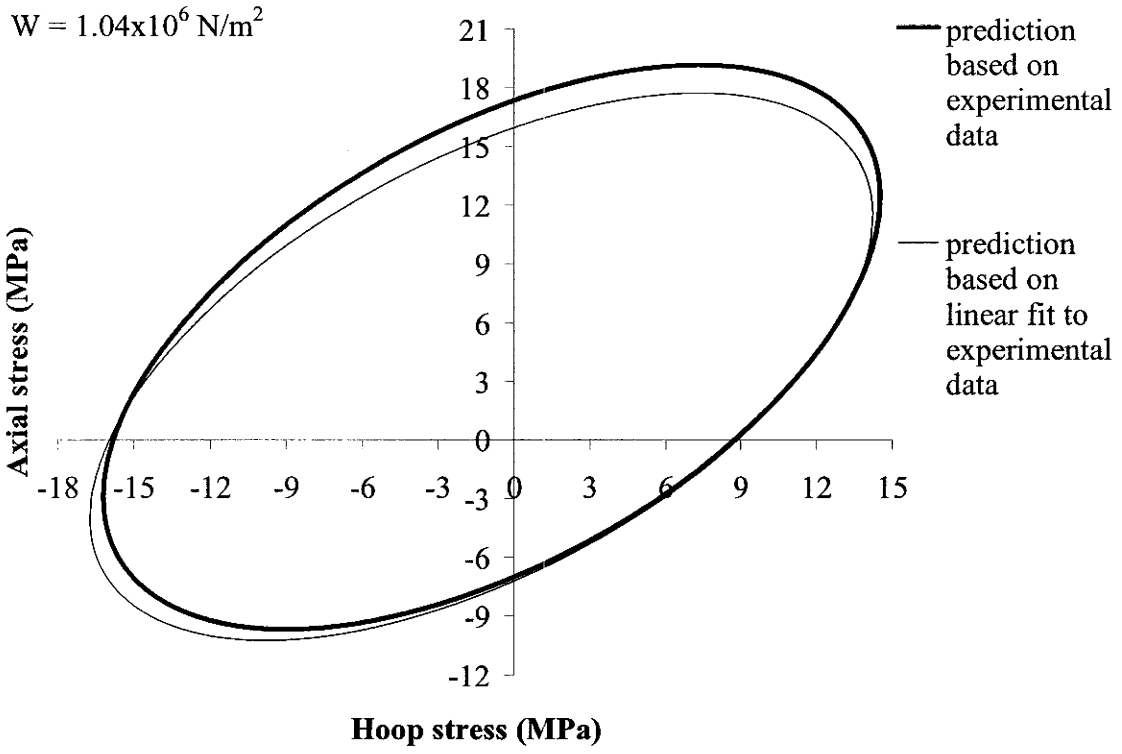

Figure 4.25 Comparison of plastic work contours obtained from fitting of the pressure-modified Hill criterion to the four uniaxial stress parameters, determined experimentally at 130°C (referred to as the "prediction based on experimental data") to that based on a linear interpolation to the uniaxial stress parameters obtained experimentally at 110°C and 150°C (referred to as the "prediction based on linear fit to experimental data"). The comparison is for a plastic work of 1.04×10^6 N/m^2.

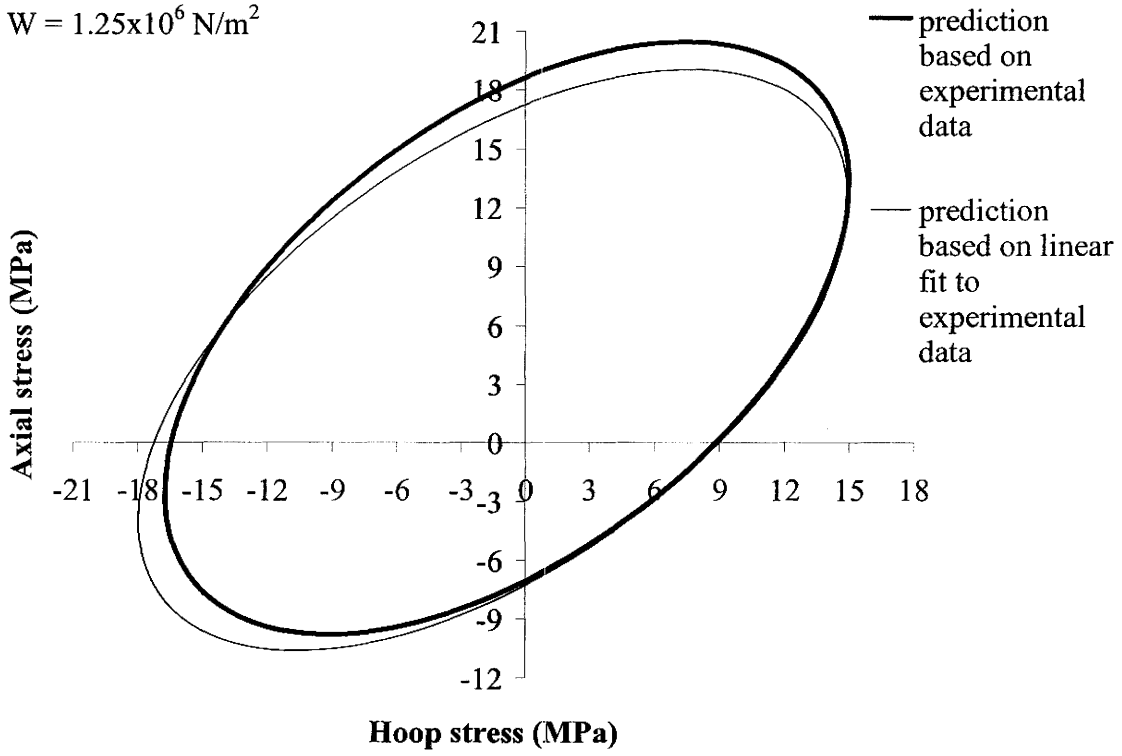

Figure 4.26 Comparison of plastic work contours obtained from fitting of the pressure-modified Hill criterion to the four uniaxial stress parameters, determined experimentally at 130°C (referred to as the "prediction based on experimental data") to that based on a linear interpolation to the uniaxial stress parameters obtained experimentally at 110°C and 150°C (referred to as the "prediction based on linear fit to experimental data"). The comparison is for a plastic work of 1.25×10^6 N/m^2.

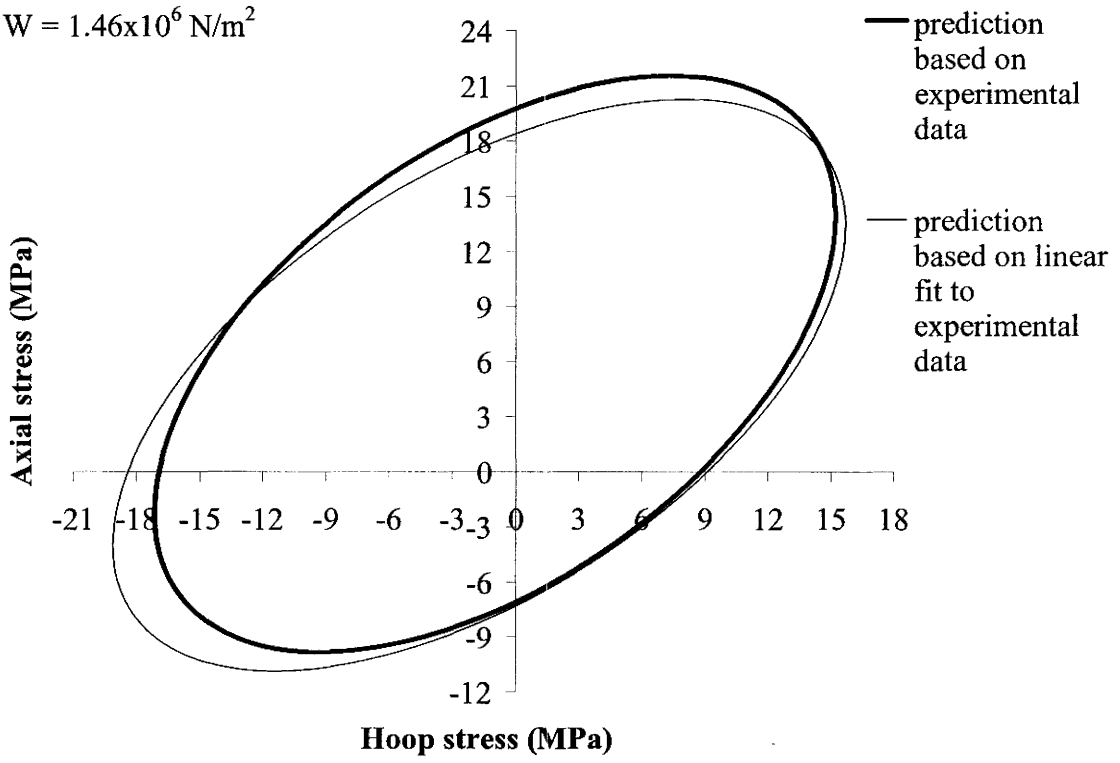

Figure 4.27 Comparison of plastic work contours obtained from fitting of the pressure-modified Hill criterion to the four uniaxial stress parameters, determined experimentally at 130°C (referred to as the "prediction based on experimental data") to that based on a linear interpolation to the uniaxial stress parameters obtained experimentally at 110°C and 150°C (referred to as the "prediction based on linear fit to experimental data"). The comparison is for a plastic work of 1.46×10^6 N/m^2.

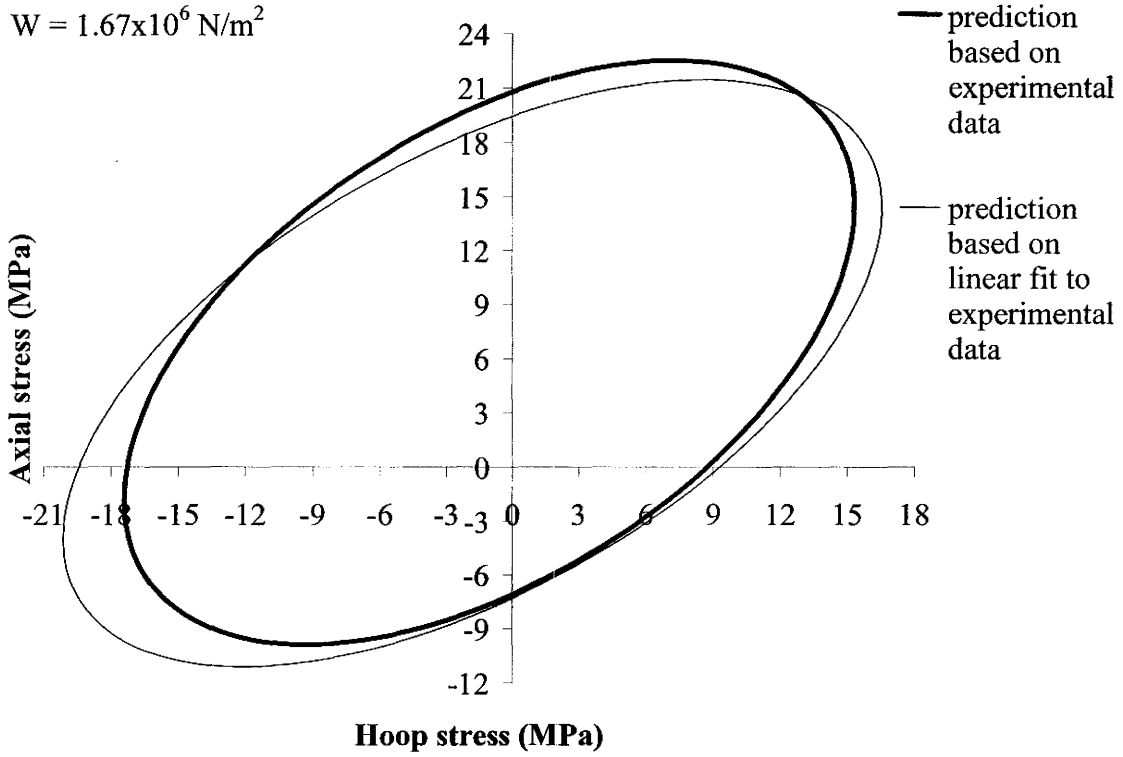

Figure 4.28 Comparison of plastic work contours obtained from fitting of the pressure-modified Hill criterion to the four uniaxial stress parameters, determined experimentally at 130°C (referred to as the "prediction based on experimental data") to that based on a linear interpolation to the uniaxial stress parameters obtained experimentally at 110°C and 150°C (referred to as the "prediction based on linear fit to experimental data"). The comparison is for a plastic work of 1.67×10^6 N/m^2.

One can conclude from the above analysis that a reasonably accurate representation of the plastic work contours for the OPP tube at different temperatures is possible using the pressure-modified Hill criterion and a linear interpolation of the uniaxial stress parameters within this criterion. In addition, the results indicate that one needs to conduct axial tensile, hoop tensile and axial compression tests at the two extremes of typical forming temperatures for OPP tube to obtain all the necessary uniaxial stress parameters to construct the temperature dependent plastic work contours. The underlying assumption here is that the hoop compressive stress parameter can be taken equal to the axial tensile stress parameter. Therefore, a total of 6 constants are required to fully define the pressure-modified Hill criterion as a function of temperature and for a given plastic work, such that:

$$T_{a,W} = C_{\theta,W} = D + ET \tag{4.2}$$

$$T_{\theta,W} = I + JT \tag{4.3}$$

$$C_{a,W} = L + M_1 T \tag{4.4}$$

where D, E, I, J, L and M_1 are empirical fit parameters as shown in Figures 4.15-4.21 and T is the temperature.

It should also be noted here that at the higher test rate (i.e. 0.044/second), a linear relationship between temperature and each uniaxial stress parameter in the pressure-modified Hill criterion, for varying degrees of plastic work was also observed for the temperature range between 110°C and 150°C. Refer to Appendix D for figures showing

the effect of temperature on the four uniaxial stress parameters corresponding to various levels of plastic work and corresponding to a strain rate of 0.044/second.

4.4.2 Approach 2 – use of modified G'Sell constitutive model

A second approach in the prediction of the temperature dependent plastic work contours for the OPP tube involves the use of a one-dimensional temperature dependent constitutive model. For materials that are anisotropic, pressure dependent and harden anisotropically, such as the oriented polypropylene tubes used in this study, the selection and/or development of an appropriate constitutive model becomes somewhat more difficult. The use of a one-dimensional constitutive model should allow the prediction of the temperature dependent tensile and compressive response of the material along each of its principal directions, once the model parameters have been determined for each mode of deformation along a particular direction. Once the temperature dependent unaixial tensile and compressive response of the material can be predicted along its principal directions, plastic work theory can be used to determine the temperature dependent plastic work contours for the material (as described in Section 4.1).

The true stress-strain curves generated from uniaxial experiments on the OPP tube along the axial and hoop directions showed good agreement with the constitutive model put forth by G'Sell et al. (1983) (refer to Chapter 2). For convenience, the final form of the G'Sell model is restated here:

$$\sigma(\varepsilon,\dot{\varepsilon}) = K[1-\exp(-B_1\varepsilon)]\exp(h_1\varepsilon^2)\dot{\varepsilon}^m \tag{4.5}$$

where σ is the stress, ε and $\dot{\varepsilon}$ are the strain and strain rate and K, B_1, h_1 and m are constants. However, it was found that the constants h_1, B_1, and K in Equation (4.5) varied with strain rate. This indicated that the effect of strain and strain rate could not be expressed separately in a multiplicative manner to describe the behaviour of these oriented materials. In addition, modifications were made to the G'Sell model to account for the effect of temperature as described in the following section. The modified model will further be referred to as the modified G'Sell model.

4.4.2.1 Development of modified G'Sell constitutive model

Since the effect of strain and strain rate could not be expressed separately in a multiplicative manner, the first modification involved the removal of the $\dot{\varepsilon}^m$ term from Equation (4.5). In order to account for temperature, T, it was assumed that its effect could be incorporated into Equation (4.5) in a multiplicative manner. It has been shown that an Arrhenius-type of dependency of stress on temperature for oriented thermoplastics can be assumed (Tate et al., 1988) such that:

$$\sigma = S \cdot \exp\left(\frac{Q}{RT}\right) = S \cdot \exp\left(\frac{V}{T}\right) \tag{4.6}$$

where S is a constant, Q is an activation energy, and R is the universal gas constant. Equation (4.6) combines Q/R into the constant V. Incorporating Equation (4.6) into Equation (4.5) with the removal of the strain rate term, one obtains:

$$\sigma = K\left[1 - \exp\left(-B_1\varepsilon\right)\right]\exp\left(h_1\varepsilon^2\right)\exp\left(\frac{V}{T}\right) \tag{4.7}$$

One final modification was made to the G'Sell model such that it could predict the initial yield point of the material at a given strain rate and as a function of temperature. The term $[1-\exp(-B_1\varepsilon)]$ in Equation (4.7) was modified to include a parameter, such that at zero plastic strain, Equation (4.7) reduced to the yield stress of the material at a given temperature and strain rate. The final form of the modified G'Sell model is then given by:

$$\sigma = K[1 - N\exp(-B_1\varepsilon)]\exp(h_1\varepsilon^2)\exp\left(\frac{V}{T}\right) \tag{4.8}$$

N is the added parameter used to describe the yield stress of the material at zero plastic strain and is given by:

$$N = \frac{-\sigma_0}{K\exp(V/T)} + 1 \tag{4.9}$$

where σ_0 is the yield stress of the material at a given strain rate and temperature. It is important to note here that the full true stress strain curve could be predicted via Equation (4.8) by removing the N term. However, if the yield stress is to be predicted (i.e. using an offset method), the N term can be retained in Equation (4.8) and the plastic stress strain curve predicted. Experimental evidence from this study showed that the K, N, B_1, and h_1 parameters in Equation (4.8) are constant with temperature, and, therefore, not in conflict with the formulation of the model in which the effects of strain and temperature were accounted for separately in a multiplicative manner.

4.4.2.2 Determination of parameters in modified G'Sell model

Appendix E outlines the procedure for the determination of the parameters within the modified G'Sell model. This procedure was used to determine the value of the model parameters for the axial tensile, hoop tensile and axial compression tests on the OPP tube. It should be noted here that in order to plot the plastic stress strain curves, from the experimental true stress strain curves, a 0.5% offset rule was employed. This allowed the determination of the cut-off between the elastic and plastic portion of the true stress-strain curve.

As an example, Tables 4.4 and 4.5 show the values of the parameters determined at four temperatures and two strain rates for the axial tensile tests of the OPP tube. An average value for each parameter (i.e. h_1, V, K, N and B_1) is also indicated in each table, and was subsequently used in the model. As indicated in Tables 4.4 and 4.5, none of the five parameters vary significantly with temperature or strain. This is consistent with the way in which the model was formulated, whereby the effects of strain and temperature, not strain rate, were expressed explicitly in a multiplicative manner.

		Model parameters				
Temperature (°C)	Strain rate (/second)	h_1	V (Kelvin)	K (Pa)	N	B_1
110	0.0022	1.28	3423	6728	0.707	6
130	0.0022	1.18	3423	7147	0.737	6
140	0.0022	1.18	3423	6992	0.743	6
150	0.0022	1.24	3423	6726	0.749	6
AVERAGE		1.22	3423	6898	0.734	6

Table 4.4 Modified G'Sell model parameters obtained from axial tensile at a strain rate of 0.0022/second.

		Model parameters				
Temperature (°C)	Strain rate (/second)	h_1	V (Kelvin)	K (Pa)	N	B_1
110	0.044	1.53	4121	1832	0.498	6
130	0.044	1.52	4121	1974	0.496	6
140	0.044	1.46	4121	1984	0.517	6
150	0.044	1.48	4121	1901	0.541	6
AVERAGE		1.50	4121	1923	0.513	6

Table 4.5 Modified G'Sell model parameters obtained from axial tensile at a strain rate of 0.044/second.

As indicated in Equation (4.6), V would take the value of Q/R, where Q is the activation energy of the material and R is the universal gas constant. From Table 4.5, the value of V at a strain rate of 0.044/second is 4121 Kelvin. One can then calculate a value of Q based on this value of V. The value obtained is 34.3 kJ/mol which falls within the range of activation energies (34 kJ/mol - 44 kJ/mol) reported for polypropylene close to its melting point by Muke et al. (2001).

4.4.2.3 Comparison of experimental and model results corresponding to axial tensile test

Figures 4.29 and 4.30 compare the stress strain curve obtained from the axial tensile test to the model prediction at four temperatures and a strain rate of 0.0022/second and 0.044/second respectively. In general, good agreement exists between the experimental curves and the predicted curves at the temperatures and strain rates studied. It is also important to note the ability of the model to accurately capture the initial yield point of the material in the range of temperatures and strain rates considered.

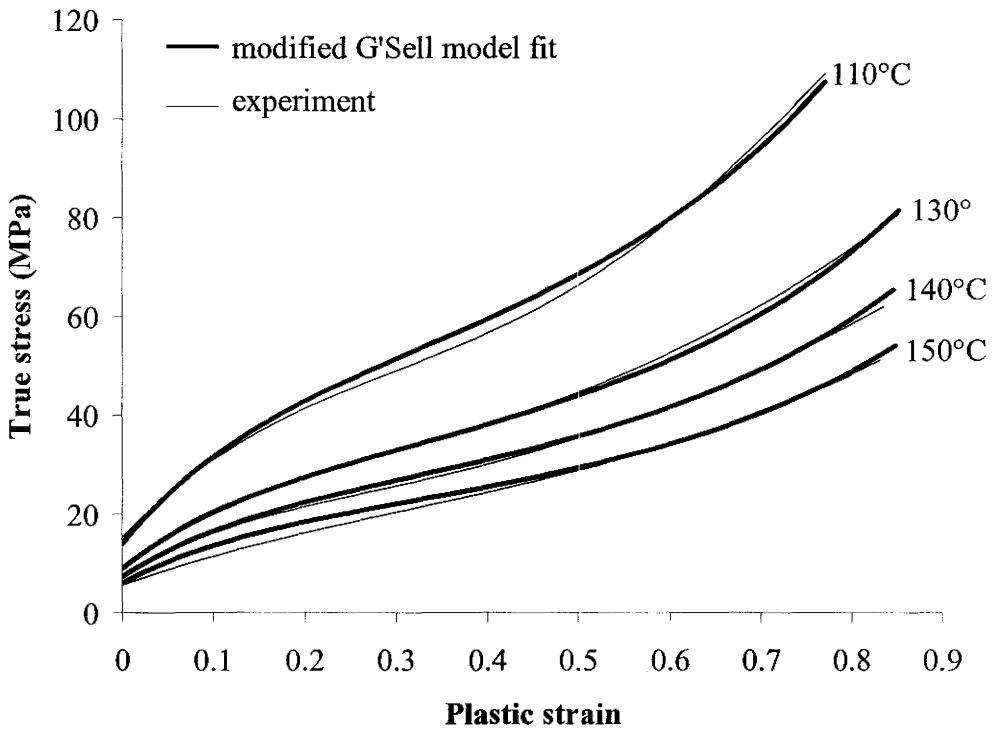

Figure 4.29 Comparison of experimental axial tensile test curves with prediction from modified G'Sell model at four temperatures and a strain rate of 0.0022/second.

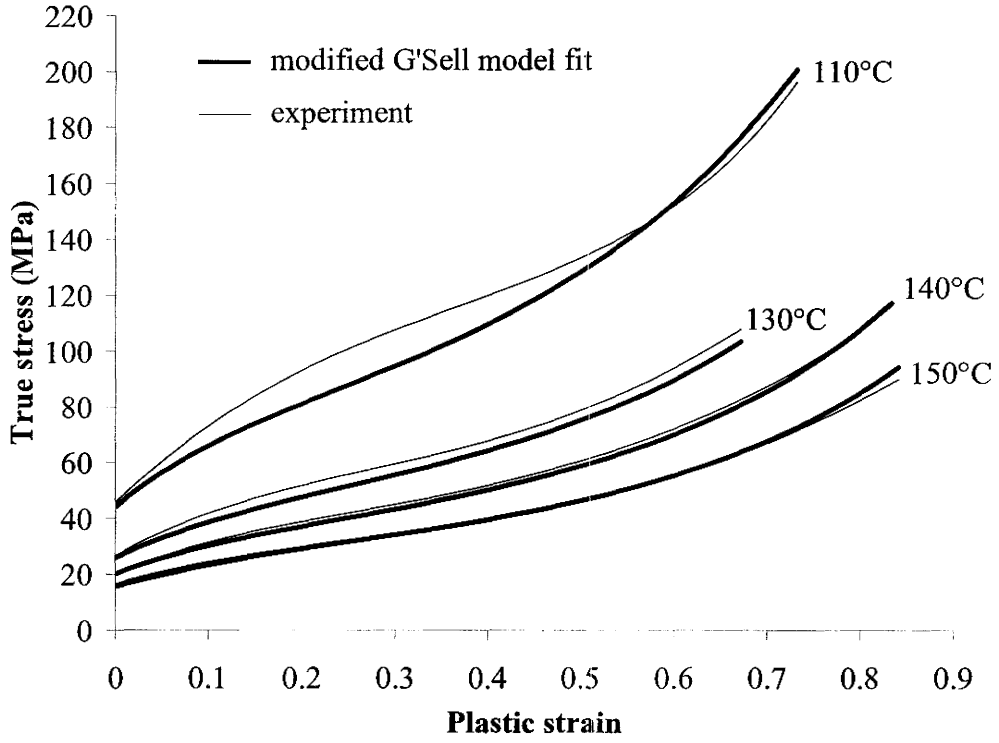

Figure 4.30 Comparison of experimental axial tensile test curves with prediction from modified G'Sell model at four temperatures and a strain rate of 0.044/second.

4.4.2.4 Comparison of experimental and model results corresponding to hoop tensile test

As in the axial tensile case, the constitutive model parameters used to predict the hoop behaviour were determined from the plastic stress-strain curves obtained from the hoop tension test. The values of the parameters were not influenced by temperature. Figure 4.31 compares the stress strain curves obtained from the hoop tensile test at four temperatures and a strain rate of 0.0022/second (tube draw ratio 4.0) to the prediction using the modified G'Sell model. Good agreement exists between the experimental curves and those predicted by the modified G'Sell model over the entire strain range. The model is also able to capture the initial yield point at the conditions studied.

4.4.2.5 Comparison of experimental and model results corresponding to axial compression test

The constitutive model parameters used to predict the axial compressive behaviour were determined from the plastic stress-strain curves obtained from the axial compression test. The values of the parameters were not influenced by temperature. Figure 4.32 compares the stress strain curves obtained from the axial compression test at four temperatures and a strain rate of 0.0022/second (tube draw ratio 4.0) to the model prediction. Once again, relatively good agreement exists between the experimental curves and those predicted by the modified G'Sell model over the entire strain range.

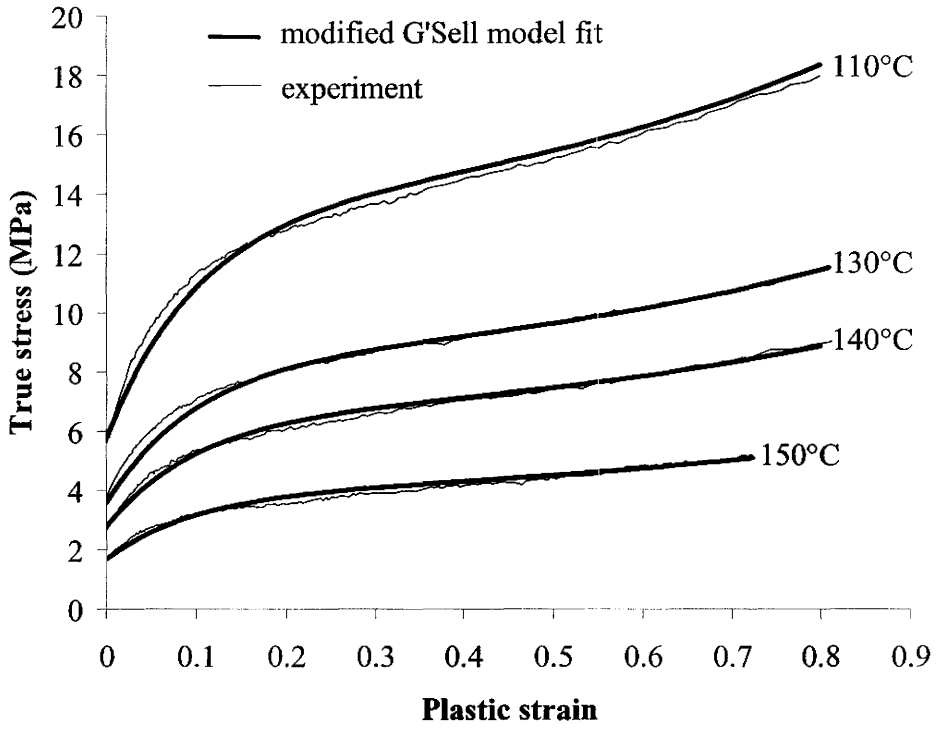

Figure 4.31 Comparison of experimental hoop tensile test curves at four temperatures and a strain rate of 0.0022/second (tube draw ratio 4.0) with prediction from modified G'Sell model.

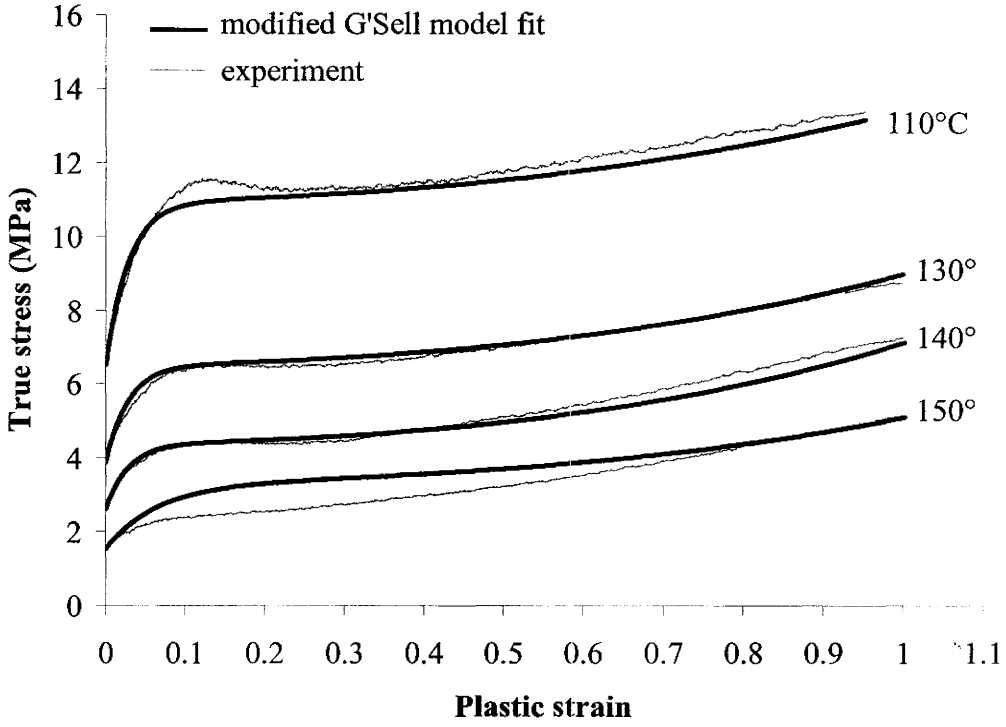

Figure 4.32 Comparison of experimental axial compression test curves at four temperatures and a strain rate of 0.0022/second (tube draw ratio 4.0) with prediction from modified G'Sell model.

Some important points regarding the use of the modified G'Sell model should be discussed here. Firstly, in order to be able to predict the temperature dependent uniaxial tensile and compressive response of the material along the axial and hoop directions, six experiments are required. More specifically, experiments at two temperatures are required along the axial direction in tension, along the hoop direction in tension and along the axial direction in compression (as in approach 1). Also, as with approach 1, it is assumed that the axial tensile and hoop compressive properties can be taken as equal. The experiments at the two temperatures are required for the determination of the parameter, V, within the model for a given mode of deformation along a given direction. All of the other parameters are assumed to be independent of temperature, and therefore, can be determined at any given temperature. The one drawback to approach 2 is that more analysis is required to determine the parameters within the model along the axial and hoop direction and for more than one mode of deformation along the axial direction. This analysis is required prior to using the predicted uniaxial curves and the concept of plastic work theory to define the temperature dependent plastic work contours for the material. For this reason, approach 1 is subsequently used in the prediction of the forming limits for the OPP tube.

4.5 Strain relations for describing OPP tube forming process

The flow rules corresponding to the pressure-modified Hill yield criterion were given in Chapter 2 (Equations (2.24) to (2.26)). Using Equations (2.24) and (2.25), the ratio of axial to hoop strains, or the strain ratio, ρ, is given by:

$$\rho = \frac{d\varepsilon_a}{d\varepsilon_\theta} = \frac{2H\sigma_a - H\sigma_\theta + 0.5K_a}{F\sigma_\theta + H\sigma_\theta - H\sigma_a + 0.5K_\theta} \tag{4.15}$$

where the x, y and z directions in Equations (2.24) to (2.26) refer to the axial (a), hoop (h) and thickness (t) directions of the tube respectively.

The strain ratio, ρ, corresponding to a given stress state and a given plastic work is obtained by selecting H, F, K_a and K_θ values at the same plastic work. It is also important to point out here that the value of ρ may not necessarily be constant, even if the stress ratio is constant. This is because the values of H, F, K_a and K_θ are continually changing with increasing plastic work values.

In order to calculate the individual strain components (i.e. axial and hoop) associated with a given plastic work increment, W_{inc}, and a given stress state, the relation expressing the plastic work per unit volume will be evoked. It can be written in terms of the stress and strain components as (assuming stress is the thickness direction of the tube is approximately zero):

$$W_{inc} = \sigma_\theta d\varepsilon_\theta + \sigma_a d\varepsilon_a \tag{4.16}$$

Assuming an increment of plastic work, in which the strain path is known within this increment, Equation (4.16) can be rearranged to give the increment of hoop strain as:

$$d\varepsilon_\theta = \frac{W_{inc}}{\sigma_\theta + \sigma_a \rho} \tag{4.17}$$

Equations (4.15) and (4.17) will be used, as described in Section 4.8, to predict the forming limits for the OPP tube along various strain paths and at different forming temperatures.

4.6 Strain path predictions and comparison with experiments

4.6.1 Biaxial tube tests

It is useful to establish the extent to which the model is able to predict realistic strain paths observed during the forming of OPP tubes. For this purpose, the results of continuous strain measurements, using the ARAMIS system as described earlier, on 2 different forming tests namely stress path 1 and stress path 4 (refer to Table 4.1) were utilized. Figure 4.33 shows the 2 deformed sample used in this comparative study. Note here that the tube test along stress path 1 was taken close to burst and, hence, the bulge became asymmetric as indicated in Figure 4.33 (a). In this case the strain history was extracted from the right side of the bulge, at the location of maximum strain.

The strain path associated with the point of maximum strain on the surface of the deforming tube would be used for comparison with the model result. For illustration purposes, Figure 4.34 (a) and (b) show the ARAMIS major (or hoop) strain map for

stress path 1 sample corresponding to a maximum hoop strain of 5.4% and 10.5% respectively. As shown in this figure, the strains are known across the surface of the entire sample as it deforms. In addition, the strain history at any point along the surface of the deforming tube (shown as 'stage points' in Figure 4.34) can be obtained. It should also be noted here that there are some square regions where the strain information is "unknown" due to poor image quality.

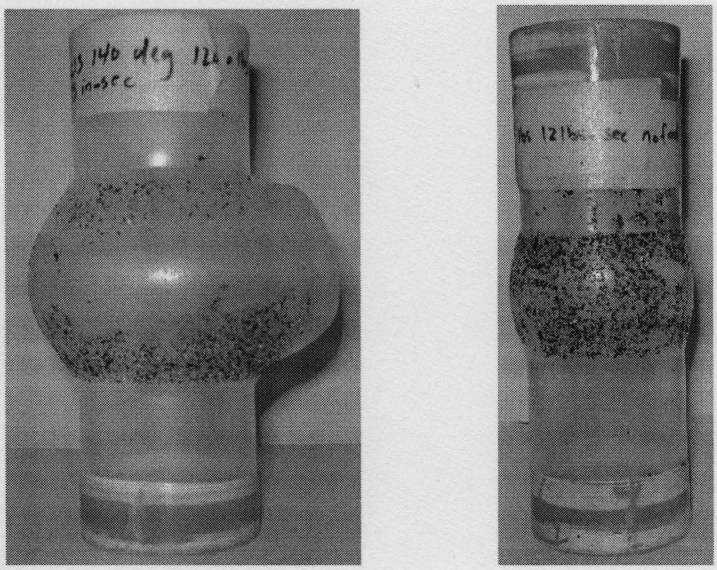

Figure 4.33 Deformed tube samples tested at 140°C (a) stress path 1 (b) stress path 4 (refer to Table 4.1 for test details)

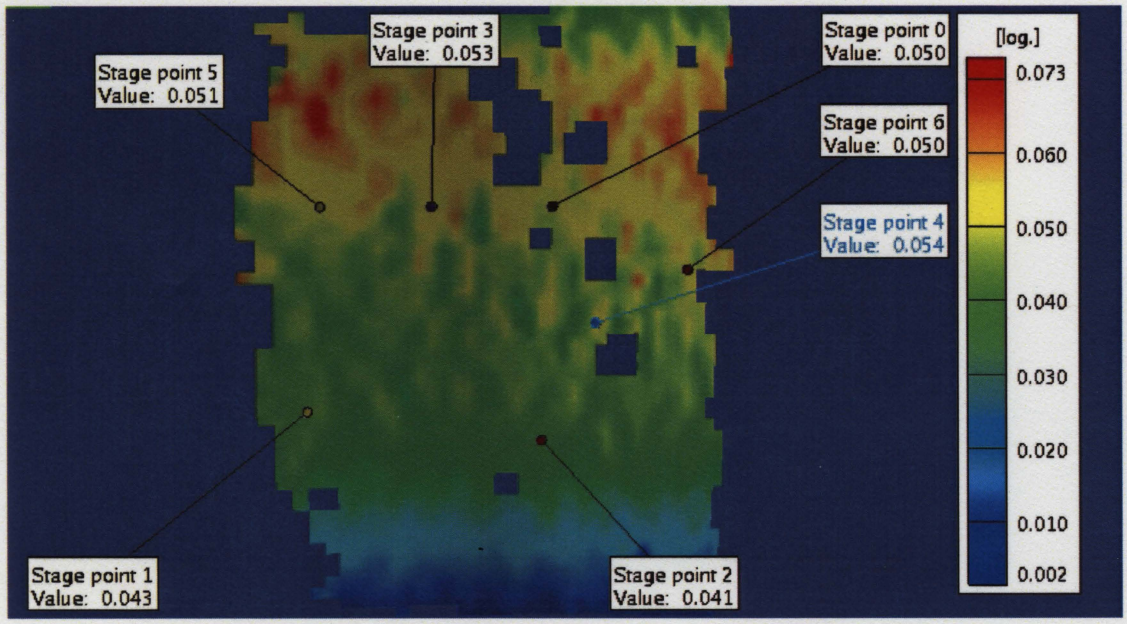

(a)

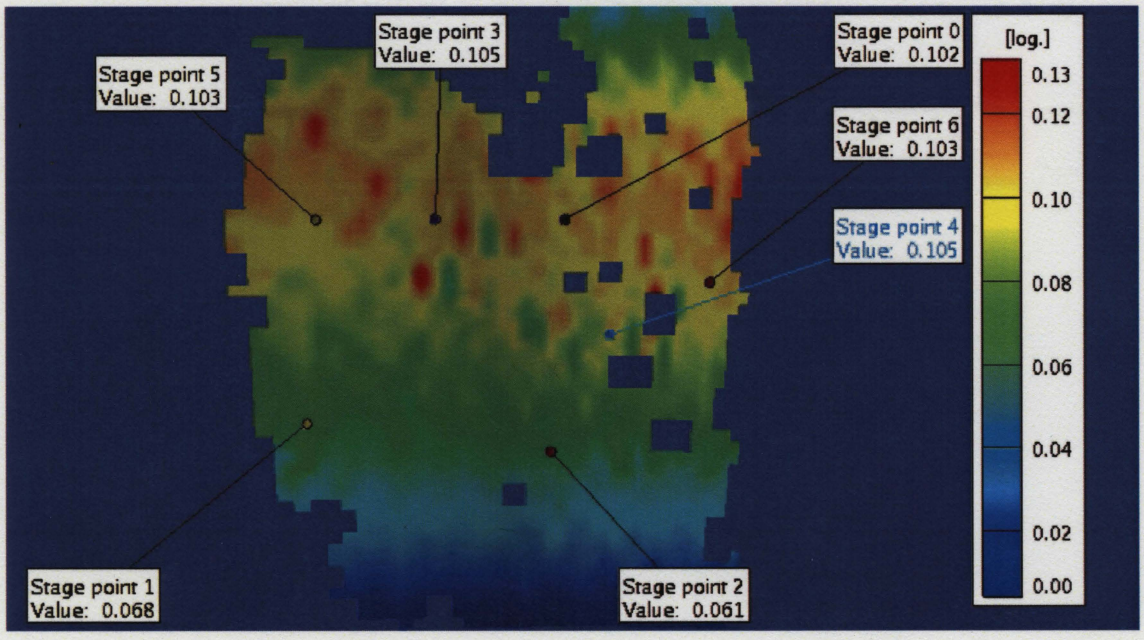

(b)

Figure 4.34 Typical hoop strain maps obtained with ARAMIS and corresponding to stress path 1 (a) hoop strain of 5.4% (b) hoop strain of 10.5%.

For the model predictions, the calculation procedure in the form of a flow chart is presented in Figure 4.35. Note here that the experimentally obtained stress paths, corresponding to stress path 1 and stress path 4, used in the model prediction, were shown earlier in Figures 4.9 and 4.12 respectively.

Figures 4.36 and 4.37 compare the predicted and experimental strain paths corresponding to stress path 1 and 4 respectively. As described in Figure 4.35, the experimentally determined stress path obtained from each test was used to predict the resulting strain path. As shown in Figures 4.12, stress path 4 is more linear in shape compared with stress path 1. Note here that stress path 1 involves axial end feeding whereas stress path 4 does not. Hence, the strain path associated with stress path 1 is significantly more non-linear than that resulting from stress path 4. However, as shown through Figures 4.36 and 4.37, the model is able to capture both linear and non-linear strain paths associated with the tube forming tests with and without the use of axial end feeding.

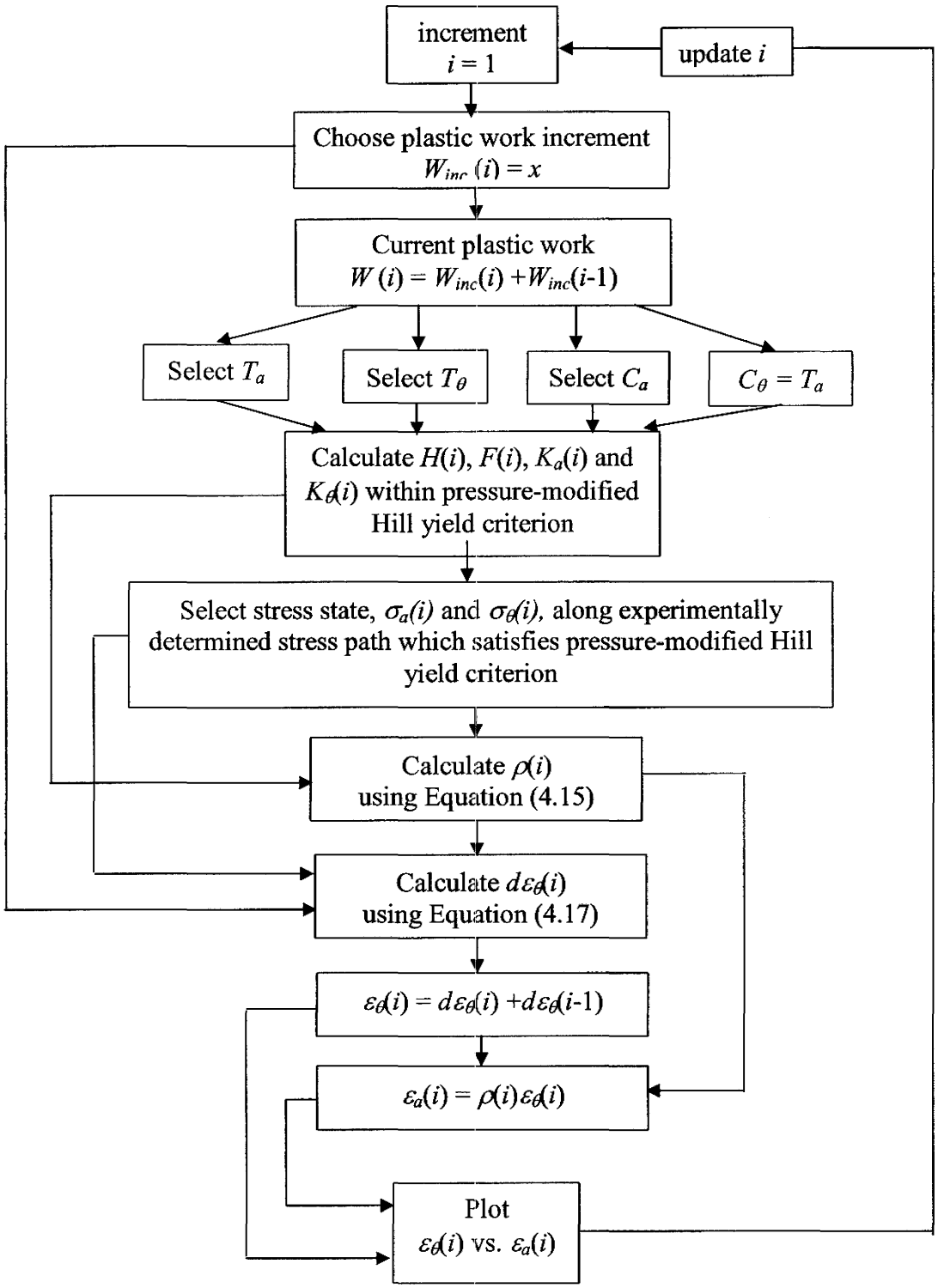

Figure 4.35 Calculation procedure for predicting strain path via the analytical model.

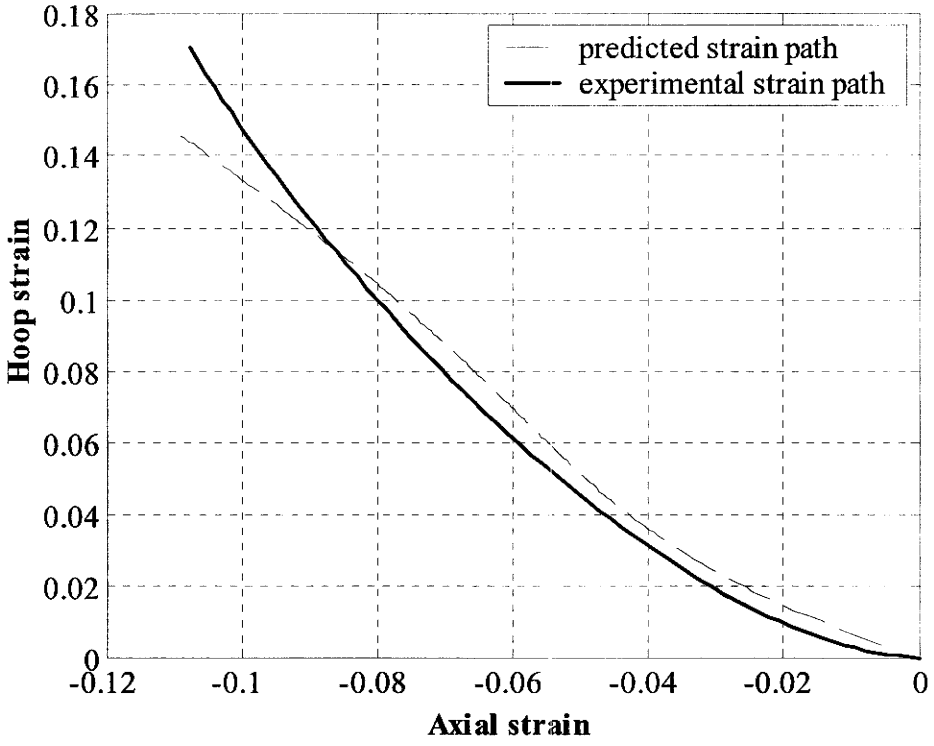

Figure 4.36 Comparison of strain path obtained from the experiment and via the analytical model for the tube tested at 140°C and corresponding to stress path 1 (refer to Table 4.1).

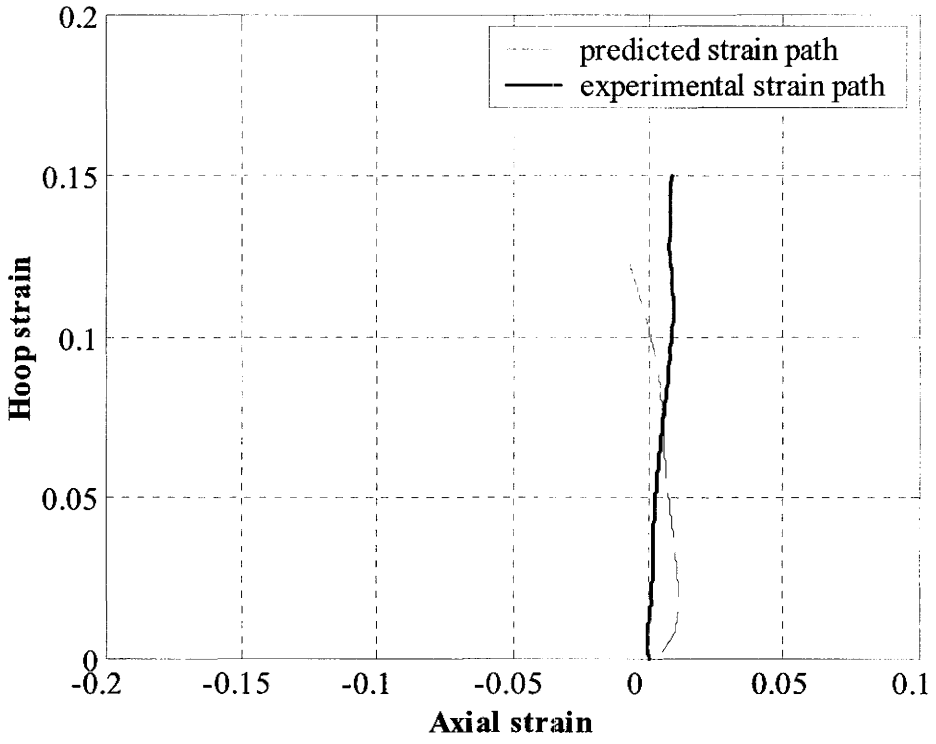

Figure 4.37 Comparison of strain path obtained from the experiment and via the analytical model for the tube tested at 140°C and corresponding to stress path 4 (refer to Table 4.1).

4.6.2 Ring hoop tension test

A comparison of the experimental strain paths determined from the ring hoop tension test at various temperatures will also be compared with the predictions via the analytical model. The results will be compared at three temperatures, 110°C, 140°C and 150°C. Once again, the experimental measurement of the strain path was determined with the use of the ARAMIS system. In this case, the strain path associated with the point of maximum strain on the surface of the deforming sample would be used for comparison with the model result. As an example, Figure 4.38 shows the strain contour maps obtained with ARAMIS for a ring hoop tension test at 110°C at various stages of the deformation. Also shown in each of the plots are the hoop strains at four specific points along the sample. Note here that stage point 0 is taken as the point of maximum strain.

For the model predictions, the flowchart given in Figure 4.35 was utilized. In this case, however, the stresses along the axial and thickness directions were assumed to be equal to zero (uniaxial stress state). Therefore, for a given plastic work increment and the corresponding calculated values of $H(i)$, $F(i)$, $K_a(i)$ and $K_\theta(i)$, the value of the hoop stress could be determined such that it satisfied the pressure-modified Hill yield criterion.

Figures 4.39 to 4.41 show that, in general, good agreement exists between the strain paths determined from the experiments and those predicted via the analytical model at the three temperatures considered. Good agreement is obtained for tests conducted at

110°C and 130°C. However, at 140°C, there appears to be some divergence of the predicted path from the experimental path at an axial strain close to –0.1.

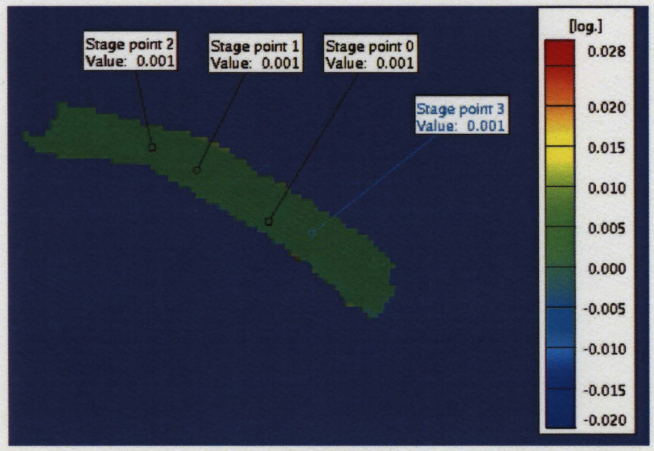

(a)

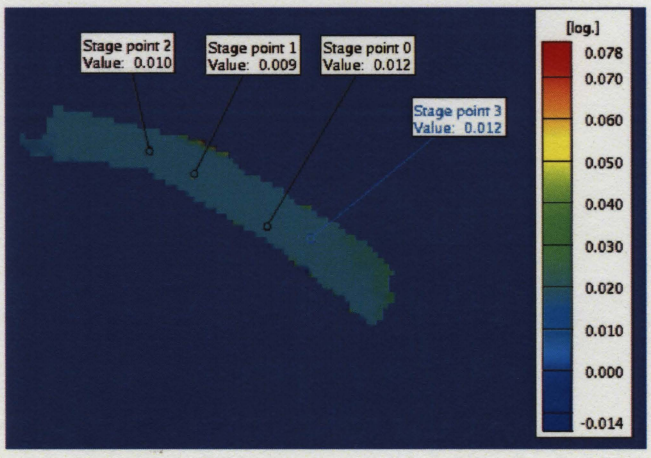

(b)

Figure 4.38 Hoop strain contour plots obtained from ARAMIS for the ring hoop tension test at 110°C. The hoop strain at stage point 0 is given as (a) 0.001 (b) 0.012.

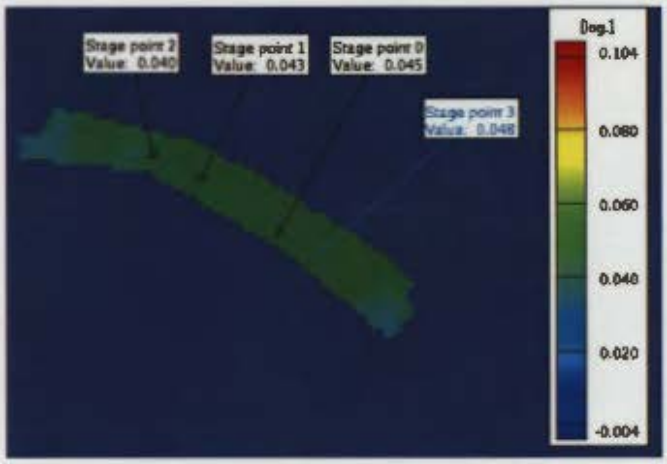

(c)

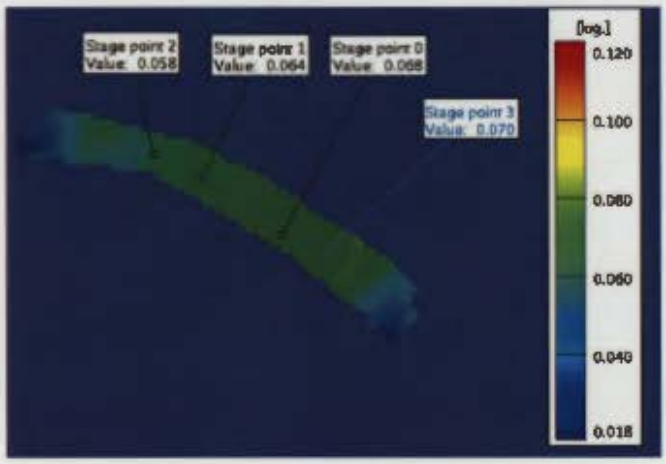

(d)

Figure 4.38 *cont.* Hoop strain contour plots obtained from ARAMIS for the ring hoop tension test at 110°C. The hoop strain at stage point 0 is given as (c) 0.045 (d) 0.068.

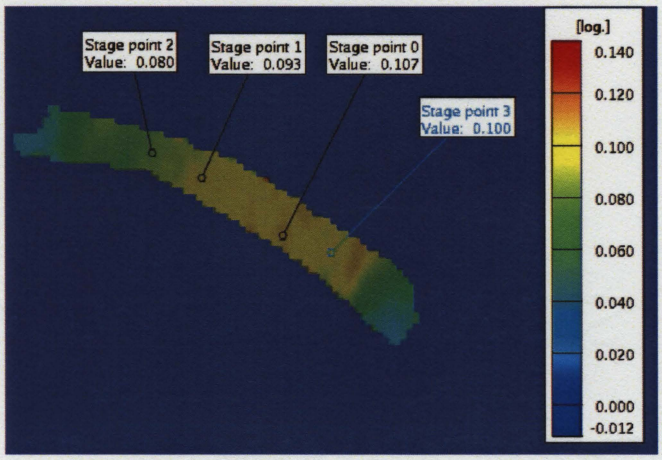

(e)

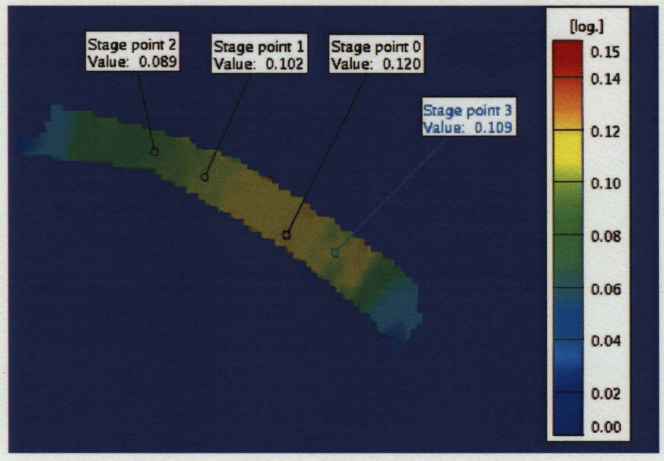

(f)

Figure 4.38 *cont.* Hoop strain contour plots obtained from ARAMIS for the ring hoop tension test at 110°C. The hoop strain at stage point 0 is given as (e) 0.107 (f) 0.120.

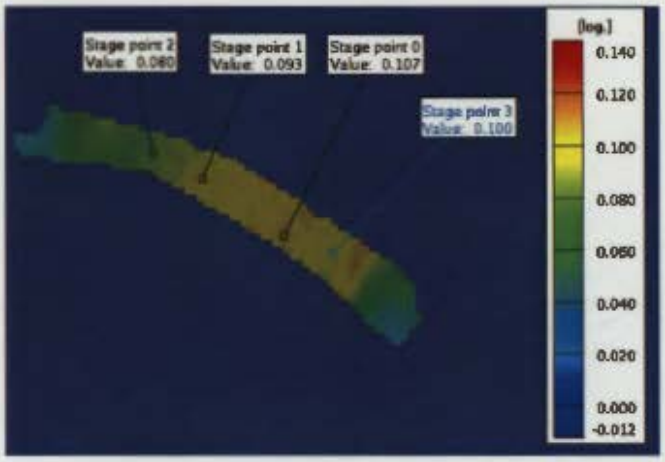

(e)

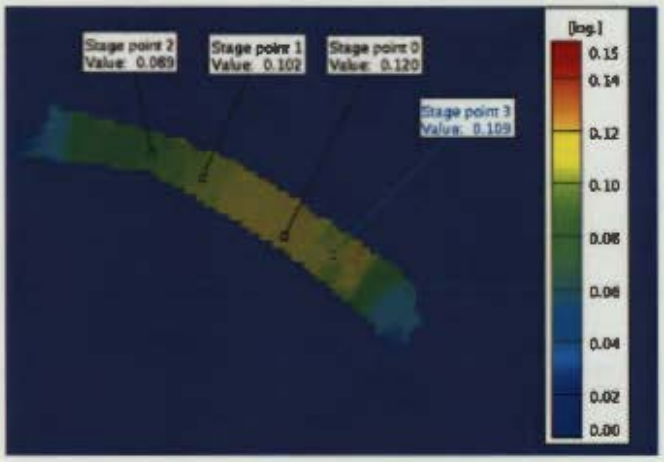

(f)

Figure 4.38 *cont.* Hoop strain contour plots obtained from ARAMIS for the ring hoop tension test at 110°C. The hoop strain at stage point 0 is given as (e) 0.107 (f) 0.120.

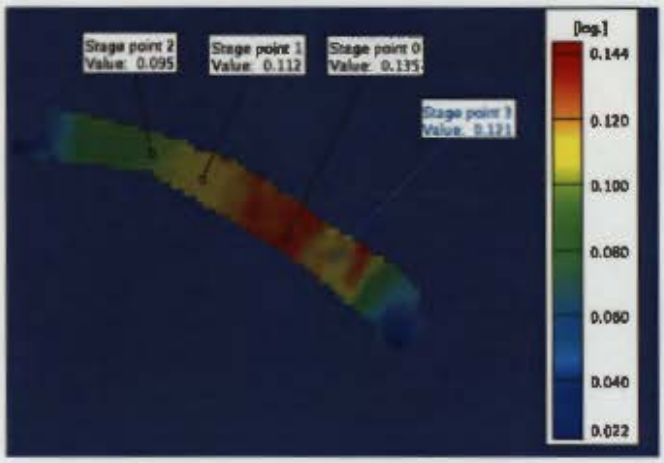

(g)

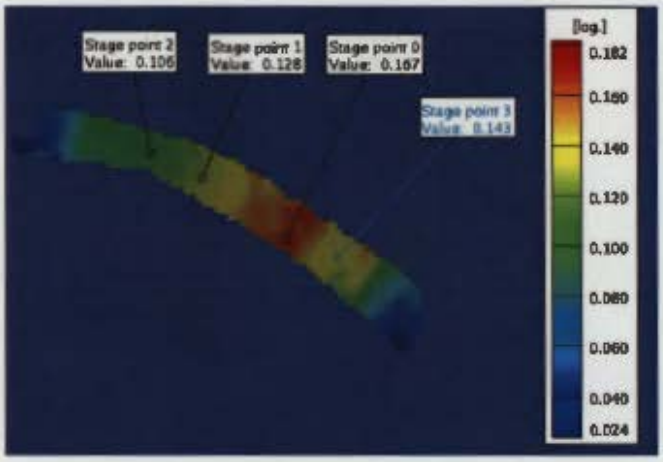

(h)

Figure 4.38 *cont.* Hoop strain contour plots obtained from ARAMIS for the ring hoop tension test at 110°C. The hoop strain at stage point 0 is given as (g) 0.135 (h) 0.167.

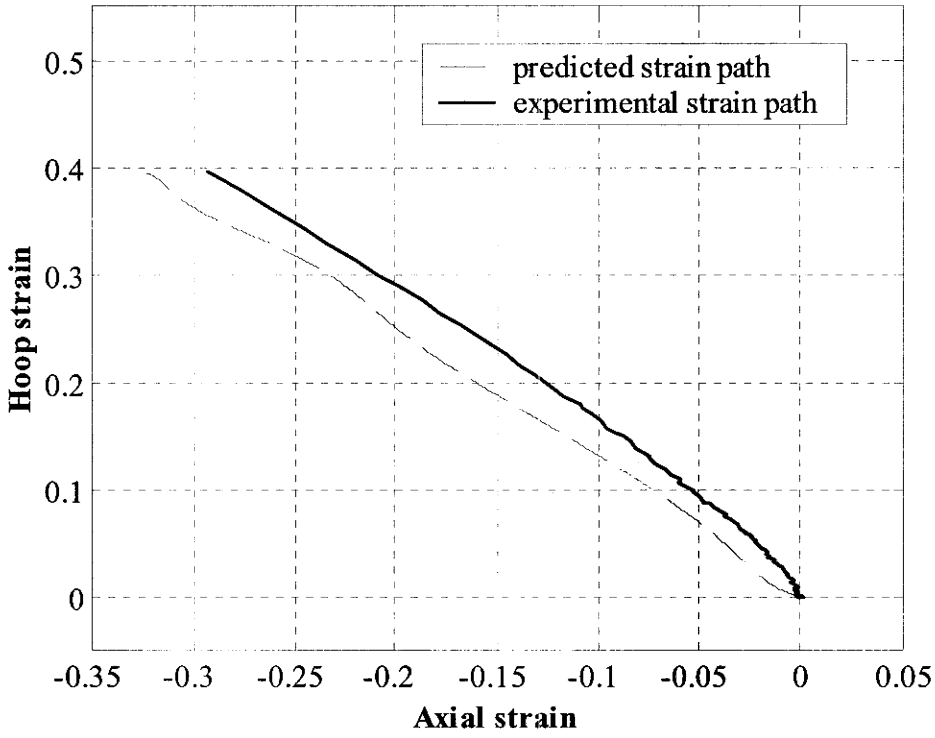

Figure 4.39 Comparison of strain path determined from the experiment and via the analytical model for the ring hoop tension test at 110°C.

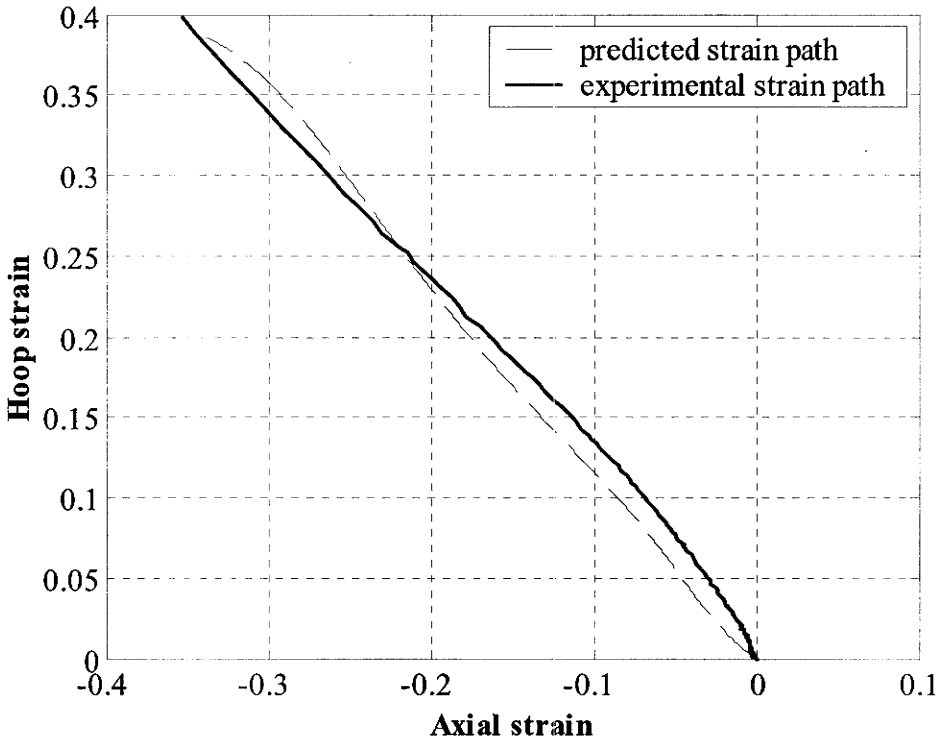

Figure 4.40 Comparison of strain path determined from the experiment and via the analytical model for the ring hoop tension test at 130°C.

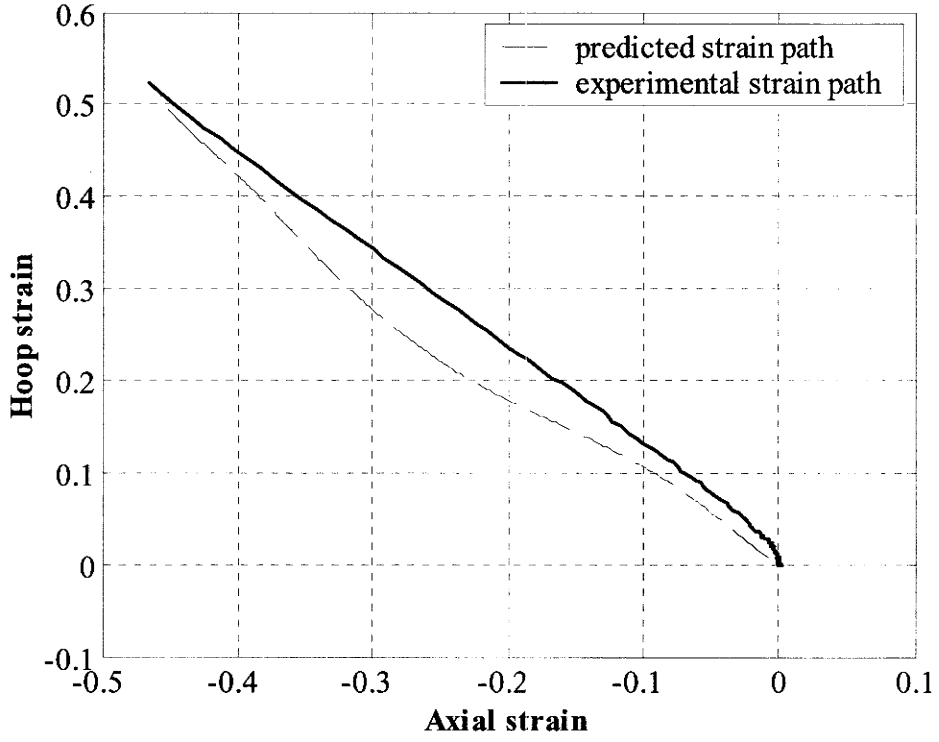

Figure 4.41 Comparison of strain path determined from the experiment and via the analytical model for the ring hoop tension test at 140°C.

4.6.3 Axial tensile test

A comparison of the experimental strain path determined from the axial test at 130°C will also be compared with the predictions via the analytical model. For the model predictions, it was assumed that the stresses along the hoop and thickness directions were equal to zero.

Figure 4.42 compares the experimental axial tension strain path with that obtained from the model prediction at 130°C. Reasonable agreement is observed between the experimental curve and the predicted curve for the strain range represented.

4.7 Criterion for localized necking of OPP tube during forming

The criterion for localized necking, taken as the point when the force in the hoop direction of the tube reached a maximum, was derived earlier in Chapter 2. The final form of the criterion is expressed as:

$$\frac{d\sigma_\theta}{\sigma_\theta} = -d\varepsilon_t \tag{4.18}$$

As an example, Figure 4.43 shows the change in the hoop force with hoop strain during forming. The figure was generated from the analytical model and was taken at a strain ratio of –0.85 at two representative temperatures, 130°C and 140°C. Section 4.8 gives the details of the method in which both the hoop force and the hoop strain were calculated for increasing levels of plastic work. Figure 4.43 shows that at both temperatures, the hoop force reaches a maximum before decreasing as the hoop strain

continues to increase. Since strain localization is assumed to occur at the point when the hoop force reaches a maximum, the hoop strain at localization is greater in the case of 140°C compared with the 130°C case.

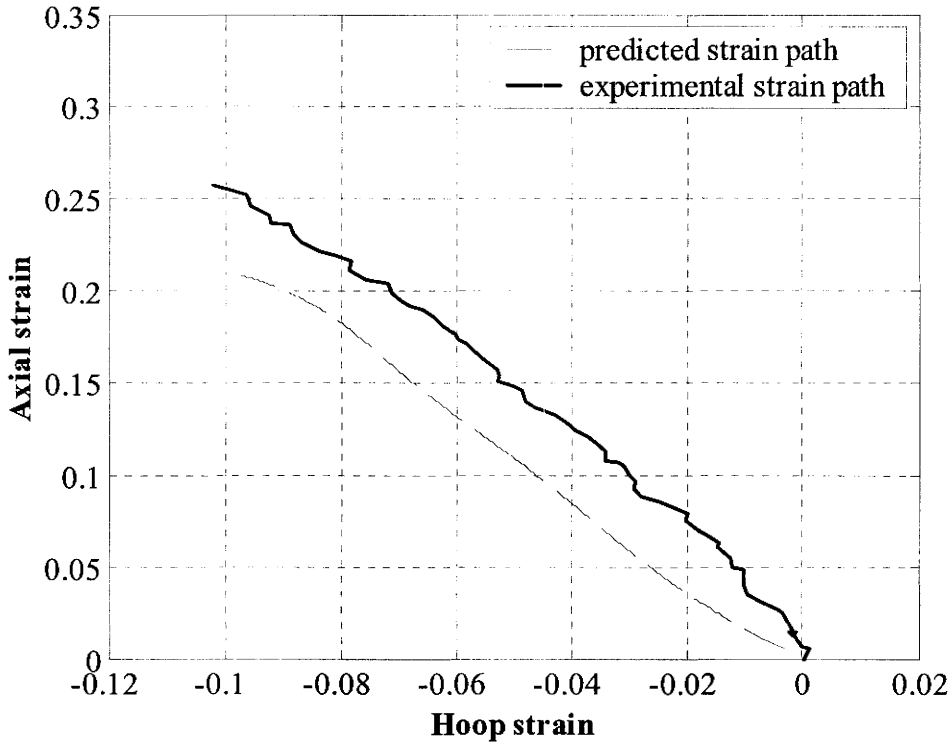

Figure 4.42 Comparison of strain path obtained from the experiment and via the analytical model for the axial tensile test at 130°C.

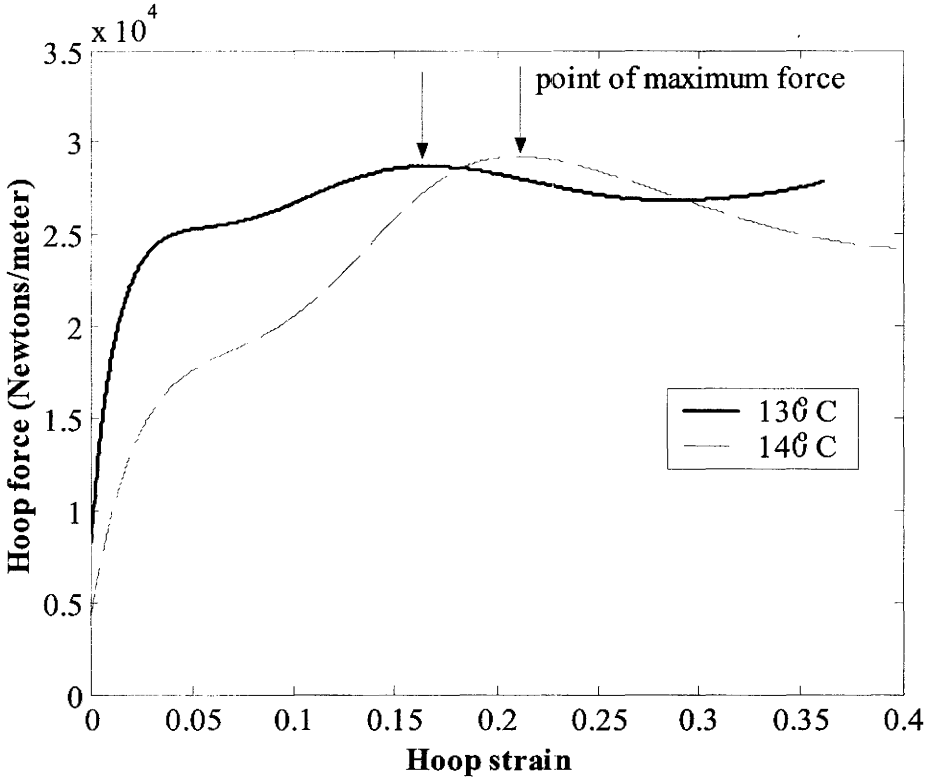

Figure 4.43 Typical hoop force vs. hoop strain plot at 130°C and 140°C (corresponding to a strain ratio of –0.85) obtained from the analytical model. Strain localization is assumed to occur at the point of maximum force.

4.8 Calculation flowchart for prediction of forming limits for OPP tube

Figure 4.44 is the main flowchart summarizing the methodology for prediction of the forming limits for the OPP tube. Sub flowchart 1 (Figure 4.45) details the uniaxial tests along the axial and hoop directions of the tube at two temperatures that need to be performed. Sub flowchart 2 (Figure 4.46) details the procedure for predicting the values of the uniaxial stress parameters in the pressure-modified Hill criterion, corresponding to a given plastic work value and at a temperature at which the forming limits are to be predicted. At a given temperature and strain ratio, sub flowchart 3 (Figure 4.47) outlines how the stresses, strains and hoop force within the deforming tube are calculated from the results of sub flowcharts 2 and 3. The point at which the hoop force reaches a maximum is the point at which strain localization is assumed. If the hoop force has not reached a maximum, the plastic work value is updated and the calculation procedure repeated as indicated in the main flowchart.

4.9 Predicted temperature dependent forming limit curves for OPP tube

Based on the calculation flowchart described above, the forming limit diagram for the OPP tube as a function of temperature can be constructed. Figure 4.48 shows the forming limit diagram for the material at four temperatures. As indicated in this figure, as the temperature increases, the hoop strains at localization, corresponding to a given strain path also increases.

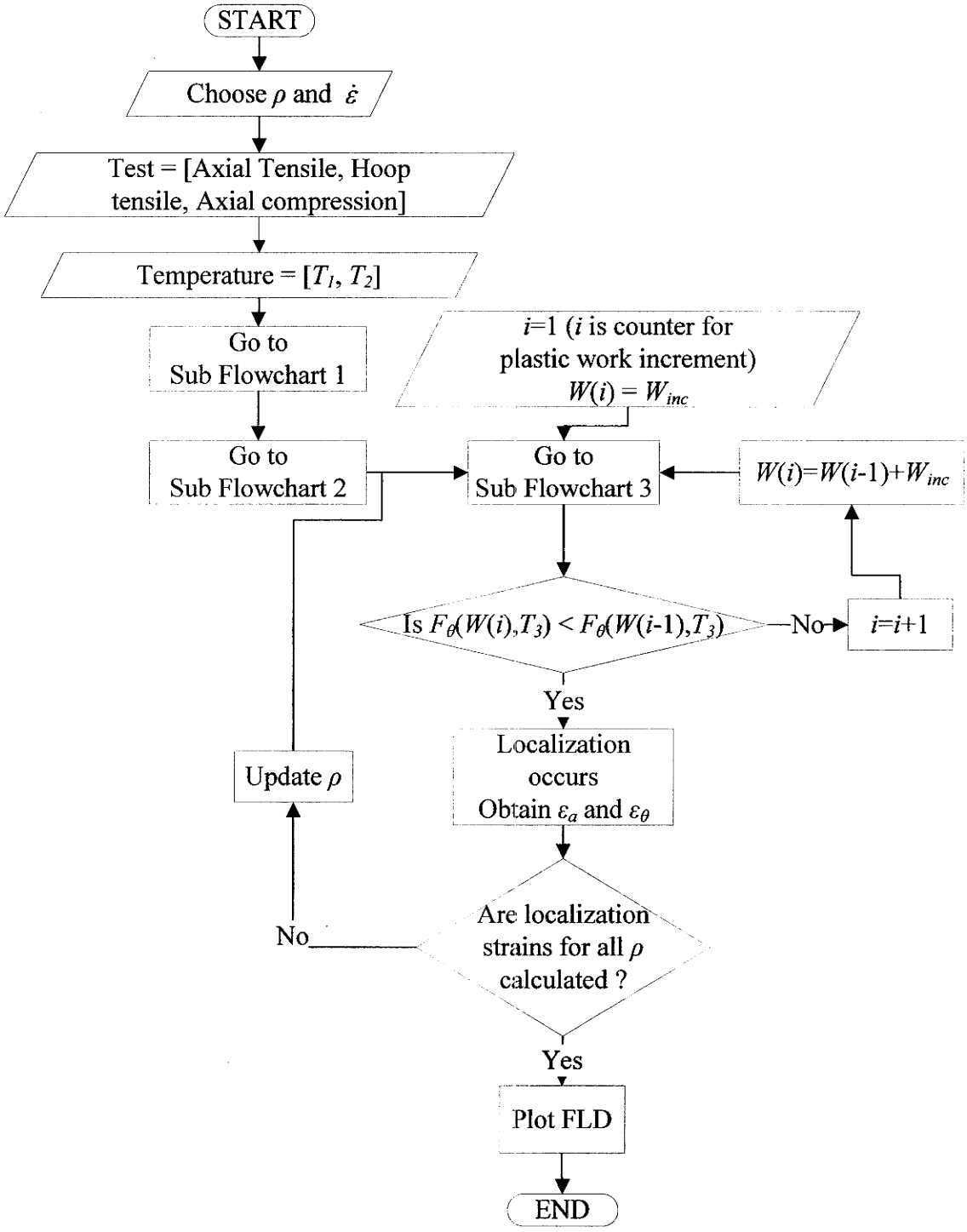

Figure 4.44 FLD prediction main flowchart.

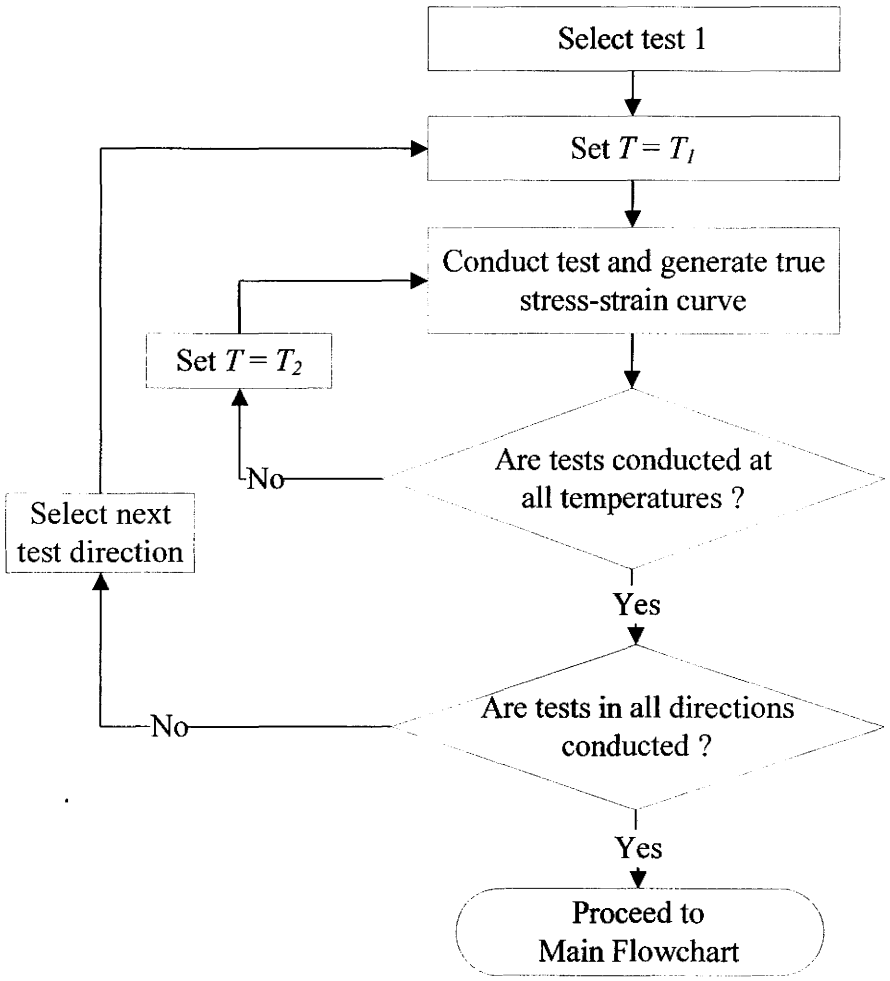

Figure 4.45 FLD prediction sub flowchart 1.

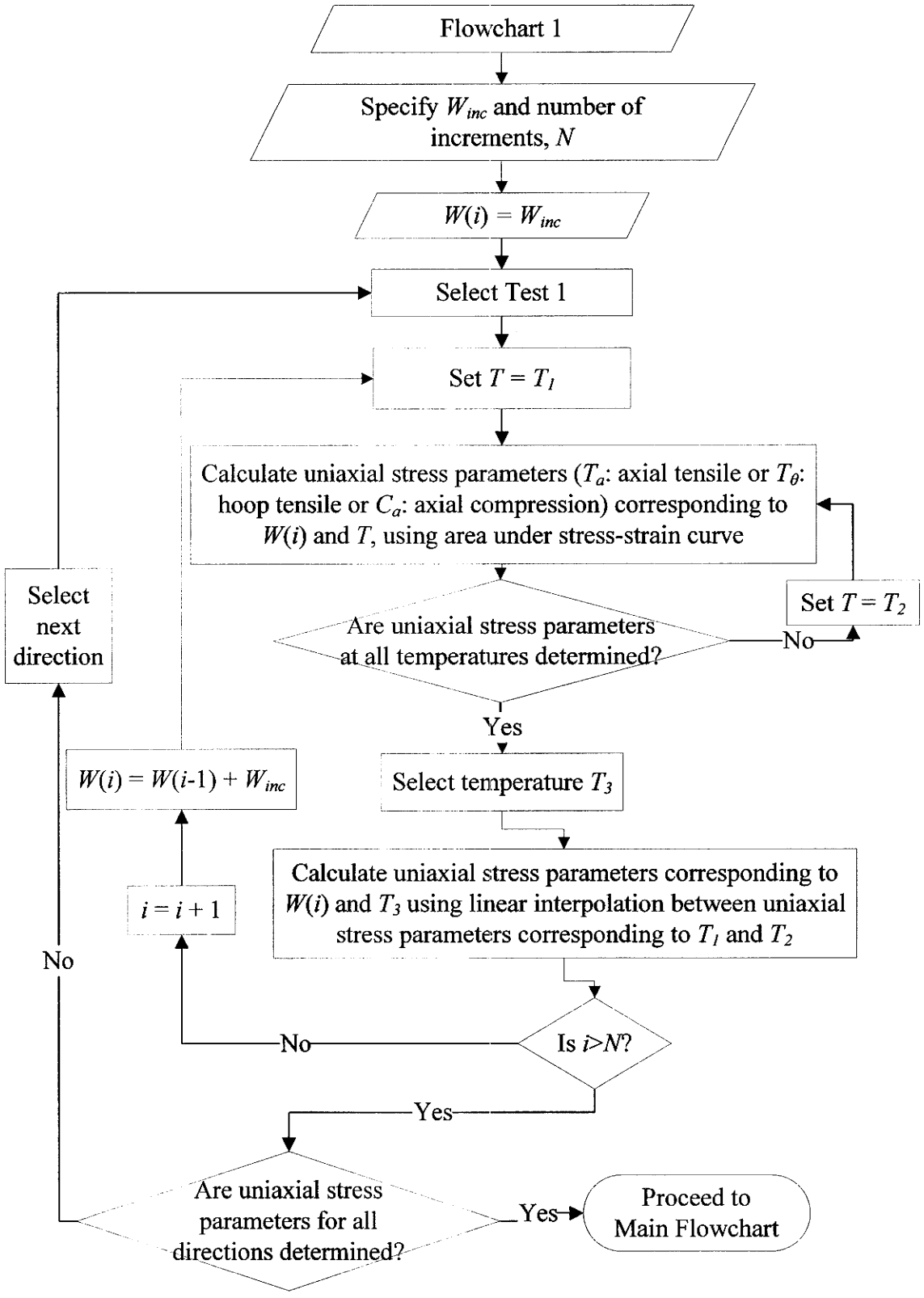

Figure 4.46 FLD prediction sub flowchart 2.

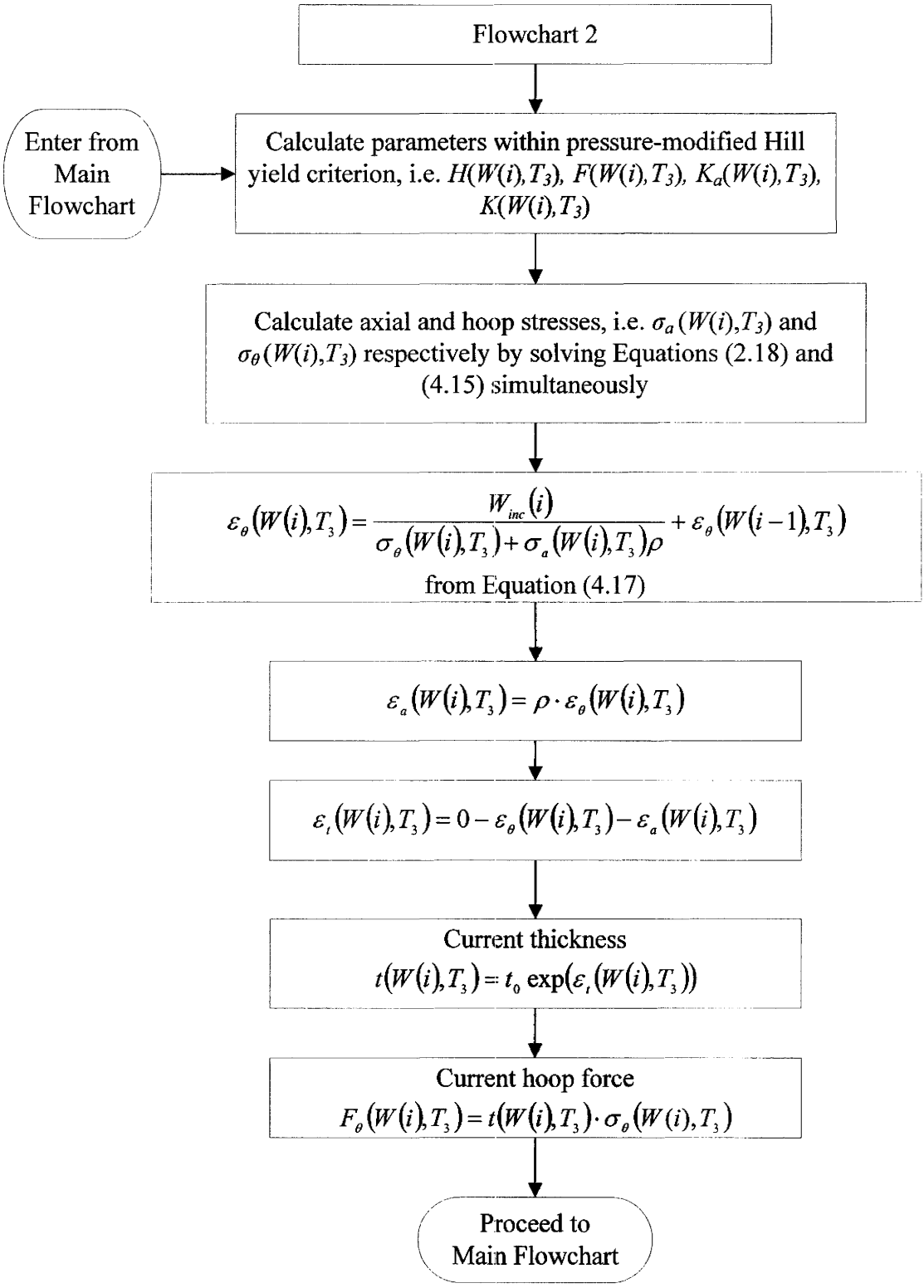

Figure 4.47 FLD prediction sub flowchart 3.

Figure 4.48 also shows that for strain paths corresponding to the left hand side of the FLD, increasing the temperature has a greater effect on increasing the forming limits compared with strain paths on the right hand side of the FLD. For the strain path corresponding to plane strain, a hoop strain of approximately 0.15 can be achieved before localization at 150°C.

Figures 4.49 and 4.50 compare the effect of draw ratio on the predicted forming limits for the OPP tube at 140°C and 150°C respectively and corresponding to a strain rate of 0.0022/second. At both temperatures, the lower draw ratio tube (i.e. 4.0) results in higher limit strains for all of the strain paths considered. This indicates that as the anisotropy of the material decreases, the forming limits increase. For example, Figure 4.50 shows that a 5% increase in the hoop strain is achievable when the draw ratio is reduced from 5.0 to 4.0 along the plane strain path.

Figure 4.51 compares the predicted forming limits for the OPP tube at room temperature, 110°C and 150°C. It is important to note here that the room temperature FLD was determined through a linear extrapolation of the value of the uniaxial stress parameters (axial tensile and hoop tensile) at 130°C and 140°C to obtain the values at room temperature. Only uniaxial compressive data along the axial and hoop direction at room temperature was available. The room temperature forming limits for this material is substantially lower compared to the other two temperatures. For the room temperature case, the hoop strain at localization does not reach or exceed 5% for any of the strain paths considered. This suggests the poor room temperature formability of these

materials, and verifies the need for elevated temperature forming if realistic forming strains are to be achieved without areas of localized thinning.

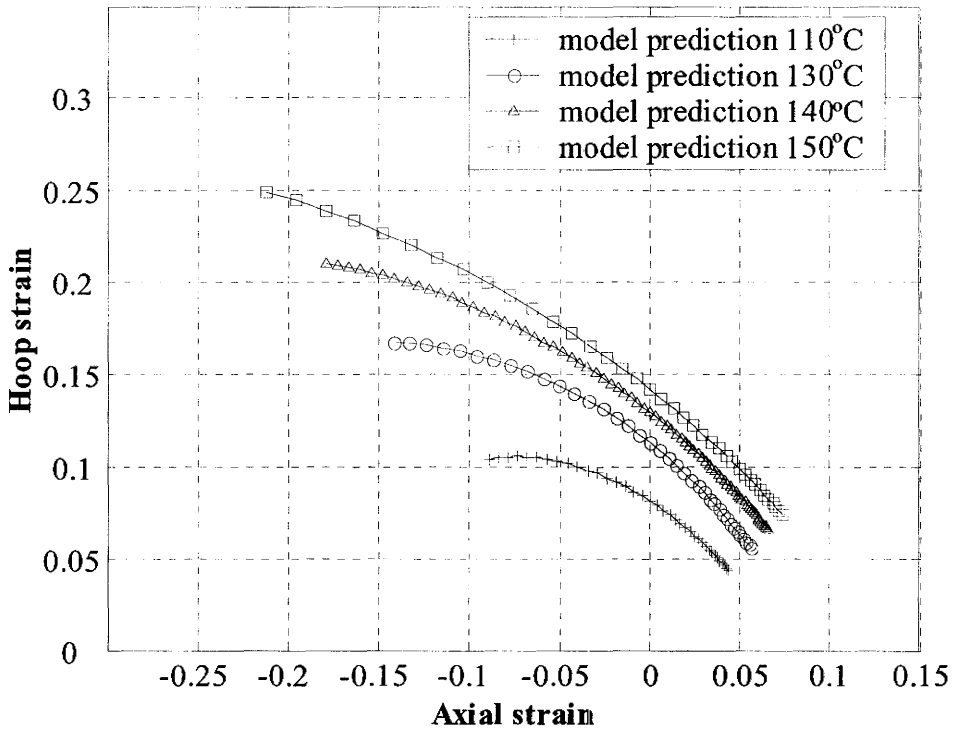

Figure 4.48 Predicted forming limit diagram for OPP tube at various temperatures.

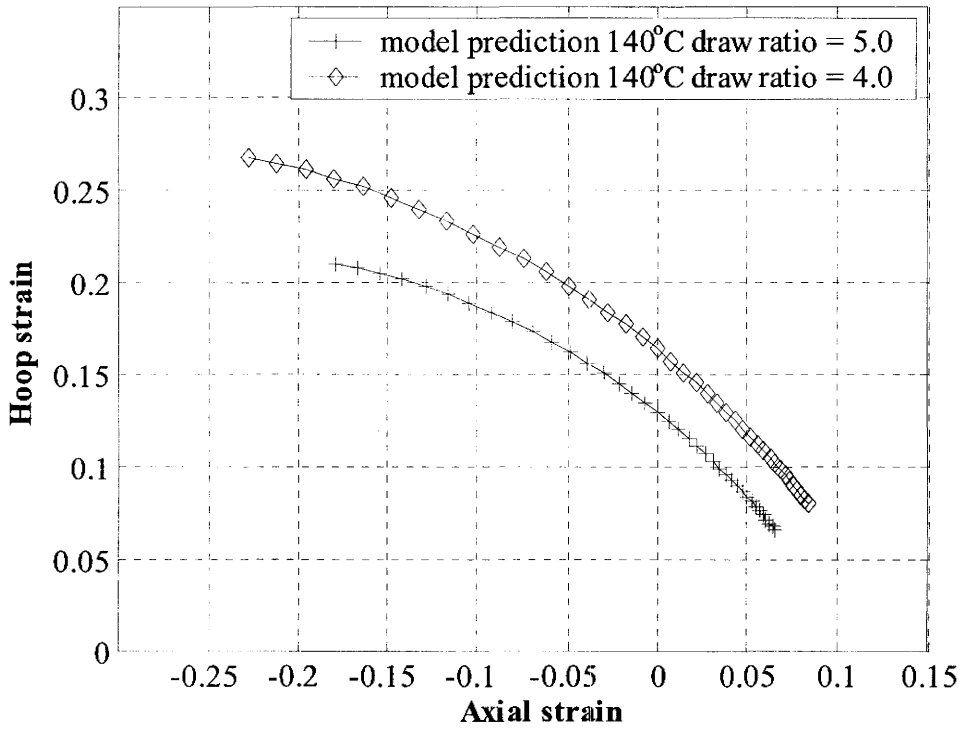

Figure 4.49 Comparison of predicted forming limit diagram for OPP tube at 140°C and a strain rate of 0.0022/second and corresponding to a draw ratio of 4.0 and 5.0.

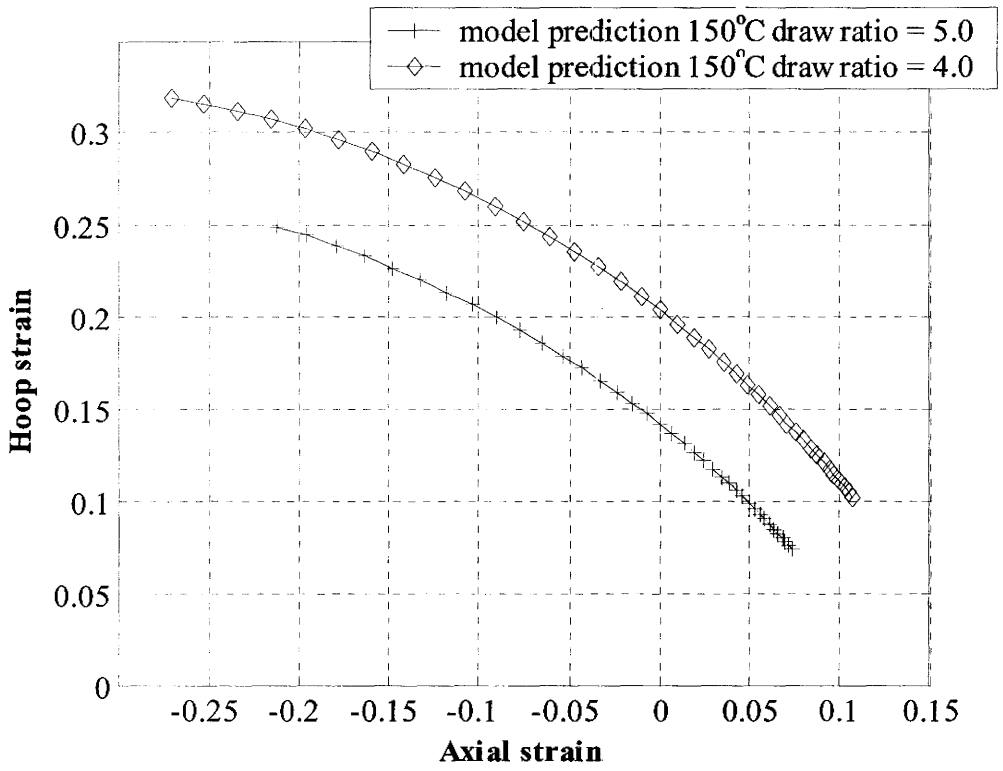

Figure 4.50 Comparison of predicted forming limit diagram for OPP tube at 150°C and a strain rate of 0.0022/second and corresponding to a draw ratio of 4.0 and 5.0.

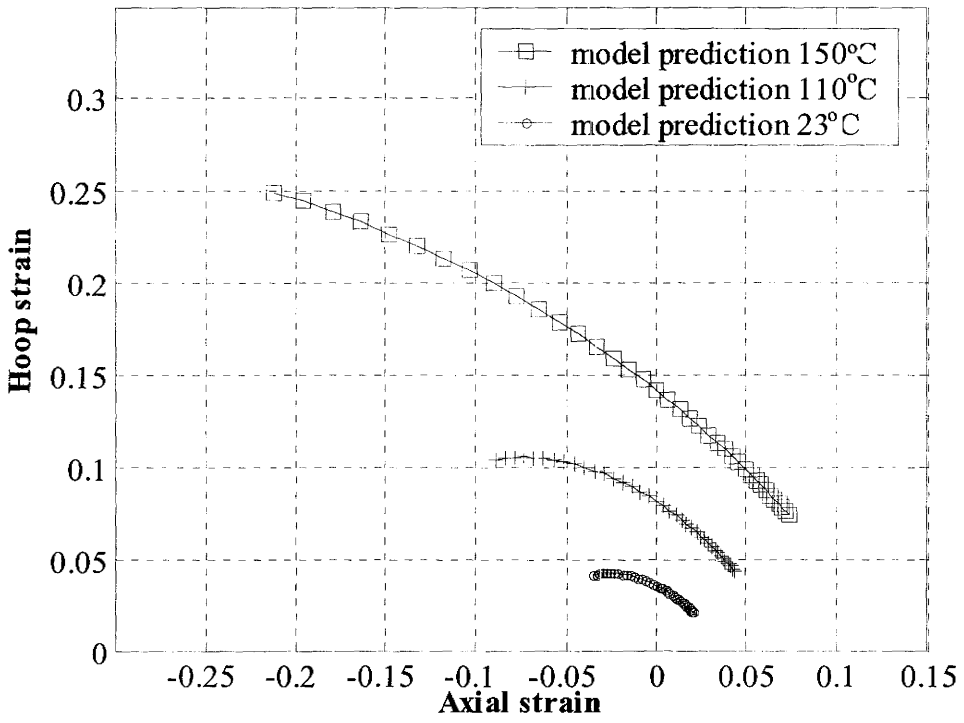

Figure 4.51 Comparison of predicted forming limit diagram for OPP tube at room temperature and at 110°C and 150°C.

This chapter outlined the development of an analytical model for predicting the forming limits for the OPP tube at various temperatures. The model is fully defined by six constants and requires performing six mechanical tests on the tube, including an axial tensile, axial compression and hoop tensile test at two temperatures within the range of interest. The model is able to capture the temperature dependent plastic work contours of the tube through the use of a temperature dependent yield function, which also accounts for the anisotropy and pressure sensitivity exhibited by the material. The forming limits predicted in this chapter will be compared to the forming limits obtained experimentally via tube forming tests in Chapter 5.

CHAPTER 5

VALIDATION OF PREDICTED FORMING LIMITS FOR OPP TUBE

This chapter begins by describing the method used to validate the predicted forming limits presented in Chapter 4. More specifically, a localization criterion is described which makes use of the results from the experimental tube forming tests using the ARAMIS strain measurement system. Using this criterion, results of the hoop strain at localization are extracted from the ARAMIS strain data and compared with the localization strain predicted using the analytical model for various tube tests. Section 5.2 describes a novel tube forming experiment, using an elliptical die, which allows strain paths close to balanced biaxial tension to be achieved. This test is subsequently used to validate the predicted forming limits corresponding to the right hand side of the forming limit diagram. The last section of this chapter presents a comparison of the predicted forming limits with those obtained experimentally, via the tube forming tests, at various temperatures.

5.1 Method of validation of predicted forming limits

The experimental determination of the forming limit curve for tubular materials was reviewed in Chapter 2. As indicated in Chapter 2, tests in which the material is subjected to simultaneous internal pressure and axial load is a common method for the determination of the experimental forming limits for tubular materials. In most cases, as in the forming of metal tubes at room temperature, the strains at the point of tube bursting, typically when the internal pressure is reduced suddenly, is taken as the limit strains. It is often assumed that the time from strain localization (or fracture initiation) to final failure is very small, such that the strains at burst can be taken as the forming limit strains.

In the case of tubular materials that locally neck or thin, but fracture considerably after significant thinning has occurred, alternate methods for experimental forming limit determination are required. These methods would be used to compare the experimental results with the model predictions. However, a clear physical indication that local necking has occurred (as in the case of bursting) is likely not available or may be subjective in the case of the experiments. This has been observed with the oriented polypropylene tubes tested at elevated temperatures for the purposes of this study.

Before a method for extracting the point of strain localization from the experimental tube forming tests is outlined, one should briefly recount the localization criterion that was used in the analytical model predictions. In this case, strain localization was assumed to take place when the hoop force per unit length of the tube reached a

maximum. Using this criterion, one could compare the hoop force versus hoop strain curve obtained from the analytical model for a tube test, at given temperature, strain rate and strain path, to the hoop force versus hoop strain obtained experimentally from a tube forming test at the same conditions. Figure 4.2 (Chapter 4) outlines the method used to calculate the axial and hoop stresses for an experimental tube test. In this case, the hoop force per unit length of the tube is simply the product of the hoop stress and the thickness at a given stage of the deformation. It is to be noted that the same formula was used to calculate the hoop force in the analytical model prediction.

Figures 5.1 and 5.2 compare the hoop force versus hoop strain curve obtained experimentally with that predicted via the analytical model for the tube tests corresponding to stress path 3 and 4 respectively as given in Table 4.1 of Chapter 4. In the case of Figure 5.1, the model is able to capture the overall shape of the hoop force vs. hoop strain curve, although it tended to over predict the value of the maximum force. Although the maximum force predicted by the model was larger than that given by the experimental result, the strain at the point of maximum force, given by the model and the experiment appear to differ by approximately 0.02 or 2% strain. The same is true for Figure 5.2, however, the strain at the point of maximum force, given by the model and the experiment are approximately equal. Therefore, once can conclude that the hoop strain at localization predicted by the analytical model using the maximum force criterion, is in good agreement with the experimental results obtained from the tube forming tests.

The above discussion shows that good agreement occurs between the predicted hoop strain at localization, associated with the peak force in the hoop direction of the tube, compared with the experimental result. However some justification that the strain at which the maximum hoop force occurs, can be associated with the physical occurrence of necking within the material, is required. This method of verification will come once again from the tube forming tests along with the use of the ARAMIS optical strain measurement system.

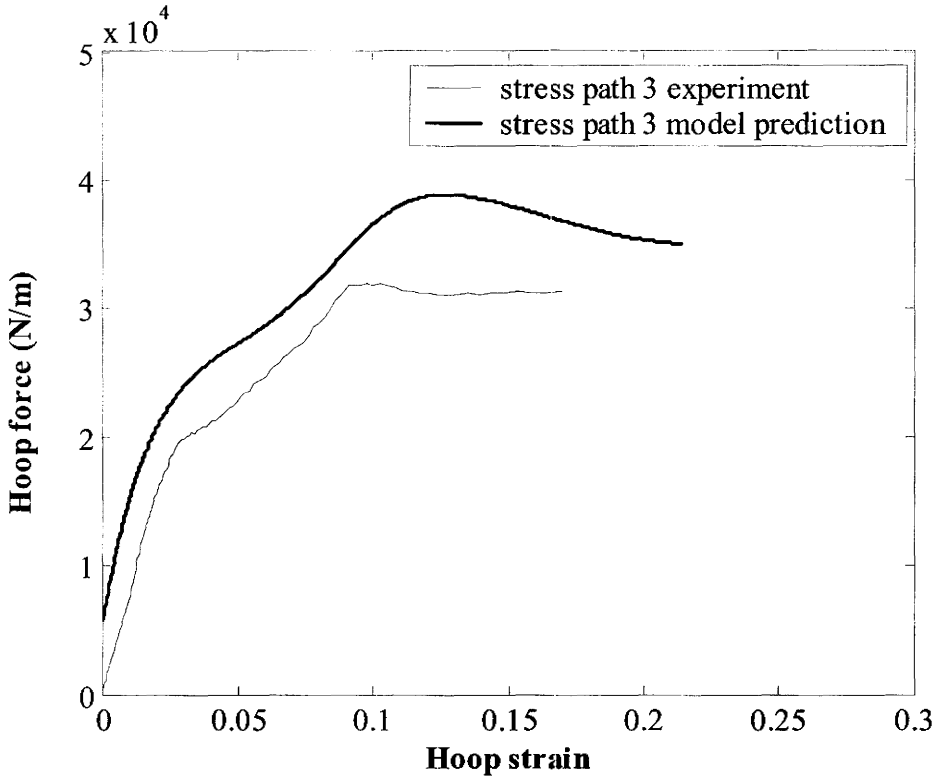

Figure 5.1 Comparison of hoop force vs. hoop strain curve obtained experimentally from tube test at 140°C, corresponding to stress path 3 of Table 4.1 and the prediction via the analytical model.

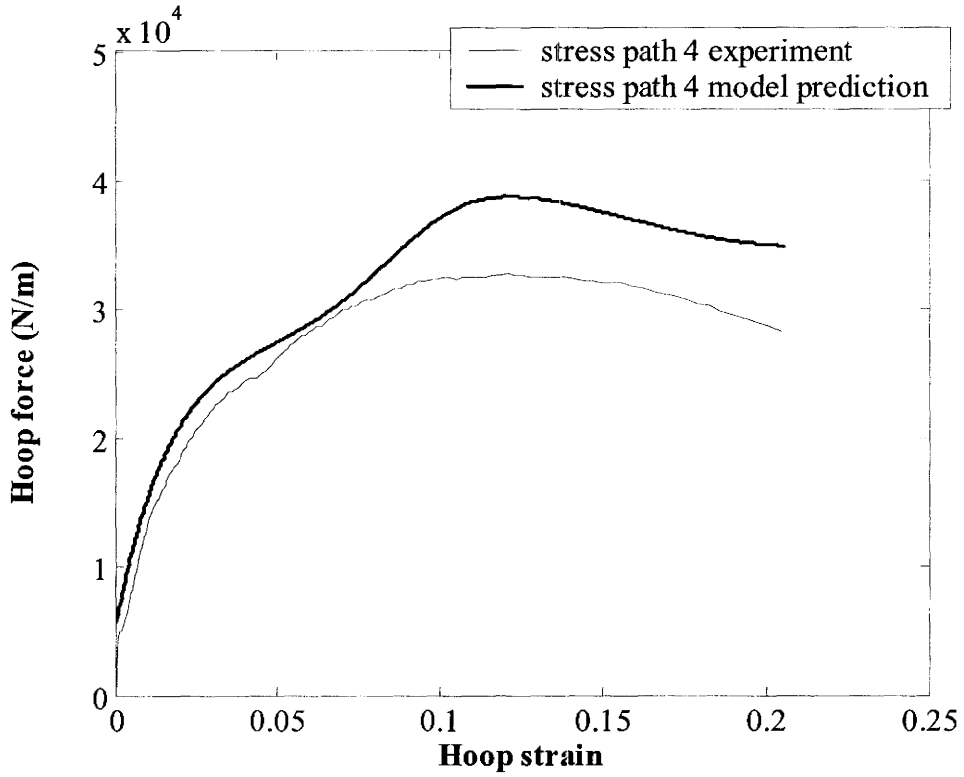

Figure 5.2 Comparison of hoop force vs. hoop strain curve obtained experimentally from tube test at 140°C, corresponding to stress path 4 of Table 4.1 and the prediction via the analytical model.

Figure 5.3 (a) to (m) shows the distribution of major strain across the surface of the deforming tube for the tube test given by stress path 3 (refer to Table 4.1 of Chapter 4). The strain contour plots are obtained directly from the ARAMIS system. The major strain at four points (labeled as 'stage point') have also been indicated on each figure, with each point lying on a horizontal line. For this representative tube test, the hoop strains are initially uniform across the middle section of the tube. This is indicated in Figures 5.3 (a) to (e) in which the maximum strains range from 0.004 to 0.057 respectively. As the deformation progresses beyond this point, a region of maximum strain eventually develops toward the center of the tube. As the tube deforms further, the strains continue to increase at a higher rate within this highly thinned region compared to the regions adjacent to it (refer to Figure 5.3 (g) to (i)). The final stage involves bursting of the tube at the weakest location (the strain image at the point of bursting was not captured by the ARAMIS system). Visual observation of tubes after bursting indicated that the neck was oriented parallel to the axial direction of the tube.

In Figure 5.3 (a) to (m), stage point 0 and 3 are taken as the point of maximum and minimum strain respectively. One can then take the point of strain localization as the point when the strain rates of these two characteristic points begin to diverge by a given amount (i.e. 3%). For the case of thermoplastics tested at elevated temperatures, this can be taken as the point of initiation of strain localization, since after this point, the material may continue to undergo large strains within the thinned region before final bursting takes place.

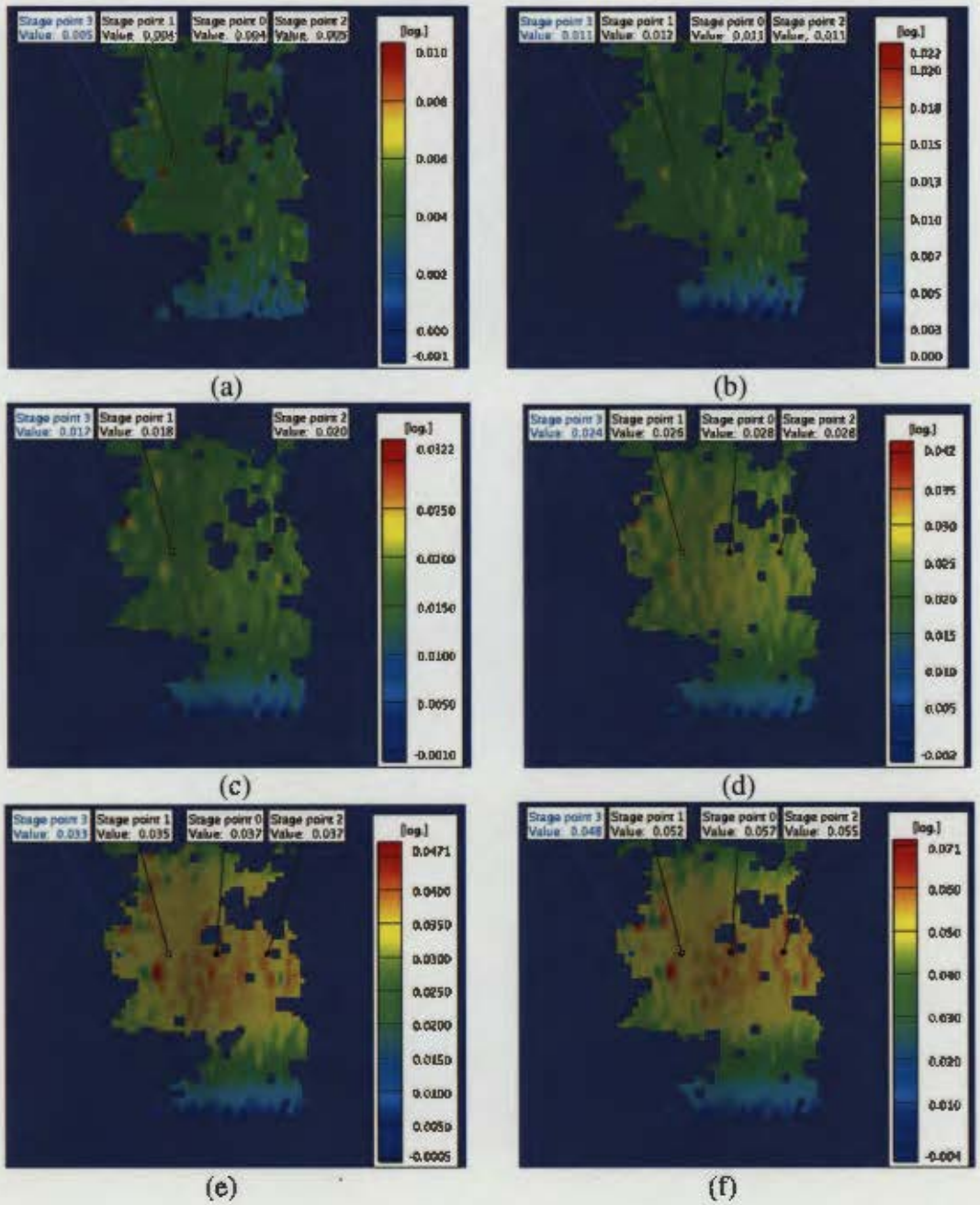

Figure 5.3 Hoop strain contour plots corresponding to tube test along stress path 3 at various stages of the deformation, determined using ARAMIS. Maximum hoop strain occurs at stage point 0 and is given by (a) 0.004 (b) 0.011 (c) not calculated (d) 0.028 (e) 0.037 (f) 0.057.

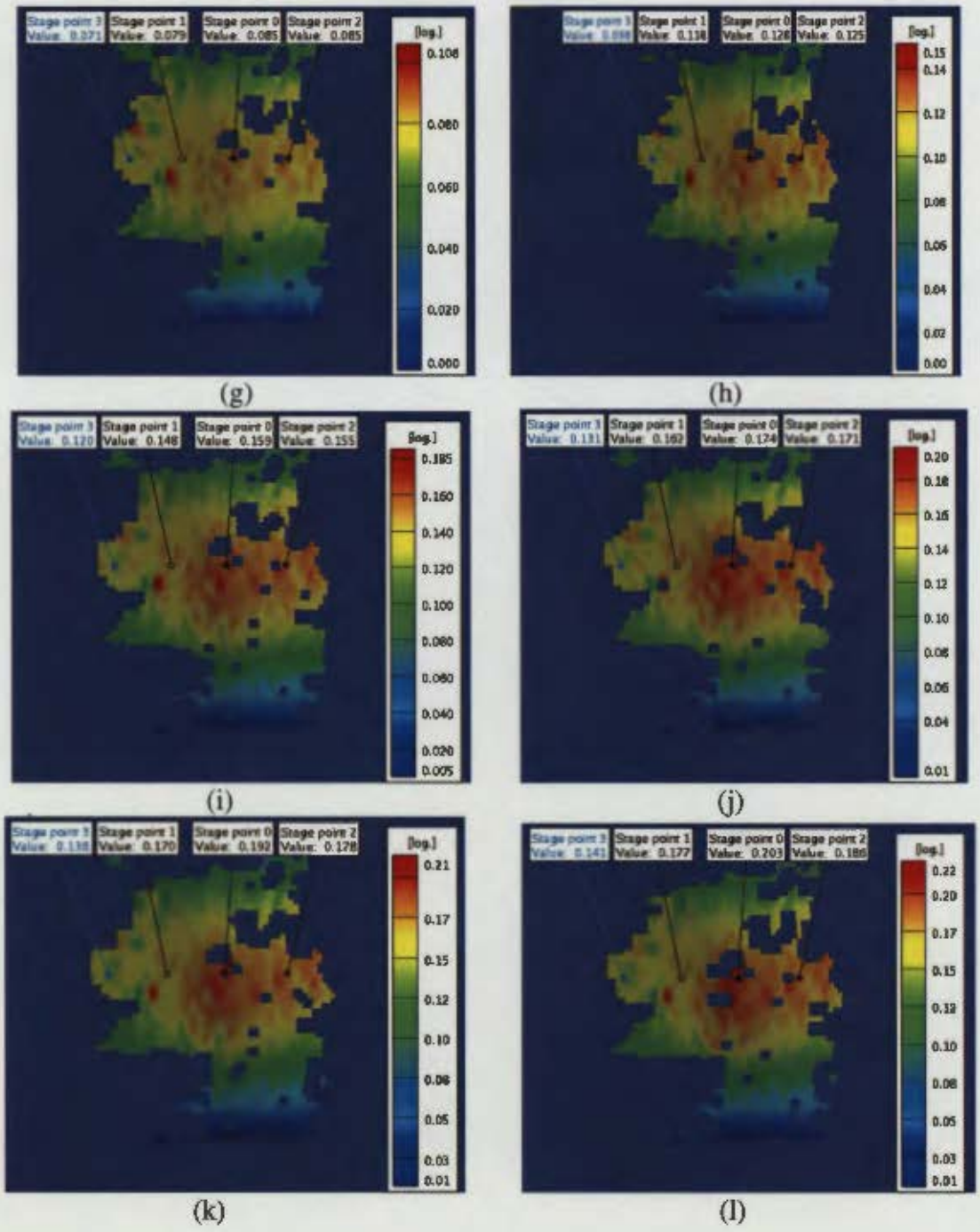

Figure 5.3 *cont.* Hoop strain contour plots corresponding to tube test along stress path 3 at various stages of the deformation, determined using ARAMIS. Maximum hoop strain occurs at stage point 0 and is given by (g) 0.085 (h) 0.128 (i) 0.159 (j) 0.174 (k) 0.192 (l) 0.203.

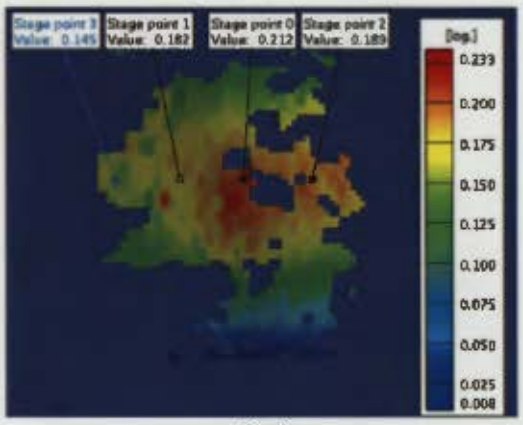

(m)

Figure 5.3 *cont.* Hoop strain contour plots corresponding to tube test along stress path 3 at various stages of the deformation, determined using ARAMIS. Maximum hoop strain occurs at stage point 0 and is given by (m) 0.212.

In order to illustrate this point, an OPP tube tested at 130°C will be considered. In this case, the pressurization took place at a rate of 2.76 x 10^4 Pa/second, with no axial end feeding. This test will subsequently be referred to as path 6. Two points were used for comparison along a horizontal line containing the point of maximum strain along the surface of the deforming tube. The two points are referred to as the points of 'maximum' and 'minimum' strain along the horizontal line. Figure 5.4 compares the hoop strain rate versus time curve for both the maximum and minimum strain points. As indicated in this figure, at a time close to 47 seconds, the two strain rate curves begin to diverge. A value of hoop strain close to 0.13, corresponding to the point of maximum strain at this time, is taken as the hoop strain at localization (refer to Figure 5.5). This value is in good agreement with the hoop strain at which the peak force in the hoop direction occurs (refer to Figure 5.6) from the analytical model prediction.

A similar analysis was performed for a tube test at 110°C in which the pressurization took place at a rate of 2.76 x 10 Pa/second, with no axial end feeding. It will be subsequently referred to as path 7. Figure 5.7 compares the hoop strain rate versus time curve for both the maximum and minimum strain points (along the same horizontal). As indicated in this figure, at a time of 74 seconds, the two strain rate curves begin to diverge. The hoop strain of close to 0.10, corresponding to the point of maximum strain at this time, is taken as the hoop strain at localization (refer to Figure 5.8). This value for the hoop strain is in good agreement with the hoop strain at which the peak force in the hoop direction occurs (refer to Figure 5.9), obtained from the analytical model.

The above analysis suggests that the hoop strain at which the peak force in the hoop direction is reached can be used as an appropriate localization criterion for the OPP tube. This allows for localization strains to be predicted from the analytical model and without the use of the ARAMIS optical strain measurement system.

5.2 Experimental tube forming tests using an elliptical die

Free (or dieless) tube bulging experiments were carried out with internal oil pressure and axial end feed to obtain strain paths on the left hand side of the FLD space. In addition, a new elliptical tube bulging test is utilized to obtain biaxial tensile strain paths. In this test, the tube wall inflates through an elliptical die opening (see Figure 5.10). The expansion process is continuously captured using the ARAMIS strain system and later analyzed to obtain strain paths.

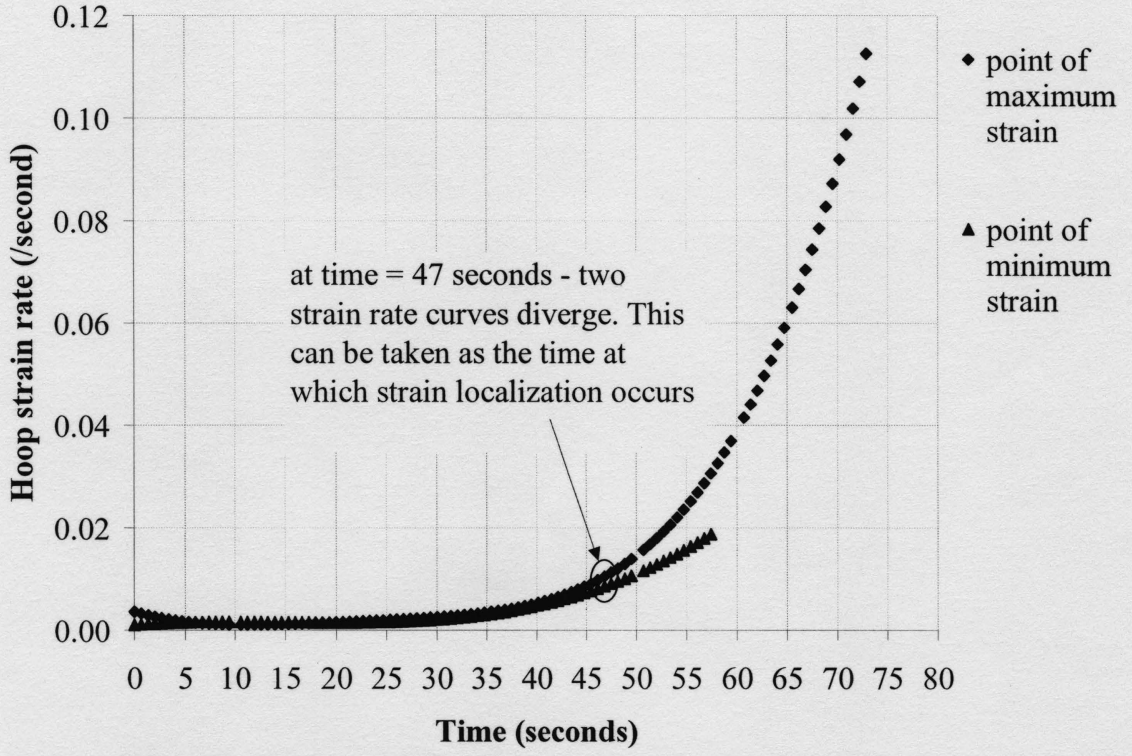

Figure 5.4 Hoop strain rate vs. time plot corresponding to maximum and minimum strain point along a horizontal (containing point of maximum strain) for the tube test at 130°C, and corresponding to path 6.

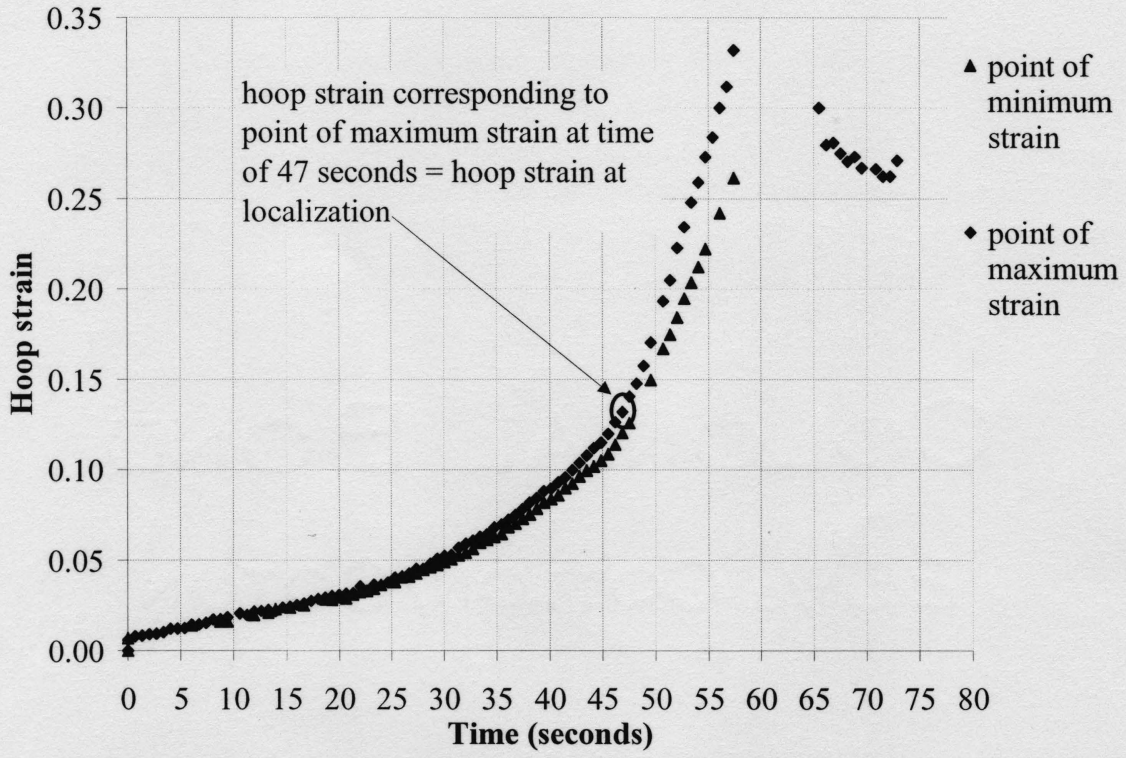

Figure 5.5 Hoop strain vs. time plot corresponding to maximum and minimum strain point along a horizontal (containing point of maximum strain) for the tube test at 130°C, and corresponding to path 6.

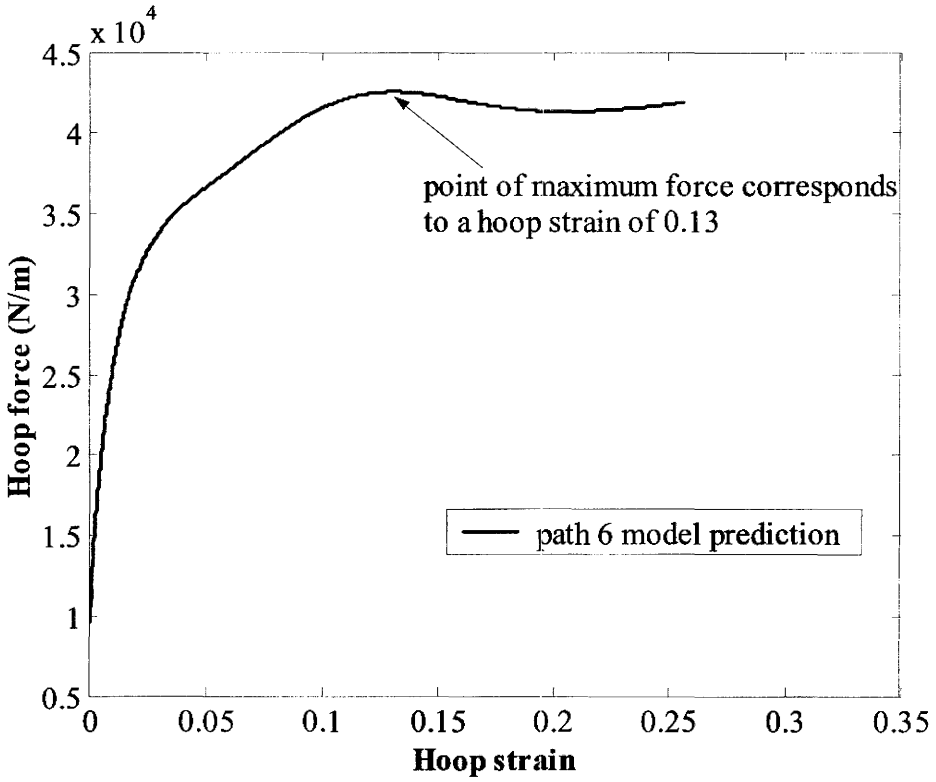

Figure 5.6 Hoop force vs. hoop strain curve obtained from analytical model for the tube test at 130°C, and corresponding to path 6.

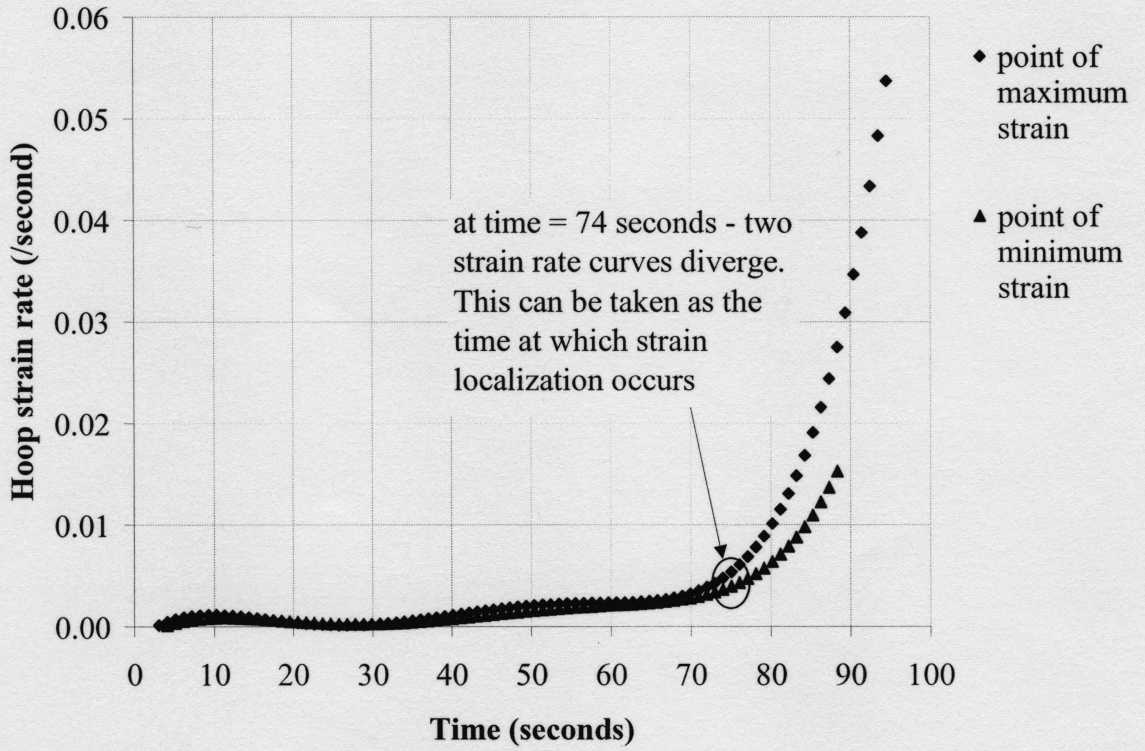

Figure 5.7 Hoop strain rate vs. time plot corresponding to maximum and minimum strain point along a horizontal (containing point of maximum strain) for the tube test at 110°C, and corresponding to path 7.

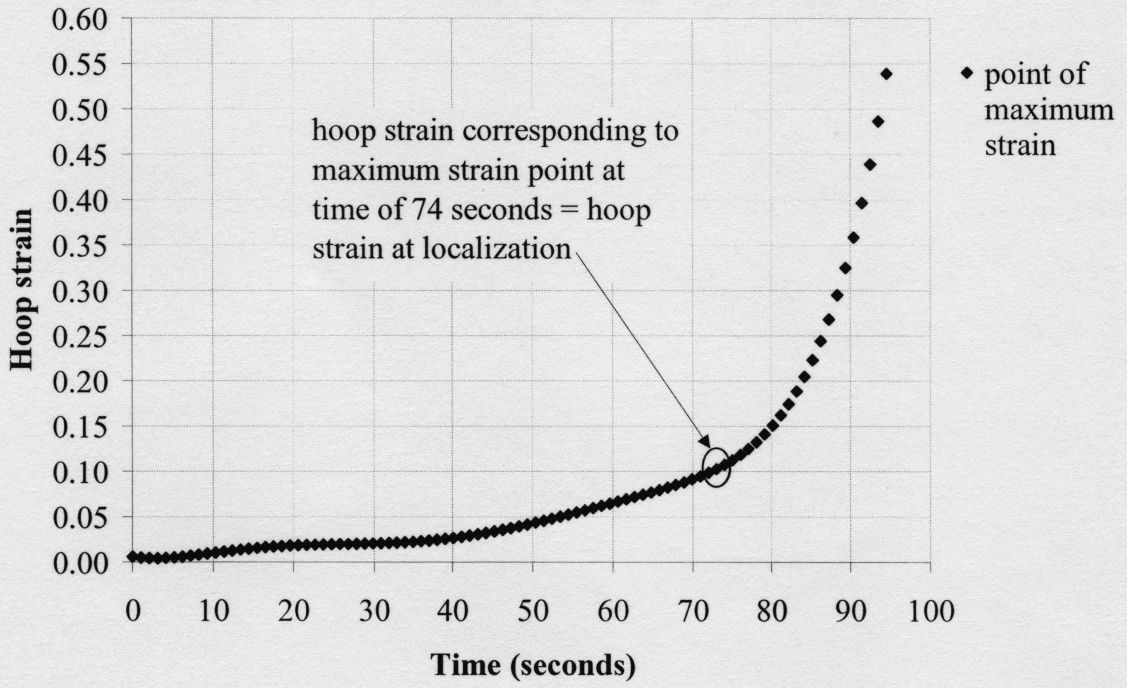

Figure 5.8 Hoop strain vs. time plot corresponding to maximum and minimum strain point along a horizontal (containing point of maximum strain) for the tube test at 110°C, and corresponding to path 7.

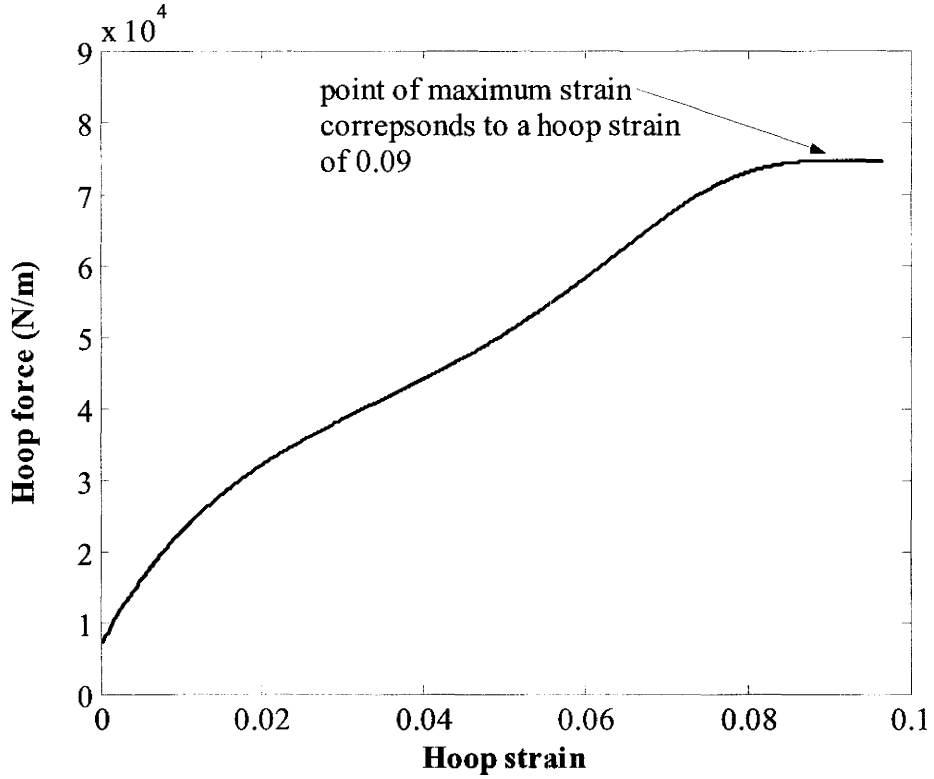

Figure 5.9 Hoop force vs. hoop strain curve obtained from analytical model for the tube test at 110°C, and corresponding to path 7.

The details of the design and selection of the elliptical die opening geometry based on an analysis of required strain paths is presented in Appendix F. It should be mentioned here that prior to selecting suitable dimensions for an elliptical die, a die with a circular opening was also considered. However, calculations of the resulting strains at the pole due to a given bulge height, would require a circular hole of diameter less than 13 mm. It should be mentioned that the problem associated with employing a hole with such a small area is that a large internal pressure would be required to deform the material. The magnitude of the pressures required was greater than what could be supplied by the test machine used here. Therefore, the elliptical die geometry appeared to be a more feasible choice.

For the selected elliptical die geometry with a major axis length of 31 mm and a minor axis length of 19 mm, tube tests were conducted at various temperatures, where the tube was subjected to internal pressure only. Figures 5.11 (a) and 5.12 (a) show the development of major and minor strains at the point of maximum strain for a tube tested at 140°C and 150°C respectively. Note that in both cases the tubes were subjected to a pressure rate of 2.76×10^4 Pa/second. Although the strain ratio was not exactly 1 (refer to Figure 5.11 (b) and Figure 5.12 (b)), the case of the tube tested at 140°C produced a much closer result to the balanced biaxial strain state. In any case, the current test enabled experimental forming limits close to the balanced biaxial state to be obtained for model validation purposes.

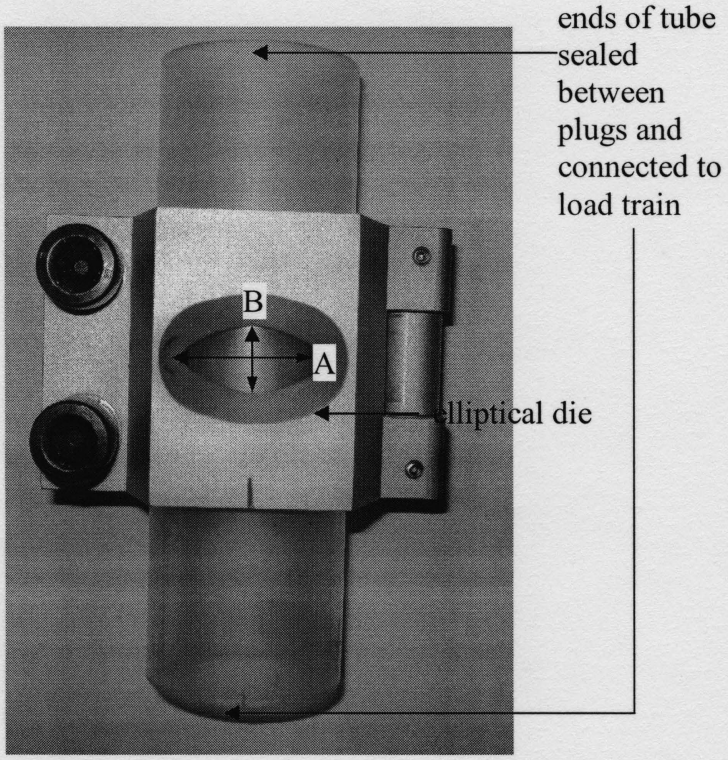

Figure 5.10 Elliptical die used in tube forming test showing major and minor axis, *A* and *B* respectively.

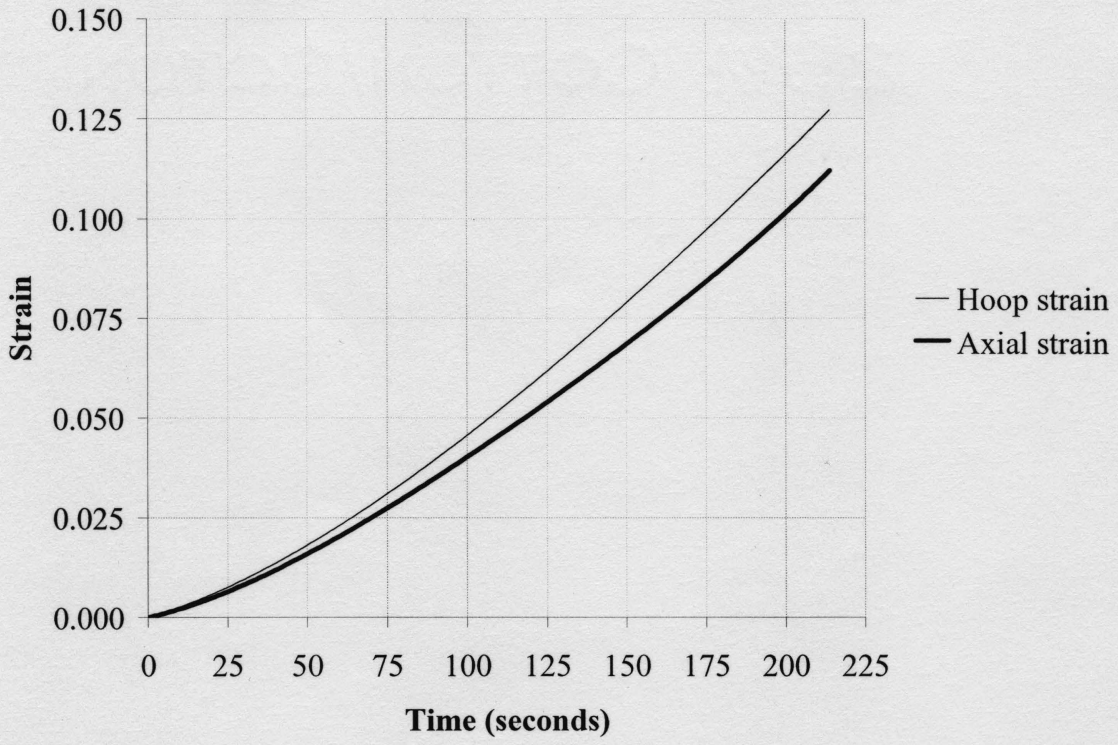

(a)

Figure 5.11(a) Development of hoop and axial strains, corresponding to the point of maximum strain, for tube test using an elliptical die with dimensions A = 31 mm and B = 19 mm. The test was conducted at 140°C and the tube was subjected to a pressure rate of 2.76 x 10^4 Pa/second.

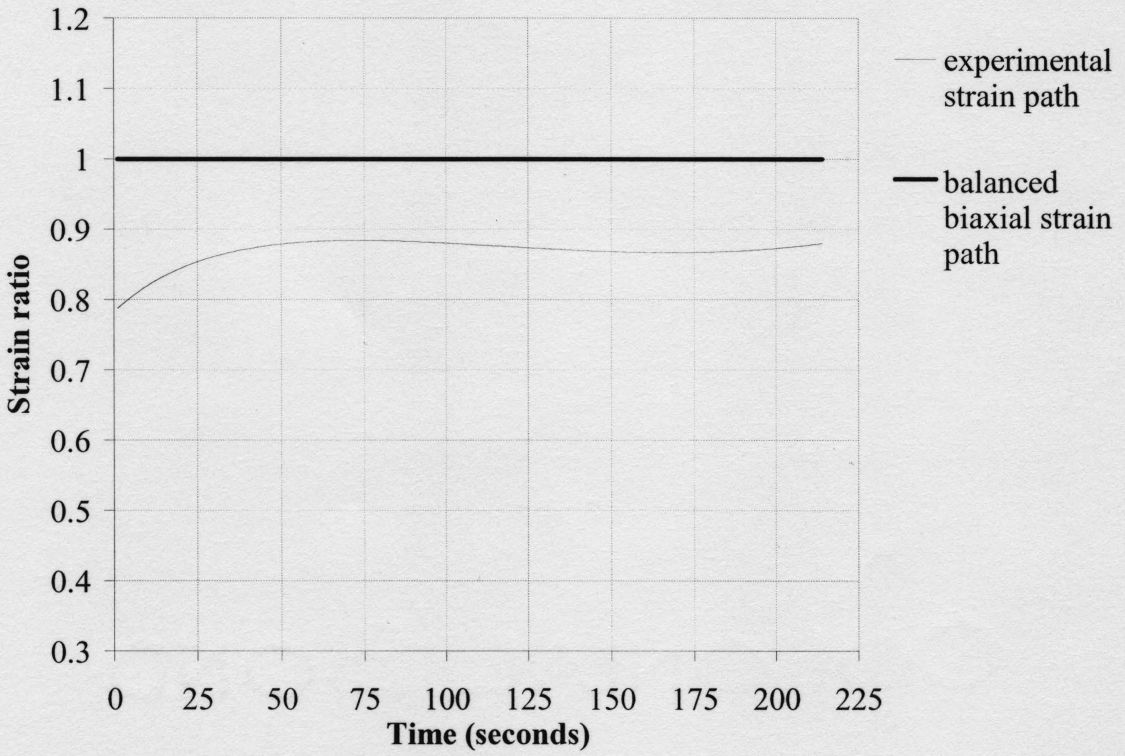

(b)

Figure 5.11(b) Strain ratio versus time, corresponding to the point of maximum strain, for tube test using an elliptical die with dimensions A = 31 mm and B = 19 mm. The test was conducted at 140°C and the tube was subjected to a pressure rate of 2.76 x 10^4 Pa/second.

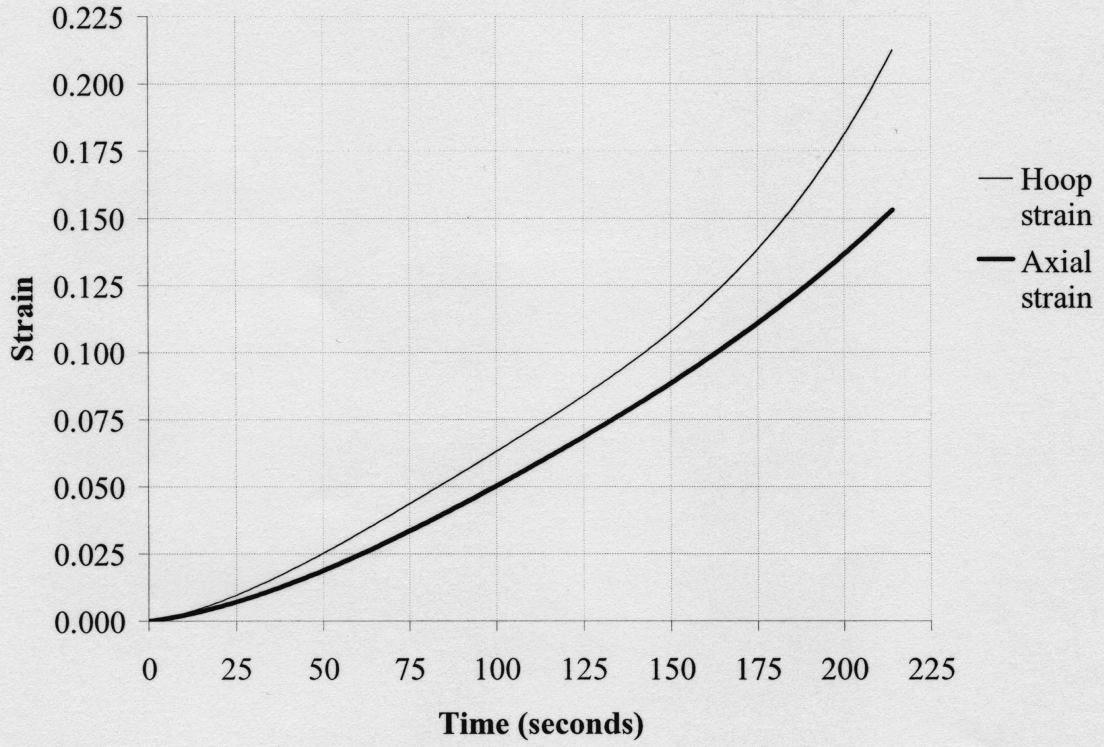

(a)

Figure 5.12(a) Development of hoop and axial strains with time, corresponding to point of maximum strain, for tube test using an elliptical die with dimensions A = 31 mm and B = 19 mm. The test was conducted at 150°C and the tube was subjected to a pressure rate of 2.76 x 10^4 Pa/second.

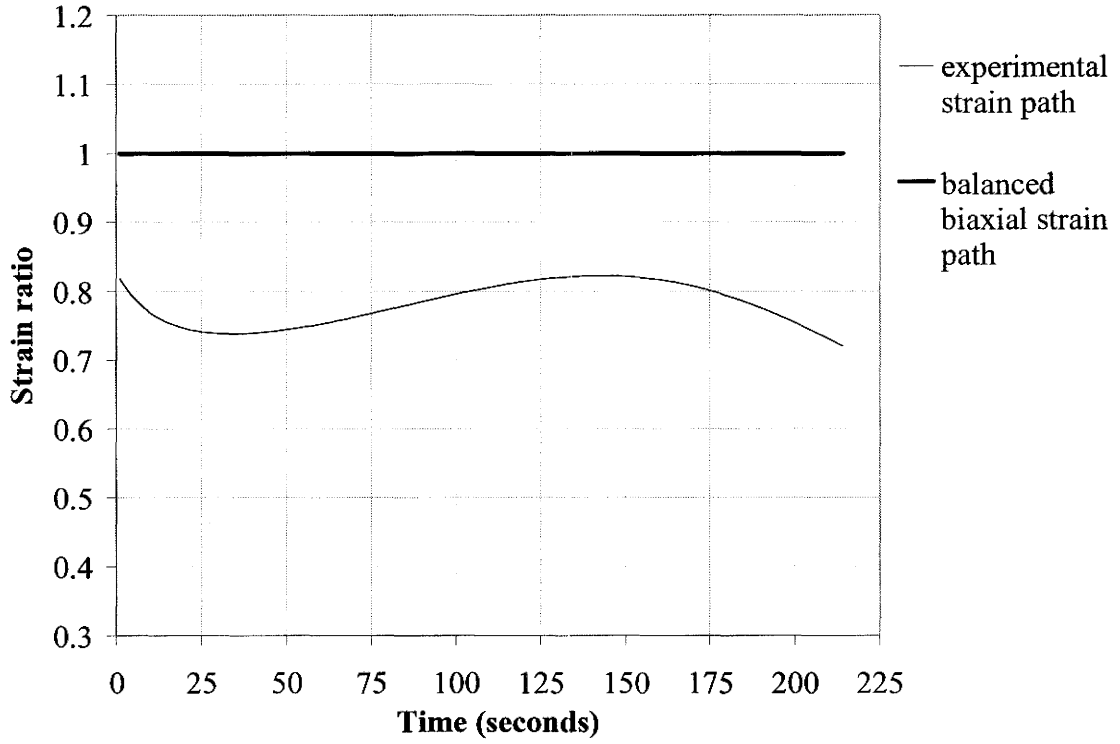

(b)

Figure 5.12(b) Strain ratio versus time, corresponding to point of maximum strain, for tube test using an elliptical die with dimensions A = 31 mm and B = 19 mm. The test was conducted at 150°C and the tube was subjected to a pressure rate of 2.76 x 10^4 Pa/second.

5.3 Comparison of experimental forming limits with predicted forming limits

This section presents a comparison of the predicted forming limits for the OPP tube (draw ratio 5.0) tested at a rate of 0.0022/second, with the experimentally obtained limits from tube forming tests at various temperatures. Note here that each of the experimental tube forming tests were repeated at least two times to ensure reproducibility of the limit strains. As described earlier, localization was taken at the point when the strain rate curves associated with the maximum and minimum strain points (along the horizontal containing the point of maximum strain) begin to diverge. Also, with respect to the experimental strain paths, the termination point of each path indicates the axial and hoop strain corresponding to strain localization. Photographs of respective test samples are included in the FLD's.

Figure 5.13 shows the predicted forming limits at 110°C. The model predicts a hoop strain of close to 0.08 corresponding to the plane strain condition, which is in good agreement with the experimental result. Figure 5.14 shows the model prediction at 130°C. As indicated in this figure, the model predicts a hoop strain of 0.12 at localization corresponding to the plane strain condition. Figure 5.14 also presents the experimental forming limits obtained from two tube forming tests, one following a strain path slightly to the left of plane strain and the other following a strain ratio close to 0.8. Generally, good agreement is observed between the experimental and predicted forming limits.

Figures 5.15 and 5.16 compare the experimental and model prediction of the forming limits at 140°C and 150°C respectively. Figure 5.15 shows that good agreement

between the experimental forming limits and the predicted values for the various strain paths exists. Figure 5.15 also shows that the two experimental strain paths on the extreme left hand side of the forming limit diagram are significantly non-linear. However, the strain paths on the positive biaxial strain side of the FLD show nearly linear behaviour. This indicates that the introduction of axial end feeding introduces some degree of non-linearity to the strain paths. This fact is also evident for tube tests conducted at the various other temperatures.

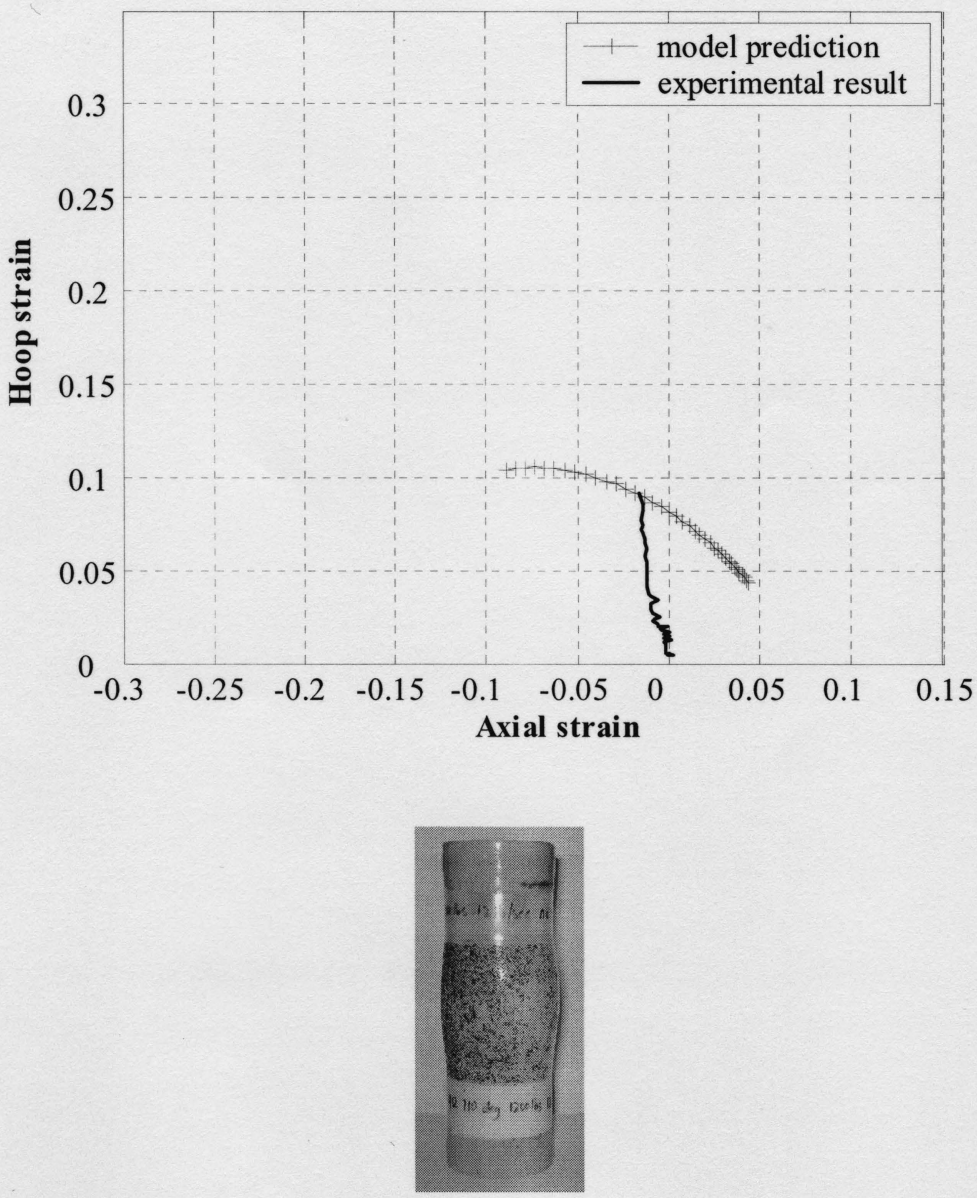

Figure 5.13 Comparison of predicted forming limits at 110°C with the result from an experimental tube forming test.

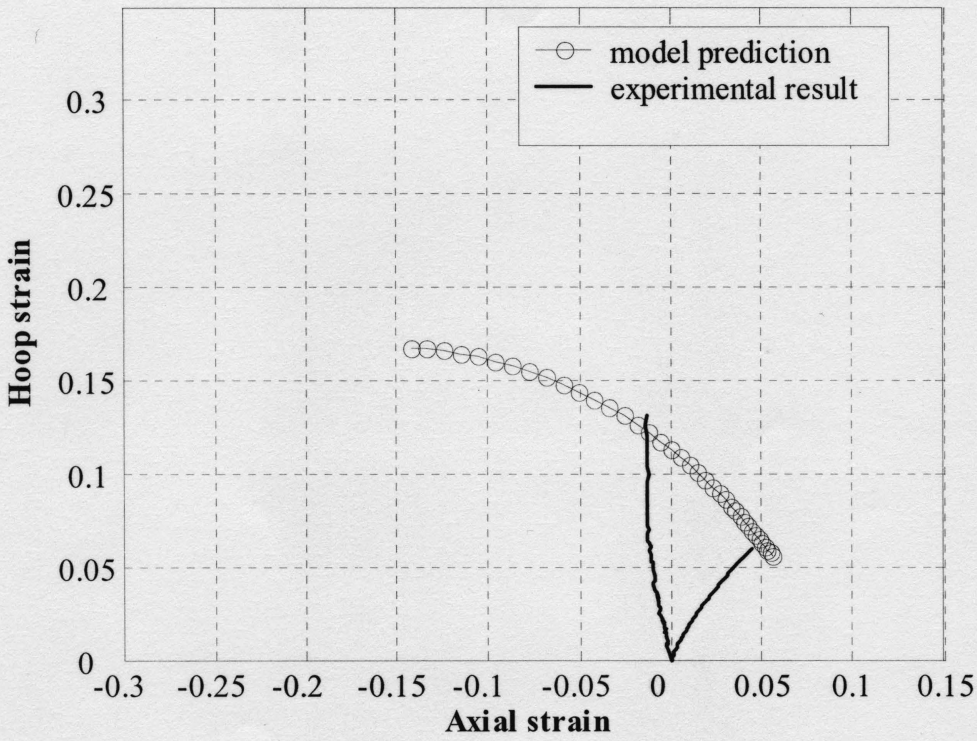

Figure 5.14 Comparison of predicted forming limits at 130°C with the results from experimental tube forming tests. Samples from left to right correspond to experimental forming limit curves from left to right respectively.

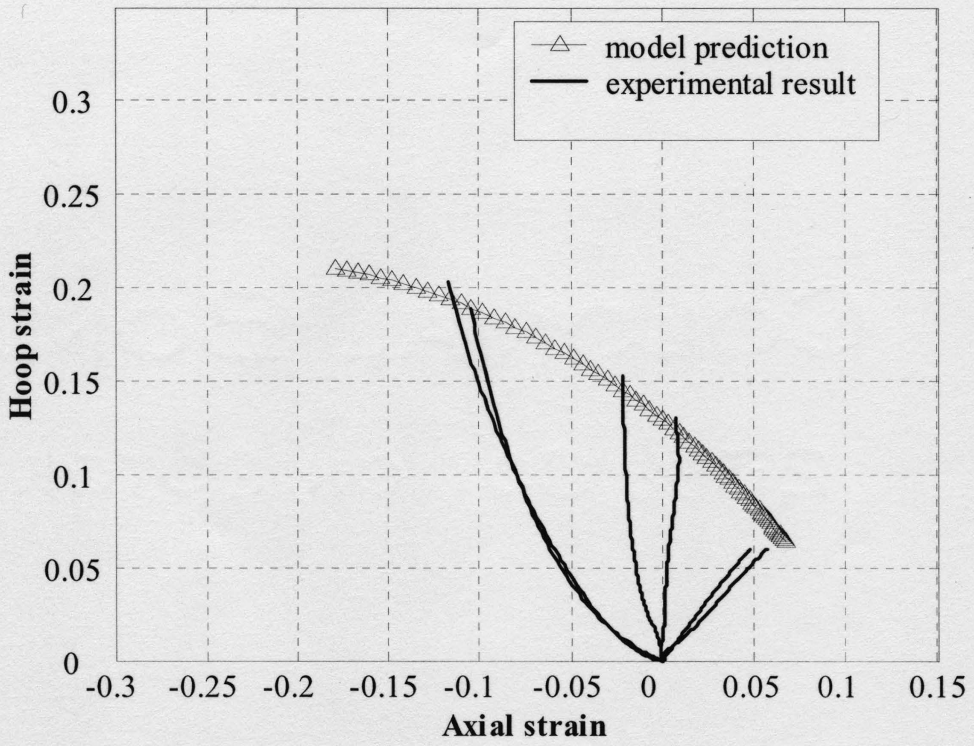

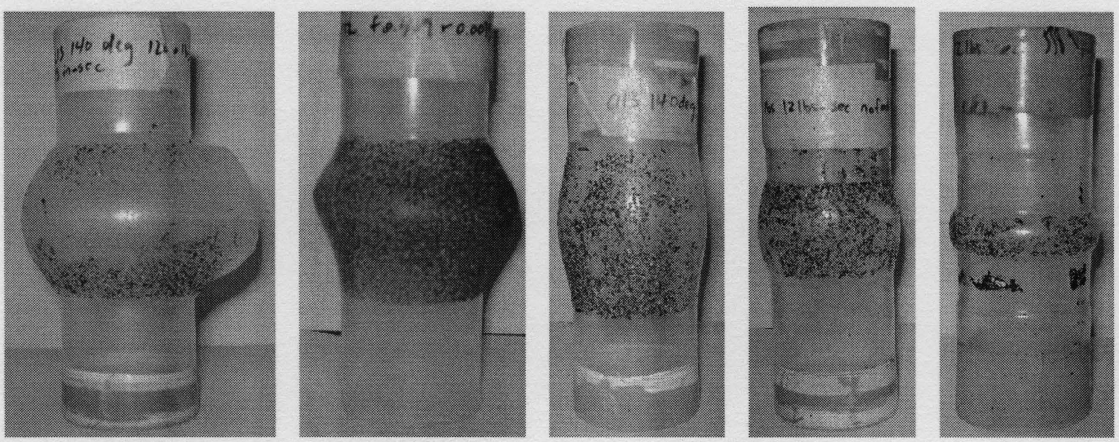

Figure 5.15 Comparison of predicted forming limits at 140°C with results from experimental tube forming tests. Samples from left to right correspond to experimental forming limit curves from left to right respectively.

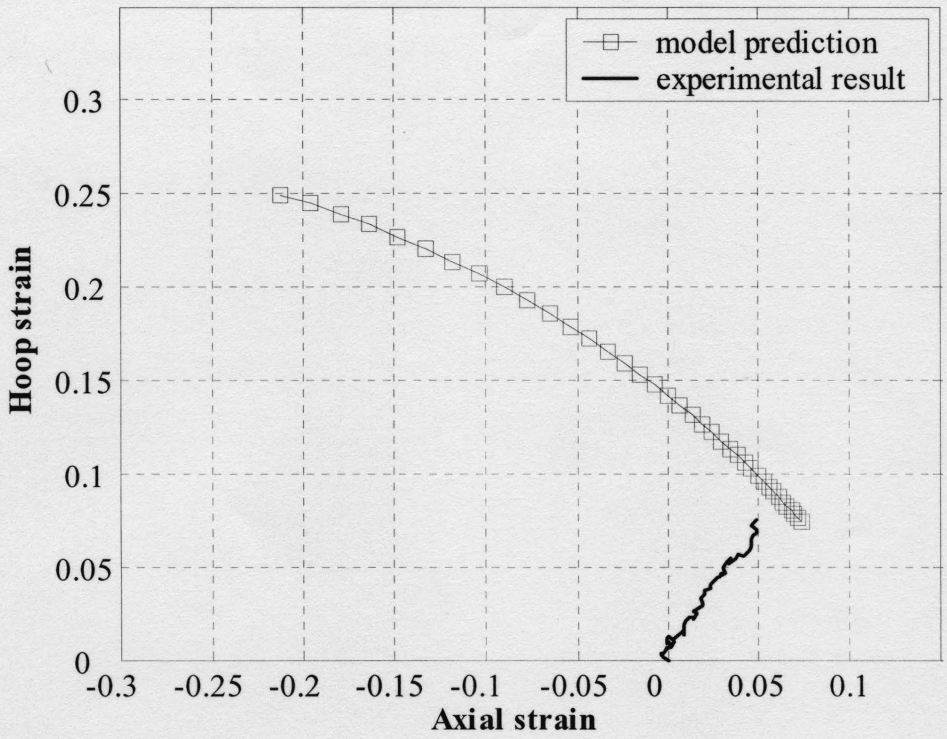

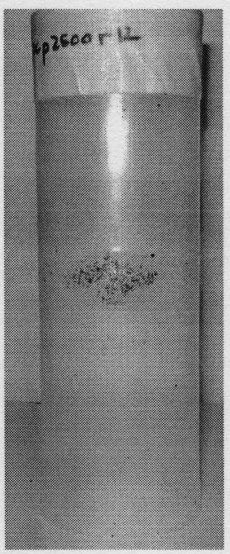

Figure 5.16 Comparison of predicted forming limits at 150°C with the result from an experimental tube forming test.

This chapter presented a method for using continuous strain data, from a tube forming experiment, to delineate the point of strain localization for subsequent comparison to model predictions. In general, good agreement between the model predictions of strain localization and the experimental results were observed. A novel tube forming test using an elliptical die was also described, which allowed strain paths close to balanced biaxial tension to be achieved. This type of test could then be used to validate the right hand side of the predicted FLDs. Chapter 6 presents a discussion of the validity of some of the assumptions employed in this research, the novelty of certain aspects of the experimental work as the significance of the results from an industrial standpoint. Also, some discussion around the practical aspects of the forming of these oriented polypropylene tubular materials is presented, i.e. the need for the cooling of the tube after forming to avoid shrinkage etc.

CHAPTER 6

DISCUSSION

This chapter will begin with a discussion of the key assumptions used in the development of the analytical model in this research. A further discussion of the results of this study as well as their implication on the forming of oriented thermoplastic tubes from an industrial standpoint will also be presented.

In the analysis used for the prediction of the forming limits for the OPP tube, it was assumed that the tube could be considered "thin-walled". Therefore, the stress along the thickness direction was assumed to be zero (i.e. $\sigma_t = 0$). One example of where this assumption was employed was in the expression for the plastic work per unit volume (i.e. Equation (4.16)). In this case, there was no contribution to the total plastic work along the thickness direction since the stress along this direction was assumed to be equal to zero. As mentioned in Appendix B, the OPP tubes used in this study had an inner radius of 22.43 mm and a wall thickness of 2.34 mm, giving an inner-radius-to-wall-thickness

ratio of approximately 9.6. In general, "thin-wall" refers to a vessel having an inner-radius-to-wall-thickness ratio of 10 or more (Hibbeler, 1993). In this case, the thin-walled tube assumption can be used, without the introduction of significant error.

Chapter 2 detailed the experimental test methods for obtaining the uniaxial mechanical properties of the tube, along the principal directions, in both tension and compression. It is important to note here that the specimens used for the tests were machined directly from the oriented tube. For practical application of this material to potential automotive structural components, the tubes used for forming would normally be either ram extruded and/or die drawn. In this case, there is a need to obtain properties from specimens machined directly from the final tube as opposed to from a solid oriented rod of material that would subsequently be machined into a tube. The latter method of specimen preparation would require an extra step in the production process, thereby rendering it less attractive for large volume automotive applications.

In addition, assuming that the hoop properties (both tensile and compressive) are equal to the thickness properties can be taken to be satisfactory from a simple discussion of the structure of these oriented materials. Referring to Figure 6.1 (taken from Figure 2.5 of Chapter 2), subjecting the material to tension along the y direction means deforming the material along a direction parallel to the molecular chain orientation. The material is strongest along this direction, hence, the stress-strain curve obtained along this direction would be much different than that obtained from pulling the material along the x –direction. However, since groups of fibrils are also packed in the z (or thickness

direction), one would expect that properties along the x and z direction would be similar since the pulling direction is perpendicular to the chain orientation direction in both cases. Also, similar chain folding within the microfibrils is expected along he x-y plane as well as the y-z plane.

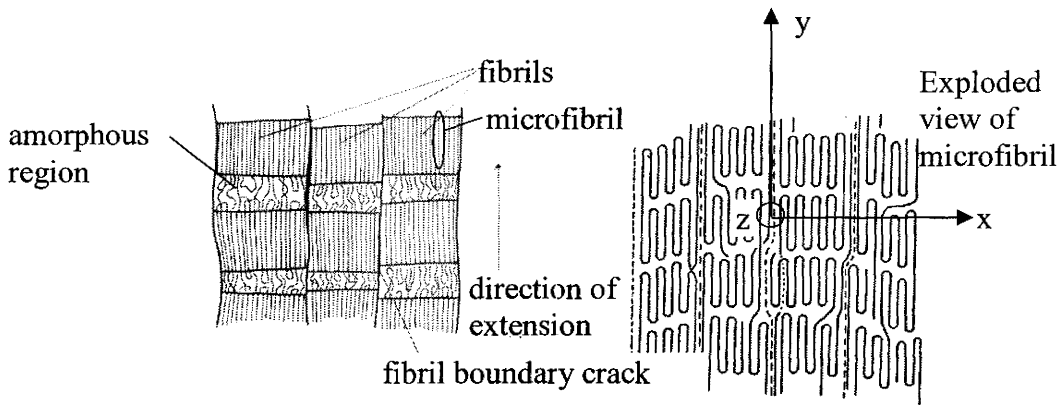

Figure 6.1 Fibrillar structure of an oriented polymer showing principal material directions (McCrum et al., 1997).

The novelty of certain aspects of the experimental work in this study should also be emphasized here. For example, a new ring compression test was employed to obtain the axial compressive properties of the tube up to large strains. The key was to use very short specimens, which would prevent buckling of the sample during compression. In addition, the ring hoop tension test was extended to obtain the hoop tensile properties of the oriented polypropylene tube at elevated temperatures and up to large strains with the use of the ARAMIS system. This allowed full field strain measurements of the sample along its thickness surface to be determined continuously during the deformation. This was particularly useful for the testing of this material in tension along the hoop direction,

since a localized neck developed in the sample, early on in the deformation process. The formation of the localized neck was followed by drawing of the material within the neck as the tensile extension continued. The ARAMIS system allowed both major and minor strains within the localized necked region to be determined for the subsequent determination of the true stress curve.

In order to validate the accuracy of the forming limit model for the OPP tube presented in Chapter 4, experimental forming limits for this material corresponding to both the left and right hand side of the forming limit diagram (FLD) were required. Tube forming tests involving simultaneous axial end feeding and internal pressurization are successful in yielding experimental forming limits corresponding to strain paths on the left hand side of the forming limit diagram. Similarly, forming tests involving internal pressurization of the tube with no axial end feeding, are typically able to subject the tube to close to the plane strain condition. However, obtaining strain paths on the right hand side of the FLD close to the balanced biaxial strain path requires alternate experimental test methods. One such method involves decreasing the length of the free section of the tube, and then subsequently pressurizing the tube with no axial end feeding. The disadvantage, however, is that various experimental trials, to optimize the length of the free section, for obtaining a given strain path would be required. A second possibility would involve equipping the testing machine with the capability of simultaneously pulling the tube in tension along the axial direction while subjecting it to internal pressure. In this case, specialized clamps for gripping and stretching the tube without slippage would be required. This becomes a more difficult task when the tubes are tested

at elevated temperatures and significant softening of the material occurs within the clamped section, thereby increasing the chances of the tube slipping.

Turning to the experimental biaxial testing of the tube, the elliptical bulge test, typically applied to sheet materials was adapted and extended for use with the tubular material used in this study. The elliptical dies were designed to subject the material to strain paths close to balanced biaxial tension at elevated temperatures. The ARAMIS strain measurement system was used to measure the biaxial strains developing in the material as the deformation progressed. Through the use of ARAMIS, analytical calculations of the strains at the pole were not required as direct measurements of the strains were possible This allowed the predicted forming limits to be validated for strain paths corresponding to the right hand side of the forming limit diagram.

It should also be mentioned here that tube forming tests were also carried out with the use of the Interlaken tube forming system located in the Materials Forming Laboratory. Unlike the hot oil tube forming test rig described in Chapter 3, the Interlaken system uses gas as the pressurizing medium, forms the tube within a closed die and allows one or both ends of the tube to be fed via the use of hydraulic actuators. Figure 6.2 shows the Interlaken system including the forming die and the actuators used for axial feeding of the tube ends. This gas forming system allowed limit strains to be obtained under conditions closer to a real tube forming process involving heated dies. For a typical tube forming experiment involving this system, the following were the sequence of steps followed:

1. Preheat tube in an external oven set to desired temperature.
2. Remove tube from oven and place inside heated lower die (set to desired temperature).
3. Seal tube between feed actuators.
4. Close die and heat further so that tube and die are uniformly brought to the required temperature.
5. Form the tube by simultaneous axial end feeding and internal pressurization. The rate at which the feeding and pressurization take place, as well as their respective magnitudes, influence the overall strain path followed by the material.
6. Once the forming stage is complete, the tube is cooled under pressure to a temperature of 80°C or less. This avoids shrinkage/warpage of the tube which occurs if the pressure is rapidly released while the tube is still hot.
7. Pressure released from tube.
8. Die is opened and tube is removed.

One important point to note here is the importance of cooling the tube under pressure after forming. Figure 6.3 shows three tube samples that were formed under the same conditions at 150°C. However, each was cooled for different time, and hence, reached a different temperature after the feeding and pressurization sequence was complete and prior to pressure release. As indicated in Figure 6.3, the sample that was cooled to 80°C proved to exhibit the least part shrinkage. This additional tube cooling feature added to the forming process worked to "freeze" in the formed shape and

eliminate shape distortion and localized necking resulting from the rapid release of pressure after the feeding and pressurization stage. This has a practical implication on the forming of these materials. If part shrinkage and/or warpage is to be avoided, rapid cooling of the part must be incorporated into the forming cycle for these materials.

Figure 6.4 shows a selection of OPP tubes formed using the Interlaken gas forming system at a temperature of 150°C. The process conditions at which the tubes were formed were: (a) temperature of 150°C (b) axial feed of 38.1 mm (c) maximum internal pressure of 2.76 MPa and (d) tube cooled to 80°C once it reached the maximum temperature.

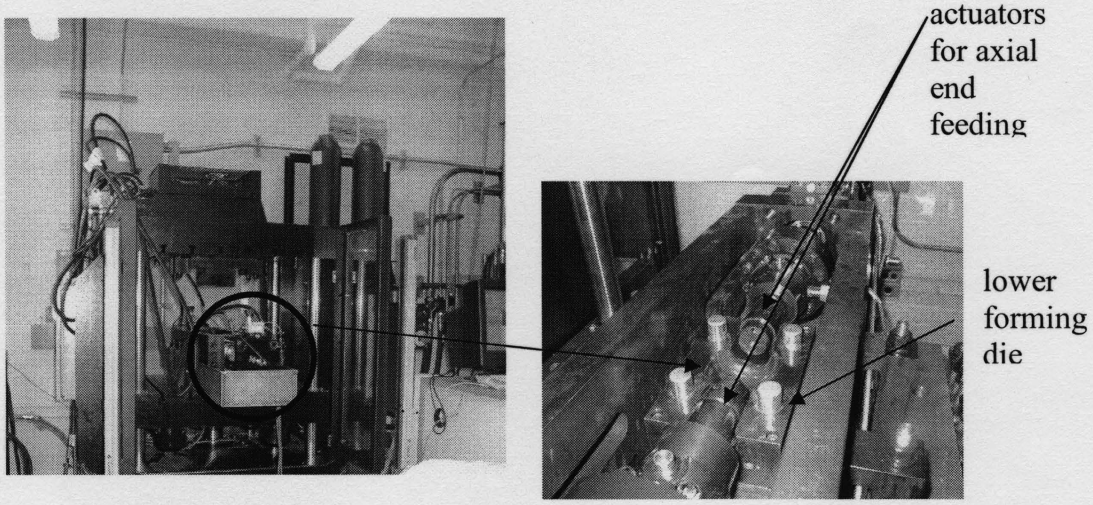

Figure 6.2 Interlaken axial feed hot tube gas forming system based on Servopress 150 mechanical test system.

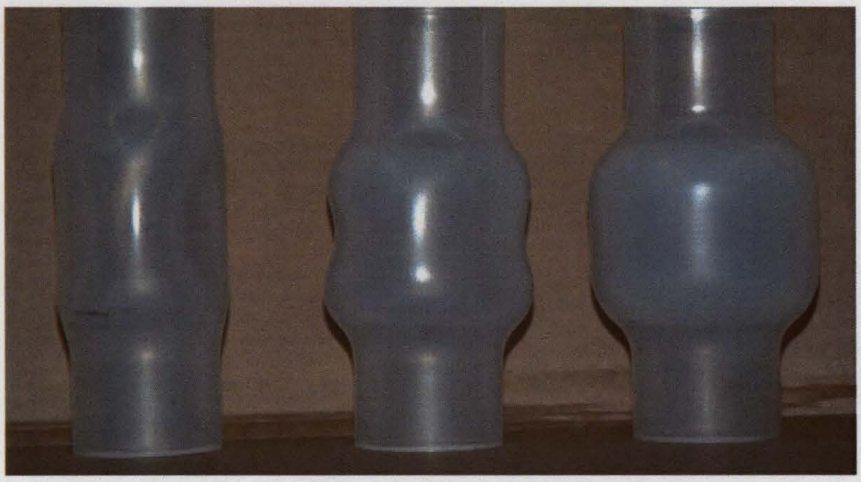

no cooling | cooling for 15 minutes to 130°C | cooling for 45 minutes to 80°C

Figure 6.3 Effect of cooling time on OPP tube formed shape.

Figure 6.4 OPP tube samples formed using Interlaken gas forming system.

A discussion of some aspects of the development and use of the modified G'Sell model should also be presented. Section 4.4.2.1 of Chapter 4 described how the modified G'Sell model could be used to predict the true stress strain curve (in tension or compression along a given tube direction) or the plastic stress strain curve by removing or retaining the N term respectively. The value of the predicted yield stress depends, for example, on the offset method used to define the yield point from the experimental true stress strain curves. The offset method used (i.e. 0.5% offset used in this study) delineates the cut-off between the elastic and fully plastic portion of the experimental stress strain curve. Ideally, loading and unloading experiments, in the transition region between the elastic and plastic behaviour, would be required to accurately specify the yield point from the experimental stress strain curve.

As shown in Chapter 4 (Sections 4.4.2.3-4.4.2.5), the modified G'Sell model was shown to accurately predict the temperature dependent axial tensile, hoop tensile and axial compressive behaviour of the OPP tube. These predicted uniaxial curves could then be used to predict the temperature dependent plastic work contours for the material. The temperature dependent forming limit diagram for the OPP tube determined using the modified G'Sell model (approach 2) showed good agreement with that determined using approach 1. Note here that in approach 1, a linear relationship between the uniaxial stress parameters in the pressure-modified Hill criterion and temperature was assumed. The one drawback to approach 2 is that significantly more analysis is required to determine the parameters within the modified G'Sell model along the axial and hoop direction and for more than one mode of deformation along the axial direction. Therefore, this

approach to predicting the temperature dependent forming limits for OPP tube material becomes less attractive than approach 1.

As discussed in Chapter 2, the condition of instability in either a uniaxial or a biaxial test of a material, is often related to the attainment of a maximum force or pressure. For the case of a tube subjected to internal pressure and axial feeding, two characteristic points are the point at which the maximum pressure is reached and the point when the maximum hoop force is reached. The prediction of the axial and hoop strain at the point at which the maximum force in the hoop direction was reached showed good agreement with the experimentally determined localization strains for the OPP tube using ARAMIS. The point at which the maximum pressure was reached occurred before the point at which the maximum hoop force was reached. Therefore, use of the maximum pressure criterion tended to under predict the strains at localization for the material. This is shown in Figure 6.5 for a test at 130°C and a rate of 0.0022/second.

The form of the predicted forming limits in earlier Figure 4.52 (Chapter 4) is different from the typical 'V" shape normally reported for room temperature tests with sheet materials. However, in the present work for the temperatures studied, the forming limits decrease continuously and non-linearly with an increase in the strain ratio. The decrease in the forming limits with increasing strain ratio was also found to occur in aluminum sheet (AA6061) at 450°C by Chow et al. (2005). The authors presented the development of a localized necking criterion applicable to materials exhibiting strain softening behaviour, and further used this criterion to predict the forming limits for the

above-mentioned aluminum sheet. The theoretical prediction was compared satisfactorily with their test results at four strain rates. Both the predicted and test results from this study are presented in Figure 6.6. They indicate that the decrease in the forming limits may be more influenced by temperature, which induces strain softening behaviour in the material, rather than the geometry of the material (i.e. sheet versus tube).

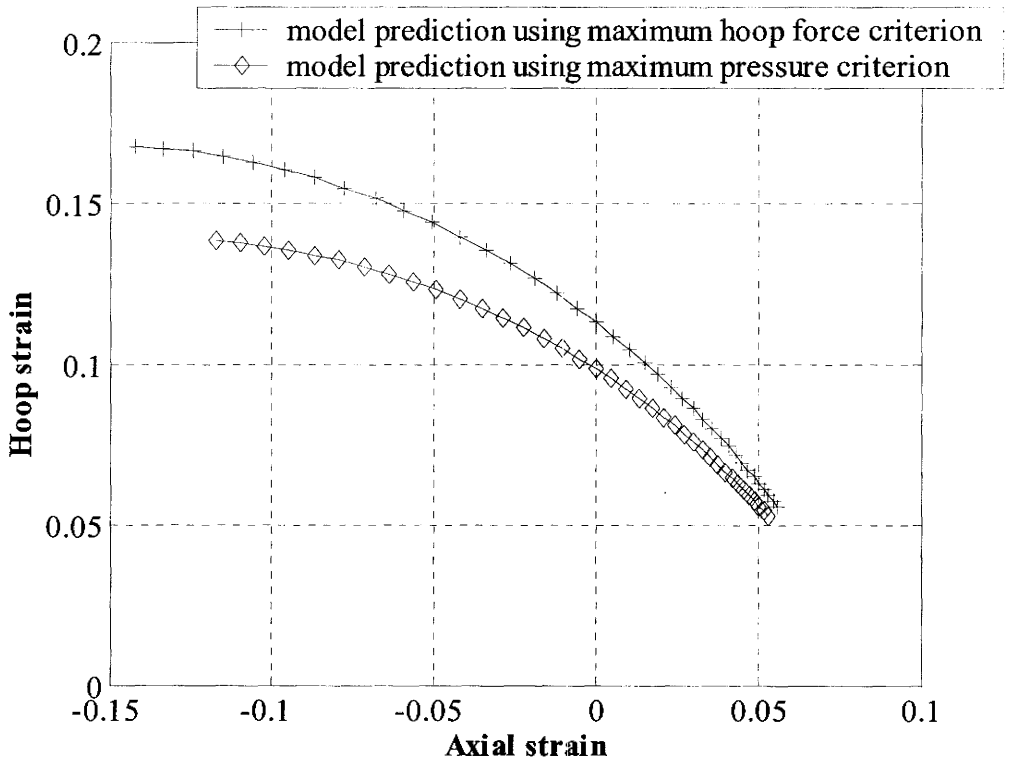

Figure 6.5 Analytical model prediction of forming limits for OPP tube tested at 130°C comparing maximum pressure and maximum hoop force localization criteria.

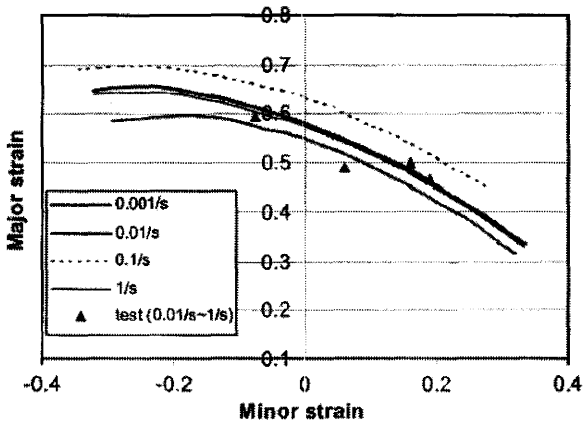

Figure 6.6 Predicted forming limits for AA6061 at 450°C at four strain rates with test results (Chow et al., 2005).

The forming limits for the OPP tube determined in this study have useful implications for forming. For example, Figure 4.52 shows that increasing the forming temperature, close to 150°C, significantly increases the forming limits for the material along all strain paths, although the effect is more pronounced along strain paths involving axial end feeding. The forming limits of the material at 110°C are significantly lower, indicating that this temperature may not be suitable for the large strain forming applications of this material. It is also important to point out that increasing the temperature much beyond 150°C may result in material instabilities associated with bringing the material close to melting, even though one may expect the forming limits to increase as the temperature increases. Further study to determine the limiting temperature, which maximizes the forming limits, while maintaining material stability during forming is required.

Figure 4.52 also shows the potential of axial end feeding applied to the tube forming of these materials in delaying strain localization. The limiting strains achieved with axial end feeding are markedly higher than those in which no axial end feeding was used (i.e close to the plane strain path) which is what would be expected if the conventional blow molding process were applied to these materials. In addition, since the forming limits continue to decrease as the strain ratios increase, forming these materials under biaxial tensile strain paths will result in considerably lower forming limits compared with the cases in which axial end feeding is employed. Therefore, temperature and strain path selection remain critical if these materials are to be adequately exploited both for their lighter weight and for the lower load requirements of the press used to form them at elevated temperatures.

The results of this study have shown how a combined experimental/analytical approach can be used to predict the forming limits for oriented thermoplastic tubular materials. The approach utilizes simple uniaxial mechanical tests of the tube in addition to plasticity theory to predict the forming limits. The primary advantage of this approach is that it avoids the need for a purely experimental determination of the forming limits at various temperatures via tube forming tests. There are a number of problems associated with conducting high temperature tube forming tests, aside from the fact that they can be difficult and time consuming to carry out. One of the primary problems is associated with sealing of the tube. As mentioned in Chapter 3, specialized tapered plugs are required to adequately seal the tubes. The chosen angle of the taper must accommodate variations in the tube wall thickness resulting from the extrusion process as well as

changes in the diameter and length of the tube due to heating and prior to forming. A second issue is related to the uniformity of heating of the tube along its entire surface. Non-uniform heating of the tube can result in "hot spot" locations where the increased temperature can lead to premature strain localization. This is especially true in the case of thermoplastic materials that are sensitive to temperature and prone to creep. The final issue is associated with the continuous measurement of the biaxial strains and radii of curvature of the tube during forming. Since the tubes are enclosed in a furnace, an optical strain measurement system, as was used in this study, is ideally suited to measure large strains on the surface of the tube through the transparent window in the furnace. However, this can be a costly technique for strain measurement compared to the use of strain gauges and/or extensometers. Attachments of extensometer and spherometer for continuous measurement of strains and radii of curvature in a bulging tube inside the furnace can be difficult and clearly does not typically provide ARAMIS type field data over a large region of the specimen. Accurate determination of the radius of curvature of the tube along the axial and hoop direction is required for the calculation of the stresses at the pole of the deforming tube.

CHAPTER 7

CONCLUSIONS AND RECOMMENDATIONS

7.1 Conclusions

The objectives of this study as stated in Chapter 1 were:

[1]. Assessment of the pressure-modified Hill yield criterion put forth by Caddell et al. (1973) for hot forming applications of oriented polypropylene (OPP) tubes. This objective will involve the development of experimental test methodologies for determination of the uniaxial stress parameters within this yield criterion, along the principal directions of the tube, in tension and compression at various temperatures and strain rates.

[2]. Prediction of the plastic work contours for the OPP tube as a function of temperature and for a given strain rate.

[3]. Development of an analytical model for predicting the forming limits of OPP tubes at various temperatures based on:

1. The yield criterion put forth by Caddell et al. (1973) (refer to objective 1).
2. Prediction of the plastic work contours for the material as a function of temperature (refer to objective 2).
3. A criterion for localized necking of the tube.
4. Mechanics of hot gas (or high temperature) axial-feed tube forming process.

[4]. Validation of the predicted forming limits via tube forming tests using an in-house tube bursting test rig and an on-line optical strain measurement system (ARAMIS) both located in the Materials Forming Laboratory (MFL) in the Mechanical Engineering Department.

With respect to objective #1, the following conclusions can be drawn:

- Uniaxial mechanical testing of the OPP tube in both tension and compression along the axial and hoop direction showed the material to exhibit both anisotropy and pressure sensitivity at the various elevated temperatures studied (ranging from 110°C to 150°C) and strain rates (0.0022/second and 0.044/second).
- The concept of contours of plastic work in stress space can be used to represent the plastic work contours for the OPP tube at the various temperatures of interest. These contours can be constructed using both the true stress-strain curves generated from the uniaxial mechanical tests as well from tube forming tests.
- At a given temperature and strain rate, the anisotropic, pressure-dependent yield criterion put forth by Caddell et al. (1973) (also referred to as the pressure-modified

Hill criterion) can be fit to each plastic work contour. This is accomplished by using the uniaxial stress parameters in the pressure-modified Hill criterion calculated for the value of plastic work associated with a given contour.

- Good agreement existed between the predicted plastic work contours, via the pressure-modified Hill yield criterion, and the experimental contours constructed from both uniaxial and biaxial testing of the tube.

With respect to objective #2, the following conclusions can be drawn:

- Each of the uniaxial stress parameters within the pressure-modified Hill yield criterion (i.e. T_a, T_θ, C_a and C_θ) were found to linearly decrease with temperature for the temperature range being studied. This trend also held true for increasing levels of plastic work.
- Based on examination of the effect of temperature on the value of T_a and C_θ, it was determined that for the range of temperatures under study, the above two uniaxial stress parameters could be taken as equal. Although it was found that for increasing levels of plastic work, the difference between the two values became more significant, neglecting this difference had only a minimal effect on the resulting yield surface predicted with the pressure-modified Hill yield criterion.
- As mentioned above, the uniaxial stress parameters in the pressure-modified Hill criterion were found to vary linearly with temperature. In this case, six uniaxial experiments (i.e. axial tension at two temperatures, hoop tension at two temperatures and axial compression at two temperatures) and, hence, six constants are required to

predict the temperature dependent plastic work contour for the OPP tube for a given plastic work. Note here that the axial tensile stress parameter, T_a, is assumed to be equal to the hoop compressive stress parameter, C_θ.

- The modified G'Sell model was shown to accurately predict the temperature dependent axial tensile, hoop tensile and axial compressive behaviour of the OPP tube. These predicted uniaxial curves can then be used to predict the temperature dependent plastic work contours for the material using the concept of plastic work. The one drawback to this approach is that more analysis is required to determine the parameters within the modified G'Sell model, along the axial and hoop direction and for more than one mode of deformation along the axial direction. Therefore, this approach to predicting the temperature dependent forming limits for OPP tube material is less feasible compared with approach 1.

With respect to objective #3, the following conclusions can be drawn:

- An analytical model for predicting the forming limits of the OPP tube at various temperatures and a given strain rate was developed. This involved the use of the temperature dependent pressure-modified Hill criterion, the mechanics of the hot gas tube forming process and a criterion for localized necking, the latter was taken as the strain when the maximum force in the hoop direction of the tube was reached.
- The hoop strain at the point of maximum hoop force predicted by the analytical model is in good agreement with the strain obtained experimentally via tube forming tests under the same conditions.

- The analytical model is able to predict linear and non-linear strain paths. Tube forming tests involving axial end feeding result in strain paths that are more non-linear compared with tests without end feeding.
- For the range of temperatures for which the forming limits for the OPP tube were predicted, the forming limits continued to decrease from the left hand side to the right hand side of the FLD.
- As the temperature increases, the forming limits corresponding to a given strain path also increase.

With respect to objective #4, the following conclusions can be drawn:

- For the OPP tubes used in this study, after local necking or thinning occurs, the material can undergo significant strains within this necked region prior to tube bursting or fracture.
- The criterion that was used to delineate localized necking of the tube during deformation involved examination of the strain rate versus time curve for a point of minimum strain and a point of maximum strain along a horizontal line containing the point of maximum strain. The values of the strain on the surface of the deforming tube were measured using the ARAMIS optical strain measurement system. Localized necking was assumed to occur when the strain curves of the above mentioned points began to diverge. The hoop strain corresponding to this occurrence showed good agreement with the value of the hoop strain obtained at the point of maximum hoop force via the analytical model.

- Experimental forming limits obtained from the tube forming tests and the ARAMIS strain measurement system showed good agreement with those predicted by the analytical model for the range of temperatures studied.

7.2 Recommendations

With the intent of developing an analytical forming limit model for oriented thermoplastic tubes in which simple mechanical tests are used to characterize its properties and the number of experimentally determined parameters are kept to a minimum, further testing and study is required. The main areas of study include:

- Incorporating the effect of strain rate into the currently defined temperature dependent pressure-modified Hill criterion. This would allow for a more complete understanding of the effects of strain rate and temperature on the forming of these materials.
- Further testing to establish the strain path dependency/independency of the forming limit diagram for oriented thermoplastic tubes. This would involve conducting tube test along various linear and non-linear strain paths.
- Determining the effect of tube draw ratio on the resulting forming limits.
- Determining if residual stresses from the extrusion process are present in the tube and if so, examining the effect of pre-heating (i.e. temperature and time) on the relaxation of these stresses.

BIBLIOGRAPHY

Alexander, J.M., and P.J. Wormell. 1971. A preliminary investigation of the hydrostatic extrusion of polymers. *Annals CIRP* 19: 21-28.

ARAMIS version 4.7 manual. 2000. GOM, Braunschweig, Germany.

Arruda, E.M., M.C. Boyce, and R. Jayachandran. 1995. Effects of strain rate, temperature and thermomechanical coupling on the finite strain deformation of glassy polymers. *Mechanics of Materials* 19: 193-212.

Ball, R., M. Doi, S.F. Edwards, and M. Warner. 1981. Elasticity of entangled networks. *Polymer* 22: 1010-1018.

Barata da Rocha, A., F. Barlat, and J.M. Jalinier. 1985. Prediction of the forming limit diagrams of anisotropic sheet in linear and non-linear loading. *Journal of Materials Science* 68: 151–164.

Barlat, F., Y. Maeda, K. Chung, M. Yanagawa, J.C. Brem, Y. Hayashida, D.J. Lege, K. Matsui, S.J. Murtha, S. Hattori, R.C. Becker, and S.J. Makosey. 1997. Yield function development for aluminum alloy sheets. *Journal of the Mechanics and Physics of Solids* 45: 1727–1763.

Bekhet, N.E., D.C. Barton, and G. Craggs. 1993. The unixial behaviour of highly-oriented polymers. *Processing of Advanced Materials* 3: 199-207.

Bekhet, N.E., D.C. Barton, and G. Craggs. 1994. Biaxial yielding behaviour of highly oriented polypropylene tube. *Journal of Materials Science* 29: 4953-4961.

Bigg, D.M., and J.R. Preston. 1989. Stamping of thermoplastic matrix composites. *Polymer Composites* 10: 261-268.

Boyce, M., S. Socrate, and P. Llana. 2000. Constitutive model for the finite deformation stress-strain behaviour of poly(ethylene terephthalate) above the glass transition. *Polymer* 41: 2183-2201.

Brunet, M., S. Boumaiza, and G. Nefussi. 2004. Unified failure analysis for tubular hydroforming. *Journal of Materials Processing Technology* 148: 269-277.

Buckley, A., and H.A. Long. 1969. The extrusion of polymers below their melting temperatures by the application of high pressures. *Polymer Engineering & Science* 9: 115-120.

Caddell, R.M., R.S. Ragahava, and A.G. Atkins. 1973. A yield criterion for anisotropic and pressure dependent solids such as oriented polymers. *Journal of Materials Science* 8: 1641-1646.

Caddell, R.M., and A.R. Woodliff. 1977. Macroscopic yielding of oriented polymers. *Journal of Materials Science* 12: 2028-2046.

Chow, C.L., M. Jie, and X. Wu. 2005. Localized necking criterion for strain-softening materials. *Journal of Engineering Materials and Technology* 127: 273-278.

Chu, C.C. 1982. An investigation of the strain path dependence of the forming limit curve. *International Journal of Solids and Structures* 18: 205–215.

Coates, P.D., and I.M. Ward. 1979. Drawing of polymers through a conical die. *Polymer* 20: 1553-1560.

Craggs, G. 1990. Mechanics analysis of the die drawing process for producing oriented polyethylene terephthalate (PET) tube. *Journal of Process Mechanical Engineering* 204: 43-50.

Crosby, J.M. 1988. Recent advances in thermoplastic composites. *Advanced Materials and Processes Incorporating Metal Progress* 133: 56-59.

Davies, R., G. Grant, D. Herling, M. Smith, B. Evert, S. Nykerk et. al. 2000. *Formability investigation of aluminum extrusions under hydroforming conditions*. Pennsylvania: Society of Automotive Engineers (SAE). SAE Technical Paper, 2000-01-2675.

Dieter, G. 1961. *Mechanical Metallurgy.* Tokyo: McGraw-Hill.

Throne, J. 1999. *Understanding Thermoforming.* Cincinnati: Hanser Gardner Publications, Inc.

Duffo, P., B. Monasse, J.M. Haudin, C. G'Sell, and A. Dahoun. 1995. Rheology of polyporpylene in the solid state. *Journal of Materials Science* 30: 701-711.

Fallon, M.R. 1989. Thermoplastic sheet stamping: Ready for the big time. *Plastics Technology* 35: 95-103.

Farrell, C.J., and A. Keller. 1977. Direct ram extrusion of polyethylene; a correlation between chain folding and tensile modulus. *Journal of Materials Science* 12: 966-974.

Ferron, G., and A.J. Makinde. 1988. Design and development of a biaxial strength testing device. *Journal of Testing and Evaluation* 16: 253–256.

Freire, J.L.F., and W.F. Riley. 1980. Yield behavior of photoplastic materials. *Experimental Mechanics* 37: 118-125.

Gibson, A.G., and I.M. Ward. 1980. The manufacture of ultra-high modulus polyethylene by drawing through a conical die. *Journal of Materials Science* 15: 979-986.

Gibson, A.G., I.M. Ward, B.N. Cole, and B. Parsons. 1974. Hydrostatic extrusion of linear polyethylene. *Journal of Material Science* 9: 1193-1196.

Glenz, W., and A. Peterlin. 1971. Infrared studies of drawn polyethylene. Part 1. Changes in orientation and conformation of highly drawn linear ppolyethylene. *Journal of Macromolecular Science, Part B: Physics* 4: 473-490.

Gol'denblat, I.I., and V.A. Koponov. 1965. Strength of glass –reinforced plastics in the complex stress state. *Polymer Mechanics.* 1 (2): 54-59.

Gotoh, M. 1985. A class of plastic constitutive equations with vertex effect—IV: Applications to prediction of forming limit strains of metal sheets under nonproportional loadings. *International Journal of Solids and Structures* 21: 1149–1163.

Graf, A, and W.F. Hosford. 1993. Effect of changing strain paths on forming limit diagram of Al 2008-T4. *Metallurgical Transactions A* 24: 2503–2512.

Graf, A, and W.F. Hosford. 1994. The influence of strain-path changes on forming limit diagram of Al 6111 T4. *International Journal of Mechanical Sciences* 10: 897–910.

G'Sell, C., N.A. Aly-Helal, and J.J. Jonas. 1983. Effect of stress triaxiality on neck propagation during the tensile stretching of solid polymers. *Journal of Materials Science* 18: 1731-1742.

Haythornthwaite, R.M. 1968. A more rational approach to strain-hardening data. In *Engineering Plasticity*, ed. J. Heyman, and F.A. Leckie, 201-218. Cambridge: Cambridge University Press.

Hecker, S.S. 1976. Experimental studies of yield phenomena in biaxially loaded metals. In *Constitutive Equations in Viscoplasticity: Computational and Engineering Aspects*, ed. J.A. Stricklin, and K.H. Saczalski, 1-33. New York: American Society of Mechanical Engineers.

Hibbeler, R.C. 1993. *Statics and Mechanics of Materials*. New York: Macmillan Publishing Company.

Hill, R. 1948. A theory of the yielding and plastic flow of anisotropic metals. *Proceedings of the Royal Society of London* 193A: 281-297.

Hill, R. 1967. The essential structure of constitutive laws for metal composites and polycrystals. *Journal of the Mechanics and Physics of Solids* 15: 79-95.

Hill, R., and J.W. Hutchinson. 1992. Differential hardening in sheet metal under biaxial loading: A theoretical framework. *Journal of Applied Mechanics* 59: 1–9.

Hill, R., S.S. Hecker, and M.G. Stout. 1994. An investigation of plastic flow and differential work hardening in orthotropic brass tubes under fluid pressure and axial load. *International Journal of Solids and Structures* 31: 2999–3021.

Holliday, L., and I.M. Ward. 1975. A general introduction to the structure and properties of oriented polymers. In *Structure and Properties of Oriented Polymers*, ed. Ian M. Ward, 1-35. New York: Halsted Press.

Hope, P.S., A.G. Gibson, B. Parsons, and I.M. Ward. 1980. Hydrostatic extrusion of linear polyethylene in tubular and non-circular sections. *Polymer Engineering and Science* 18: 540-552.

Hope, P.S., A. Richardson, and I.M. Ward. 1981. Manufacture of ultra-high modulus poly(oxymethylenes) by die-drawing. *Journal of Applied Polymer Science* 26: 2879-2896.

Hosford, W.F. 1979. On yield loci of anisotropic cubic metals. In *Proceedings of the 7th North American Metalworking Research Conference,* by The Society of Manufacturing Engineers. Dearborn, Michigan: The Society of Manufacturing Engineers, 191-196.

Hosford, W.F., and R.M. Caddell. 1993. *Metal Forming Mechanics and Metallurgy*. New Jersey: PTR Prentice Hall.

Hsu, T.C. 1966. Definition of the yield point in plasticity and its effect on the shape of the yield locus. *The Journal of Strain Analysis* 1: 331-338.

Ikeda, S., and T. Kuwabara. 2004. Work hardening behavior of IF and low carbon steel sheets under biaxial tension. *Tetsu-to-Hagane'* 90: 1016–1022 (in Japanese).

Inouye, K. 1954. Studies on the hot-working strength of steels (II) (high-temperature deforming strength of various steels) *Tetsu to Hagane* 41: 593-601 (in Japanese).

Johnson, W., and J.L. Duncan. 1965. The use of the biaxial test extensometer. *Sheet Metal Industries* 42: 271–275.

Jones, B.H., and P.B. Mellor. 1967. Plastic flow and instability behaviour of thin-walled cylinders subjected to constant-ratio tensile stress. *The Journal of Strain Analysis* 2: 62–72.

Karger-Kocsis, J., ed. 1999. *Polypropylene: An A-Z Reference.* Dordrecht: Kluwer Publishers.

Kim, J., S. Kim, W. Song, and B. Kang. 2005. Analytical and numerical approach to prediction of forming limit in tube hydroforming. *International Journal of Mechanical Sciences* 47: 1023-1037.

Kim, S., and Y. Kim. 2002. Analytical study for tube hydroforming. *Journal of Materials Processing Technology* 128: 232-239.

Koc, M., and T. Altan. 2001. Overall review of the tube hydroforming (THF) technology. *Journal of Materials Processing Technology* 108: 384-393.

Kuroda, M., and V. Tvergaard. 2000. Effect of strain path change on limits to ductility of anisotropic metal sheets. *International Journal of Mechanical Sciences* 42: 867–887.

Kuwabara, T. 2007. Advances in experiments on metal sheets and tubes in support of constitutive modeling and forming simulations. *International Journal of Plasticity* 23: 385-419.

Kuwabara, T., M. Ishiki, M. Kuroda, and S. Takahashi. 2003. Yield locus and work-hardening behavior of a thin-walled steel specimen subjected to combined tension-internal pressure. *Journal de Physique IV* 105: 347–354.

Kuwabara, T., M. Umemura, K. Yoshida, M. Kuroda, and S. Hirano. 2005. Forming limits of 5000 series aluminum alloys with different magnesium contents. In *Proceedings of the 8th ESAFORM Conference,* by The Publishing House of the Romanian Academy. Romania: The Publishing House of the Romanian Academy, 399.

Kuwabara, T., S. Ikeda and T. Kuroda. 1998. Measurement and analysis of differential work hardening in cold-rolled steel sheet under biaxial tension. *Journal of Materials Processing Technology* 80–81: 517–523.

Lee, J.H., and J.H. Vogel. 1995a. Investigation of necking instability in fiber reinforced polypropylene. *Journal of Engineering Materials and Technology* 118: 80-87.

Lee, J.H., and J.H. Vogel. 1995b. Investigation of the formability of long fiber thermoplastic composite sheets. *Journal of Engineering Materials and Technology* 117: 127-132.

Logan, R., and W.F. Hosford. 1980. Upper bound anisotropic yield locus calculations assuming <111> - pencil glide. *International Journal of Mechanical Sciences* 22: 419-430.

Lowden, M.A.W., and W.B. Hutchinson. 1975. Texture strengthening and strength differential in titanium–6Al–4V. *Metallurgical Transactions A* 6: 441–448.

Maeda, Y., M. Yanagawa, F. Barlat, K. Chung, Y. Hayashida, S. Hattori, K. Matsui, J.C. Brem, D.J. Lege, S.J. Murtha, and T. Ishikawa. 1998. Experimental analysis of aluminum yield surface for binary Al–Mg alloy sheet samples. *International Journal of Plasticity* 14: 301–318.

McCrum, N.G., C.P. Buckley and C.B. Bucknall. 1997. *Principles of Polymer Engineering*. Oxford: Oxford University Press.

Michaeli, W., and M. Jehrke. 1993. Diaphragm forming of continuous-fibre reinforced thermoplastics suitable for medium scale production. In *Proceedings of the International Conference on Advanced Composite Materials* by The Minerals, Metals & Materials Society (TMS). Warrendale, Pennsylvania: The Minerals, Metals & Materials Society, 869-873.

Michno, M.J., Jr., and W.N. Findley. 1976. An historical perspective of yield surface investigations for metals. *International Journal of Non-Linear Mechanics* 11: 59–82.

Muke, S., I. Ivanov, N. Kao, and S.N. Battacharya. 2001. The melt extensibility of polypropylene. *Polymer International* 50: 515-523.

Nakamura, K., and K. Imada, and M. Takayanagi. 1972. Solid-state extrusion of isotactic polypropylene through a tapered die. I. Phenomenological analysis. *International Journal of Polymer Materials* 18: 71-88.

Ogorkiewwicz, R.M., ed. 1970. *Engineering properties of thermoplastics*. New York: John Wiley and Sons.

Osakada, K., M. Shiraishi, S. Murakai, and M. Tokuoka. 1991. Measurement of flow stress by the ring compression test. *JSME International Journal Series 1* 34: 312-318.

Parsons, B., and I.M. Ward. 1982. The production of oriented polymers by hydrostatic extrusion. *Plastics and Rubber Processing and Applications* 2: 215-224.

Paul, B. 1968. Macroscopic criteria for plastic flow and brittle fracture. In *Fracture: An Advanced Treatise, Volume II: Mathematical Fundamentals,* ed. H. Liebowitz, 315-489. New York: Academic Press.

Peguy, A., and R.J. Manley. 1984. Ultra-drawing of high molecular weight polypropylene. *Polymer Communications* 25: 39-46.

Peterlin, A. 1969. Plastic deformation of polyethylene by rolling and drawing. *Kolloid-Zeitschrift & Zeitschrift für Polymere* 233: 857-862.

Peterlin, A. 1971. Chain scission and plastic deformation in the strained crystalline polymer. *Journal of Polymer Science, Part C: Polymer Symposia* 32: 297-317.

Peterlin, A. 1975. Molecular aspects of oriented polymers. In *Structure and Properties of Oriented Polymers*, ed. Ian M. Ward, 36-56. New York: Halsted Press.

Raghava, R.S. 1972. Macroscopic yielding behaviour of polymeric materials. Ph.D. diss., University of Michigan.

Raghava, R.S., and R.M. Caddell. 1973. A macroscopic yield criterion for crystalline polymers. *International Journal of Mechanical Sciences* 15: 967-974.

Raghava, R.S., and R.M. Caddell. 1974. Yield locus studies of oriented polycarbonate: An anisotropic and pressure-dependent solid. *International Journal of Mechanical Sciences* 16: 789-799.

Raghava, R.S., R.M. Caddell, and G.S. Yeh. 1973. The macroscopic yield behavior of polymers. *Journal of Materials Science* 8: 225-232.

Ranta-Eskola, A.J. 1979. Use of the hydraulic bulge test in biaxial tensile testing. *International Journal of Mechanical Sciences* 21: 457–465.

Richardson, A., B. Parsons, and I.M. Ward. 1986. Production and properties of high stiffness polymer rod, sheet, and thick monofilament oriented by large-scale die drawing. *Plastics and Rubber Processing and Applications* 6: 347-361.

Robinson, T., H. Ou, and C. Armstrong. 2004. Study on ring compression test using physical modeling and FE simulation. *Journal of Materials Processing Technology* 153-154: 54.

Rosato, D.V., ed. 1989. *Blow molding handbook.* New York: Hanser Publishers.

Selwood, A., I.M. Ward, and B. Parsons. 1987. The Production of oriented polymer tube by the die-drawing process. *Plastics and Rubber Processing and Applications* 8:49-58.

Shinozaki, D., and G.W. Groves. 1973. The plastic deformation of oriented polypropylene: Tensile and compressive yield criteria. *Journal of Materials Science* 8: 71-78.

Shiratori, E., and K. Ikegami. 1968. Experimental study of the subsequent yield surface by using cross-shaped specimens. *Journal of the Mechanics and Physics of Solids* 16: 373–394.

Singh, H. 2003. *Fundamentals of hydroforming.* Dearborn, MI: Society of Manufacturing Engineers.

Smiley, A.J., and R.B. Pipes. 1988. Analysis of the Diaphragm Forming of Continuous Fiber Reinforced Thermoplastics. *Journal of Thermoplastic Composite Materials* 1: 298-321.

Sokolowski, T., K. Gerke, M. Ahmetolgu, and T. Altan. 2000. Evaluation of tube formability and material characteristics: Hydraulic bulge testing of tubes. *Journal of Materials Processing Technology* 98: 34-40.

Spitzig, W.A., R.J. Sober, and O. Richmond. 1975. Pressure dependence of yielding and associated volume expansion in tempered martensite. *Acta Metallurigca* 23: 885–893.

Stassi-D'Alia, F. 1967. Flow and fracture of materials according to a new limiting condition of yielding. *Meccannica* 2: 178-195.

Stassi-D'Alia, F. 1969. Limiting conditions of yielding for anisotropic materials. *Meccannica* 4: 349-364.

Stout, M.G., S.S. Hecker, and R. Bourcier. 1983. Evaluation of anisotropic effective stress-strain criteria for biaxial yield and flow of 2024 aluminum tubes. *Journal of Engineering Materials and Technology* 105: 242-249.

Sweeney, J., T.L.D. Collins, P.D. Coates, and I.M. Ward. 1997. Application of an elastic model to the large deformation, high temperature stretching of polypropylene. *Polymer* 38: 5991-5999.

Taraiya, A., A. Richardson, and I.M. Ward IM. 1987. Production and properties of highly oriented polypropylene by die drawing. *Journal of Applied Polymer Science* 33: 2559-2579.

Tate, K.R., A.R. Perrin, and R.T. Woodhams. 1988. Tensile flow stress model for oriented polypropylene. *Polymer Engineering and Science* **28**: 740-742.

Tozawa, Y., and M. Nakamura. 1972. New method for testing sheet under biaxial compression. *Journal Japan Society for Technology of Plasticity* 13: 538–541 (in Japanese).

Tsahalis, D.T., S.G. Pantelakis, and V. Schulze. 1990. Modelling of the diaphragm forming technique applied to continuous fiber reinforced thermoplastic composites. *Processing of Polymers and Polymeric Composites* 19: 91-101.

Tsai, S.W., and E.M. Wu. 1970. A general theory of strength for anisotropic materials. *Journal of Composite Materials* 5: 58-80.

Tuttle, M.E., M. Semeliss, and R. Wong. 1992. The elastic and yield behaviour of polyethylene tubes subjected to biaxial loadings. *Experimental Mechanics* 32: 1-10.

Voce, E. 1948. The relationship between stress and strain for homogeneous deformation. *Journal of the Institute of Metals* 74: 537-562.

Wang, H., R. Bouchard, R. Eagleson, P. Martin, and W.R. Tyson. 2002. Ring hoop tension test (RHTT): A test for transverse tensile properties of tubular materials. *Journal of Testing and Evaluation* 30: 382-391.

Ward, I.M. 1971. Review: The yield behavior of polymers. *Journal of Materials Science* 6: 1397-1417.

Ward, I.M. 1989. Developments in oriented polymers. *SERC Bulletin* 4: 12-13.

Ward, I.M., A.K. Taraiya, and P.D. Coates. 2000. Solid state extrusion and die drawing. In *Solid Phase Processing of Polymers*, ed. I.M. Ward, P.D. Coates, and M.M. Dumoulin, 328-367. Cincinnati: Hanser Gardner Publishers.

Williams, T. 1973. Hydrostatically-extruded polypropylene. *Journal of Material Science* 8: 59-70.

Woo, D.M., and P.J. Hawkes. 1968. Determination of stress/strain characteristics of tubular materials. *Journal of the Institute of Metals* 96: 357-359.

Yoshida, K., and T. Kuwabara. 2007. Effect of strain hardening behavior on forming limit stresses of steel tube subjected to non-proportional loading paths. *International Journal of Plasticity* 23: 1260-1284.

Young, R.F., J.E. Bird, and J.L. Duncan. 1981. An automated hydraulic bulge tester. *Journal of Applied Metalworking* 2: 11–18.

Zhou, Y., and P.K. Mallick. 2002. Effects of temperature and strain rate on the tensile behaviour of unfilled and talc-filled polypropylene. Part II: Constitutive equation. *Polymer Engineering and Science* 42: 2461-2470.

APPENDIX A

Derivation of flow rules for pressure-modified Hill yield criterion

The pressure-modified Hill yield criterion in three dimensions is given by:

$$H(\sigma_a - \sigma_\theta)^2 + F(\sigma_\theta - \sigma_t)^2 + H(\sigma_t - \sigma_a)^2 + K_a\sigma_a + K_\theta\sigma_\theta + K_\theta\sigma_t = 1 \qquad \text{(A.1)}$$

where σ_a is the axial stress, σ_θ is the hoop stress and σ_t is the thickness stress (which is assumed to be zero). Also,

$$H = \frac{1}{2T_a|C_a|} \qquad \text{(A.2)}$$

$$F + H = \frac{1}{T_\theta|C_\theta|} \qquad \text{(A.3)}$$

$$K_a = \frac{|C_a| - T_a}{|C_a|T_a} \qquad \text{(A.4)}$$

$$K_\theta = \frac{|C_\theta| - T_\theta}{|C_\theta|T_\theta} \qquad \text{(A.5)}$$

where T_a and T_θ are the tensile yield strengths in the axial and hoop direction respectively and C_a and C_θ are the compressive yield strengths in the axial and hoop direction respectively. Note here that it is assumed that the tensile and compressive properties along the hoop and thickness direction of the tube are equal.

Assuming that the plastic potential and yield function are equivalent, the flow rules developed from the yield function given by Equation (A.1) are derived using:

$$d\varepsilon_{ij} = d\lambda \frac{df}{d\sigma_{ij}} \tag{A.6}$$

Therefore,

$$d\varepsilon_a = d\lambda \frac{df}{d\sigma_a} \tag{A.7}$$

$$= d\lambda\left[4H\sigma_a - 2H\sigma_\theta + K_a\right] \tag{A.8}$$

$$= 2d\lambda\left[2H\sigma_a - H\sigma_\theta + 1/2K_a\right] \tag{A.9}$$

Also,

$$d\varepsilon_\theta = d\lambda \frac{df}{d\sigma_\theta} \tag{A.10}$$

$$= d\lambda\left[2(H+F)\sigma_\theta - 2H\sigma_a + K_\theta\right] \tag{A.11}$$

$$= 2d\lambda\left[(H+F)\sigma_\theta - H\sigma_a + 1/2K_\theta\right] \tag{A.12}$$

Finally,

$$d\varepsilon_t = d\lambda \frac{df}{d\sigma_t} \tag{A.13}$$

$$= 2d\lambda\left[-F\sigma_\theta - H\sigma_a + (F+H)\sigma_t + 1/2K_t\right] \tag{A.14}$$

however, since $\sigma_t = 0$ (plane stress),

$$d\varepsilon_t = 2d\lambda\left[-F\sigma_\theta - H\sigma_a + 1/2K_t\right] \tag{A.15}$$

APPENDIX B

Production of oriented polypropylene (OPP) tubes

Before discussing the extrusion process used to produce the oriented tubes, a description of the preparation of the tubular billets, which would subsequently be used for the extrusion, will be described first. The starting tubular billet used for the extrusion was machined from a solid cylindrical block of natural polypropylene. The first of two steps involved the machining of a 44.5 mm hole in the center of each solid cylindrical block. The outer diameter of the tubular billet was then machined to various sizes depending on the desired draw ratios. Figure B.1 shows, in detail, the steps involved in the machining of the tubular billet.

The draw ratio, *dr*, is defined as the ratio of the cross-sectional area of the tubular billet, A_{billet}, to that of the final extruded tube, A_{final_tube} i.e:

$$dr = \frac{A_{billet}}{A_{final\_tube}} \tag{B.1}$$

Assuming the dimensions of the final tube as it exited the die during the extrusion were constant (i.e. extrusion die fixed outer dimension of the final tube and mandrel fixed the inner diameter of the final tube), as well as the inner diameter of the tubular billet, Equation (B.1) could be used to calculate the required outer diameter of the starting billet to achieve a given draw ratio. The outer diameter of the starting tubular billet was then machined to the size required to produce a given draw ratio. Based on the existing capabilities of the extrusion machine at PSA, tubes of draw ratio 4.0, 4.5 and 5.0 were produced. Table B.1 shows the dimensions of the tubular billet used to produce the three draw ratios.

It is important to note here that nominal draw ratio values are given in Table B.1. This is because the exact dimensions of the tube as it exited the die were not known, since they were dependent on the rate of cooling of the tube as it emerged from the die as well as the amount of draw tension applied to the tube as it exited. In any case, final tube dimensions were estimated so that the required outer diameter of the tubular billet to be machined could be calculated via Equation (B.1). It should also be noted that the inner diameter of the tubular billet was smaller than the size of the mandrel. This is because the tubular billets required preheating prior to insertion of the mandrel in the inner diameter. The preheating caused some expansion in the billet to occur, therefore, the inner diameter of the starting billet was machined slightly smaller to account for this expansion. The inner diameter of the tubular billet, prior to pre-heating was used to calculate the required outer diameter of the tubular billet based on a nominal draw ratio.

The tubular billets were then ram extruded and die-drawn. The procedural steps were as follows:

(a) The starting tubular billets were preheated in a large external oven to a temperature of 150°C (refer to Figure B.2).

(b) The mandrel was placed in the inner diameter of the heated tubular billet. As mentioned previously, the presence of the mandrel kept the inner diameter of the final extruded tube consistent with that of the starting billet.

(c) The preheated tubular billet, along with the inserted mandrel, was placed inside the heated extrusion chamber (refer to Figure B.3).

(d) The ram was attached to the mandrel, positioned in place and the extrusion started.

(e) After approximately 0.3 m of the extruded tube emerged from the die, the tube was then clamped and drawn out of the die using a nearly constant load of 2050 N (refer to Figure B.4). Note that an arrangement of pipes was used, in conjunction with compressed air to cool the tube as it emerged form the die (refer to Figure B.5).

(f) The last segment of the extruded tube (approximately 0.3 m from the end) was pulled (or drawn) at a larger load, close to 5340 N, in order to release it completely from the extrusion die (refer to Figure B.5).

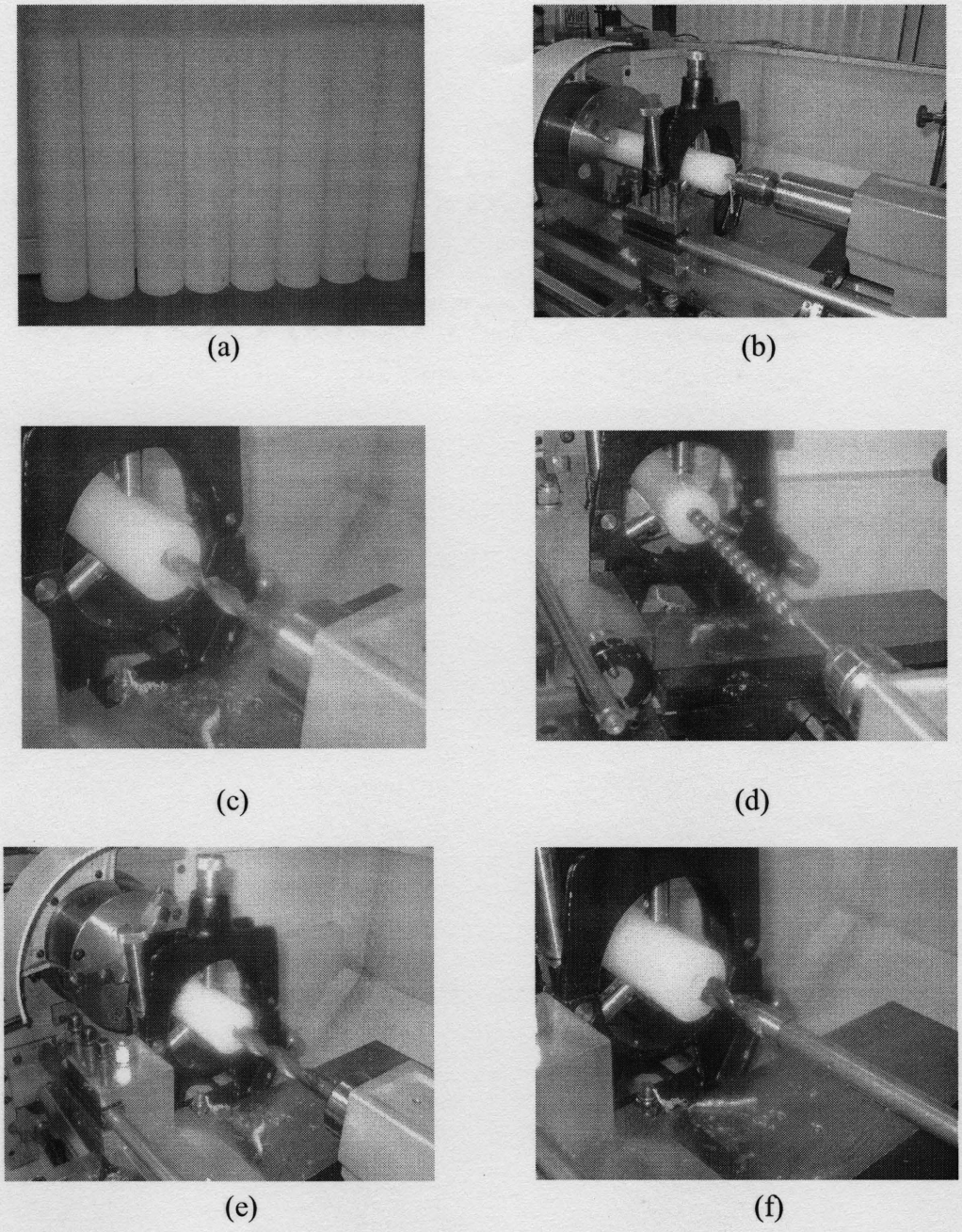

Figure B.1 Detailed steps involved in machining of tubular polypropylene billets (a) starting solid cylindrical polypropylene material (b) center drilling (c) 19.1 mm short drilling (d) 19.1 mm spiral drilling (e) 25.4 mm short drilling (f) 25.4 mm long drilling.

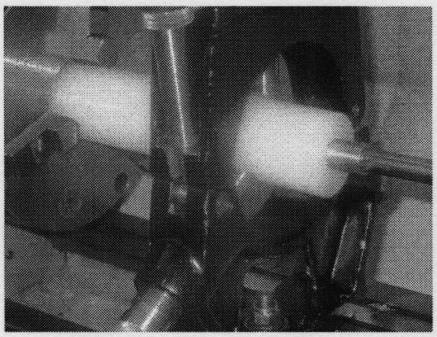

(g)

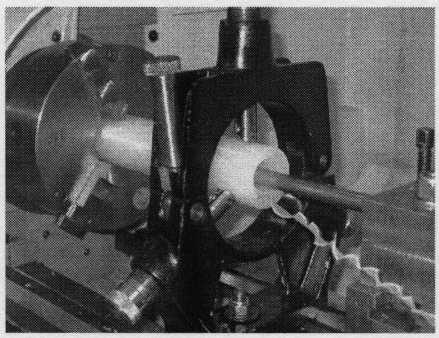

(h)

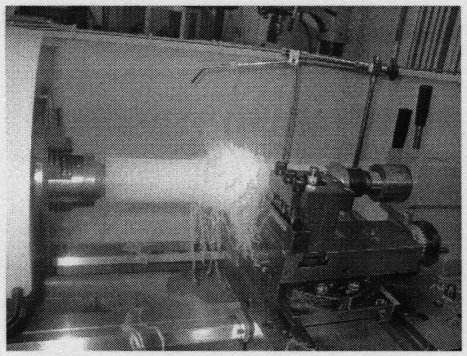

(i)

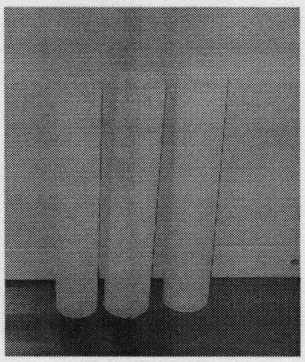

(j)

Figure B.1 *cont.* Detailed steps involved in machining of tubular polypropylene billets (g) boring of 44.5 mm hole using bushing (h) boring continued (i) machining of outer diameter of billet (j) final tubular billets.

Nominal draw ratio	Final extruded tube dimensions		Tubular billet dimensions	
	Outer diameter (fixed by extrusion die) (mm)	Inner diameter (fixed by size of mandrel) (mm)	Outer diameter (mm)	Inner diameter (mm)
4.0	49.5	44.9	64.2	44.2
4.5	49.5	44.9	66.3	44.2
5.0	49.5	44.9	68.3	44.2

Table B.1 Tubular billet dimensions to achieve three draw ratios.

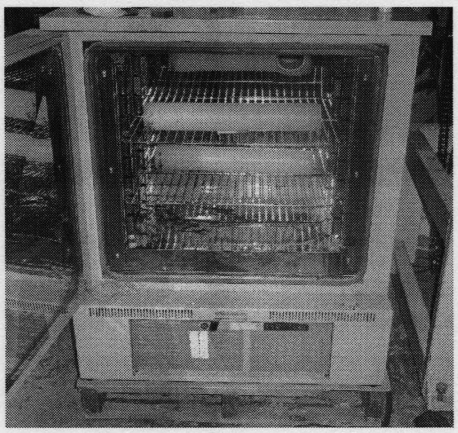

Figure B.2 Pre-heating of billets in external oven.

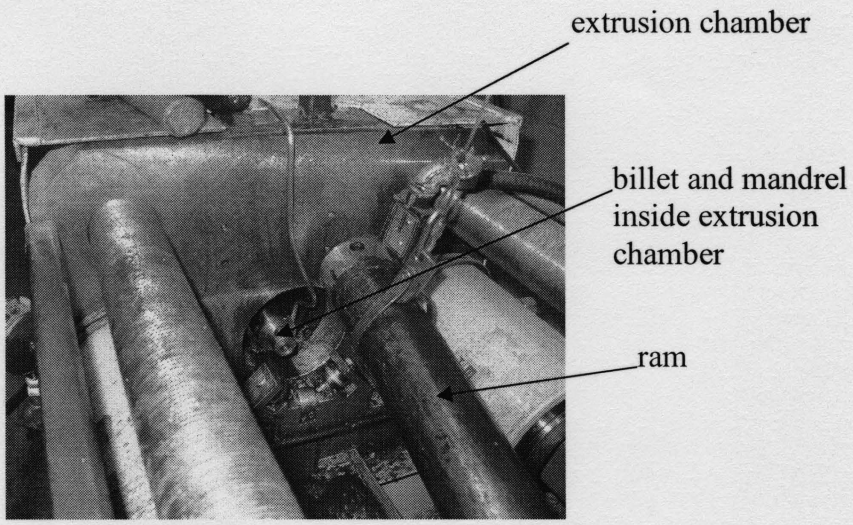

Figure B.3 Insertion of billet with mandrel into extrusion chamber.

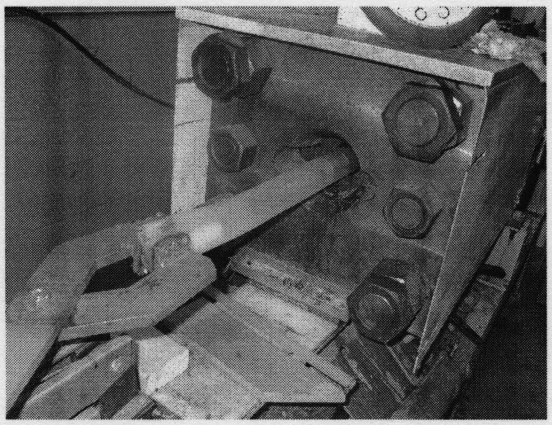

Figure B.4 Drawing of tube out of die using a constant force.

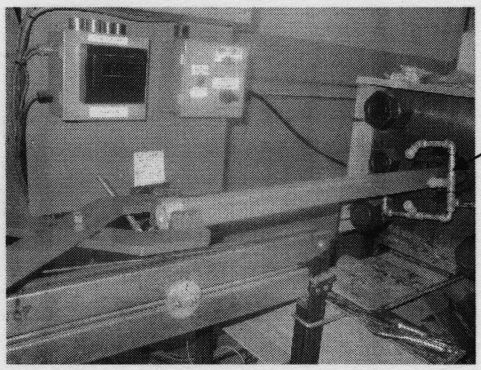

Figure B.5 Drawing out last segment of tube from extrusion die.

Since the die drawing load applied to the tube affects its level of orientation, only the middle section of the extruded tubes were used for all subsequent mechanical testing. The first 0.3 m of the tube (head) which emerged from the extrusion die had no die drawing load applied to it and the last 0.3 m (tail) had a much higher drawing load applied to it than the middle section of the tube (which had a constant 2050 N load applied). Therefore, the head and tail sections of the tube were discarded.

APPENDIX C

Repeatability of experimental load-displacement curves determined from axial compression test

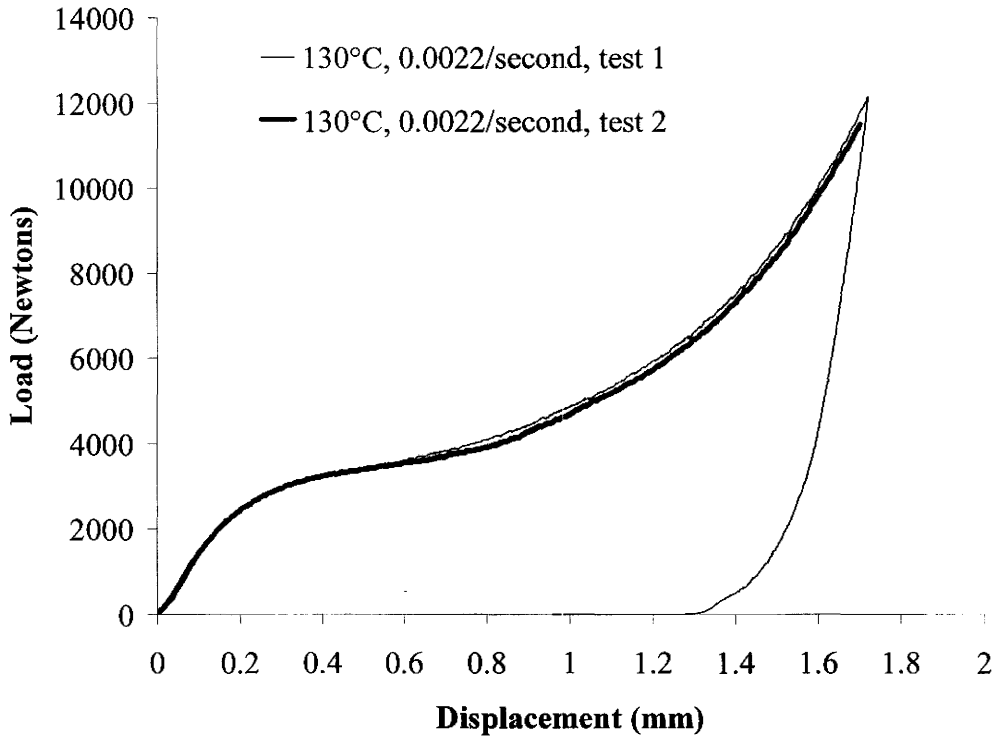

Figure C.1 Experimental load-displacement curves determined from two axial compression tests conducted at the same conditions (130°C and a rate of 0.0022/second).

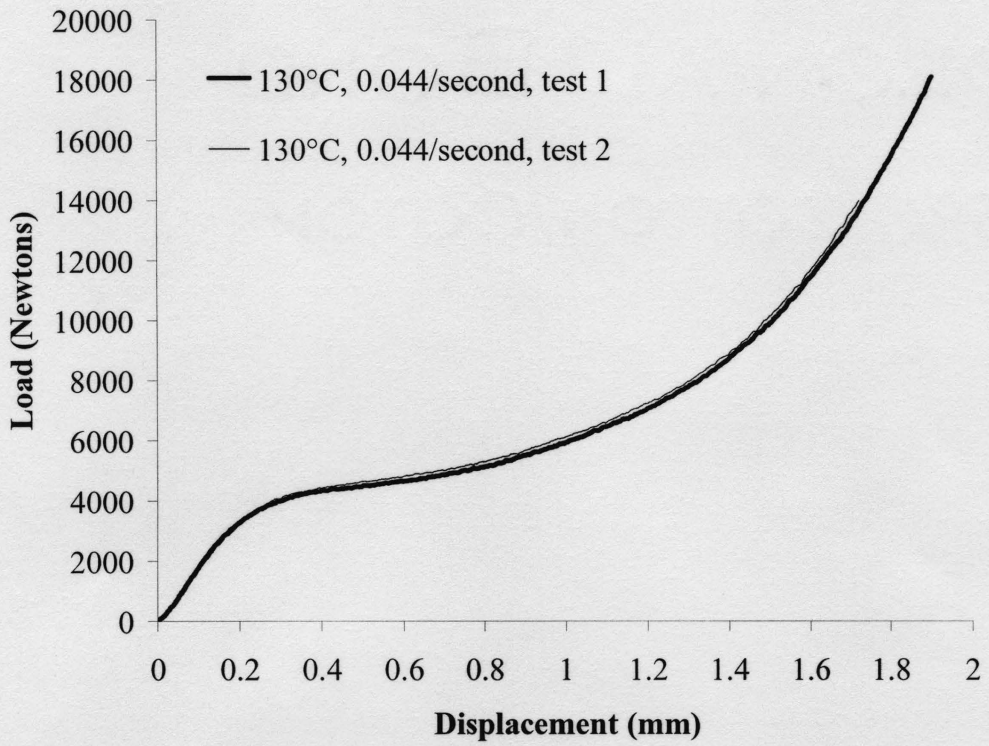

Figure C.2 Experimental load-displacement curves determined from two axial compression tests conducted at the same conditions (130°C and a rate of 0.044/second).

APPENDIX D

Effect of temperature on uniaxial stress parameters in pressure-modified Hill criterion for OPP tube of draw ratio 5.0 and tested at a strain rate of 0.044/second

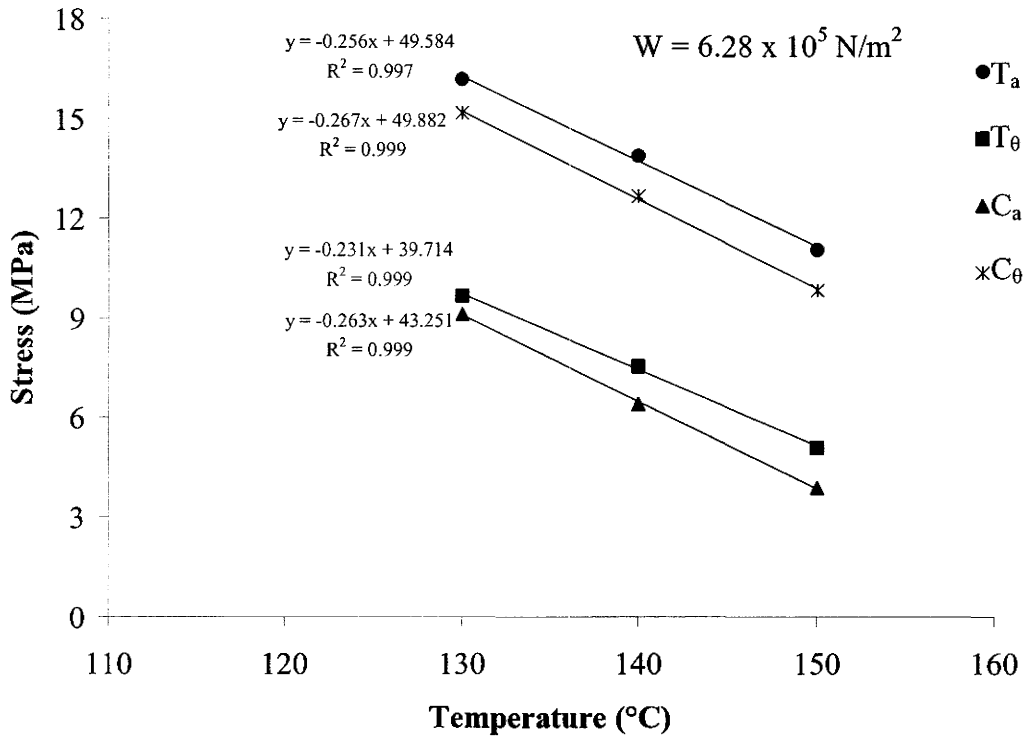

Figure D.1 Effect of temperature on uniaxial stress parameters at a plastic work of 6.28×10^5 N/m^2 for the OPP tube of draw ratio 5.0 and tested at a strain rate of 0.044/second.

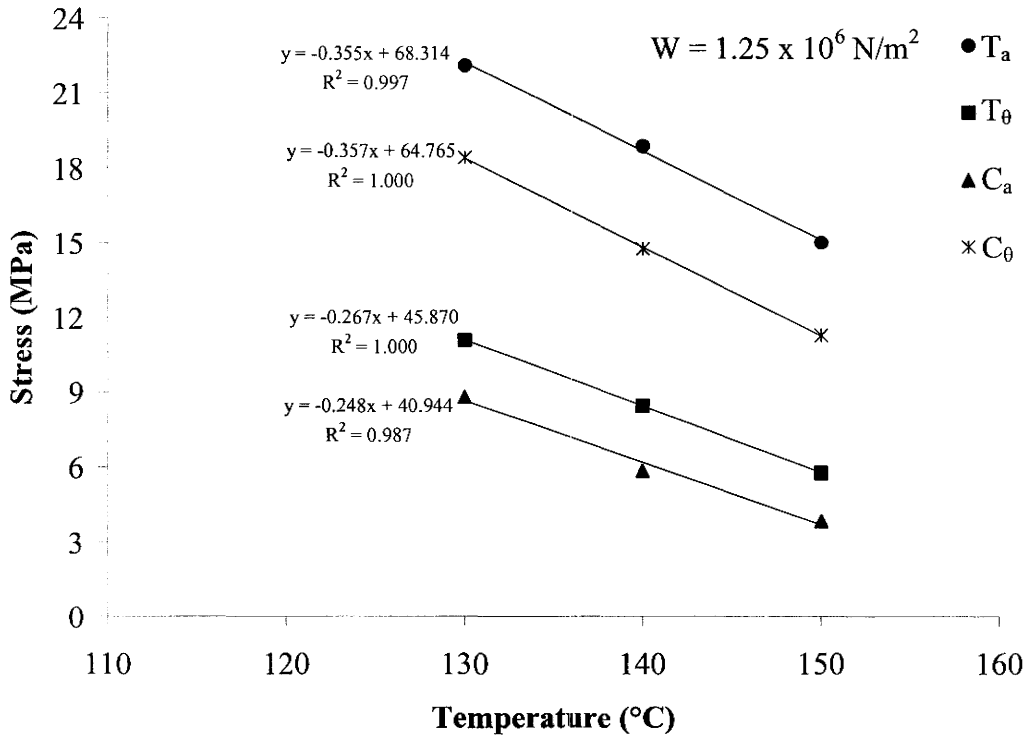

Figure D.2 Effect of temperature on uniaxial stress parameters at a plastic work of 1.25×10^6 N/m^2 for the OPP tube of draw ratio 5.0 and tested at a strain rate of 0.044/second.

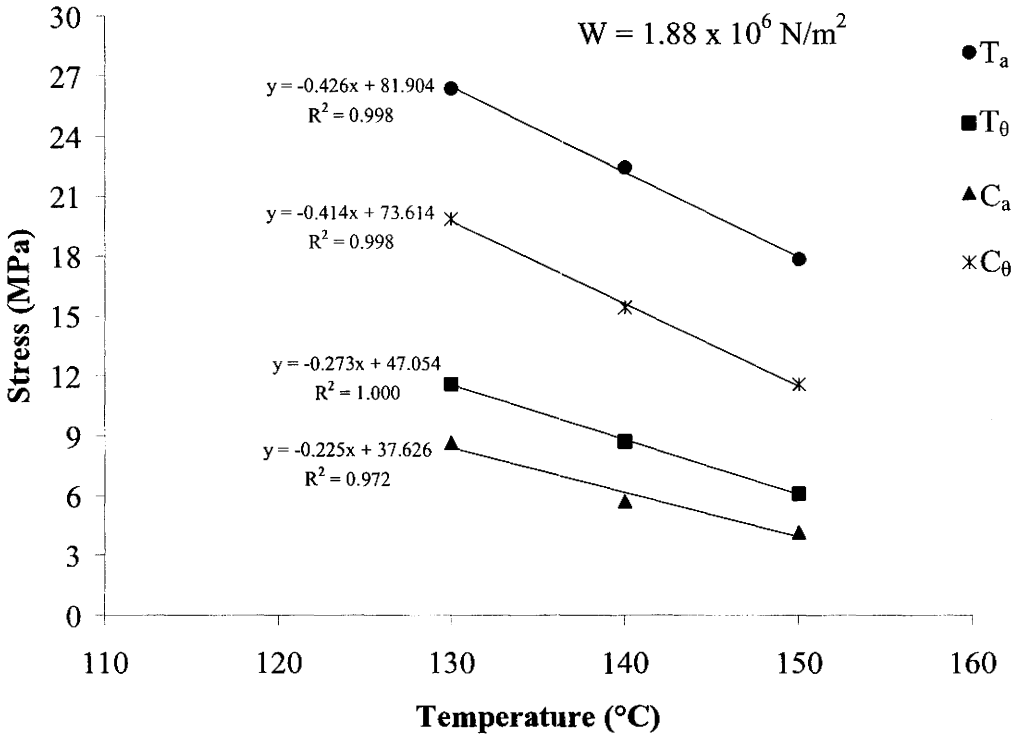

Figure D.3 Effect of temperature on uniaxial stress parameters at a plastic work of 1.88×10^6 N/m^2 for the OPP tube of draw ratio 5.0 and tested at a strain rate of 0.044/second.

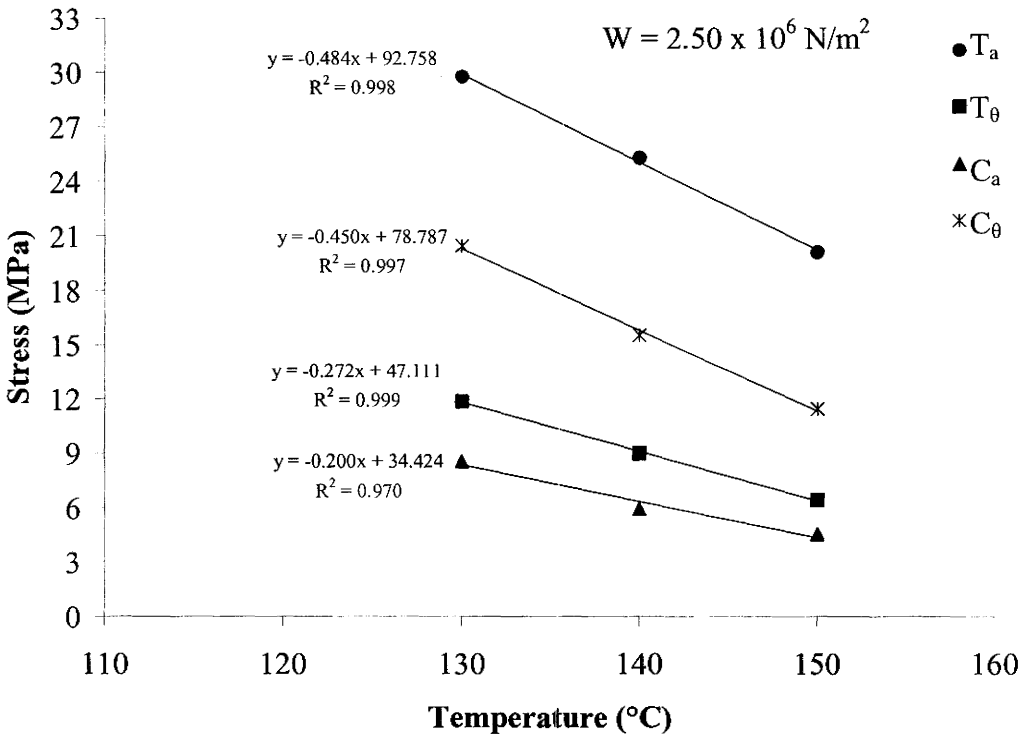

Figure D.4 Effect of temperature on uniaxial stress parameters at a plastic work of 2.50×10^6 N/m^2 for the OPP tube of draw ratio 5.0 and tested at a strain rate of 0.044/second.

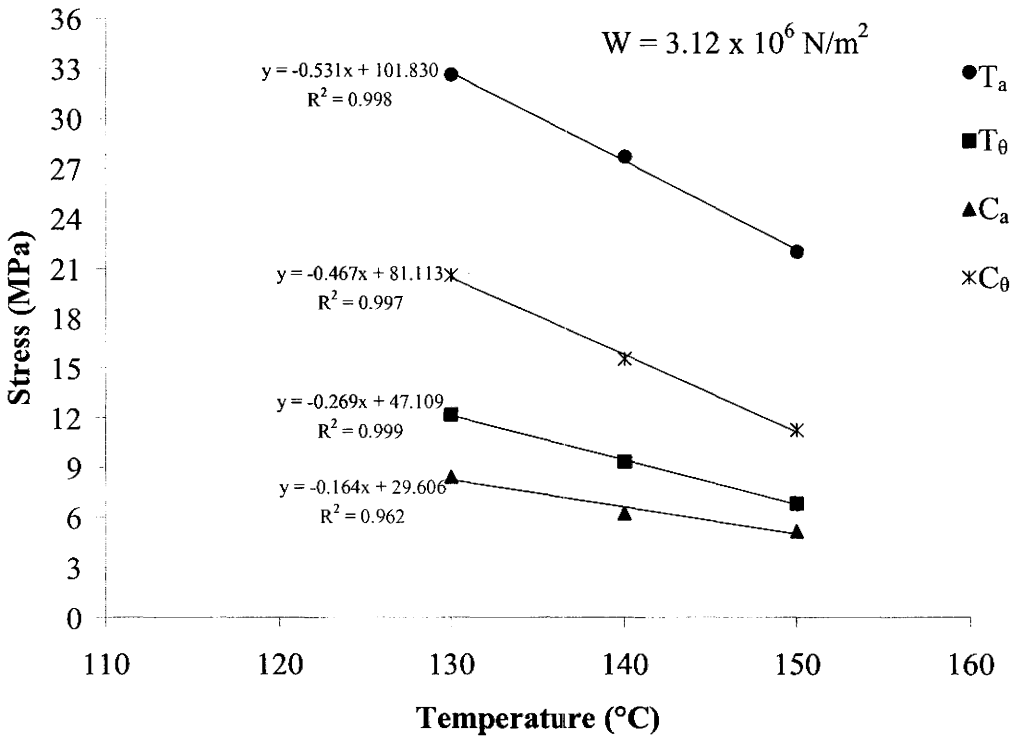

Figure D.5 Effect of temperature on uniaxial stress parameters at a plastic work of $3.12x10^6$ N/m^2 for the OPP tube of draw ratio 5.0 and tested at a strain rate of 0.044/second.

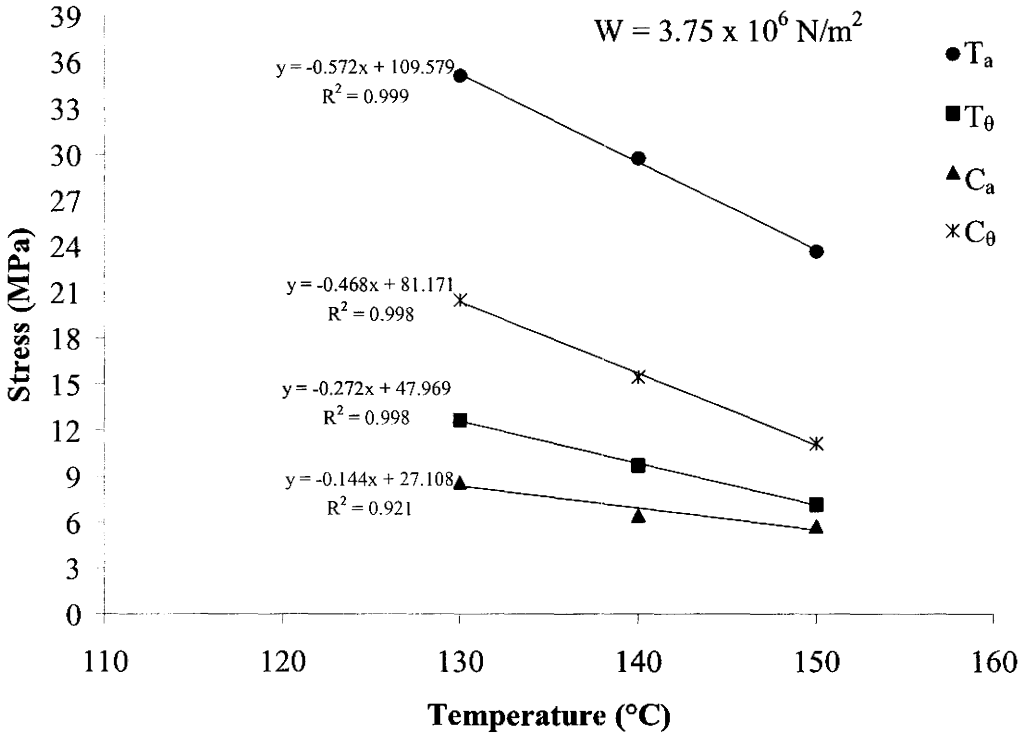

Figure D.6 Effect of temperature on uniaxial stress parameters at a plastic work of 3.75×10^6 N/m^2 for the OPP tube of draw ratio 5.0 and tested at a strain rate of 0.044/second.

APPENDIX E

Procedure for determination of parameters in modified G'sell model

The final form of the modified G'Sell model is given by:

$$\sigma = K\left[1 - N\exp\left(-B_1\varepsilon\right)\right]\exp\left(h_1\varepsilon^2\right)\exp\left(\frac{V}{T}\right) \tag{E.1}$$

At large plastic strains, Equation (E.1) reduces to:

$$\sigma = K\exp\left(h_1\varepsilon^2\right)\exp\left(\frac{V}{T}\right) \tag{E.2}$$

Since the effect of strain and temperature are expressed separately in a multiplicative way, Equation (E.2) can be rewritten such that the effect of temperature on stress is given by:

$$\sigma = f_0\exp\left(\frac{V}{T}\right) \tag{E.3}$$

where f_0 is a constant. Taking the natural logarithm of both sides of Equation (E.3) and plotting $ln\ \sigma$ versus $1/T$ (at a given strain and strain rate) yields a linear curve whose slope is the constant V. Knowing the value of V, Equation (E.2) can be rewritten as:

$$\frac{\sigma}{\exp(V/T)} = K\exp\left(h_1\varepsilon^2\right) \tag{E.4}$$

Taking the natural logarithm of both sides of Equation (E.4) and plotting $\ln\left[\frac{\sigma}{\exp(V/T)}\right]$ versus ε^2 (at large strains and at given strain rate) yields a straight line whose slope and intercept are h_1 and $\ln K$ respectively.

Lastly the values of N and B_1 require determination. The parameters N and B_1 are within the term $\left[1-N\exp(-B_1\varepsilon)\right]$ (refer to Equation (E.1)), and are only active at small strains. Therefore for small values of strain, Equation (E.1) can be rewritten as:

$$\sigma = K\left[1-N\exp(-B_1\varepsilon)\right]\exp\left(\frac{V}{T}\right) \tag{E.5}$$

Rearrangement of Equation (E.5) yields:

$$\frac{-\sigma}{K\exp(V/T)}+1 = N\exp(-B_1\varepsilon) \tag{E.6}$$

Taking the natural logarithm of both sides of Equation (E.6) and plotting $\ln\left[\frac{-\sigma}{K\exp(V/T)}+1\right]$ versus ε (at small values of strain and at a given strain rate) yields a straight line whose slope is $-B_1$ and intercept is $\ln N$. Knowing the value of N, one can then use Equation (4.9) to predict the initial yield stress for various temperatures and a given strain rate.

APPENDIX F

Details of design of elliptical die used for tube forming test

Preliminary calculations were required for estimation of the size of the elliptical opening, i.e. the length of the major and minor axis, which would yield results close to the balanced biaxial state. Figure F.1 shows the OPP tube installed with the elliptical die, whose major and minor axes lengths are given as the variables A and B respectively. The elliptical die is placed as a collar around the tube and tested with the hot oil system presented earlier in Figure 3.28.

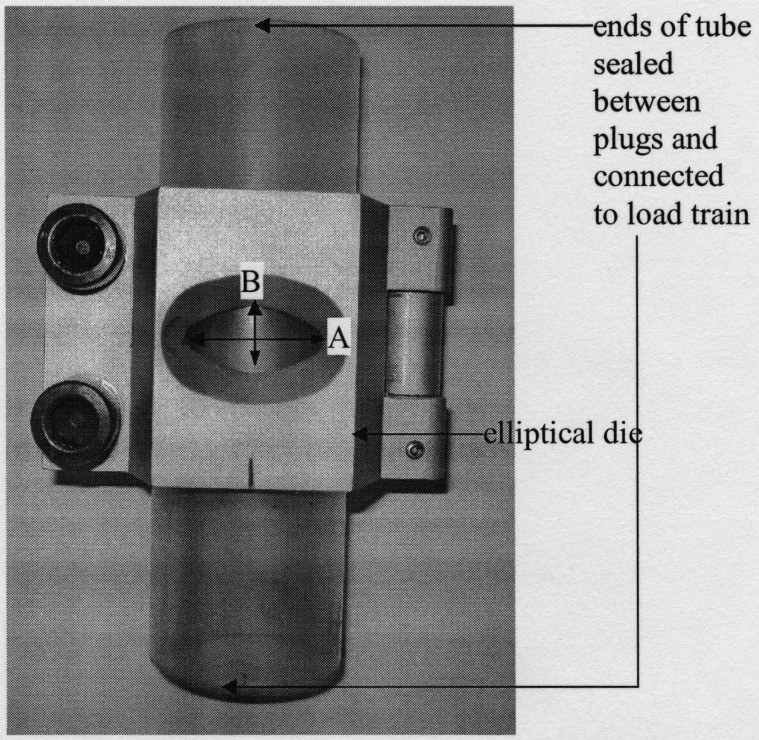

Figure F.1 Elliptical die used in tube forming test showing major and minor axis, A and B respectively.

With an elliptical die whose major and minor axis lengths are A and B respectively, fitted to the tube, various bulge heights, h, are assumed as the material is pressurized. The bulge height refers to the vertical distance from the initial surface of the tube to the deformed surface at the pole of the bulge. Figure F.2 shows this dimension and all of the other relevant dimensions from the perspective of the hoop deformation. Table F.1 gives a qualitative description of the dimensions shown in Figure F.2. For simplicity, scale drawings of the initial tube and a given die opening geometry, in addition to the deformed geometry associated with a given bulge height, were drawn using AutoCAD. The values of θ_{hi}, R_h and θ_h were obtained (as in Figure (F.2)) from the drawings. The quantities l_{hi} and l_h were calculated using:

$$l_{hi} = (R_{hi})(\theta_{hi}) \tag{F.1}$$

$$l_h = (R_h)(\theta_h) \tag{F.2}$$

The hoop strain, ε_θ, associated with a given die opening geometry and bulge height, h, was calculated using:

$$\varepsilon_\theta = \ln\left(\frac{l_h}{l_{hi}}\right) \tag{F.3}$$

A similar procedure was used in the calculation of the strain along the axial direction of the tube associated with a bulge height, h, and die opening geometry. Figure F.3 shows all of the relevant dimensions from the perspective of the axial deformation. Table F.2 gives a qualitative description of the dimensions shown in Figure F.3. Once again, the values of R_a and θ_a were determined using AutoCAD. The quantity l_a was calculated using:

$$l_a = (R_a)(\theta_a) \tag{F.4}$$

The axial strain, ε_a, associated with a given die opening geometry and bulge height, h, was calculated using:

$$\varepsilon_a = \ln\left(\frac{l_a}{B}\right) \tag{F.5}$$

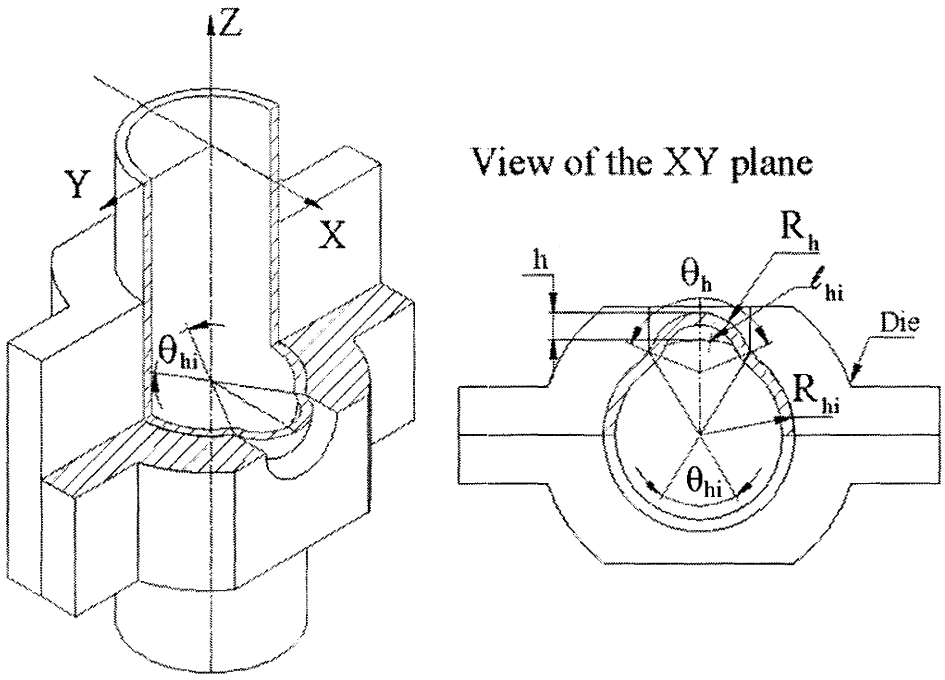

Figure F.2 Tube bulging using an elliptical die viewed from the perspective of deformation along the hoop direction with appropriate dimensions shown. Note that the two figures are identical.

Dimension (refer to Figure E.2)	Description (corresponds to deformation along the hoop direction)
h	bulge height
R_{hi}	initial radius of tube
l_{hi}	arc length along the outer radius of the undeformed tube between the die opening
θ_{hi}	angle subtended between the die opening along the outer radius of the undeformed tube
R_h	radius of the deformed arc associated with bulge height, h
l_h	arc length along the outer radius of the deformed tube between the die opening
θ_h	angle subtended between the die opening along the outer radius of the deformed tube

Table F.1 Qualitative description of critical dimensions associated with tube bulging using an elliptical die viewed from the perspective of deformation along the hoop direction.

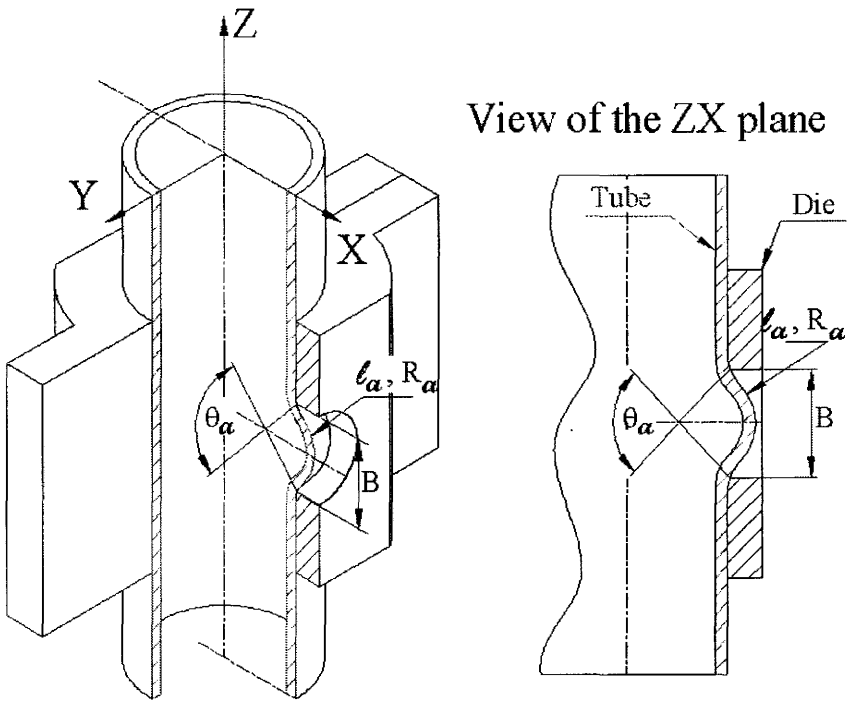

Figure F.3 Tube bulging using an elliptical die viewed from the perspective of deformation along the axial direction with appropriate dimensions shown.

Dimension (refer to Figure E.3)	Description (corresponds to deformation along the axial direction)
B	Length of minor axis of elliptical opening
R_a	radius of the deformed arc associated with bulge height, h
l_a	arc length along the outer radius of the deformed tube between the die opening
θ_h	angle subtended between the die opening along the outer radius of the deformed tube

Table F.2 Qualitative description of critical dimensions associated with tube bulging using an elliptical die viewed from the perspective of deformation along the axial direction.

In order to select the elliptical die geometry (i.e. length of major and minor axis) which would yield strains close to the balanced biaxial state, various geometries were considered. Tables F.3 to F.5 outline the results of the simple design study for selected elliptical die geometries. Table F.4 shows that the die with A = 31 mm gives an average strain ratio close enough to 1, and for this reason, this was the chosen geometry.

Elliptical die geometry – A = 25.4 mm B = 19 mm

h	R_{hi}	θ_{hi}	l_{hi}	R_h	θ_h	l_h	Hoop strain (ε_θ)	l_{ai} (or B)	R_a	θ_a	l_a	Axial strain (ε_a)	Strain ratio ($\varepsilon_a/\varepsilon_\theta$)
4	25.4	57.725	25.577	14.08	121.068	29.736	0.151	19	13.28	91.335	21.159	0.108	0.715
5	25.4	57.725	25.577	13.29	134.518	31.186	0.198	19	11.52	111.03	22.312	0.161	0.813
6	25.4	57.725	25.577	12.79	146.995	32.797	0.249	19	10.52	129.103	23.692	0.221	0.888

Table F.3 Calculation of the strain ratio at the pole of the bulge based on an elliptical die geometry having A = 25.4 mm and B = 19 mm. All length dimensions are in millimeters and angles in degrees.

Elliptical die geometry – A = 31 mm B = 19 mm

h	R_{hi}	θ_{hi}	l_{hi}	R_h	θ_h	l_h	Hoop strain (ε_θ)	l_{ai} (or B)	R_a	θ_a	l_a	Axial strain (ε_a)	Strain ratio ($\varepsilon_a/\varepsilon_\theta$)
4	25.4	75.213	33.326	17.59	123.612	37.930	0.129	19	13.28	91.335	21.159	0.108	0.837
5	25.4	75.213	33.326	16.83	134.189	39.397	0.167	19	11.52	111.03	22.312	0.161	0.964
6	25.4	75.213	33.326	16.29	144.157	40.965	0.206	19	10.52	129.103	23.692	0.221	1.07

Table F.4 Calculation of the strain ratio at the pole of the bulge based on an elliptical die geometry having A = 31 mm and B = 19 mm. All length dimensions are in millimeters and angles in degrees.

Elliptical die geometry – A = 38.1 mm B = 19 mm

h	R_{hi}	θ_{hi}	l_{hi}	R_h	θ_h	l_h	Hoop strain (ε_θ)	l_{ai} (or B)	R_a	θ_a	l_a	Axial strain (ε_a)	Strain ratio ($\varepsilon_a/\varepsilon_\theta$)
4	25.4	97.181	43.060	20.7	133.921	48.359	0.116	19	13.28	91.335	21.159	0.108	0.931
5	25.4	97.181	43.060	20.14	142.09	49.921	0.148	19	11.52	111.03	22.312	0.161	1.088
6	25.4	97.181	43.060	19.73	149.863	51.580	0.181	19	10.52	129.103	23.692	0.221	1.221

Table F.5 Calculation of the strain ratio at the pole of the bulge based on an elliptical die geometry having A = 38.1 mm and B = 19 mm. All length dimensions are in millimeters and angles in degrees.